Helmholtz Resonators in Open Office Acoustics

Vidhya Rajendran

A thesis
submitted in partial fulfillment of the
requirements for the degree of

Master of Science in Architecture

University of Washington
2020

Committee:
Tomás Méndez Echenagucia
Brian R Johnson

Program Authorized to Offer Degree:
Architecture

University of Washington

Abstract

Helmholtz Resonators in Open Office Acoustics

Vidhya Rajendran

Chair of the Supervisory Committee:

Tomás Méndez Echenagucia
Department of Architecture

Acoustics is the only category in which a LEED-rated office building performs worse than a conventional office building. Exposed hard surfaces and lack of partitions cause easy propagation of conversational sounds between the workstations in an open office. Research has shown that excess speech levels in the office cause disturbance to its occupants, and it can affect their work performance. Sound absorbers are relied upon to remove the excess sound energy from the office space. But, to address the absorption of speech sounds, porous absorbers are not efficient. Resonant absorbers, particularly Helmholtz Resonators, are effective at low-frequency sounds and are applied to tackle the frequencies important for speech intelligibility in open offices.

This research discusses the basics of Helmholtz resonators and their working principles. The classical lumped approach is used for evaluating the absorption performance of a resonator. Modifications to the basic geometry of a resonator, as explored by Selamet, S.K.Tang, Y.H.Kim, and a few others, are discussed along with their analytical formulations. Models, as given by Van der Aa and Y.H.Kim to predict the performance behavior of an array of resonators are presented, since such a system of resonators can overcome the narrow performance quality of a single resonator. Differential evolution is implemented for designing the array. The application of this array or panel in an open office improves its acoustic quality. Open office acoustic parameters like Distraction distance, Spatial decay rate, Sound Pressure Level at 4m, and the background noise level are used for evaluating the acoustic comfort. Pareto front optimization is applied to analyze the trade-offs for an optimal acoustic environment.

Contents

Acknowledgments

Doing this research was not easy for me, but the journey was made enjoyable thanks to all those who helped me. I would like to thank my Thesis Committee Chair, Prof. Tomás Méndez Echenagucia, for his constant support, supervision, patience, and extensive knowledge in the field of acoustics. He pushed me in the right direction and made sure that I stayed on track throughout this research project. Besides my Committee Chair, I would like to thank my other committee member, Prof. Brian R Johnson, who helped me structure my thesis better and guided me to the right resources. My committee made sure that I was not overworked, and helped me pace out my workload.

I am eternally grateful to my family for their moral support throughout my Master's program. My dad, Rajendran Muthumari, proofread and re-read this document to offset for my careless spelling and grammar mistakes. My mom, Girija Rajendran, made sure that I remembered all my deadlines, and she was always there for me to vent to. My brother, Vasanth Kumar Rajendran, helped me refine my presentations and my public speaking skills.

My sincere thanks go to Renée Cheng, the Dean of the College of Built Environments, for providing me with financial support, which helped me spend more time on the research work rather than trying to maintain multiple jobs. I would also like to express my gratitude to the NBBJ architecture firm in Seattle, a partner in this research project. A very special thanks to my firm advisor, Ryan Mullenix, who provided insights into workplace design and helped widen the scope of this research.

The experiments would not have been possible without the help from Prof. Andy Piacsek and Technician Peter Zencak from the Department of Physics in the Central Washington University. We collaboratively built the impedance tube setup for testing my panel samples. Their efforts, especially during the COVID pandemic time, is very much appreciated. I would like to thank my professor, Roark Congdon, who lent me his 3D printer so that I could fabricate my test samples during the lock-down. A huge thanks to my professors who run the fabrication lab - Jack Hunter and Kimo Griggs.

I would like to thank Arthur van der Harten, developer of the Pachyderm Acoustics plugin, for answering my questions on using his software. Last but not the least, I appreciate the help from my friends, Zakariya Hussain and Hemanth Prabakar, in sustaining me through the lockdown and in making the trip to CWU for the experimentation.

Finally, to my other friends and flatmates who have been a part of my journey in getting there: Kevin Tom Philip, Calvin Apodaca, Vineet Kapashi, Deepthi Reddy Pailla, Roshni Somkuar, Hari Krishna, and Krishna Teja.

List of Figures

List of Tables

1 Introduction

Over the last two decades, there has been a shift in office culture from private cubicles to open-plan offices. Open offices gained prominence for promoting worker collaboration and social interaction (Bradley 2004). They are economical and improve the mental health of the occupants. Lack of intervening partitions enhances most elements of workplace comfort, viz. indoor air quality, natural lighting, and visual access to the outdoors. Unfortunately, this also enables unhindered sound propagation in the open offices. The originating sound can travel longer distances within the office. Sound from human activities and speech can interfere with the cognitive abilities of the employees (Delle Macchie et al. 2018, Ebissou et al. 2015). In open offices, the hard reflective surfaces and the insufficiency of sound barriers cause the distracting noises to affect many more people than in a conventional office setup (Hodgson 2011, Lee & Kim 2008).

Sound absorbent surfaces help to reduce the detrimental effects of noise in the work space. But with the type of office furnishings and the conventional ceiling absorbents, acoustic comfort is not attained in open offices (Delle Macchie et al. 2018). Porous absorbers are commonly used for sound absorption in open offices. They are effective in absorbing mid to high frequency sound spectrum. This emphasis on damping the mid to high frequencies is because humans are more sensitive to frequencies above 500Hz, though our audible range is between 20Hz-20kHz, and we perceive them to be loud. Most activities, speech and mechanical noises contain energy in the whole sound spectrum. Damping the mid and high frequencies causes a concentration of low-frequency sound in the space, which can be heard as a "hum". Though low frequencies are not heard as a loud sound, they can cause annoyance and stress in people (Leventhall et al. 2004, Pierre Jr et al. 2004). Long exposure to low-frequency noise in the workplace adversely affects the employee's concentration and work performance.

Unlike porous absorbers, resonant absorbers are effective in absorbing low frequencies. They attenuate the sound by the vibration motion of an air column that connects the environment having sound waves to an enclosed cavity of air (Cox & d'Antonio 2016). Helmholtz Resonators, a type of resonant absorber, are of particular interest in this research study. A Helmholtz Resonator with a specific geometrical construct can absorb a narrow range from the low-frequency spectrum. Fortunately, many such constructs are possible and each resonator design can absorb a different bandwidth from the low-frequency spectrum. By combining different sized resonators into an array, or panel, a large bandwidth could be absorbed, even larger than the sum total of individual absorption bandwidths (Griffin et al. 2000). This is made possible by their coupling effect. Such a panel can be hung from the ceiling, or applied to wall surfaces in open offices, to absorb and to obstruct the concentration of low sound frequencies.

The acoustic quality of the open office with ceiling-hung Helmholtz resonator panels fares better, compared to the offices without any low-frequency absorbers. With this inclusion, the reverberation time in each octave can be maintained within 1 second, which averts the "hum". Addressing the low-frequency problem in open-plan offices can help improve the occupant satisfaction, and thereby the work productivity of the employees (Fuchs 2013).

1.1 Previous work

Helmholtz resonators have existed for over a century now. The initial designs of a Helmholtz resonator were quite bulky for attenuating low frequencies, but over the years developments have been made to both the sound attenuation performance and its space efficiency. Ingard (Ingard 1953) investigated the effect of neck geometry (size and number of openings, cross-sectional shape, and location in relation to the cavity's central axis) on the resonance frequency of a Helmholtz resonator with either a circular or rectangular cavity. Selamet and Lee (Selamet & Lee 2003) studied the extension of the neck into the cavity to improve the low-frequency absorption capability within a limited space. Shi and Mak (Shi & Mak 2015) designed a resonator with a spiral neck to improve the absorption efficiency using the curvature effect of the spiral neck. Tang (Tang 2005) suggested a tapered neck for the resonator to increase the internal resistance, and hence its absorption. Selamet (Selamet et al. 2005) introduced porous material in the cavity of the resonator to increase its internal resistance.

Analytical models have been developed to predict the sound absorptive performance of the resonators. Johansson and Kleiner (Johansson & Kleiner 2001) developed formulas to predict the performance of a simple cylindrical resonator and the interaction between two resonators. Kim (Kim et al. 2003) provided a method to predict the absorption quality of a unit rectangular resonator and an array of such resonators in a panel. Huang (Huang et al. 2019) presented an approach to calculate the performance of a resonator with an embedded neck. Vigran (Vigran 2004) provided a matrix technique to calculate the performance of a conical neck resonator. Additional resistances in the form of perforated plates and screens to improve the absorptive performance of resonators were given by Atalla (Atalla & Sgard 2007).

Kim (Kim 2010) developed three methods to predict the performance of a panel composed of resonators of varying sizes. These methods have certain limitations in their implementation. His third method is widely applicable, and it predicts the performance of a panel quite accurately, but neglects the distribution pattern of the resonators in the panel. Van der Aa (Van der Aa 2012) provided a similar approach to calculate the sound pressure at a receiver location for sound waves reflected from a resonator panel.

1.2 Research questions and objectives

Since the inception of open offices in the 1950s, the problem of providing a positive working environment has been a persistent challenge. The occupants in open offices show dissatisfaction and reduced work productivity (Delle Macchie et al. 2018). In a research (Brennan et al. 2002) that tracked the satisfaction of employees who were relocated from traditional offices to open offices, the results showed a decrease in occupant satisfaction. Their dissatisfaction continued long after they were relocated, and there was a lower perceived job performance too. A majority of those complaints are targeted at the acoustical discomfort present in the work areas. At the same time, open offices can offer economic and cultural incentives as indicated by the Leadership in Energy and Environmental Design (LEED) rating system's preference for open offices. The acoustic challenge in open offices has led to the following research questions.

Main research questions - It is cited that employees are distracted by conversational noises in the open office (Delle Macchie et al. 2018, Ebissou et al. 2015). So, how can an absorber be designed to specifically attenuate the frequencies important for speech intelligibility in open offices? Is it possible to improve the open office acoustics with such an absorber?

Secondary questions -

- Can Helmholtz Resonators be used to address the low-frequency noise problem?
- How to design an absorber composed of Helmholtz resonators? Would it be efficient in attenuating the sound frequencies important for speech intelligibility?
- What is the impact of such an absorber in open office acoustics?
- How can this absorber be architecturally integrated into the design?
- How can this absorber be fabricated? What materials can be used for better results, and what are the constraints involved in its fabrication?

1.2.1 Aims and objectives

The goal of this research is to investigate the application of Helmholtz resonators to improve open office acoustics issues. Helmholtz resonators are used as acoustic liners for reducing noise in airplanes and automobiles. In architecture, they are used for removing room modes or standing waves, especially in engine rooms or in recording studios, which produce the same frequency or bass frequencies sound throughout (Jordan 1947). Hence, these resonators are already proven to be good at attenuating low-frequency noise. Through this research, the possibility of extending the application of Helmholtz resonators to a diffuse sound field is examined. In open offices, a wide range of sound frequencies exist in a reverberant field. In such a case, the sound incidence on the resonators could be from any direction. To address the broadband spectrum, a number of resonators working in different frequencies would have to be put together.

The main objective of this research is to design a broadband absorber composed of Helmholtz resonators of varying sizes to address the speech intelligibility complaints in open offices. The addition of porous materials to enhance the absorption capabilities of the resonator is avoided in this research, considering the possibility of dust collection in the fibers. The ideal absorber would be simple, yet efficient in improving the acoustical comfort in open offices.

1.3 Research methods

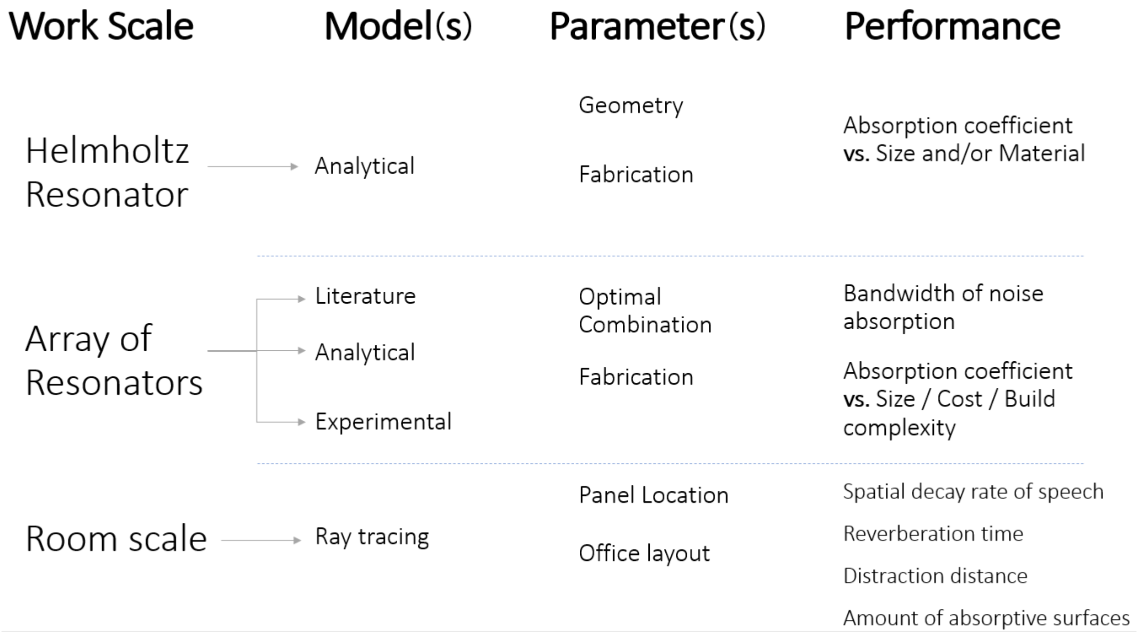

Figure 1: *Work scales and their associated models, parameters, and performance criteria*

This research is split into three work scales - individual resonators, an array of resonators in the form of a panel, and application of the panels in open offices. Though these work scales are developed sequentially, the results from one work scale influence the design in the other scales. Experimental validation has been done for the array of resonators scale. This calibration helped reduce the error accumulation in other scales as well.

At the scale of the individual resonator, the goal is to design a unit resonator which maximizes the absorption performance within the desired spectrum of sound. Analytical models are used to predict the absorption performance of the resonator. While the analysis considered only the geometrical configuration of the resonator, design considerations include probable fabrication procedures. The resonator's performance is evaluated based on the trade-off between its sizing and its maximum absorption coefficient.

At the array of resonators scale, resonators of various geometries are packed together into a system. The coupling effect improves the overall performance of the system. To maximize this system's performance, the resonators' resonant frequencies are spaced out evenly within the bandwidth of interest. Literature review of other Helmholtz resonator panels or metamaterials provided knowledge on the optimal combination of resonators. Analytical methods, as suggested by Kim (Kim 2010), are employed in designing an absorptive panel within the desired bandwidth. Experiments were conducted on a few samples to validate the results from the analytical methods. Performance of the designed panels are ranked based on its bandwidth of absorption, its peak performance, and the complexity involved in fabricating the panel.

At the room-scale, ceiling absorbers are modeled into an open office layout to analyze the optimal location of the absorbers and its efficacy in improving the acoustics of the space. Single-number acoustic values as specified in the ISO 3382-3 are used for quantifying the acoustic comfort achieved. The number of resonator panels (consequently, the amount of absorption introduced in the open office) and their heights from the floor level are the variable parameters in each simulation. The panels are arranged equally over all the workstations in the office layout. Studies are done to understand the impact of the orientation of these panels with respect to the workstations. The observations made from the resonator panel studies are applied to three open office layouts - modeled based on the existing offices in the USA. Pareto front analysis is applied between the number of absorptive panels required, and consequently the cost, to achieve good acoustics, and the single-number acoustical ratings of their performance for each office layout.

1.4 Report outline

Chapter 2 covers the background knowledge and the literature review for this research. Association of work productivity to acoustic comfort is dealt with in this chapter. Some of the answers to the secondary research questions on the acoustics issues in open offices are shared. In chapter 3, the basics of Helmholtz resonators and their working principles are reviewed. Analytical formulas developed by researchers to compute the efficiency of different kinds of Helmholtz resonators are provided. Chapter 4 discusses the advantage and ways of organizing multiple resonators into an array system. Models to predict the performance behavior of the arrays are presented. Two approaches to designing an array of resonators are explored, along with the "best" one selected for this research. Chapter 5 describes the implementation of the Helmholtz resonator panels in the open office acoustical simulation, and analyzes the improvements made. Acoustic parameters for this evaluation and bench-marking against the acoustics of conventional offices are given. Improvements made by the introduction of the designed absorber in different open office layouts are studied and presented in Chapter 6. In Chapter 7 the materials and fabrication of a resonator panel and some of the alternative designs for the resonators are discussed. This research concludes with the Experimentation Chapter that outlines the design and manufacture of an impedance tube setup and samples for testing.

2 Background

2.1 Fundamentals of acoustics

Sound consists of pressure waves. The intensity or the loudness of sound, known as Sound Pressure Level (SPL), is measured in decibels (dB). 45dB sound is as loud as the constant humming noise from a refrigerator. The pressure waves are characterized by the number of vibrations (or air compressions) per second, known as wave frequency. High-frequency sound waves have shorter wavelengths, and vice versa. The human ear is tuned to frequencies from 20Hz to 20 kHz. Hence, it can detect low, mid, and high-frequency sound waves. But, it is not equally sensitive to all the frequency ranges.

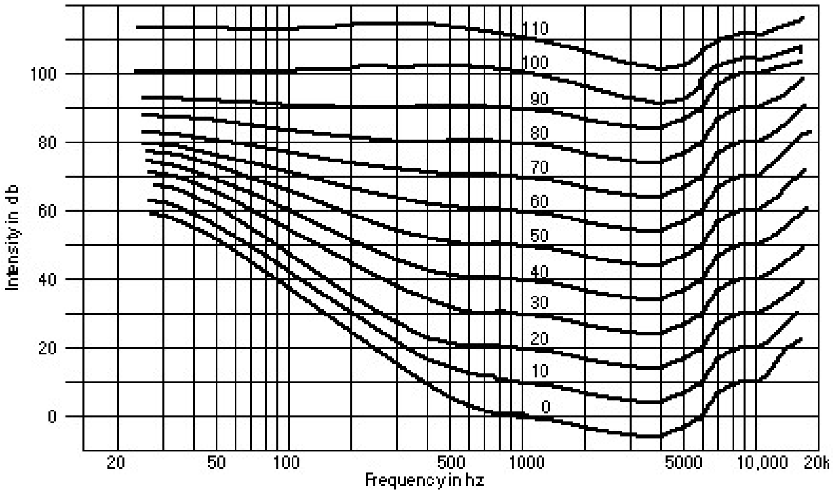

Figure 2: *Equal-loudness contours*

Equal-loudness contours (refer figure 2) reveal the correlation between the intensity or the loudness of sound and the audible frequencies. For a 10dB change in loudness (up to 50dB loudness level), humans can hardly perceive this change in the low-frequency (less than 600Hz) and in the high-frequency (over 8000Hz) spectrums. And they are most sensitive to frequencies in the range 2000Hz - 5000Hz. This variability has introduced the A-weighting system for measuring the loudness of sound that is adjusted to human sensitivity.

2.2 Performance rating of 'Green' buildings

In open offices, the noise levels could reach up to 60dB. Though open offices are designed to enhance the connectivity between teams, and to reduce the maintenance costs, they lack in providing speech privacy and a quiet working environment. Center for Built Environment (CBE) at the University of California, Berkeley designed a web-based occupant satisfaction survey to gain insights into workplace productivity. The results from the survey of over 200 office buildings are given in figure 3. LEED-rating is used as a means to categorize the office buildings into 'Green' and 'non-Green' buildings.

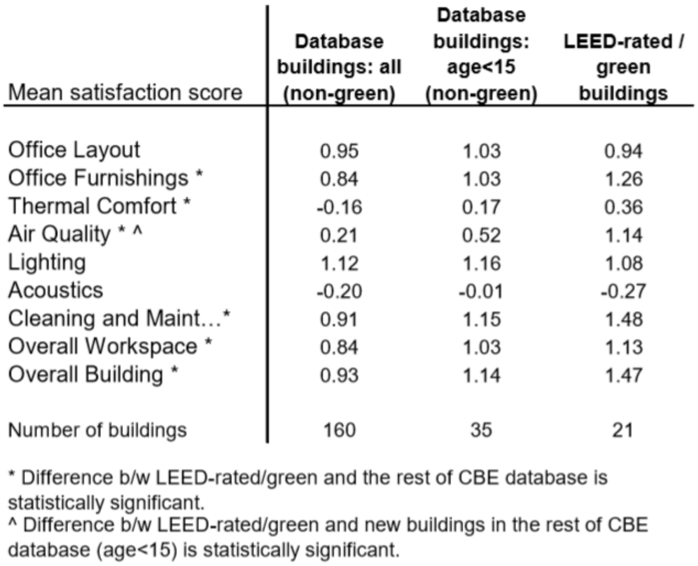

Mean satisfaction score	Database buildings: all (non-green)	Database buildings: age<15 (non-green)	LEED-rated / green buildings
Office Layout	0.95	1.03	0.94
Office Furnishings *	0.84	1.03	1.26
Thermal Comfort *	-0.16	0.17	0.36
Air Quality * ^	0.21	0.52	1.14
Lighting	1.12	1.16	1.08
Acoustics	-0.20	-0.01	-0.27
Cleaning and Maint…*	0.91	1.15	1.48
Overall Workspace *	0.84	1.03	1.13
Overall Building *	0.93	1.14	1.47
Number of buildings	160	35	21

* Difference b/w LEED-rated/green and the rest of CBE database is statistically significant.
^ Difference b/w LEED-rated/green and new buildings in the rest of CBE database (age<15) is statistically significant.

Figure 3: *Mean Satisfaction Score comparison across all CBE survey categories among three groups: database buildings, new database buildings, and LEED-rated/green buildings (Abbaszadeh et al. 2006)*

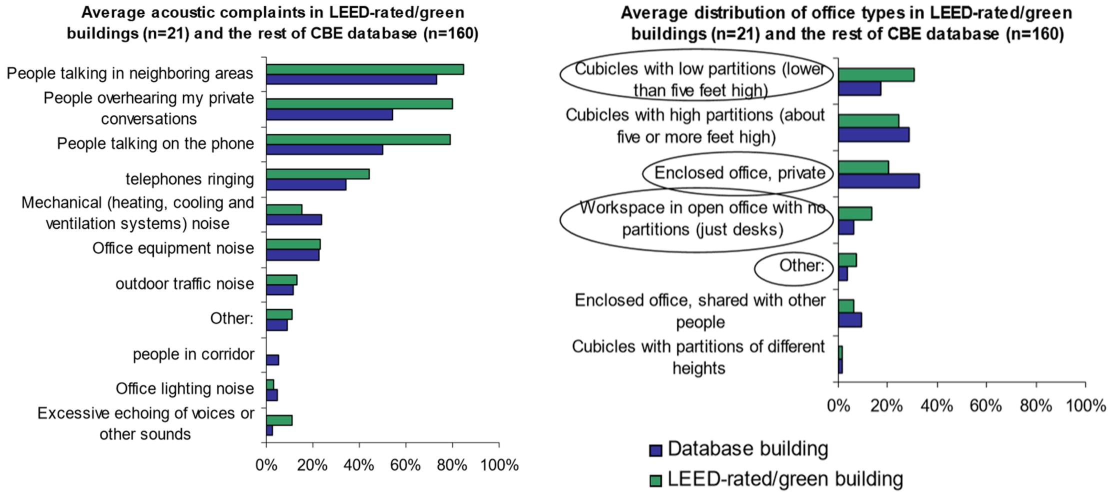

Figure 4: *(a) Mean percentage of acoustic complaints; (b) Mean percentage of office types in LEED-rated/green buildings and the rest of the CBE database (Abbaszadeh et al. 2006)*

Acoustics is the only category in which a LEED-rated office building performs worse than a conventional building (Abbaszadeh et al. 2006, Hodgson 2011, Lee & Kim 2008). This aspect is very prominent in the offices with low partition walls or open-plan offices, than in the offices with high screens. The CBE survey also branches out to include the sources of dissatisfaction and occupant complaints. Figure 4 outlines the reasons for the acoustic discomfort in LEED-rated office buildings. Employees in open offices are often disturbed by conversational sounds from neighboring areas. The hard exposed wall surfaces and the lack of sufficient partitions reflect the babble sounds within the open office. Another reason for the acoustic concern in

LEED-rated buildings is the influx of external noises which are induced by natural ventilation. But more importantly, LEED "virtually ignores acoustics" (Hodgson 2011). Hence, sufficient attention is not paid towards the acoustic comfort in the workplace environment.

2.3 Acoustics in Open offices

In open offices, the occupants are distracted by speech levels and activities occurring around them. A poor acoustic condition weakens their ability to concentrate and affects their work productivity (Ebissou et al. 2015). A decrease in task performance is correlated with Speech Transmission Index (STI) (refer figure 5). The STI is a 0 to 1 index, that represents the "transmission quality of speech", where 1 represents a perfectly speech-intelligible situation and 0 corresponds to a perfectly speech-private condition. In open offices, an STI value of 0.2 or less is required to maintain the occupant productivity levels (ISO 3382-3 2012).

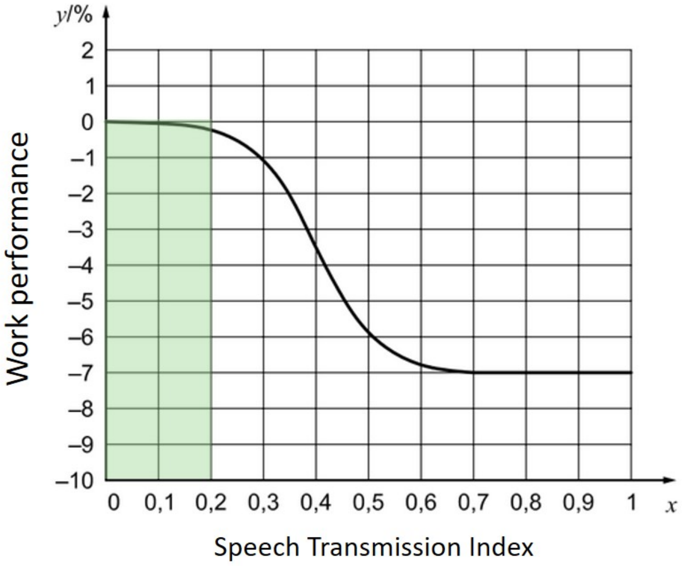

Figure 5: *STI vs Task performance (ISO 3382-3 2012)*

Two kinds of sound levels contribute to the evaluation of STI - Conversational Sound and Background Noise. While it is a common mistake to remove the background noise for better acoustic quality, the contrary is found to be true in offices (Rindel 2018). People find it comforting to work in the presence of mild background noise. This is because the background noise plays a masking role for the remote speech sounds. However, if its value is too high, it could affect the employee's work performance. To achieve an STI value of 0.25, the speech and noise levels will have to be maintained as shown in figure 6. The background noise levels will have to be slightly higher than the conversational or speech sound to effectively mask the speech and provide speech privacy.

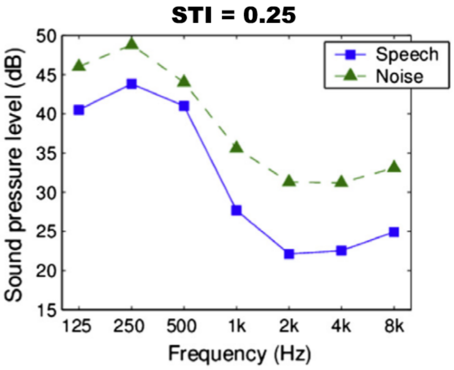

Figure 6: *Sound levels for an STI value of 0.25 (Ebissou et al. 2015)*

The typical speech levels in an open office are depicted in figure 7. It is noticeable that the Intermediate Office Speech Level (IOSL) exceeds the required speech levels for an STI value of 0.25. And this excess sound is mostly concentrated in the low-frequency range of up to 600 Hz. Hence, it is equally important to address the sound absorption of low frequencies to reduce the overall speech sounds in open offices. Tackling the speech sounds at their source helps in selectively attenuating them without completely removing the background noise. Removing the conversational sound adds a layer of speech privacy to the occupants, the lack of which is another prominent acoustic complaint.

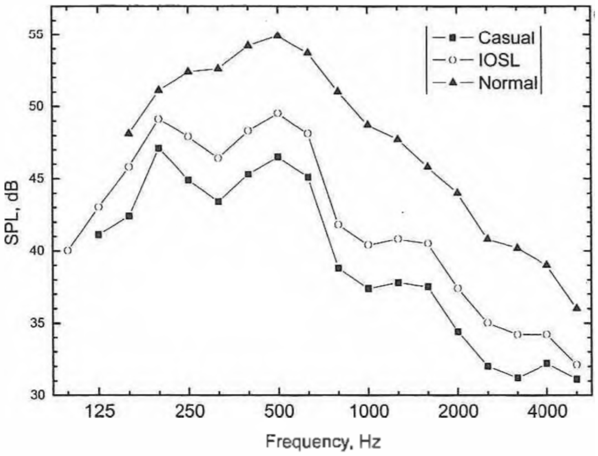

Figure 7: *Speech spectrum in Open offices (Bradley 2003)*

2.4 The low-frequency problem

The annoyance caused by low-frequency sound is underestimated (Leventhall et al. 2004, Pierre Jr et al. 2004). Low-frequency sound includes frequencies in the range 10Hz to 300Hz. Typically, A-weighting is used as a standard for measuring the loudness of sound. It factors in the sensitivity of human ears to the full audible range of frequencies (20Hz-20kHz). The A-weighting standard, though widely accepted and used in measuring the noise levels, de-emphasizes the low-frequency noise content (Pierre Jr et al. 2004). Research studies have shown that low-frequency noises, also known as "hum", are perceived by many as loud and annoying, compared to other noises of the same SPL. But the A-weighting standard has reduced the attention placed on attenuating the low-frequency noises. Unfortunately, low-frequency noises can travel long distances without losing much of their energy, and they are less attenuated by walls and other structures.

In open offices, low-frequency noises are largely generated by HVAC systems. In addition, low-frequency external noises from aircraft or vehicles are transmitted through walls, doors, and windows as they aren't greatly damped by the intervening structures. Long exposure to low-frequency noise in the workplace affects the employee's concentration and work performance (Pawlaczyk-łuszczyńska et al. 2003). The low rumble noise can affect the retaining capacity of the brain.

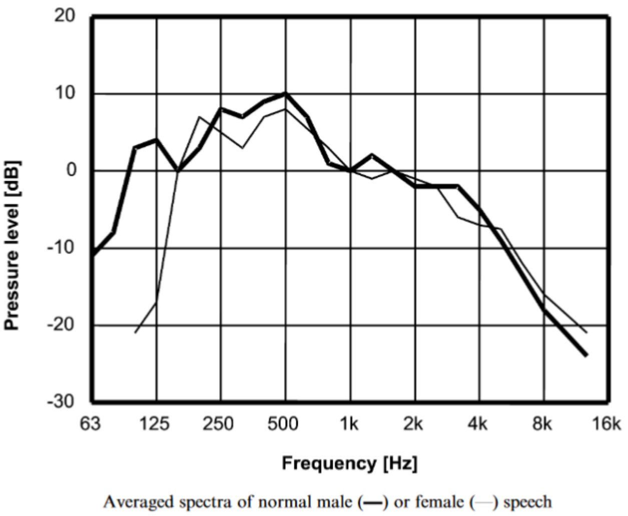

Figure 8: *Speech spectra (Fuchs et al. 2001)*

Another source of low-frequency noise in workplaces is normal human conversation. Human sentences are composed of vowels and consonants. The consonants carry the information content of speech while vowels carry the sound volume of speech. Mapping out the consonants and vowels on a frequency scale shows that consonants are largely clustered in mid to high frequencies, while vowels occupy the lower frequencies (Davidsson 2016). As shown in figure 8, both male and female speech levels have higher SPL values in the low frequencies contributed by vowels. Articulation loss of consonants, denoted %ALcons, is a measure that uses the amount of deterioration of consonants in the speech as a means for quantifying speech intelligibility. It does not factor in the impact of low-frequency vowels. In fact, the low-frequency content is amplified in rooms that have been treated with mid to high-frequency porous absorbers. This causes a rumbling noise that degrades the speech intelligibility (Fuchs et al. 2001). Unlike %ALcons, STI encompasses all the octave bands in speech and is included in the ISO standards for measuring the speech intelligibility in open office spaces.

Fuchs (Fuchs 2013) rightly points at the low-frequency problem, both in terms of measuring it and in attenuating it. Low-frequency noise can amplify certain room modes, and this not only causes uneasiness but also hinders the measurement of SPL at low frequencies. Noise is best controlled when tackled at its source. But low-frequency noises are difficult to control at their source, and can bounce around the room without losing much of their energy. Even the partitions placed in the open offices don't contribute much in attenuating low frequencies. Low-frequency sounds, because of their long wavelengths, are strongly diffracted around the edges of the partitions and also get transmitted through the screens without losing much energy.

2.5 Sound absorption in open offices

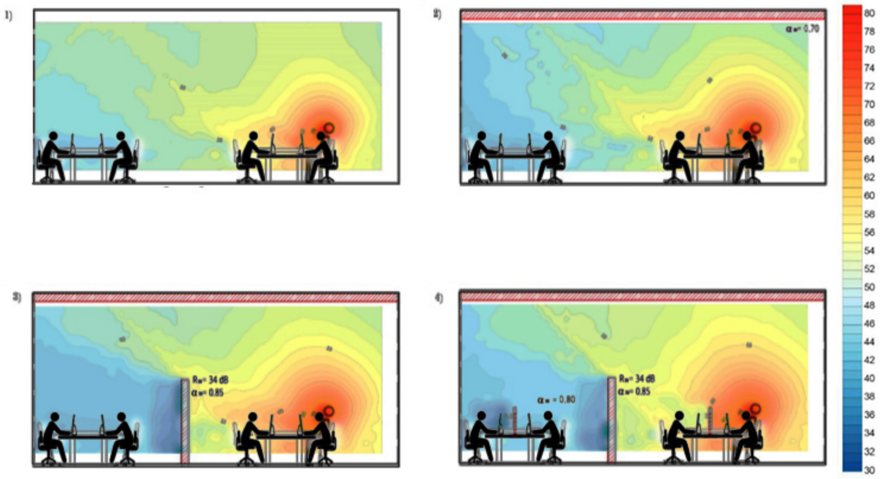

Figure 9: *Sound absorption in open offices (Delle Macchie et al. 2018)*

Typically, diffusive or rough surfaces are used to scatter the incident sound waves in the open offices. But, this strategy only ensures that the sound does not concentrate in a particular zone. On the other hand, sound absorptive surfaces remove the excess sound energy from the space. Figure 9 shows a case-wise reduction in the sectional area affected by a speaker in an open office using sound absorbers. Use of absorptive material on the ceiling is very effective in impeding the sound propagation in the open offices.

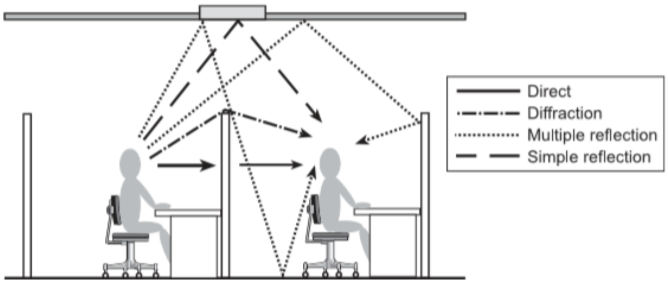

Figure 10: *Sound path between workstations (Bradley 2004)*

Porous absorbers are commonly used as acoustic insulation on the walls, as they perform well in mid to high frequencies, but it is difficult to achieve low-frequency sound absorption with them due to the required thickness of the material – porous absorbers need to be at least a quarter wavelength thick for quality sound absorption. Also, within a space, absorbers are preferred at room boundaries, and porous absorbers are not efficient at the boundaries where the wave velocity is low (Cox & d'Antonio 2016). Resonant absorbers, on the other hand, are very effective when placed at the room boundaries. They have their peak absorption in the low-frequency, but unlike porous absorbers, the sound attenuation capacity is dependant on the dimensions of the structure rather than on the material properties.

Membrane or panel absorbers and resonant absorbers are designed for trapping low frequencies (Figure 11). Diaphragmatic absorber, a popular membrane absorber, is quite efficient in tackling frequencies as low as 50Hz, but it needs a large cavity (200mm-300mm) for such low frequencies. Helmholtz resonator is also a low-frequency absorber and requires a deeper cavity for effective absorption. However, there have been recent developments in making them compact without compromising their performance. For instance, a sub-wavelength acoustic resonator, which is 75 to 80 percent shorter, can achieve the same results as a traditional Helmholtz resonator (Yuan et al. 2019). Also, resonant absorbers are considered a "healthier" alternative to porous absorbers, as they do not have any spongy components that may lead to dust accumulation (Cox & d'Antonio 2016). This also helps prevent mold formation in their pores.

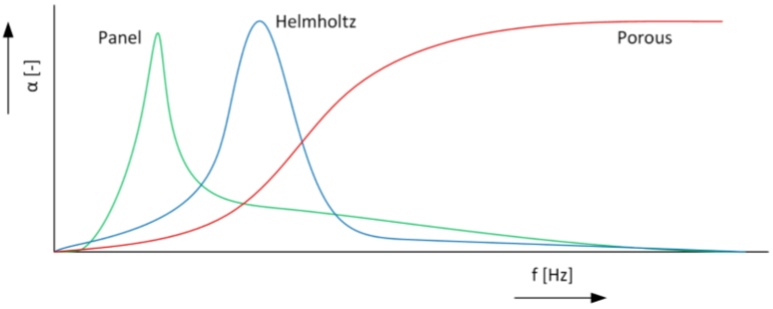

Figure 11: *Performance of different sound absorbers (Gommer 2016)*

3 Helmholtz Resonators

Long before Helmholtz resonators were studied, the Greeks designed "vessels" to modify the acoustics in their theaters. Vitruvius, a great Roman architect, in his book, described the embedding of "brass vessels" in the reflective stone or marble walls of the theater to improve the sound quality (Rindel 2011). In the 19^{th} century, the German physicist Hermann von Helmholtz studied the phenomenon of air resonance in hollow spherical cavities with short and narrow necks. He used varying sizes of these resonators to study the frequencies in music, to amplify a particular frequency in a complex sound wave. His resonator design was later named after him. Now, several modifications have been made to the original design to make it more compact and efficient.

3.1 Working principles

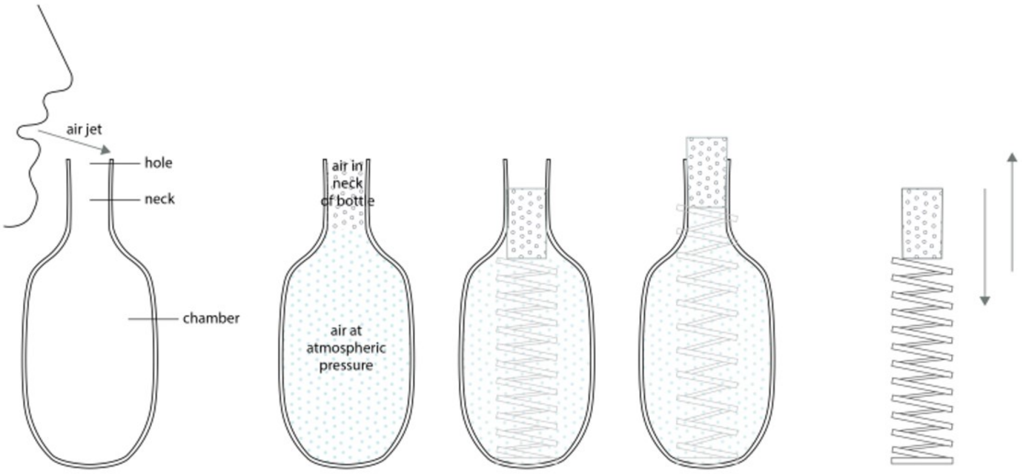

Figure 12: *Working of a Helmholtz Resonator (newt.phys.unsw.edu.au/jw/Helmholtz.html)*

Helmholtz resonators resemble an empty bottle with an open mouth. When sound waves pass over this opening, it vibrates the air column in the neck which converts sound energy into thermal losses. The plug of air in the neck acts as a vibrating mass against the spring provided by the air in the enclosed cavity (see figure 12) (Cox & d'Antonio 2016). Damping is caused by viscous losses along the surface of the neck and radiation losses at the ends of the neck. By changing the vibrating mass and the stiffness of the air spring, the Resonant Frequency of the device can be tuned, and the maximum absorption occurs at its Resonant Frequency. But its bandwidth of absorption is very narrow and limited. This drawback could be overcome by combining multiple Helmholtz resonators of varying geometries (or resonant frequencies) to achieve a broader bandwidth of absorption (refer figure 13).

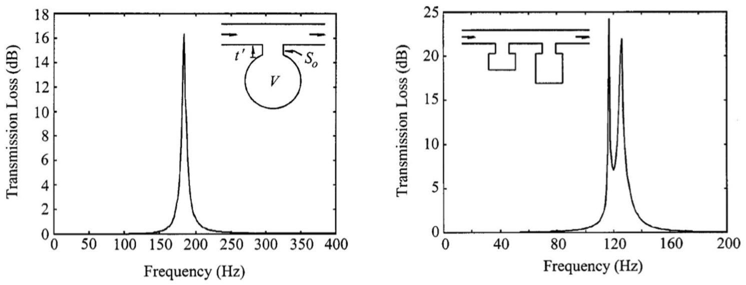

Figure 13: *(left) Sound absorption of a single resonator; (right) Sound absorption of two resonators connected in series (Griffin et al. 2000)*

3.2 Classical lumped approach

The performance of a Helmholtz resonator is measured using its absorption coefficient, i.e, the ratio of the amount of incident sound energy reflected back to the amount of incident sound energy. One way to predict the absorption coefficient of a resonator is to determine its acoustic impedance. Acoustic impedance is a measure of the resistance provided by a resonator to the flow of sound waves.

The acoustic impedance on the surface of the resonator is given by (Ver & Beranek 2006):

$$z_A = \frac{pressure}{velocity} = \frac{\widehat{p}}{U} \tag{3.1}$$

where $\widehat{p}$ is the spatially averaged sound pressure and U is the volume velocity.

The above equation can be re-written as:

$$z_A = R_m + j(X_m) \tag{3.2}$$

where $j = \sqrt{-1}$, R_m is the resistance of the resonant system, and X_m is the reactance term.

The resistance in the resonant system is offered by viscous and radiation losses in the neck. Viscous losses are induced by the friction provided by the neck material to the vibrating plug of air. Some amount of sound energy that enters the resonator is given back into the environment. This is the radiated energy. The amount of sound energy that is trapped by the resonator accounts for the radiation losses.

$$R_m = R_v + R_{rad} \tag{3.3}$$

where R_v accounts for the viscous losses (Ingard 1953) and R_{rad} the radiation losses (Meissner 2004).

$$R_v = \frac{\sqrt{2\rho_0\omega\mu}}{S_n}\left[2 + \frac{l}{r}\right] \qquad R_{rad} = \frac{\rho_0 c k^2}{2\pi} \tag{3.4}$$

where S_n is the area of the neck opening ($S_n = \pi r^2$), r is the radius of the neck, l is the length of the neck, $k = \frac{\omega}{c}$ is the wavenumber in the air, and $\omega = 2\pi f$ is the angular frequency.

The reactance of the resonant system is expressed as a mass-spring damper system (Chenzhi & Mak 2018):

$$X_m = \omega M_n - \frac{K_r}{\omega} \tag{3.5}$$

where M_n is the mass of the vibrating plug, and K_r is the stiffness of the spring provided by the air in the cavity.

$$M_n = \frac{\rho_0 l'_n}{S_n} \qquad\qquad K_r = \frac{\rho_0 c^2}{V_c} \tag{3.6}$$

where l'_n is the corrected length ($l' = l + \delta$), and V_c is the volume of the cavity.

The end corrections are given by Ingard (Ingard 1953):
ε is the ratio of the radius of the neck to the radius of the body. If $\varepsilon < 0.4$,

$$\delta_{inner} \approx 0.48(S_n)^{\frac{1}{2}}(1 - 1.25\varepsilon) \qquad\qquad \delta_{outer} \approx 0.48(S_n)^{\frac{1}{2}} \tag{3.7}$$

The system resonates when the imaginary part (reactance term) of the impedance is zero. Hence, the resonant frequency is given by (Cox & d'Antonio 2016):

$$f_0 = \frac{c}{2\pi}\sqrt{\frac{S_n}{l'V_c}} \tag{3.8}$$

3.3 Modifications to a Helmholtz resonator

This research discusses only concentric resonators, which have the center of the neck and the center of the cavity along the same axis. The resonators are considered to be loaded on a baffle to model a sound absorptive panel.

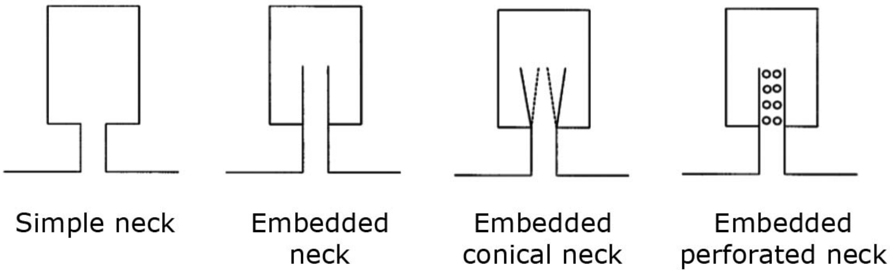

Figure 14: *Modifications suggested by Selamet (Selamet & Lee 2003)*

A simple resonator design is a cylindrical cavity with a cylindrical neck. Modification to the cross-section of the cavity introduces a square cavity attached to a cylindrical neck. Such a design is space-efficient, especially when multiple resonators are packed together into a panel. A square resonator with exact dimensions to that of the cylindrical resonator (the diameter of the cylindrical cavity equates to the edge length of the square cavity) has a lower resonant frequency and a better absorption peak value in the low frequencies.

Adaptation of the neck geometry of a simple resonator presents the embedded neck model. Instead of having the neck protrude outwards, having the neck immersed into the cavity's volume of the resonator saves space. This design shifts the performance peak to lower frequencies but maintains the peak absorption value. Another variant is developed by switching the cylindrical neck with a conical neck. This resonator shifts the resonant frequency higher with increasing taper length. Though it has a better absorption performance, its performance has a narrow bandwidth compared to a resonator with cylindrical neck.

To predict the absorption performance of a resonator, its neck and cavity impedances are calculated. The average spatial impedance, Z, of a Helmholtz resonator loaded on a baffle or wall is given by,

$$Z = \frac{Z_{HR}}{\varepsilon} \qquad Z_{HR} = Z_n + Z_c; \quad \varepsilon = \frac{S_n}{S_c} \tag{3.9}$$

where Z_n and Z_c are the impedances of the neck and the cavity, respectively, and $S_c = \pi R^2$ (if in free field) or D^2 (if attached to a baffle).

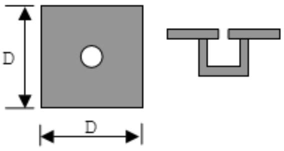

Absorption coefficient, α, is given by,

$$R = \frac{Z - Z_0}{Z + Z_0} \qquad \alpha = 1 - |R|^2 \tag{3.10}$$

where Z_0 is the characteristic impedance of air ($Z_0 = \rho_0 c$).
note: Units of Z, Z_{HR}, and Z_0 are Ns/m^3

Case 1 - Cylindrical neck and cylindrical cavity
Resistance is given by (Johansson & Kleiner 2001),

$$R_v = \sqrt{2\rho_0\omega\mu}\left[\frac{l}{r} + 2\right] \qquad R_{rad} = \frac{\rho_0 c k^2 S_n}{2\pi} \tag{3.11}$$

Impedances of the neck and the cavity (Johansson & Kleiner 2001),

$$Z_n = R_v + R_{rad} + j\omega\rho_0 l' \tag{3.12}$$

$$Z_c = j\omega\frac{\rho_0 L_c}{3}\left(\frac{S_n}{S_c}\right) - \frac{j\rho_0 c^2 S_n}{\omega V_c} \tag{3.13}$$

(Refer Appendix A for a complete derivation)

Case 2 - Cylindrical neck and square cavity

Resistance is given by (Kim et al. 2003),

$$R_v = \rho_0 \frac{l}{a}\sqrt{8\nu\omega} \qquad\qquad R_{rad} = \frac{\rho_0 c(kr)^2}{2} + j\omega\rho_0\frac{8}{3\pi}r \tag{3.14}$$

Impedances of the neck and the cavity (Kim et al. 2003),

$$Z_n = R_v + R_{rad} + j\omega\rho_0\left(\frac{8}{3\pi}r + 2\sqrt{\frac{8\nu}{\omega}}\right) + j\omega\rho_0 l\left(1 + \frac{\sqrt{\frac{8\nu}{\omega}}}{2r}\right) \tag{3.15}$$

$$Z_c = -j\frac{\rho_0 c^2 S_n}{\omega V_c} \tag{3.16}$$

(Refer Appendix B for a complete derivation)

Case 3 - Cylindrical embedded neck and cylindrical cavity

Resistance is given by (Huang et al. 2019),

$$R_v = 2\sqrt{2\rho_0\omega\eta} \qquad\qquad R_{rad} = j\omega\rho_0\delta_i \tag{3.17}$$

where δ_i is the acoustic mass end-correction.

Impedances of the neck and the cavity (Huang et al. 2019),

$$Z_n = R_v + R_{rad} + \frac{-j\rho_0\omega l}{\Psi_v} \tag{3.18}$$

$$Z_c = \frac{-jS_n\rho_c c_c^2}{\omega Vc} \tag{3.19}$$

where V_c = (Vol. of cavity - Vol. of embedded neck) and $\Psi_v = \frac{J_2(k_v r)}{J_0(k_v r)}$.

(Refer Appendix C for a complete derivation)

Case 4 - Conical neck and cylindrical cavity

Impedance at the inlet is given by (Tang 2005),

$$Z_{inlet} = j\rho_0 c\left(\frac{r_i}{r_o}\right)\frac{kl - \frac{\pi r_i r_o}{kV_c}}{1 + \frac{\pi r_i r_o l}{V_c}} \tag{3.20}$$

where radii r_i faces outside and r_o faces the cavity ($r_i < r_o$).

Impedance of the resonator is given by (Tang 2005),

$$Z_{HR} = \frac{r_i^2 R_0}{r_o^2 + \frac{r_i r_o l \pi r_o^2}{V_c} + jr_i r_o R_0\sqrt{\frac{\pi r_i r_o l}{V_c}}} \tag{3.21}$$

where R_0 is the unknown resistance of the conical resonator.

(Refer Appendix D for a complete derivation using another method)

3.4 Additional resistance to a Helmholtz resonator

Additional resistance could be added to a resonator by including a perforated plate or a screen over the neck opening, or porous material in the cavity of the resonator. Such additions increase the viscous losses in the neck. This additional resistance improves either the absorption coefficient value or the bandwidth of absorption, depending on the kind of resistance added. To achieve an optimal absorption coefficient value, the added resistance, R_s, is governed by (Pieren 2012),

$$R_s = Z_0 \left[1 + \left(\frac{2\rho_0}{\pi} \frac{D}{m} \right)^2 \right]^{-\frac{1}{2}} \tag{3.22}$$

where D is the distance of the screen from the rigid backing, and m is the surface mass density of the added resistance. And if the distance is small enough and the mass density is large, then $R_s \approx Z_0$.

Case 1 - Neck perforated plate

ϕ is the porosity of the plate, and is usually assumed between 0.5-0.6.

Resistance and end correction are given by (Atalla & Sgard 2007),

$$R_v = \sqrt{2\rho_0 \omega \eta} \left(\frac{d}{a} + 2\frac{\varepsilon}{a} \right) \qquad \varepsilon_e = 0.85a(1 - 1.14\sqrt{\phi}) \tag{3.23}$$

where d is the depth of the perforation plate, and a is the radius of the perforation.

Impedance of the perforated plate, Z_p,

$$Z_p = \left(R_v + j\omega\rho_0 \left[2\varepsilon_e + d \right] \right) \frac{1}{\phi} \tag{3.24}$$

Impedance of the resonator, Z_{total},

$$Z_{total} = Z_p + Z_c \quad ; \qquad Z_c = -j\rho_c c_c \frac{S_n \phi}{S_c} cot(k_c L_c) \tag{3.25}$$

where Z_c is the impedance of the backing cavity and ρ_c, c_c, k_c are the complex density, speed of sound, and wavenumber of the backing cavity, respectively. The complex parameters are replaced by ρ_0, c, k if the backing cavity contains only air.

Case 2 - Resistive screen

Impedance and resistance of the screen are given by (Atalla & Sgard 2007),

$$Z_s = \frac{j\omega\rho_s R_s}{j\omega\rho_s + R_s} \quad ; \qquad R_s = \sigma d \tag{3.26}$$

where ρ_s is the mass per unit area of the resistive material, R_s is the flow resistance, σ is the flow resistivity, and d is the thickness of the screen.

$$\sigma = \frac{8\eta}{\phi r^2} \tag{3.27}$$

where r is the radius and ϕ is the perforation rate of the resistive material.

Impedance of the resonator, Z_{total},

$$Z_{total} = Z_s + Z_n + Z_c \quad ; \qquad Z_s \approx R_s, \quad if R_s >> \rho_s \tag{3.28}$$

Case 3 - Porous material in the cavity

Impedance of the backing cavity with porous absorber, Z_c,

$$Z_c = -j(Z_i)cot(k_i d) \tag{3.29}$$

where Z_i and k_i are the impedance and the wavenumber of the porous material.

From the empirical equation of Delany and Bazely,

$$k_i = \frac{\omega}{c}\left[(1 + 0.0978(X)^{-0.70})j + 0.189(X)^{-0.595}\right] \tag{3.30}$$

$$Z_i = \rho_0 c\left[1 + 0.0571(X)^{-0.754} - j(0.087(X)^{-0.732})\right] \quad ; \qquad X = \frac{\rho_0 f}{\sigma} \tag{3.31}$$

where f is the frequency and σ is the flow resistivity.

3.5 Digital simulation

The impedance formulas given in section 3.3 for each resonator geometry were verified by reproducing the absorption performance graphs obtained from the literature. The given graphs in other research papers have been validated against the experiment's results. This benchmarking is necessary to reduce the error accumulation further down in the research process. Additional information on reproducing these graphs are given in Appendix G.

Trends in the absorption performance of a resonator by varying each parameter were analyzed. Increasing the size of the neck opening decreases the peak absorption value of the resonator, while increasing the length of the neck increases the peak value. These trends are caused by the frictional resistance provided by the neck. The relationship between the neck geometry and the viscous losses is given in Eqn. 3.4 - The neck opening (S_n) is inversely proportional, while the neck length (l) is directly proportional, to the viscous losses. These relationships help determine the peak performance value of the resonator. In the trends observed in the resonator's cavity, increasing the cavity radius increases the peak value, while increasing the cavity depth has only a marginal impact on the peak value. These are governed by the stiffness of the spring provided by the air in the cavity (given in Eqn. 3.6). In general, increasing the volume of the cavity reduces the stiffness of the spring, and hence enables increased vibrations in the neck of the resonator. This improves the the resonator's peak performance value.

3.5.1 Benchmarking

Case 1 - Cylindrical neck and cylindrical cavity

Performance graph from (Komkin et al. 2017):

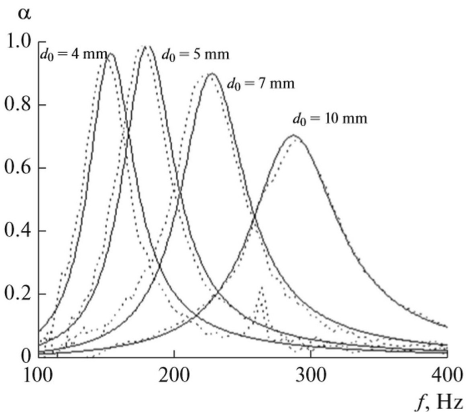

Calculated (—) and experimental (·····) dependences of the absorption coefficient on frequency for different diameters of the resonator neck.

Reproduced graph:

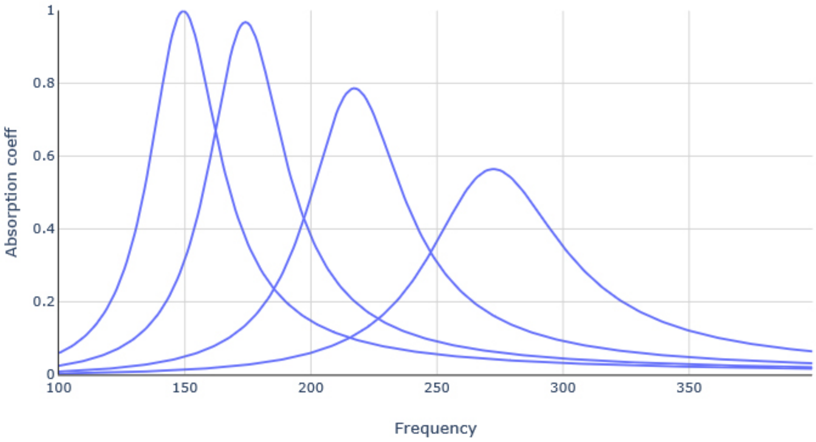

Case 2 - Cylindrical neck and square cavity

Performance graph from (Kim et al. 2003):

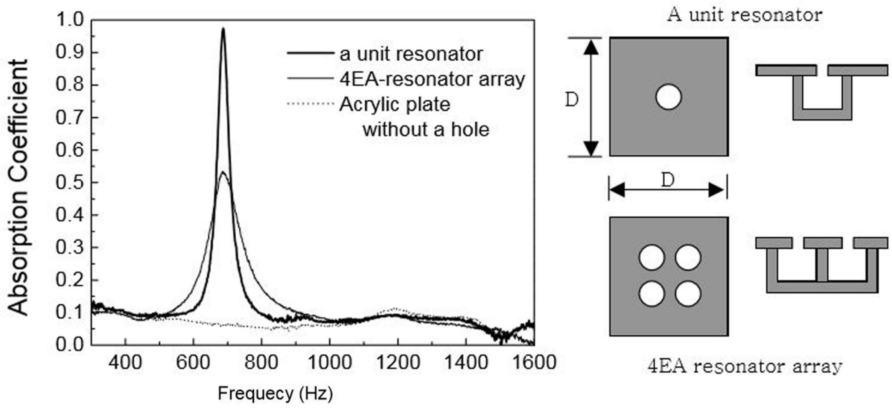

Absorption coefficients of Helmholtz resonator units at normal incidence *a=5mm, l=10mm, V=27000mm^3, D=100mm*

Reproduced graph of a unit resonator:

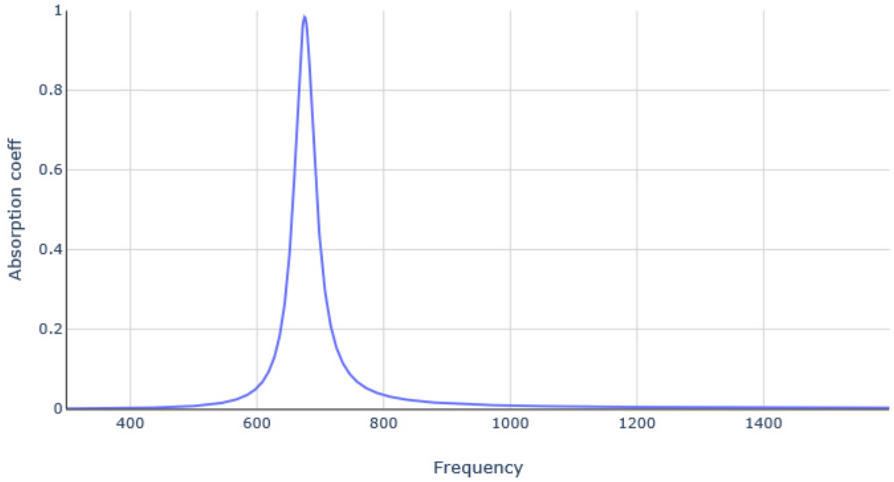

Case 3 - Cylindrical embedded neck and cylindrical cavity

Performance graph from (Huang et al. 2019):

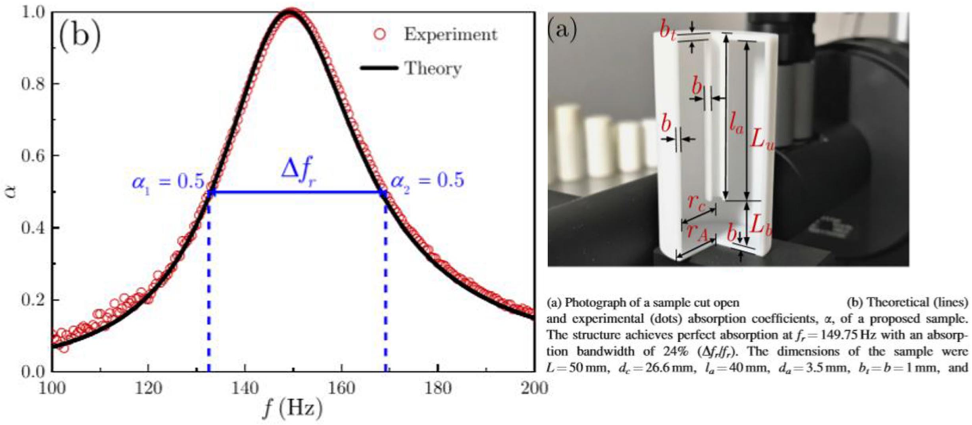

(a) Photograph of a sample cut open (b) Theoretical (lines) and experimental (dots) absorption coefficients, α, of a proposed sample. The structure achieves perfect absorption at $f_r = 149.75$ Hz with an absorption bandwidth of 24% ($\Delta f_r / f_r$). The dimensions of the sample were $L = 50$ mm, $d_c = 26.6$ mm, $l_a = 40$ mm, $d_a = 3.5$ mm, $b_t = b = 1$ mm, and

Reproduced graph of the embedded sample:

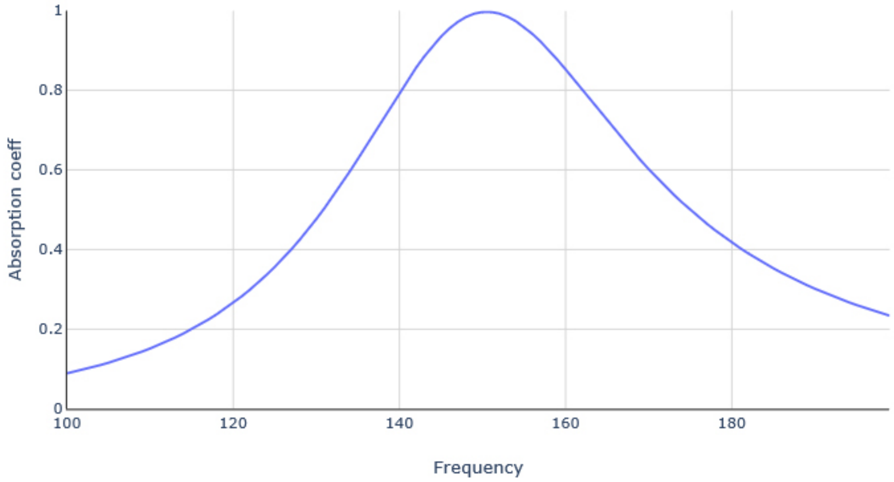

3.5.2 Helmholtz Resonator performance metrics

The quality factor Q, a dimensionless measurement, is used for comparing two individual resonators. It is defined as the ratio of resonant frequency to the bandwidth over which the absorption coefficients are greater than half the absorption coefficient at the resonant frequency.

$$Q = \frac{f_{res}}{\Delta f} \quad ; \quad Q = \frac{Z_n''}{Z_n'} \tag{3.32}$$

The quality factor is also defined as the ratio between the imaginary and the real parts of the total impedance in the resonator's neck (Ver & Beranek 2006).

$$Z_{neck} = Z_n' + jZ_n'' \tag{3.33}$$

where Z_n' is the real part of the neck impedance, and it is the sum of viscous and radiation resistance in the neck, and Z_n'' is the imaginary part contributed by the vibration of the plug of air in the neck.

$$Z_n' = R_v + R_{rad}; \quad R_v = \sqrt{2\rho_0\omega\mu}\left[2 + \frac{l}{r}\right]; \quad R_{rad} = \frac{\rho_0 c k^2 S_n}{2\pi} \tag{3.34}$$

$$Z_n'' = \omega\rho_0(l + \Delta l'); \quad endcorrection, \Delta l' = 2\left(\frac{8a}{3\pi}\right) \tag{3.35}$$

Small values of the Q-factor produce a broader absorption curve (Ver & Beranek 2006). Hence, to achieve a small value the viscous and radiation losses in the neck (Z_n') have to be large. This could be attained using additional resistance in the neck (refer section 3.4). Yet, the Helmholtz resonators have an inherent nature of narrow bandwidth of absorption.

4 Array of resonators

A single resonator is not very effective in absorbing a wide spectrum of frequencies. As shown in figure 13, combining two or more dissimilar resonators broadens the bandwidth of absorption. When unit resonators are placed close to one another, they influence each other due to the 'coupling effect'. This interaction becomes weaker as the distance between the resonators is increased (Johansson & Kleiner 2001). It is cited that resonators with similar resonant frequencies, when placed in close proximity, can maximize the absorption of the system compared to resonators with very dissimilar resonant frequencies (Van der Aa 2012).

4.1 The coupling effect

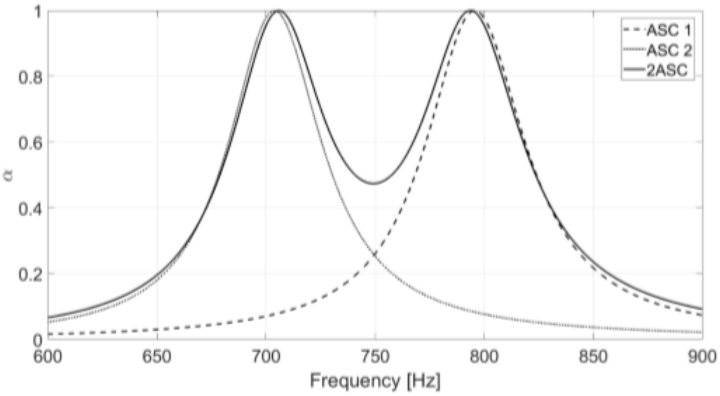

Figure 15: *Effect of mutual interaction between two resonators (Carvalho De Sousa et al. 2019)*

The coupling effect is depicted in figure 15. The bold line represents the absorption performance of the system of two different resonators placed next to each other, and the other two lines represent the individual performance of the resonators. The difference between the valley where the individuals' performances cross over and the trough in the system's performance is caused by the interaction between the two resonators.

To account for this interaction in the absorption calculation, an additional term known as "mutual radiation impedance" is added to the radiation impedance as discussed in section 3.2. The mass of air vibrating in the neck is modeled as a circular piston moving up and down. The movement expends radiation energy as shown in figure 16. When the source excites the resonators, the circular pistons are set in motion, which produces radiation waves. The resonators in the vicinity of a radiating resonator face the additional radiation on top of the self-radiation due to direct excitation by the source. This causes the mutual interaction effect observed in the graph (figure 15). As the resonators are moved away from each other, the impact of one's radiation on another becomes weaker and their combined performance tapers.

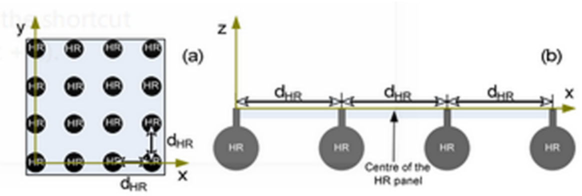

Plan and section of the 4*4 panel

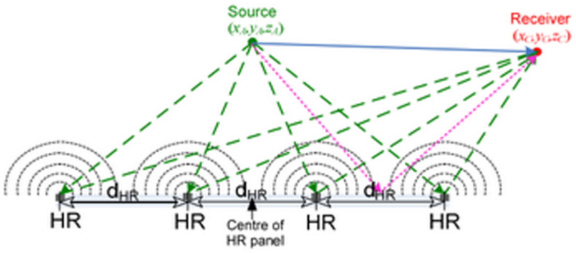

Working of the HR panel

Figure 16: *Radiation energy from a Helmholtz resonator panel of 4*4 identical resonators (Polychronopoulos et al. 2014)*

The additional impedance term that has to be added to the radiation impedance to account for this effect is given by (Chazot & Guyader 2007, Kim 2010),
Self radiation impedance, Z_{nn},

$$Z_{nn} = \rho c \left[1 - e^{-jka}\right] \tag{4.1}$$

where a is the radius of the neck.

Mutual radiation impedance, Z_{mn},

$$Z_{mn} = \frac{j\rho\omega}{2\pi}\left(\frac{e^{-jkd}}{d}\right) S_n \tag{4.2}$$

where d is the distance between the radiators and S_n is the area of the neck.

4.2 Absorption coefficient models

The models proposed by Van der Aa and Kim are analyzed to choose the appropriate one that fits the problem space of this research. To derive the absorption coefficient of a panel of resonators, the overall surface impedance of the panel has to be calculated. This parameter depends on the inlet sound pressures acting on the neck openings and the velocities of the air plugs in the necks (refer Eqn. 3.1). Van der Aa uses a matrix of resonator impedances and a vector of inlet pressures in his models to arrive at the coupled velocities in the necks. This can be used to calculate the absorption coefficient of the whole panel. Kim uses the acoustic impedance formulas (discussed in section 3.3) in his models to directly calculate the sound absorption of the panel.

Van der Aa (Van der Aa 2012) developed a model to predict the sound pressure at a receiver for a point source sound waves reflected by an array of resonators. This approach determines the

impact of the panel in its surround and gets complicated for complex environments. Van der Aa accounts for the direct waves, reflected waves from the top panel of the baffled resonators, and the radiated waves from the neck openings of the resonators. To calculate the radiated waves, he derives the inlet velocity matrix from a Gaussian elimination of the impedance matrix of N x N resonators, and the inlet pressure at the resonator openings. The impedance matrix includes the self and mutual radiation impedance as discussed above.
Impedance matrix by Van der Aa:

$$A = \begin{bmatrix} Z_{11} & -g_{21} & -g_{31} & \cdots & -g_{m1} \\ -g_{12} & Z_{22} & -g_{32} & \cdots & -g_{m2} \\ \cdots & \cdots & \cdots & \cdots & \cdots \\ -g_{1n} & -g_{2n} & -g_{mn} & \cdots & Z_{mn} \end{bmatrix} \tag{4.3}$$

where $Z_{mn} = Z_{HR}$ - $Re(\rho c(1 - e^{-jka_n}))$ and g_{mn} is the mutual radiation impedance.

$$g_{mn} = \frac{j\omega\rho}{2\pi} S_n \frac{e^{-jkd}}{d} \tag{4.4}$$

where d is the distance between the radiators and S_n is the area of the neck.

Matrix multiplication ($A * b = c$) would solve for b the vector for coupled velocities, where c is the vector for inlet pressures.

$$b = \begin{bmatrix} v_1 \\ v_2 \\ \cdots \\ v_n \end{bmatrix} \qquad c = \begin{bmatrix} q_0(2G(r_{o,1})) \\ q_0(2G(r_{o,2})) \\ \cdots \\ q_0(2G(r_{o,n})) \end{bmatrix} \tag{4.5}$$

From the velocities, the source strength of each radiating resonator is calculated by,

$$q_n^{'} = \frac{j\omega\rho S_n}{2\pi} v_n \tag{4.6}$$

And thus, the total pressure from direct, reflected, and radiated sound waves is given by (Maennel et al. 2013),

$$p(x, y, z) = q_0 \left[G(r_d) + G(r_r)\right] + \sum_{i=1}^{N} q_i G(r_i); \qquad G(r) = \frac{e^{-jkr}}{r} \tag{4.7}$$

where q is the strength of the point source, and $G(r)$ is the Green function in which r represents the distance between the two points.

Kim (Kim 2010) arrives at three effective methods to calculate the absorption performance of an array of Helmholtz resonators of varying sizes. The panel is assumed to be composed of periodic unit cells of size $L_x * L_y$ containing different sized resonators. The incident sound wave is a plane wave which has a complex amplitude of P_{in}, a polar angle θ_{in}, and an azimuth angle ϕ_{in}. Plane-wave, p_{in},

$$p_{in} = P_{in} e^{-j(k_x x + k_y y - k_z z)} \tag{4.8}$$

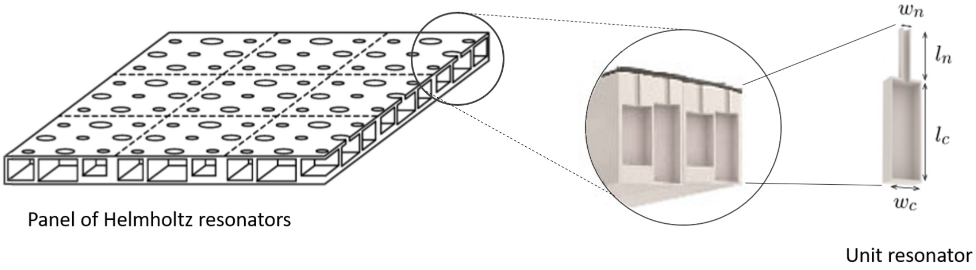

Figure 17: *Panel composed of Helmholtz resonators of varying sizes (Kim 2010)*

Method 1 - Equivalent surface impedance method

This method regards the top perforated surface as a homogeneous surface with an equivalent surface impedance. The main assumption is that the periodic unit cell is smaller than the wavelength of frequencies under consideration. Hence, the unit cells would have to be small for mid to high frequencies.

Absorption coefficient for a polar angle θ,

$$\alpha = \frac{4Re(Z_{surf}^{avg})(\rho_0 c) cos\theta_{in}}{\left[\rho_0 c + Re(Z_{surf}^{avg}) cos\theta_{in}\right]^2 + \left[Im(Z_{surf}^{avg}) cos\theta_{in}\right]^2} \tag{4.9}$$

Random incidence absorption coefficient, α_{st},

$$\alpha_{st} = \frac{1}{\pi} \int_0^{2\pi} \int_0^{\frac{\pi}{2}} (\alpha) cos\theta_{in} sin\theta_{in} d\theta_{in} d\phi_{in} \tag{4.10}$$

Averaged surface impedance for a resonator array panel composed of many identical resonators,

$$Z_{surf}^{avg} = \frac{Z_{HR}}{\varepsilon}; \qquad \varepsilon = \frac{A}{L_x L_y} \tag{4.11}$$

Spacially averaged impedance for a resonator array panel that has various kinds of resonators,

$$\frac{1}{Z_{surf}^{avg}} = \sum_{i=1}^{N} \frac{\varepsilon_i}{Z_{HR,i}}; \qquad \varepsilon_i = \frac{A_i}{L_x L_y} \tag{4.12}$$

where N is the number of resonators in a unit cell, and subscript i denotes each resonator.

The resonator impedance Z_{HR} includes the end corrections and the mutual effect between the resonators. ε is the surface porosity, which is the ratio between the area of the neck and the area of a unit cell. Refer paper (Kim et al. 2003) for a worked-out example.

Method 2 - Fourier-Rayleigh method

This method was not studied in this research because of its complexity and inherent drawbacks. There is a restriction on the size of the unit cell for this method to be applicable. $\left[\frac{max(L_x,L_y)}{\lambda} < 0.5\right]$

Method 3 - Radiation impedance method

This method accounts for the mutual radiation impedances between resonators. Unlike the equivalent surface impedance method, the top surface is not considered homogeneous, and the surface impedances of each inlet of resonators are calculated. This method does not have the restriction on the size of the unit cell as imposed in the Fourier-Rayleigh method.

Pressure at the inlet of any of the resonator is given by,

$$p_{in,i'} = P_{in} e^{-j(k_x x_{c,i'} + k_y y_{c,i'})} \tag{4.13}$$

assuming that z_c is 0, i.e. it is on the panel, and $k_x = ksin\theta_{in}cos\phi_{in}$, $k_y = ksin\theta_{in}sin\phi_{in}$, and $k_z = kcos\theta_{in}$.

The inlet pressure can be given in terms of all the impedances acting on the inlet,

$$\sum_{i=1}^{N} (\overline{Z}_{r,i',i} + \zeta_{i',i} Z_{surf,i}) u_i = -2p_{in,i'} \quad for \quad i' = 1, 2, 3, ..., N \tag{4.14}$$

where $\overline{Z}_{r,i',i}$ is the total radiation impedance, either self or mutual, and $\zeta_{i',i} = 1$ if $i' = i$, else 0.

For a circular inlet of a resonator,

$$\overline{Z}_{r,i',i} = \rho_0 c \frac{\pi a_i^2}{L_x L_y} \sum_{m=-\infty}^{\infty} \sum_{n=-\infty}^{\infty} \frac{jk}{\sqrt{\beta_{mn}^2 - k^2}} \frac{2J_1\left(a_{i'}\beta_{mn}\right)}{a_{i'}\beta_{mn}} \frac{2J_1\left(a_i\beta_{mn}\right)}{a_i\beta_{mn}} \\ \times e^{j\left[(2\pi m/L_x - k_x)\left(x_{c,i'} - x_{c,i}\right) + (2\pi n/L_y - k_y)\left(y_{c,i'} - x_{y,i}\right)\right]} \tag{4.15}$$

where $\beta_{mn} = \sqrt{(2\pi m/L_x - k_x)^2 + (2\pi n/L_y - k_y)^2}$

Sound absorption is given by,

$$\alpha = \sum_{i=i}^{N} \rho_0 c \frac{\pi a_i^2}{L_x L_y} \frac{Re(Z_{surf,i})}{cos\theta_{in}} \left| \frac{u_i}{P_{in}} \right|^2 \tag{4.16}$$

Refer paper (Kim et al. 2006) for a worked-out example.

4.2.1 Comparison between the models

Of the different approaches discussed above, Kim's radiation impedance method is a very straightforward and practical approach for this research. Both Van der Aa's pressure model and Kim's radiation impedance method account for the mutual interaction between the resonators through a N x N matrix calculation. Though it might be computationally expensive for larger resonator arrays, they are more precise and have no limitations on the size of the array. But it might be circuitous to apply Van der Aa's pressure model to derive the absorption performance of the resonator array. It involves calculating the coupled velocities in the necks from the individual resonator impedances, and then uses this vector to calculate the overall surface impedance of the panel. Hence, it is a long and an indirect method to arrive at the panel's absorption performance. The other two methods of Kim have restrictions on the size of the unit cell. Though this research is largely focused on low frequencies, and such restrictions do not have a huge impact on the unit cell sizing, having the flexibility to expand this research into mid and high-frequency is valuable. Therefore, Kim's radiation impedance method will be used for deriving the absorption performance of a panel of resonators.

4.2.2 Computational implementation

Figure 19 is the absorption performance of two specimens (Kim et al. 2006). Specimen A is composed of identical resonators, while specimen B is composed of non-identical resonators. The graphs show a comparison between Kim's proposed radiation impedance method, the conventional method, and the experimental results. There is a good agreement between Kim's method and the results obtained from an impedance tube experiment.

Using the same formulas, the graphs for specimen A and specimen B were replicated to ensure its correct usage. This was done on Python programming language, and libraries such as Numpy and Plotly were used for the matrix calculation and the graph representation, respectively.

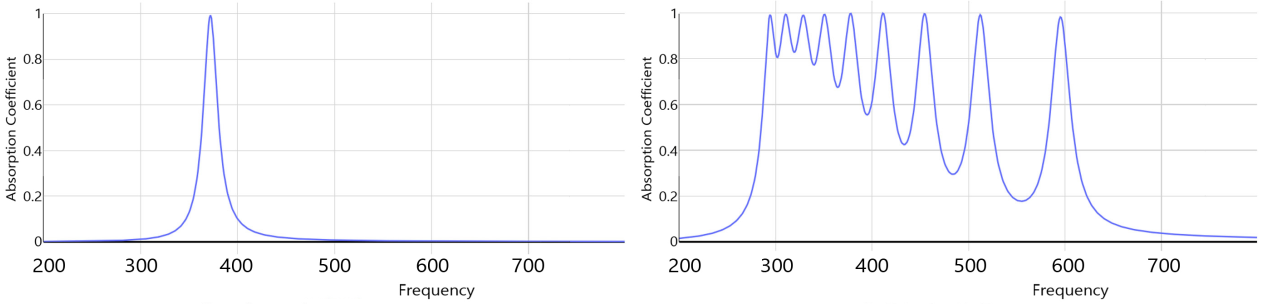

Specimen A

Specimen B

Figure 18: *Graph replications of Specimen A B using Kim's method 3*

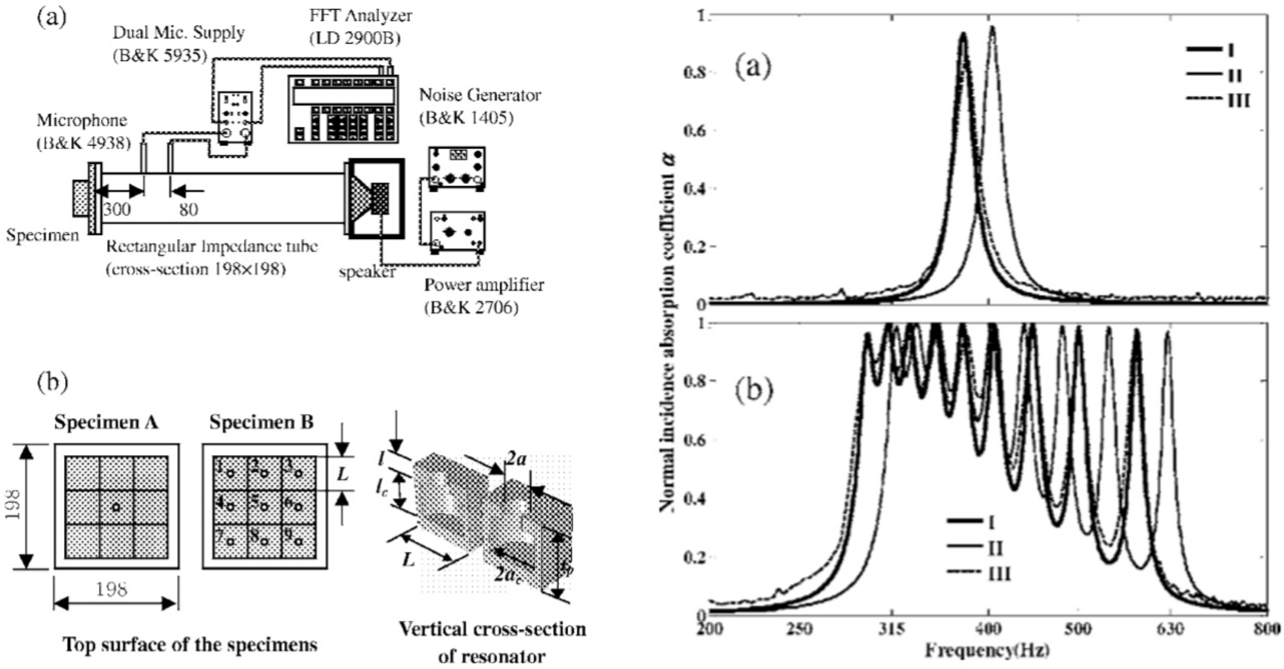

__Figure 19:__ (Left) Experimental setup and the specimens; (Right) Comparison of predicted and measured absorption coefficients for the specimen A (a) and specimen B (b). Graph I points to the predictions from Kim's radiation impedance method, graph II represents the conventional method, and graph III represents the experimental result (Kim et al. 2006)

4.3 Approach 1 - Automated resonator array design

To achieve a broadband absorber, multiple resonators of varying sizes (varying resonant frequencies) are put together in a panel. A resonator has four geometrical variables that could be changed to achieve a resonant frequency. Though a particular resonant frequency could be reached through multiple combinations, not all of them will have the same absorption performance. A few might have a smaller absorption value at their resonant frequency. As the number of resonators increase, the number of geometrical variables also increases along with the panel variables, such as the panel depth and distance between the resonators. To handle this complexity, an evolutionary solver is engaged to automate the process of finding the right geometrical combinations to achieve an effective panel.

Differential evolution (DE), one of the evolutionary solvers, was used in this study to find the optimal solution. It works on the same principle as Darwin's "survival of the fittest". A large search space is combed through by favoring those search points which score the highest on the fitness function (Storn & Price 1997). A fitness function is a rating system that analyzes the search point and produces a single-number value for comparison with other search points. Initially, randomly selected search points are assigned to the first generation of the population. The features of the high scoring "individuals" on the fitness function are passed on to the next generation. And those which score the least are dropped out to keep the population constant.

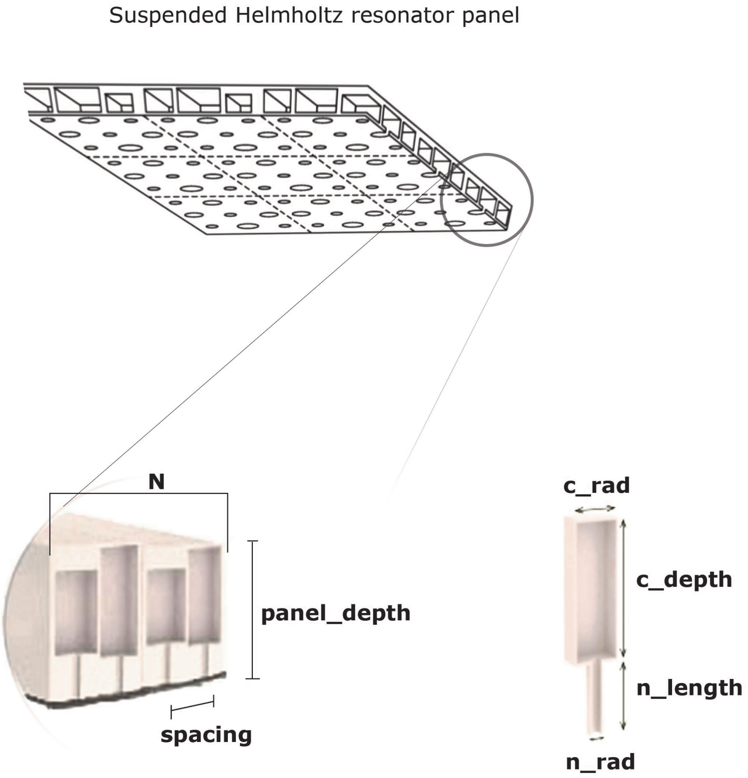

Figure 20: *Variables involved in the design of a panel composed of varying Helmholtz resonators*

Crossover and mutation help in diversifying the search points. The best features in two high performing "individuals" are crossed over to look for a better performing "offspring". A stochastically chosen "individual" is mutated by changing one of its features to prevent from localizing the solver. A couple of generations, in the magnitude of hundreds or thousands, are termed one evolution, and the solver typically runs for a few hundred evolutions to converge on a solution. The output from the solver is not the best solution in the search space, but rather an optimal one.

4.3.1 Fitness functions

In solving for resonator array design by using DE, the search space is the set of possible values for the resonator's geometry. Three fitness functions are studied to find the appropriate one that does not include any biases. The left-side image in figure 21 explains the Bandwidth fitness function. The single number is derived by multiplying the width of the curve (frequency bandwidth) at $\alpha = 0.5$ and its resonant frequency's α value (peak height). Hence, the function does not favor both narrow-tall and broad-short curves. The right-side image in figure 21 depicts the area under the curve fitness function. The Area Coverage function favors broadband absorbers. The third fitness function (Combination function) is a combination of the other two functions.

Bandwidth fitness function, $F_1(x) = \text{BW x } \alpha_{peak}$; (parameters depicted in the figure 21 graph)

Area Coverage function,

$$F_2(x) = \int_{f_{lower}}^{f_{upper}} \alpha(f) df$$

where $\alpha(f)$ is the absorption coefficient at frequency f;

Combination function, $F_3(x) = F_1(x) + F_2(x)$

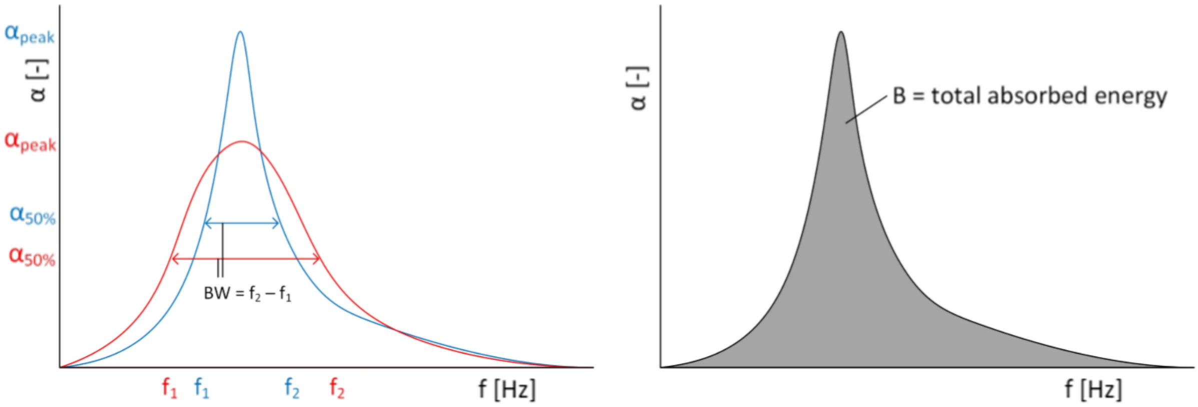

Figure 21: *Fitness functions used for the evolutionary solver (Gommer 2016)*

4.3.2 Evaluation of the fitness functions

All the three fitness functions were tested on the DE for the same search space. Refer to Appendix E for the detailed report. In the figure 22, the blue line is the frequency-dependent absorption performance and the red line is the octave filtered absorption values (discussed further in section 4.6). For the rest of this chapter, the blue line will be used for observing the trends. The bandwidth fitness function tends to clump together the resonant frequencies. As the slicing line, $\alpha = 0.5$, is raised up in stages of 0.1 from 0.7 (i.e., $\alpha = 0.7$, 0.8, and 0.9), the clumped peaks merge together into one prominent broad peak. This function is ideal for cases where all the sound energy within narrow bandwidths of sizes 100-150 Hz needs to be attenuated.

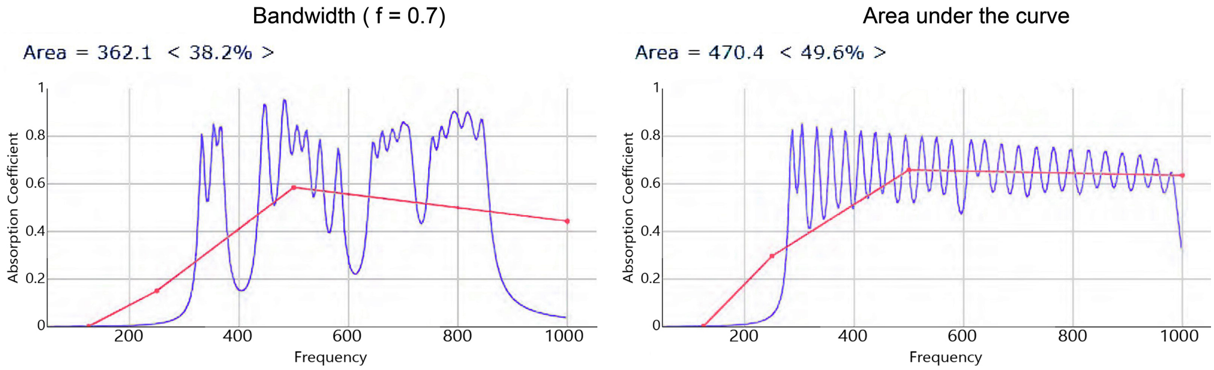

Figure 22: *Comparison between bandwidth and area under the curve fitness functions*

The area under the curve fitness function spaces out the resonant frequencies equally. The first resonant frequency is located around 275 Hz, because the search space used does not include geometrical values for a low-frequency resonator. This could easily be corrected by expanding the search space. This fitness function maximizes the bandwidth of absorption even though the peak absorption values are not as high as the ones achieved with the other fitness function. To overcome the disadvantages faced in both the fitness functions, the values from these functions were added to form the third fitness function. This combined fitness function did not yield a straight-forward relationship; the absorption curves produced did not have a pattern. Because the two fitness functions added having opposing nature - one tries to overlap the resonant frequencies while the other aims to evenly space them out.

The area under the curve fitness function is favorable for producing a broadband panel absorber. Its disadvantage could be circumvented by using additional neck resistance (as discussed in section 3.4) in the resonators that would increase their peak absorption values.

4.3.3 Variables and Constraints used in the solver

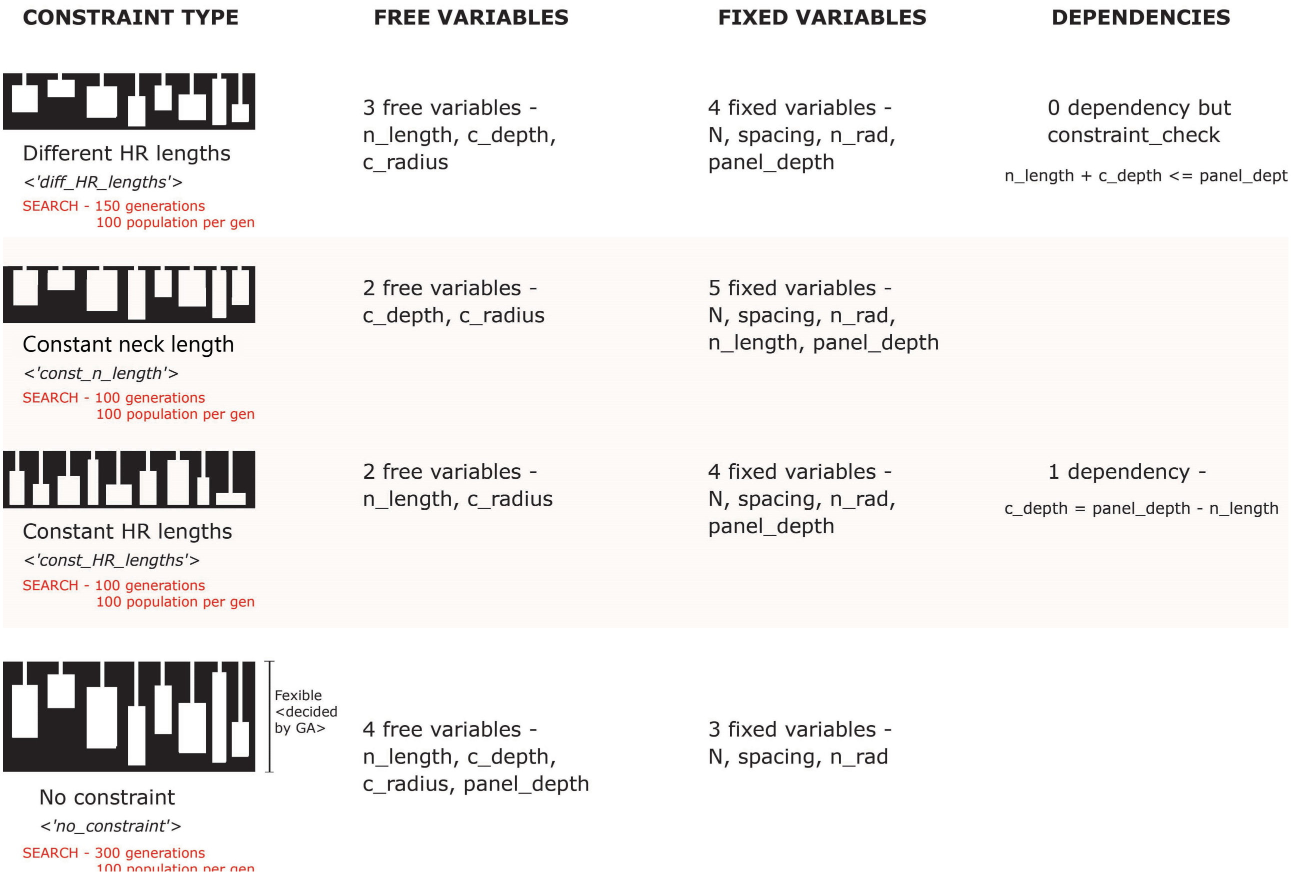

CONSTRAINT TYPE	FREE VARIABLES	FIXED VARIABLES	DEPENDENCIES
Different HR lengths <'diff_HR_lengths'> SEARCH - 150 generations 100 population per gen	3 free variables - n_length, c_depth, c_radius	4 fixed variables - N, spacing, n_rad, panel_depth	0 dependency but constraint_check n_length + c_depth <= panel_dept
Constant neck length <'const_n_length'> SEARCH - 100 generations 100 population per gen	2 free variables - c_depth, c_radius	5 fixed variables - N, spacing, n_rad, n_length, panel_depth	
Constant HR lengths <'const_HR_lengths'> SEARCH - 100 generations 100 population per gen	2 free variables - n_length, c_radius	4 fixed variables - N, spacing, n_rad, panel_depth	1 dependency - c_depth = panel_depth - n_length
Fexible <decided by GA> No constraint <'no_constraint'> SEARCH - 300 generations 100 population per gen	4 free variables - n_length, c_depth, c_radius, panel_depth	3 fixed variables - N, spacing, n_rad	

Figure 23: *Different constraint types and its associated variables*

Different types of panels can be produced by setting certain constraints on the search space. Figure 23 outlines the four types of constraints used in the DE simulations. Fixed variables are those geometrical values that are set by the user and not chosen by the DE algorithm. This is done to limit the size of the design space in the DE solver. Constraining the search space by having fixed variables helps achieve an optimal solution within a few hundred generations. It is heuristic to nudge the solver to look for a solution in a certain direction. This also allows the user to control the way the optimal panel looks. Free variables are geometrical values chosen by the DE algorithm from a domain of possible values. Each variable has a different domain of values. The dependent variable's value is derived from the equation provided. For this study, a simple Helmholtz resonator geometry is used, i.e. cylindrical neck attached to a cylindrical cavity. The panel is assumed to be a square panel with N resonators along each edge.

Constraint type 1 - Different HR lengths
HR length is the sum of the neck length (n_length) and the cavity depth (c_depth). The number of resonators in the panel (N^2), the distance between the resonators (spacing), and the depth of the panel (panel_depth) are fixed by the user. By fixing the location of the resonators, we can rule out the possibility of overlapping geometry. Resonator's geometrical variables, except the neck radius (n_rad), are chosen by the DE solver. The domains of each of these variables are set based on the spacing and the panel_depth.

Constraint type 2 - Constant neck length
This constraint type was introduced to make the fabrication of the panel easy. The n_length is constrained and all the cavities are aligned to a plane parallel to the top of the panel. The gradation of the resonant frequencies is achieved by varying the resonator cavities (c_depth and c_radius). Such a panel could be fabricated in two parts - the top board with neck perforations drilled in and the bottom block with milled out cavities.

Constraint type 3 - Constant HR lengths
This constraint type makes the fabrication of panels simple. The cavities and the necks can be milled out from a block and clamped together to a bottom flat board. The DE solver picks out the values for the n_length and c_radius. The dependency relationship makes sure that the cavity (c_depth) reaches all the way to the bottom plate.

Constraint type 4 - No constraint
This constraint has the least number of fixed variables, thus expanding the scope of the search space. The panel_depth is made a free variable. n_length and c_depth are not constrained to fit within the panel_depth's value. This opens up a large set of combinations for the DE solver, and hence the number of generations is also increased to allow for the solver to reach an optimal solution.

4.3.4 Advantages of fixing certain variables

All the constraint types have the number of resonators in the panel (N^2), the distance between the resonators (spacing), and the neck radius (n_rad) in the fixed variables. By fixing the location of the resonators and the size of their neck openings, the calculation of mutual radiation impedance (Z_{mut}) can be done only once and reused in subsequent simulations. The formula for Z_{mut} is given in equation 4.15.

The Z_{mut} on resonator i is calculated by summing up all the mutual impedances from resonators $i' = 0, 1, 2, ..., N, ..., N^2$. Hence, the number of times the above formula is used to calculate the mutual impedances of all the resonators in one panel is N^4. This is computationally heavy for higher values of N. For a realistic broadband panel, N has to be at least 5, i.e. 25 resonators in the panel. In one generation in the DE solver, 100 individual panels exist. And the solver is run for 100-300 generations. Thus, for one DE simulation the formula is run for at least 250,000 times. This takes up a lot of computational power and time.

To simplify this time-consuming task, a heuristic is designed to precompute the Z_{mut} matrix for the whole panel. In the above formula, the variables are the neck radius (a), the edge dimensions of the panel (L_x, L_y), and the distance between the resonators (x, y coordinates). If these values are made constant across all the panels in each population, the Z_{mut} matrix can be computed once and reused multiple times throughout one DE simulation. Hence, we could bring down the computation time from running the formula 250,000 times to a mere 625 times.

4.4 Panel studies

Various studies were performed to understand the patterns of a panel's performance by varying the fixed variables - N, spacing, panel depth, and *n_rad*. Though the fixed variables were maintained constant in each DE simulation, they were gradually increased or decreased in subsequent simulations to understand their impact on the panel's absorption performance. This was done for all the panel constraint types discussed in the previous section. Refer Appendix F for the detailed report. Note that the other fixed variables were kept constant across all the simulations to understand the impact of varying just one fixed variable.

4.4.1 Effect of varying N

As N is increased, in steps of 1 from 3*3 panel to 8*8 panel, the peak height of the absorption curve drops for all constraint types. In the simulations for the different HR lengths type, it starts as an equally spaced out curve for $N = 3$ but becomes uneven for higher values of N. As N increases, the DE would have to provide geometrical values to more number of resonators, and hence it would need an increased number of generations to reach an optimal solution. The same reasoning is valid for the No constraint type. There is no conceivable pattern in the absorption graphs because of prematurely terminating the optimization.

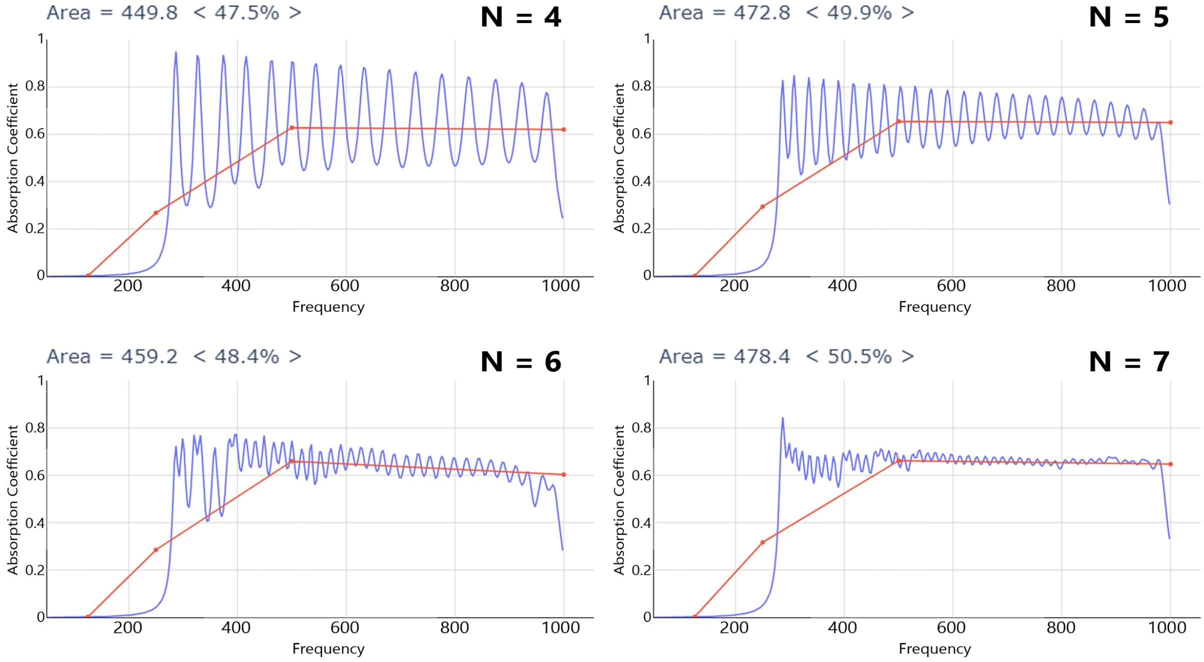

Figure 24: *Impact of varying N on the absorption performance using the Constant neck length type*

Constant neck length type shows consistent results with increasing N, even though the number of generations in the simulations are the same. There is equal spacing between the resonant frequencies. In the Constant HR length type, the resonant frequencies are clumped together within a certain bandwidth, because the search space is very constrained to be able to produce resonators beyond that bandwidth limit. An arching pattern is evident as N increases, again because of overly constraining the search space.

4.4.2 Effect of varying spacing

Increasing the spacing reduces the panel's absorption performance. This trend can be attributed to the coupling effect, which decreases with increasing distance between the resonators. There is a good agreement between the graphs of the Different HR lengths type and the Constant neck length type. Unlike the previous case, changing the spacing does not affect the scope of the search space. Hence, optimal results were attained in both the types within the specified generation count. Another visible trend is that the curves shift towards the lower frequencies as the spacing increases. The cavity size could be expanded because of increased distances between the resonators, and hence opens up the possibility for low-frequency resonators. Again, in the No constraint type, the simulation is terminated prematurely causing the graph to be haphazard. In the Constant HR lengths type, over-constraining has caused the solver to not find resonators beyond a certain bandwidth.

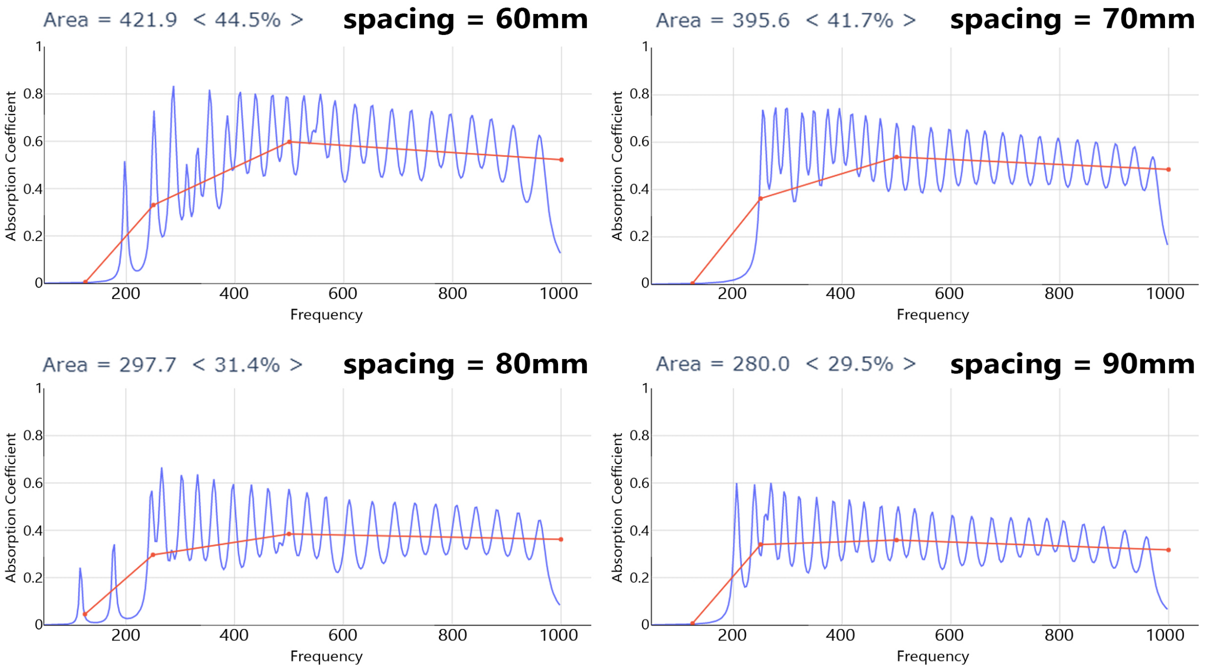

Figure 25: *Impact of varying spacing on the absorption performance using the Different HR lengths type*

4.4.3 Effect of varying panel depth

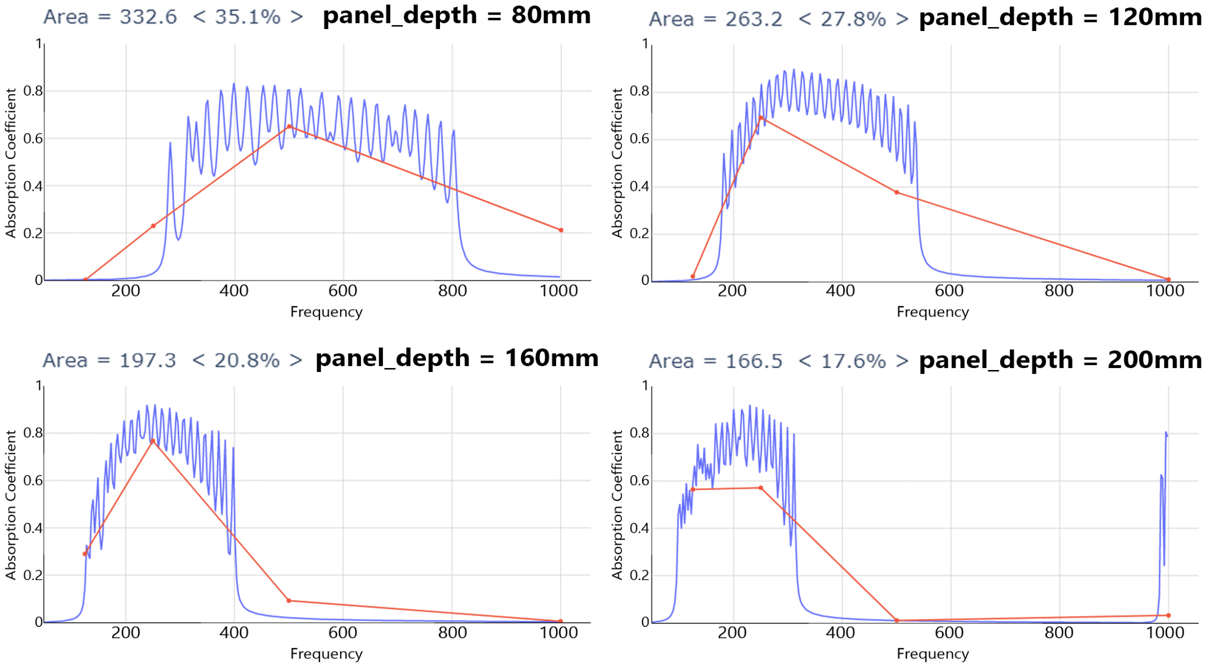

Figure 26: *Impact of varying panel depth on the absorption performance using the Constant HR length type*

Varying the panel depth does not affect the performance peak of the panels. There is a consistent pattern in all the types, except the No constraint type. Increasing the panel depth does not affect the area under the curve but it shifts the curve towards the lower frequencies. This is because a deeper panel allows for longer resonators that can absorb sound in the lower frequencies. In the Constant neck length type the troughs drop with increasing panel depth, because it tries to maintain equal spacing (between a fixed number of resonant frequencies), while the bandwidth of absorption increases. In the Constant HR lengths type the bandwidth of absorption gets narrower and moves toward the lower frequencies. To maintain a constant HR length the resonators were elongated to reach the bottom surface plate, and such long resonators do not have their resonant frequencies in the mid-high ranges.

4.4.4 Effect of varying *n_rad*

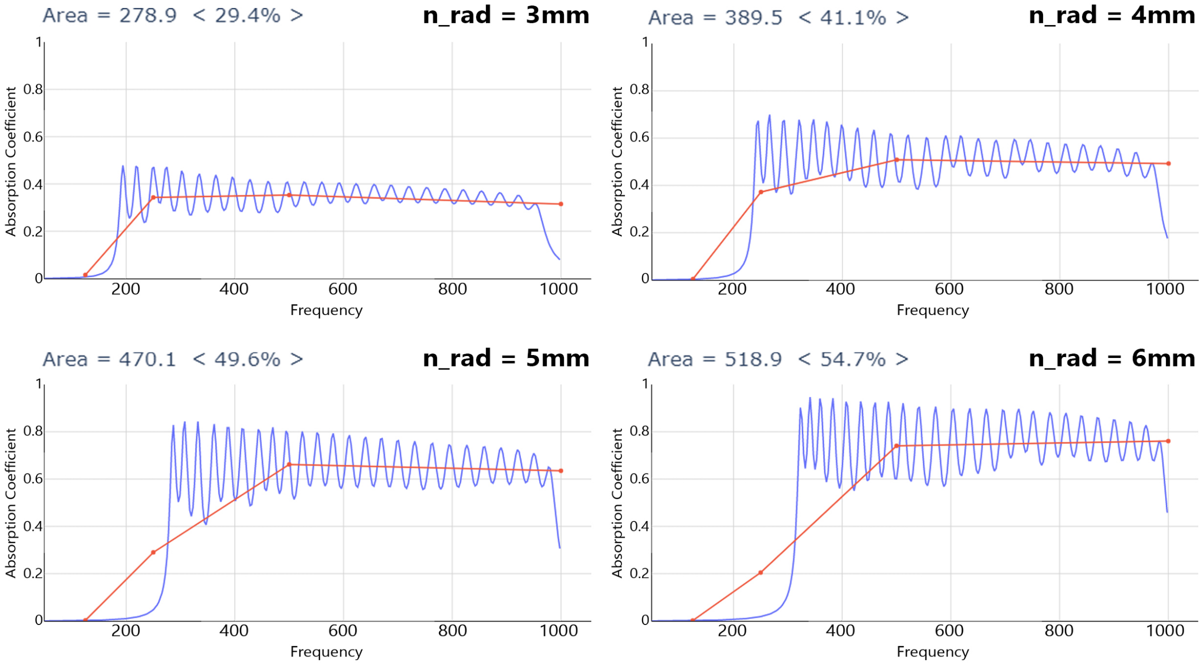

Figure 27: *Impact of varying n_rad on the absorption performance using the Constant neck length type*

Increasing *n_rad* improves the absorption performance of all the panel types. This trend suggests that the mutual impedance increases with the neck radius as it will have a larger area to act on. All the panel types, except the No constraint type, exhibit a shift towards the higher frequencies. The neck area is directly proportional to the resonant frequency. Thus, increasing the neck size shifts their resonant frequencies higher. Another trend is that the curves get noisier as n_rad increases, i.e. the bandwidth of an individual resonator's performance reduces. This can be understood by analyzing the viscous losses in the neck - it reduces with increasing neck size.

The No constraint type does not produce optimal results within the specified 300 generations whose DE simulation takes at least 100 minutes. Striking the right balance between the scope of the search space and the computation time is necessary to achieve quality results. Over-constrained search space (Constant HR length type) tampers with the results, while under-constraining it (No constraint type) requires a longer computation time to reach optimal results. Constant neck length type has consistent results, and strikes the right balance between the search space constraints and the computation time.

4.4.5 Distribution of resonators in the array

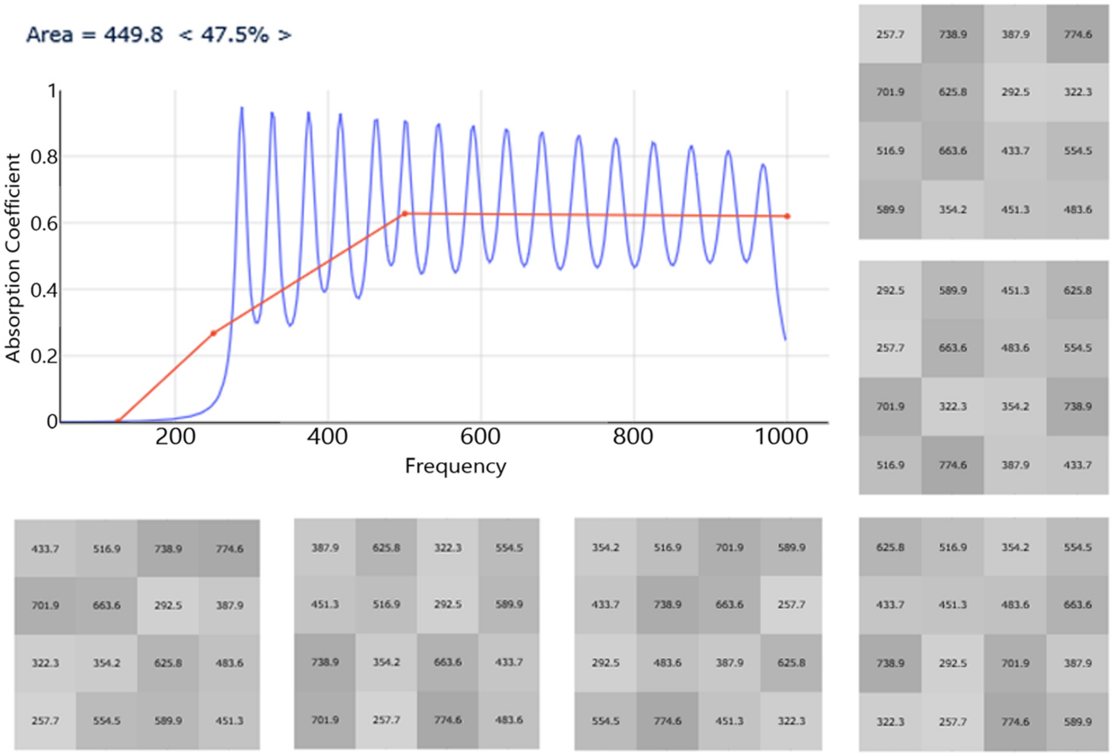

257.7	738.9	387.9	774.6
701.9	625.8	292.5	322.3
516.9	663.6	433.7	554.5
589.9	354.2	451.3	483.6

292.5	589.9	451.3	625.8
257.7	663.6	483.6	554.5
701.9	322.3	354.2	738.9
516.9	774.6	387.9	433.7

433.7	516.9	738.9	774.6
701.9	663.6	292.5	387.9
322.3	354.2	625.8	483.6
257.7	554.5	589.9	451.3

387.9	625.8	322.3	554.5
451.3	516.9	292.5	589.9
738.9	354.2	663.6	433.7
701.9	257.7	774.6	483.6

354.2	516.9	701.9	589.9
433.7	738.9	663.6	257.7
292.5	483.6	387.9	625.8
554.5	774.6	451.3	322.3

625.8	516.9	354.2	554.5
433.7	451.3	483.6	663.6
738.9	292.5	701.9	387.9
322.3	257.7	774.6	589.9

Figure 28: *Different arrangements of the same set of resonators produce the same absorption graph*

The arrangement of the resonators associated with the optimal results produced by the constant neck length panel type did not show a discernible pattern. For the same set of resonators, the panel's absorption performance was calculated for different arrangements of these resonators along the surface of the panel. They all produced the same results (refer figure 28). The only element that changes in these different arrangements is the relative location of the resonant frequencies. Though this should have had an impact on Z_{mut}, it didn't because Z_{mut} only accounts for the neck sizes which are maintained constant. Hence, the total impedance of the panel remains the same for different distributions.

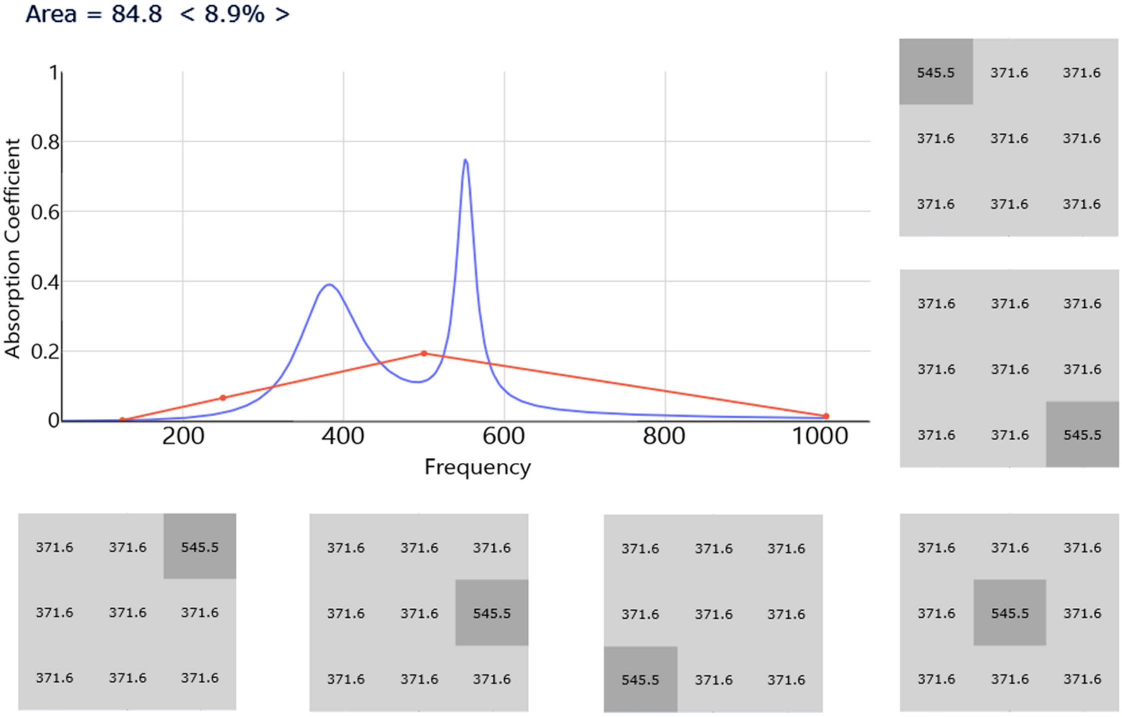

545.5	371.6	371.6
371.6	371.6	371.6
371.6	371.6	371.6

371.6	371.6	371.6
371.6	371.6	371.6
371.6	371.6	545.5

371.6	371.6	545.5
371.6	371.6	371.6
371.6	371.6	371.6

371.6	371.6	371.6
371.6	371.6	545.5
371.6	371.6	371.6

371.6	371.6	371.6
371.6	371.6	371.6
545.5	371.6	371.6

371.6	371.6	371.6
371.6	545.5	371.6
371.6	371.6	371.6

Figure 29: *Different arrangements between identical resonators and one resonator with a larger neck radius produce the same absorption graph*

The same study was repeated with identical resonators and one deviant resonator with a larger neck radius. All the arrangements produced the same absorption graph even though the deviant neck radius changes is relative location. The formula for calculating Z_{mut} does not account for this relative positioning of the resonant frequencies. This is an implicit drawback with the radiation impedance method (Kim 2010). In fact, none of the other analytical methods account for the relative positions of the resonators.

4.5 Approach 2 - Semi-automated resonator array design

Running the DE solver might be difficult for certain users, and it is also a time-consuming process. Hence, a simpler method that requires minimum input from the users was engaged for designing an optimal performing panel. In this semi-automated approach, the frequency bandwidth of the panel's performance and the panel's depth are the variables that control the panel's design. From the first set of inputs from the user - the frequency bandwidth and the distance between the resonant peaks - a set of target resonant frequencies are generated. From the next set of inputs from the user - the panel depth, the neck length, and the panel type - the resonator geometrical constraints are generated. Now, for each target resonant frequency in the set, the algorithm looks for possible resonator geometry combinations, within the geometrical constraints, that can achieve that target resonant frequency. This algorithm is based on the brute-force search which analyzes all possible combinations. Though multiple resonator constructs can have the same resonant frequency, the algorithm chooses the one that maximizes the peak absorption performance. These resonators are arranged randomly in the panel since the radiation impedance method does not factor in the distribution pattern of the resonators. A flow-chart of this algorithm in given in Appendix H along with a brief explanation of the design interface. Figure 105 shows the absorption performance of an optimal panel from a given set of inputs.

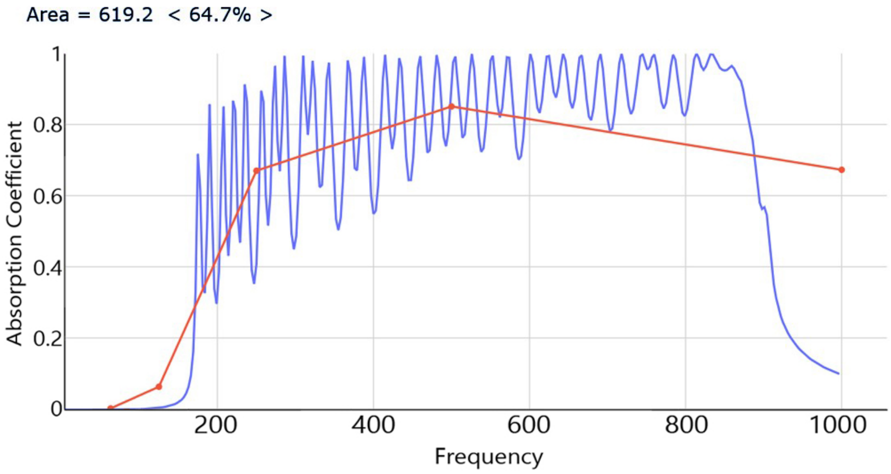

Figure 30: *Results without additional neck resistance*

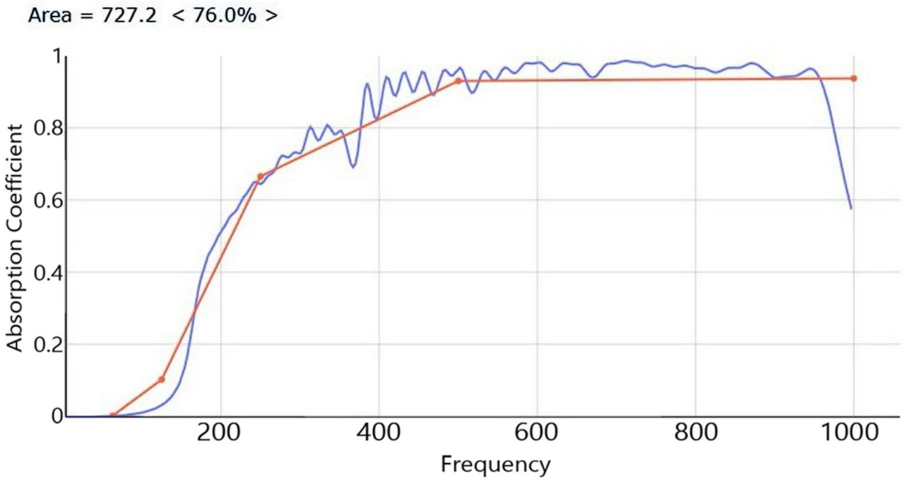

Figure 31: *Results with additional neck resistance*

4.5.1 Enhancing the performance of the panel using additional resistance

The result achieved in figure 105 has prominent valleys in between the resonant peaks. The absorption curve could be evened out using additional resistance in the neck, as discussed in section 3.4. Figure 31 shows the improvement in the absorption performance of the panel after adding neck perforations. Additional resistance improves the peak absorption value and the bandwidth of absorption. Hence, the resonant peaks merge into one another without deeper valleys.

4.6 Using the achieved absorption curve

The absorption coefficients of the panel obtained from Kim's formulas are for the entire frequency range. The blue line in the graph in figure 31 shows the frequency-dependant absorption coefficients. This cannot be directly used in geometric acoustic simulation software; they require the values in octave bands. Octave filter is used for converting the frequency-dependent values to octaves-dependant that can be used in Pachyderm Acoustics for room simulation. The formula for the Octave filter,

$$\sum_{i=F_l}^{F_h} (freq_{i+1} - freq_i) * \left|\frac{\alpha_{i+1} + \alpha_i}{2}\right| / (F_h - F_l) \tag{4.17}$$

where F_h is the higher end of frequency bandwidth and F_l is the lower end of the frequency bandwidth.

This filter produces 8 discrete absorption coefficients, one for each octave band. The octave bands are depicted by their center frequencies - 63Hz, 125Hz, 250Hz, 500Hz, 1000Hz, 2000Hz, 4000Hz, and 8000Hz. The red line in the graph in figure 31 shows the octave filtered absorption values. These values are used to describe the absorption performance of a material in the acoustics software.

4.7 Example panel studies

The advantage of the resonator panel design is that it can be customized to any frequency range. For example, to attenuate the excess noise in an engine room, a broadband absorber is not required but rather a targeted absorber. Figure 32 shows the absorption performance of a panel composed of low-frequency resonators. With just 14 resonators, the absorption coefficient achieved is good in octaves 63Hz, 125Hz, and 250Hz. However, this panel is quite bulky–the panel size of about 0.3m x 0.35m and its depth is 0.16m. The resonators have a constant neck opening of 0.02m and resonator spacing of 0.1m. All the resonators have neck perforations, and three out of those have embedded necks to lower the resonant frequencies to below 100Hz.

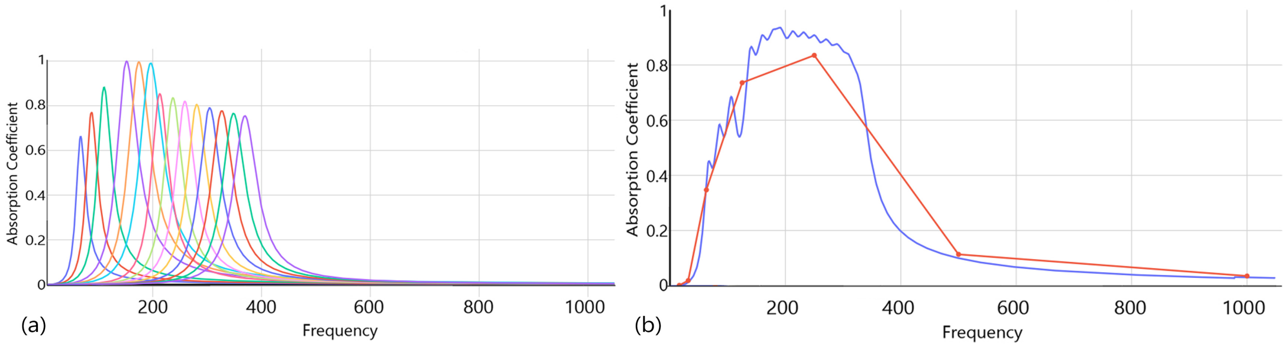

Figure 32: *Low-frequency panel: (a) Absorption performance of the individual resonators in the panel; (b) Absorption performance of the panel*

Another panel design for the mid frequencies is given in figure 33. This panel's dimensions are similar to the low-frequency panel, i.e. the area is 0.3m x 0.3m and the depth is 0.16m. However, due to the smaller size of the resonators required for attenuating mid frequencies, 36 resonators can be fit within this panel. These resonators have a neck opening of 0.01m and resonator spacing of 0.05m. This panel's performance is improved with the use of neck perforations which produces good results in octaves 250Hz, 500Hz, and 1000Hz.

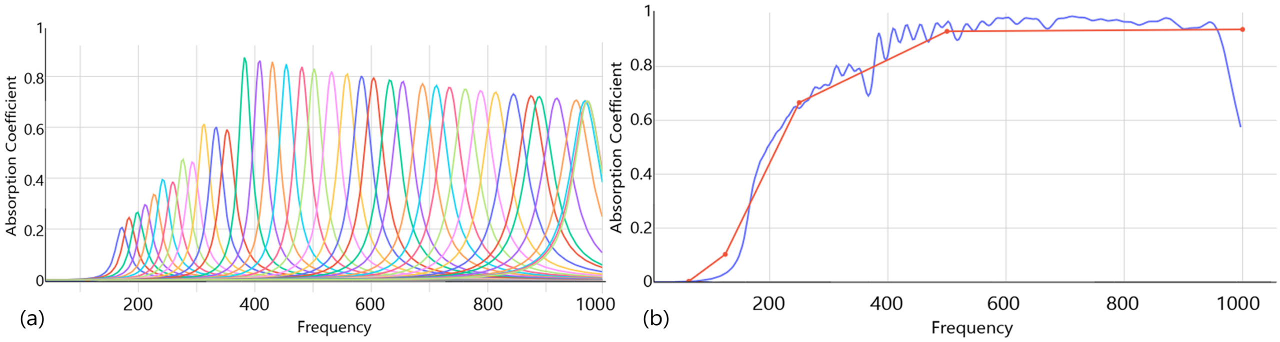

Figure 33: *Mid frequency panel: (a) Absorption performance of the individual resonators in the panel; (b) Absorption performance of the panel*

The absorption performances given do not factor in the material properties of the panel. In reality, this would further increase the absorption quality of the panel. Low-density MDF or plywood have adequate absorption in frequencies above 1000Hz, and can positively impact the overall performance of the resonator panel. Thus, the choice of material can boost the absorption bandwidth of the panel.

5 Open office acoustics

Open office acoustics have been a source of discomfort to the employees. The acoustic conditions have an impact on the psychological and physiological well-being of the employees (Ebissou et al. 2015). Most of the acoustic complaints are related to speech intelligibility and speech privacy in open offices (Delle Macchie et al. 2018). The low partitions and the hard reflective wall surfaces bounce the speech sounds around, causing distraction to the other employees. Two solutions are currently practiced in tackling this problem - sound absorption and sound masking. Sound absorption is a passive technique and can be integrated within office furnishings. Sound masking is an active technique and requires loudspeakers to be installed in the ceiling. Both the techniques are usually implemented to improve the open office acoustics (Bradley 2004, Keränen et al. 2008).

This research focuses on utilizing passive techniques in improving the open office acoustics. Instead of absorbing all the sound energy in the space and overlaying it with a masking sound, the prevalent background noise could help in masking the adverse effects of the irrelevant speech in open offices. The impact of a source speaker could be reduced by hindering the direct sound propagation and by minimizing its intensity through absorption. Frequency-specific sound absorbers, especially targeting the speech frequencies, can greatly lower the intensity of the conversational sounds. This softer speech signal overlaid by the background noise from ventilation or hardware systems would be less detrimental to the work performance of other employees (Schlittmeier & Liebl 2015).

The sample panel described in the previous section was designed specifically for attenuating frequencies important for speech intelligibility. Introducing too much absorption in the space can make it very quiet and even a small disturbance can cause a distraction to a large number of employees. Hence, it is important to optimize the number of absorptive surfaces and their locations to maximize the acoustic quality. The knowledge of the optimal location could be derived from studying the nature of sound propagation in open offices. Placing the absorbers close to the sound source has proven to be fruitful (Fuchs 2013).

5.1 Sound and its propagation

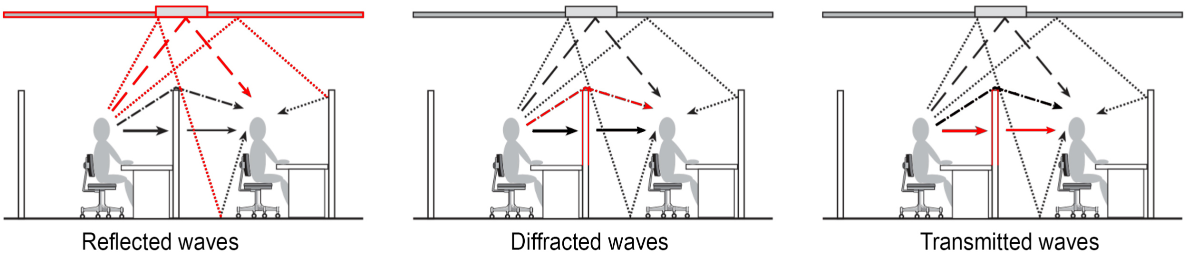

Figure 34: Types of sound propagation in open offices

Sound propagation from one workstation to another is facilitated through reflection, diffraction, and transmission of the sound waves (see figure 34). First-order reflections are usually from the ceiling while second-order reflections could be from any surrounding surfaces. Reflected sound waves travel longer distances, compared to diffracted or transmitted waves. Diffraction, or bending, of sound waves happens around the edges of the partition separating the two workstations. Transmitted waves pass through the partition wall, and travel the least distance to reach the next workstation. Diffracted and transmitted waves contribute most to the annoyance caused by a co-worker (Wang & Bradley 2002).

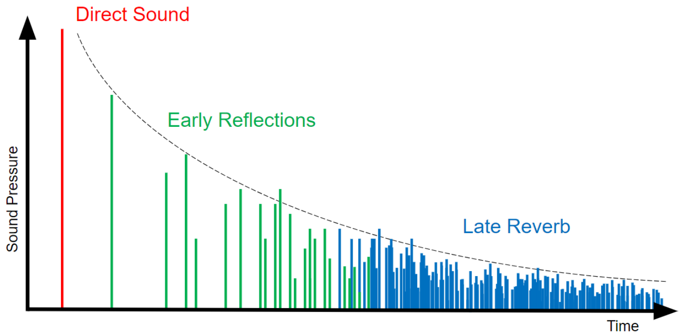

Figure 35: *Energy of sound and its reflections*

Each type of sound propagation contributes to different amounts of sound energy deposited at a receiver's location. Direct and diffracted waves are the first ones to be heard and they contain the maximum amount of sound energy due to traveling shorter distances. First and second-order reflections reach next, and they have reduced energy levels due to absorption by hard surfaces. Other orders of reflection have diminished energy, and could be heard as echoes if they are loud enough. The energy levels of direct sound and its reflections reaching a receiver's location is given in figure 35.

5.2 Single-number acoustic parameters for open offices

Parameters to measure the loudness of sound (SPL) or the speech intelligibility (STI) are spatial, i.e. they are dependant on the location of the speaker and the receiver in a space. Hence, they cannot be used to evaluate the acoustics of open offices where the speaker(s) and receiver(s) could be anywhere in the room (Schlittmeier & Liebl 2015). ISO standards for open offices (ISO 3382-3 2012) gives four single-number parameters to measure the acoustic quality of an open-plan office. Distraction distance (r_D) is the radius from the speaker up to which people in that zone are easily distracted by his (or her) speech sounds. It is derived from the spatial decay of the STI values; r_D is the distance at which the STI value falls below 0.5. The spatial decay rate of A-weighted SPL of speech ($D_{2,S}$) is the rate at which the intensity of speech decreases when the distance is doubled. It is extrapolated from A-weighted SPL values measured at different locations in the open-plan. The third parameter is A-weighted SPL of speech at 4m from the source ($L_{p,A,S,4m}$). It is a straightforward measurement but is not necessarily measured first-hand. It can be obtained from a linear regression of A-weighted SPL values measured at various positions. The last parameter is the average A-weighted background noise level ($L_{p,A,B}$). Though this parameter is time-dependant, an averaged quantity helps to estimate the masking of the intruding speech sounds.

Of the four parameters, r_D has the most direct correlation with the intrusion caused by speech sounds in open offices (Haapakangas et al. 2017). It's based on STI which factors in the masking effect of background noise through signal-to-noise ratio estimation. While $D_{2,S}$ and $L_{p,A,S,4m}$ depend on physical room parameters, such as the amount of absorption included in the room, ceiling height, shape of the room, its volume, and inclusion of partition screens (Haapakangas et al. 2017), they are not affected by the background noise level which plays a major role in the speech intelligibility (Keränen et al. 2008). Though r_D seems to be a promising indicator of the office acoustics, it cannot be solely depended upon for measuring the acoustic quality of the space without considering $D_{2,S}$, $L_{p,A,S,4m}$, and $L_{p,A,B}$. Small r_D values (which are favorable) can be obtained with high levels of background noise. But, the acoustic comfort is poor with such high background noise. Hence, it is essential to consider all the four parameters while evaluating the acoustics of an open office.

The single-number parameters are simulated for one source speaker while the rest are silent receivers. This situation is considered to be the toughest to achieve good acoustics. For, if multiple people are talking at the same time, their combined sound would create a better masking effect over the individual signals and the distraction caused is minor (ISO 3382-3 2012). The ISO also specifies target values for these parameters to achieve good open office acoustics. To better understand the impact of these independent single-number parameters on acoustic comfort in the open office, this research introduces a spider plot to capture all the parameters along with their target values.

Table 1: *Target values of single-number parameters set by ISO*

Parameter	**Symbol**	**Target value**
Distraction distance	r_D	$\leq 5m$
Spatial decay rate	$D_{2,S}$	$\geq 7dB$
SPL(A) at 4m	$L_{p,A,S,4m}$	$\leq 48dB(A)$
Background noise level	$L_{p,A,B}$	35dB - 45dB
Reverberation time	RT˙60	0.7s - 0.8s

5.3 Room acoustics simulation

To study the open office acoustics, the geometry of the space is modeled in the Rhinoceros 3D software. Real objects, like workstations and storage, are represented by 2D Surfaces in the Rhino interface. Complex geometry is abstracted to have a manageable simulation time. Pachyderm Acoustics, a plugin for the Rhino software, is used for running the acoustic simulation. It provides additional properties to the 2D Rhino surfaces - absorption, scattering, and transparency coefficients in octave bands - to reproduce the real room characteristics. A variety of acoustical analysis can be run with a source and multiple receivers.

5.3.1 Office layouts

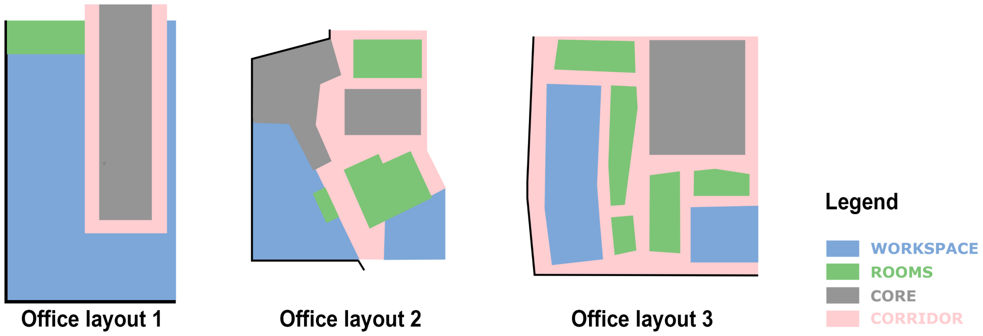

Figure 36: *Different open office layouts for simulation*

Three variants of open offices are studied to estimate the effectiveness of Helmholtz resonator panels. Figure 36 shows the layouts of the three case studies, which are modeled based on existing open offices in the USA (made anonymous). It might be computationally expensive to simulate the acoustics for the whole floor plate. Hence, a representative section of the floor plate is used for the room acoustic simulations.

The office layout 1 is a simple open-plan office with circulation around a central core and workstations organized perpendicular to the exterior face of the room. Meeting and conference rooms are organized together as a separator between rows of workstations and the common social areas - a clear buffer between noisy community space and a quiet work-space.

In the layout 2, the core is decentralized and they merge into the work-space and conference rooms. Since the core is typically used for vertical circulation, the foot traffic and movement around the work space is a lot more than in Layout 1. The buffer is provided in the form of floor height differences between the workstations and the central circulation zone.

Layout 3 is similar to layout 1, except that the work-space is decentralized and separated by groups of meeting, conference, and focus rooms. These rooms are used as a buffer between the common areas around the core and the quiet work-space.

Each type has a different background noise spectrum in the work-space area, the total area of vertical absorptive surfaces, and the workstation setup. Acoustic simulation of these layouts with and without the Helmholtz resonator panels was performed. The same was repeated with a generic ceiling tile to analyze the acoustical improvements delivered by the resonator panel.

5.3.2 Simulation models

Sound waves are vibrations in the air, characterized by frequency, amplitude (or intensity), and phase. And these waves propagate spherically from a point source. It is a computationally expensive process to apply these physics in digital simulation. Instead, these waves are substituted by sound rays that travel in a straight line and carry a fraction of the source's sound energy (Kuttruff 2016, Vorländer 2007). This is the ray-tracing model. From a point source, a specified number of sound rays are projected out in every direction, and they travel in a straight path until they hit objects or surfaces in the digital model. At this intersection, a part of the energy carried by the rays is lost to the geometry based on its absorptive properties. Depending on whether it is a diffusive or a reflective geometry surface, the direction and the number of reflected rays are altered (refer figure 37). After several reflections, the rays will lose their energy and the simulation is concluded. The SPL at receiver locations is calculated by adding the energies of the sound rays that intersect with the receiver's sphere.

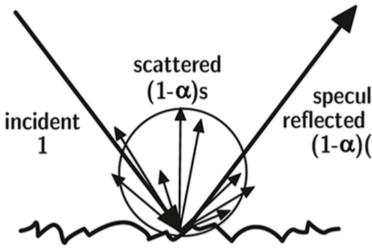

Figure 37: *Specular and diffuse reflection from a surface (Vorländer 2007)*

In the ray-tracing model, the simplification of the sound waves to sound rays also resulted in losing valuable information on the frequency and phase angle of the sound. Without these details, sound properties like edge diffraction and sound interference cannot be replicated in the digital simulation. These are the important properties of sound, which may either increase or decrease the SPL at various locations in the room. However, digital simulation is an approximation of the acoustical condition in a room. If the size of the room is large compared to the wavelength of sound, these approximations correspond to the acoustics observed in the physical room (Kuttruff 2016). This is true only if the space is completely diffuse, otherwise not accounting for room modes might tamper with the acoustic results. Those frequencies below the Schroeder frequency can cause standing waves in the room, which are unaccounted in the digital simulations due to the lack of sound wave properties.

Pachyderm Acoustics, which is used for the room acoustic simulation in this research, uses two simulation models - ray tracing and image source. In the image source model, the specular reflections from a surface are estimated by mirroring the source along the plane of the intersecting geometry. The mirrored source then shoots rays through the intersection points on the geometrical surface (refer figure 38). These rays are the reflected rays. This process is fast and efficient for early sound reflections. It is continued for a certain number of times, and the SPL at the receiver is calculated by backtracking the rays from the image sources back to the original source. By summing up the distances traveled by these rays, its total energy can be calculated using the inverse-square law. The main drawback of using the image source model is that diffusive scattering at the wall surfaces cannot be modeled (Kuttruff 2016).

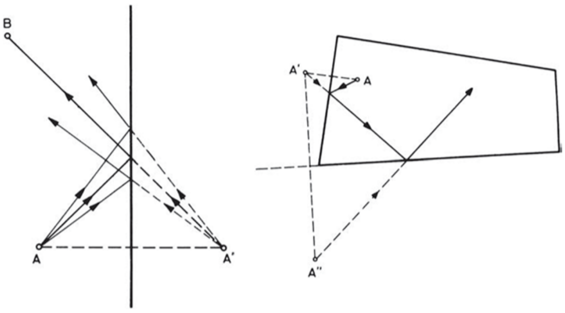

Figure 38: *Image source model for specular reflections (Kuttruff 2016)*

5.3.3 Consistency check

The same room model with absorptive surfaces was run a couple of times on Pachyderm Acoustics in Rhino 3D to check for its consistency. The results produced each time were exactly the same, which are overlaid on one another for the purpose of comparison (refer figure 39).

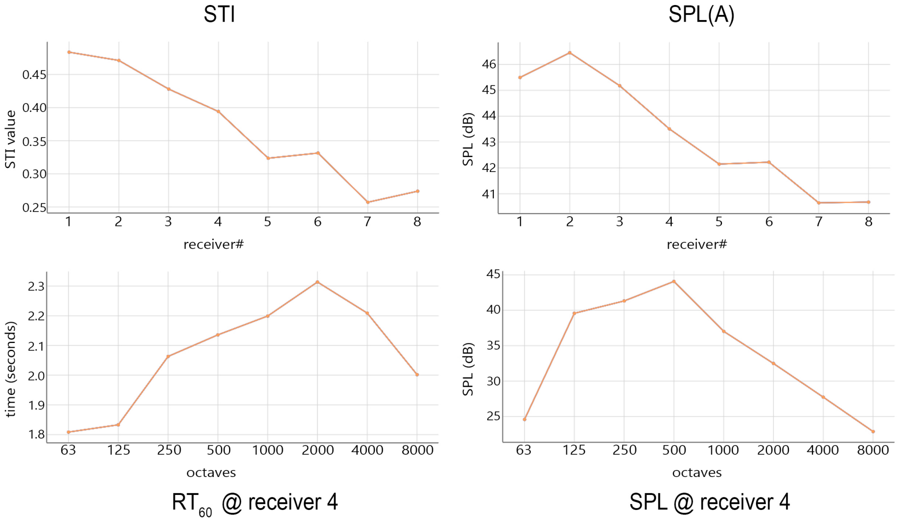
STI

SPL(A)

RT_{60} @ receiver 4

SPL @ receiver 4

Figure 39: *Consistency check for Pachyderm Acoustics*

5.3.4 Effect of ray count on the simulation results

Pachyderm provides three options of specifying the number of rays to be used in a simulation. A good number of rays is required to produce accurate results. The same room model with absorptive surfaces was run a couple of times, but with different ray count options (minimum convergence and detailed convergence). Eight simulations with specified ray count setting within the range of 50k rays to 140k rays were run. All acoustical parameters, except the Reverberation Time (RT_{60}), agree well with each other. The overlaid graphs of the results from different ray count settings are shown in figure 40.

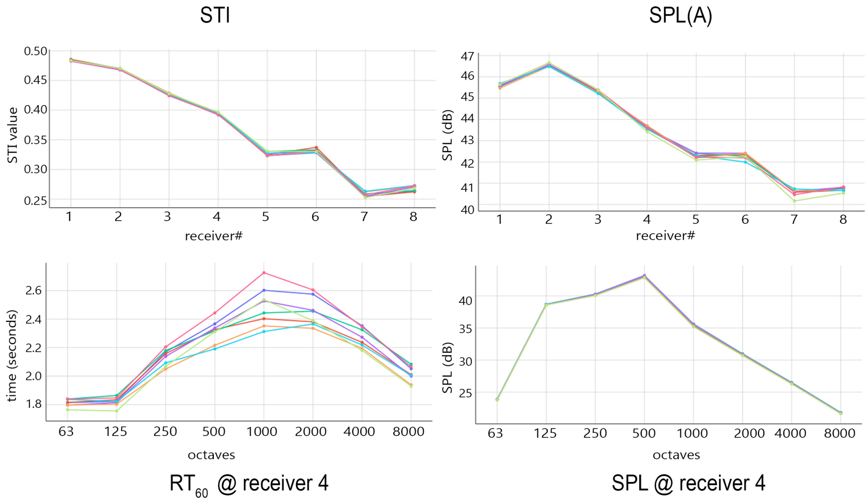
STI

SPL(A)

RT_{60} @ receiver 4

SPL @ receiver 4

Figure 40: *Effect of ray count on the simulation results*

5.4 Study methodology

To study the impact of the Helmholtz resonator panel (HR panel) on the open office acoustics, a simple office layout (figure 41) was modeled which is roughly based on case study 1 layout. It is a rectangular layout of 16m x 33.5m with a ceiling height of 3.2m and has a single main corridor that connects the workstations to the central circulation zone. Each workstation is L-shaped (dimension 2.6m x 2.4m), and groups of eight workstations make a bay. The bays are arranged parallel to each other with a 1.4m walkway.

The measurement of the acoustical quality is carried out as per the ISO standards. Two lines of measurement that overlap with the seating positions, as specified in figure 41(b), are used for simulating the acoustic condition of this layout. The position of the sound source is at the intersection of the two lines, and all the other dots are receivers. The source, a geodesic omnidirectional source, is defined with a speech power level in octave bands for normal effort speech as specified in ISO (ISO 3382-3 2012). The receiver positions have microphones for recording the impact of the source speaker at that respective location. The source and the microphones are placed at 1.2m from the floor level to mimic seated workers.

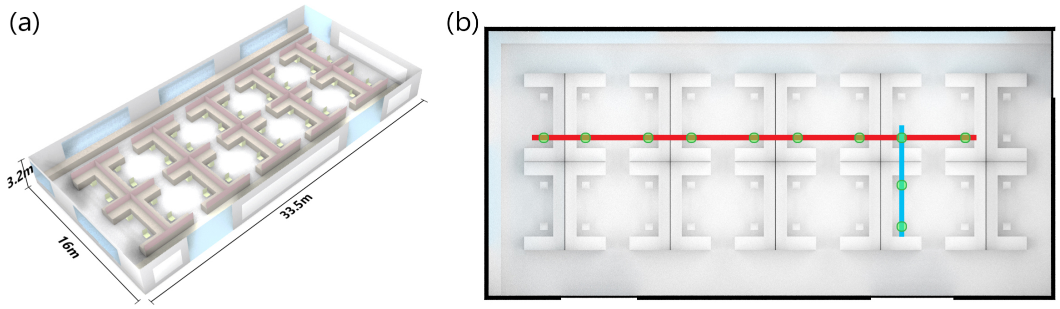

Figure 41: *(a) View of the simple layout; (b) Plan overlaid with the two lines of measurement*

The next sections would discuss the variable parameters in the study of open office acoustics. To study the influence of the number of absorptive surfaces in achieving good acoustics, a series of increasing area of HR panel distributions are designed. To optimally locate the panel in the open offices, their heights are varied in increments 0.2m from the floor level. Varying these parameters produces different acoustic environments in the office layout but to choose the optimal one, multi-objective sorting is used. In all the acoustic simulations, a background noise level is applied to imitate real office conditions. However, the results produced with the geometrical acoustic simulation might not be the exact representation of the real office conditions. The furnishing or building elements used in the office model are abstracted, and the inherent nature of the sound waves in the simulation is simplified for a practical run-time. Hence, the results derived from the studies given in the next section are for observing the trends to achieve good open office acoustics.

5.4.1 Background noise levels

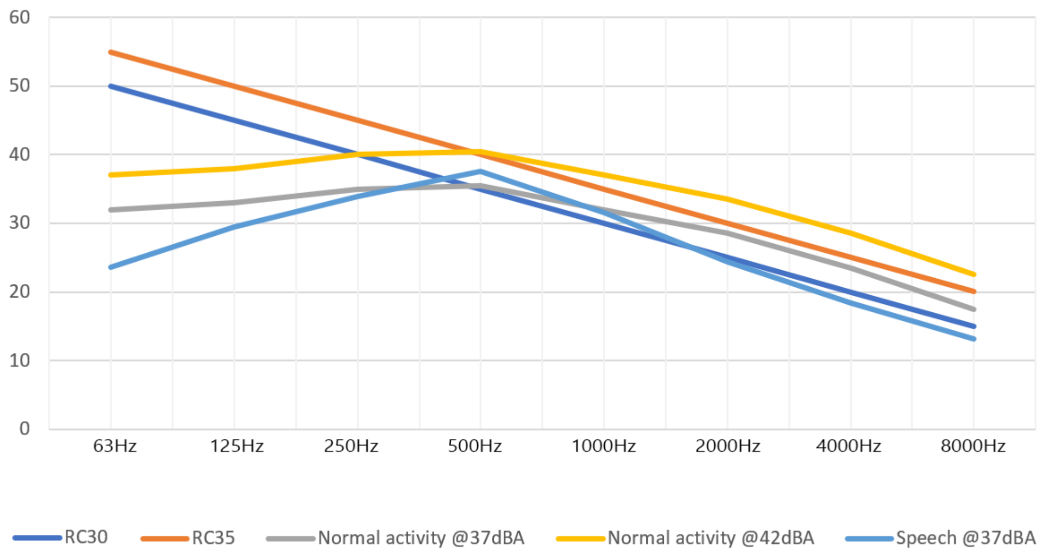

Figure 42: *Background noise levels used in the open office simulations*

Speech intelligibility in open offices is measured using STI, which factors in the useful signal to the background noise ratio. To achieve good acoustics that does not interfere with the employee's work productivity the STI value has to be maintained within 0.2 (refer figure 5). Higher levels of background noise can achieve this value but ISO sets the acceptable range to be within 35dBA - 45dBA. Hence, background noise levels of 37dBA and 42dBA were used for acoustic studies.

Room Criteria (RC) noise curves provide a range of allowable background noise levels in a room. It is specifically used for modeling the HVAC systems in a space. RC30 and RC35 curves corresponding to 37dBA and 42dBA are used for reproducing background noise from air vents in the open office simulation. Background noise levels measured in the presence of normal human activity, given in the report by (Nilsson & Hellström 2010), were also used in the studies. Finally, the speech signal (taken from (Rindel 2018)) was used as background noise to simulate multiple speakers in the open office.

5.4.2 Panel distribution in the open office

To study the influence of the number of absorptive surfaces in achieving good acoustics, a series of instances with an increasing number of ceiling-hung HR panels were introduced. The combined area of the panels in each instance is expressed as a percentage of the workstation area. The nine variations had a uniform arrangement of panels around each workstation, maximizing the mitigation of the reflected sound waves between the workstations (see figure 43).

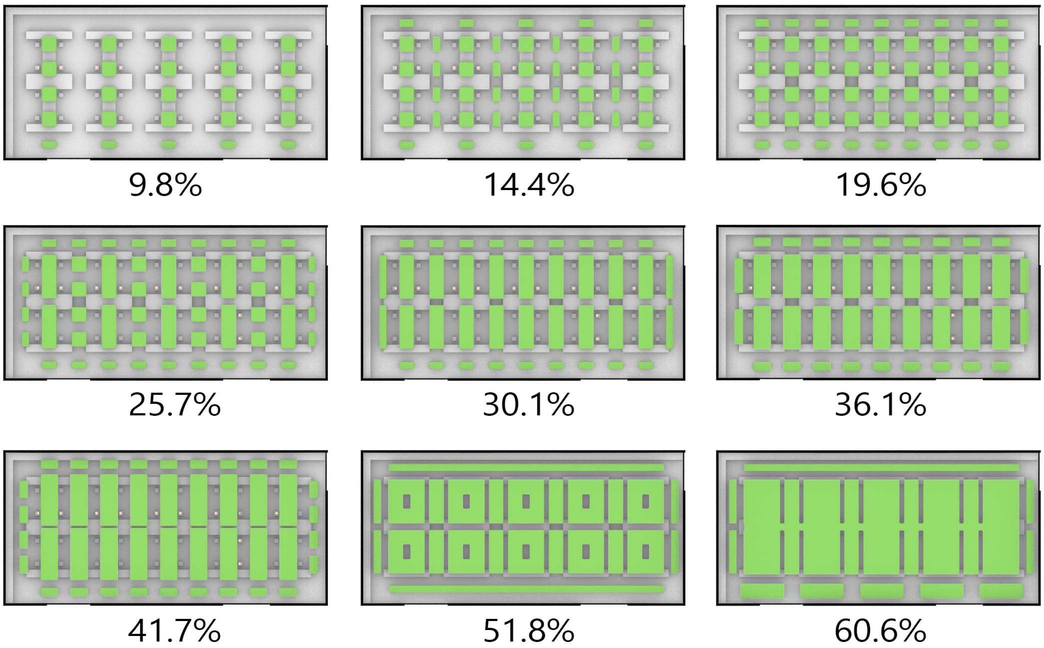

Figure 43: *Arrangement of ceiling-hung panels in each instance*

5.4.3 Panel heights

To optimally locate the panels in the open office, the heights of the ceiling-hung panels were varied from 2.1m to 3.1m in increments of 0.2m, while keeping the ceiling height fixed. The height of the panels impacts the amount of direct sound energy reaching the panels (based on solid angles) and the early reflection time of the speech sound. When the panels are closer to the source speaker, a large portion of the speech energy reaches the panels, than when the panels are farthest from the speaker. Low-hung panels reduce the travel distance of the reflected sound waves, and hence reduce the early reflection time at the receiver's location. This reduces the reverberation time as well since early reflections are the largest contributors in the measurement.

5.4.4 Multi-objective problem

There is a direct correlation between the amount of absorption and the overall sound energy in the room (top graph in figure 44). Covering the whole ceiling area with absorptive panels can result in a quiet environment. However, this does not necessarily create an acoustically comfortable environment. Employees prefer to work in the presence of ambient noise which is not too loud, since it helps mask the intruding speech signals. This essence is captured by the distraction distance parameter. Hence, r_D does not exhibit a linear relationship with the number of absorptive surfaces introduced. With an increasing area of absorptive surfaces the excess sound energy in the space decreases, which lowers the r_D. The r_D dips when it reaches the balanced ambient noise level. This is the optimal amount of absorption, since further increasing the area of absorption starts to increase the r_D (bottom graph in figure 44).

To strike the right balance in achieving good acoustics, the number of absorptive panels introduced in the space will have to be modulated with r_D and $D_{2,S}$. The spatial decay, $D_{2,S}$, controls how much of the originating sound energy gets dissipated with distance doubling. A large $D_{2,S}$ value results in a smaller overall sound energy in the room. The aim is to minimize the r_D and maximize the $D_{2,S}$ to achieve acoustic comfort in the open office. But $D_{2,S}$ cannot be maximized without degrading the r_D and vice versa. Hence, multi-objective analysis was utilized for the balancing act of finding the optimal amount of absorption that maximizes the $D_{2,S}$, but it also minimizes the r_D.

The multi-objective analysis used for this parametric study is Pareto sorting. It produces a set of optimal solutions, called Pareto Frontier, for two or more fitness functions in which each Frontier solution "dominates" the other solutions (Deb 2001). A solution is Pareto Frontier if it equals (or outperforms) another solution in all fitness functions and also outperforms it in at least one fitness function. The Frontier set has solutions that outperform each other in different fitness functions–the optimal solution set. Using the variable parameters (panel distribution and their heights) discussed in this section and the Pareto sorting, four studies are done to evaluate the optimal location and the efficiency of the HR panels in improving open office acoustics.

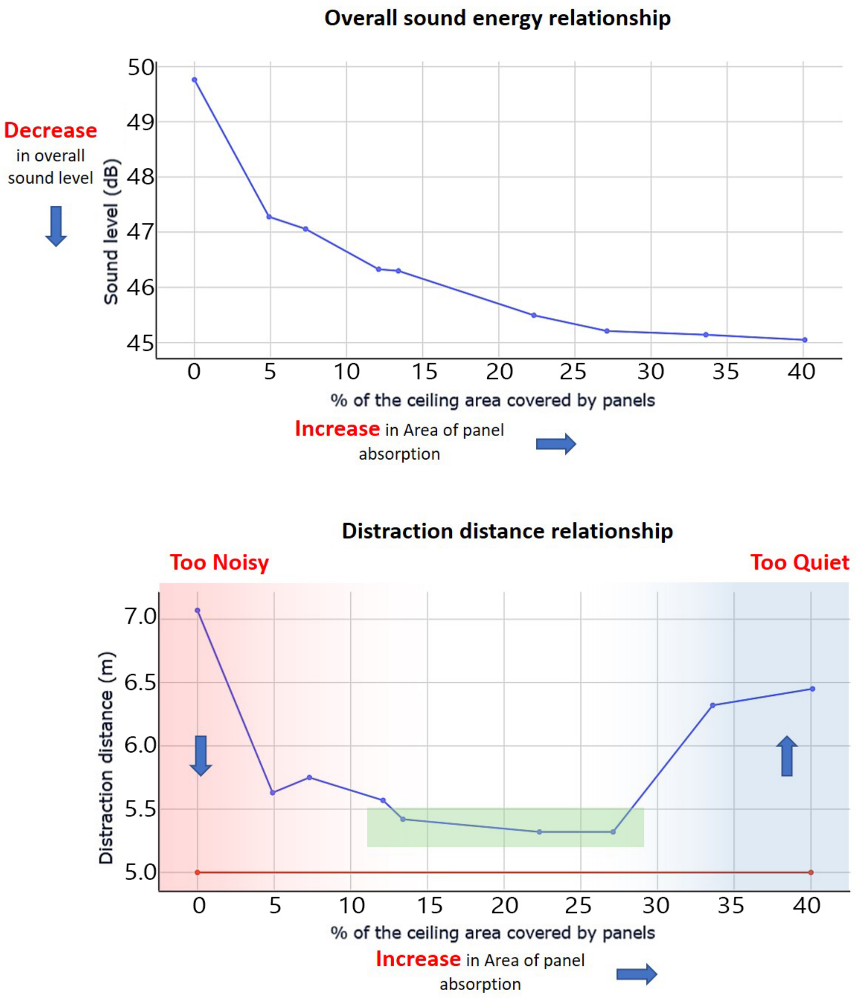

Figure 44: *(Top) Relationship between the amount of absorption and the overall sound energy; (Bottom) Relation between the amount of absorption and the distraction distance*

5.5 Study 1 - Efficiency of the HR panel

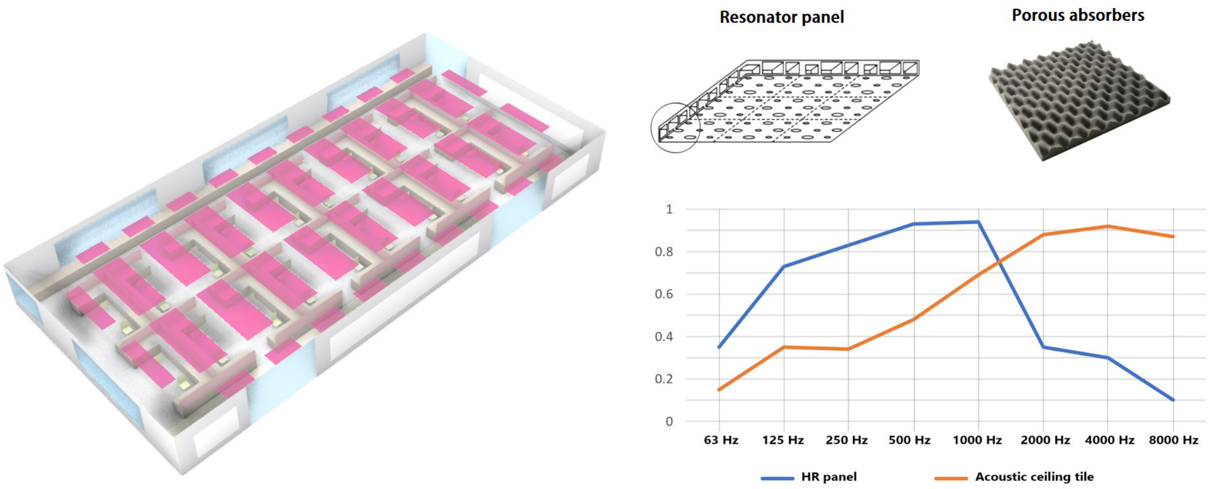

Figure 45: *(Left) Open office setup for comparing the efficiency of the resonator panels and the porous acoustic tiles; (Right) Absorption performance of the resonator panel and the porous ceiling tile*

This study was done to compare the efficiency of the commonly used porous absorber tiles and the designed resonator panel at improving the acoustics of the open office with a talking person. Both these panels are effective in different frequency ranges and this study is about finding which frequency range absorber is best suited to absorb the frequencies important for speech intelligibility. The simple office layout, as described in section 5.4, was furnished with 1.5m high desk partitions made of foamy infill with fabric encasing. Acoustic simulations were run for different ceiling-hung HR panel distributions (section 5.4.2) located at varying heights (section 5.4.3) from the floor level. Speech intelligibility (STI) was calculated using the background noise levels discussed in section 5.4.1. The results for all the single-number parameters are compiled into a matrix format - the *x-axis* representing the increasing area of ceiling-hung panels given as a percentage of the workstation area, the *y-axis* depicting the height from the floor level at which the panels were hung, and the colored boxes in the matrix are the values of the single-number parameter. The matrix of r_D measured in the presence of normal activity background noise at 37dBA and $D_{2,S}$ are presented in figures 46 and 47, respectively.

The matrix of r_D shows the fluctuating relationship with the amount of absorption introduced in the space (as highlighted in section 5.4.4). When no ceiling-hung absorbers are present (i.e. 0% column in the matrix), the background noise helps in masking the speech sounds at the receiver's location. When the HR panels are successively increased, the background noise level at the receiver's location is absorbed, which negatively impacts the r_D. Deviant cases are observed in the 2.1m and 3.1m rows in the matrix. In the 2.1m case, the panels are closer to the source. By the solid angle property, a larger portion of the source energy falls on the absorptive panels. Therefore, absorbing the speech sounds at its source benefits the r_D. In the 3.1m case, the distance traveled by the reflected sound waves to reach the receiver's location is large, which delays the early reflection time, and thus helps reduce the r_D. The negative trend in the r_D value with increasing area percentage of the HR panels reverses upon reaching a threshold. But the reversal point is different for each row (i.e. the heights of the panel from the floor level) in the matrix. This inconstancy is due to the different travel times of the reflected waves. Upon reversal, the r_D improves with increasing area percentage of the HR panels.

The trends observed in the $D_{2,S}$ matrix are quite straightforward, since $D_{2,S}$ only factors in the amount and the location of absorbers, and the room geometry. With increasing area percentage of the HR panels, the spatial decay improves. This improvement is more in the low panel heights (2.1m and 2.3m high panels). This trend is attributed to the solid angle property, i.e., a large portion of the sound energy from the source falls on the absorptive HR panels. Hence, a large number of absorbers placed closer to the source is an effectual strategy in boosting the $D_{2,S}$ value. Though the panels placed at 2.1m height from the floor level is desirable for better acoustics, it is shorter than the permissible ceiling height of 2286mm given in the International Building Code (IBC). However, sparsely spaced ceiling clouds at 2.1m height integrated with lighting fixtures or HVAC could be a design possibility.

	0.0%	9.8%	14.4%	19.6%	25.7%	30.1%	36.1%	41.7%	51.8%	60.6%
3.1m	5.2	5.1	5.1	5.3	5.1	5.3	5.1	5.2	4.5	3.8
2.9m	5.2	5.2	5.3	4.8	5.1	4.8	4.8	4.9	4.1	4.0
2.7m	5.2	5.2	5.8	5.3	5.2	5.4	5.1	5.1	3.8	4.3
2.5m	5.2	5.2	5.3	5.3	5.1	5.1	5.1	5.1	3.4	4.0
2.3m	5.2	5.1	5.4	5.5	5.4	5.5	5.1	5.3	3.2	3.9
2.1m	5.2	4.8	4.8	5.1	4.8	4.9	4.7	4.9	3.3	4.0

Figure 46: *Matrix of* r_D

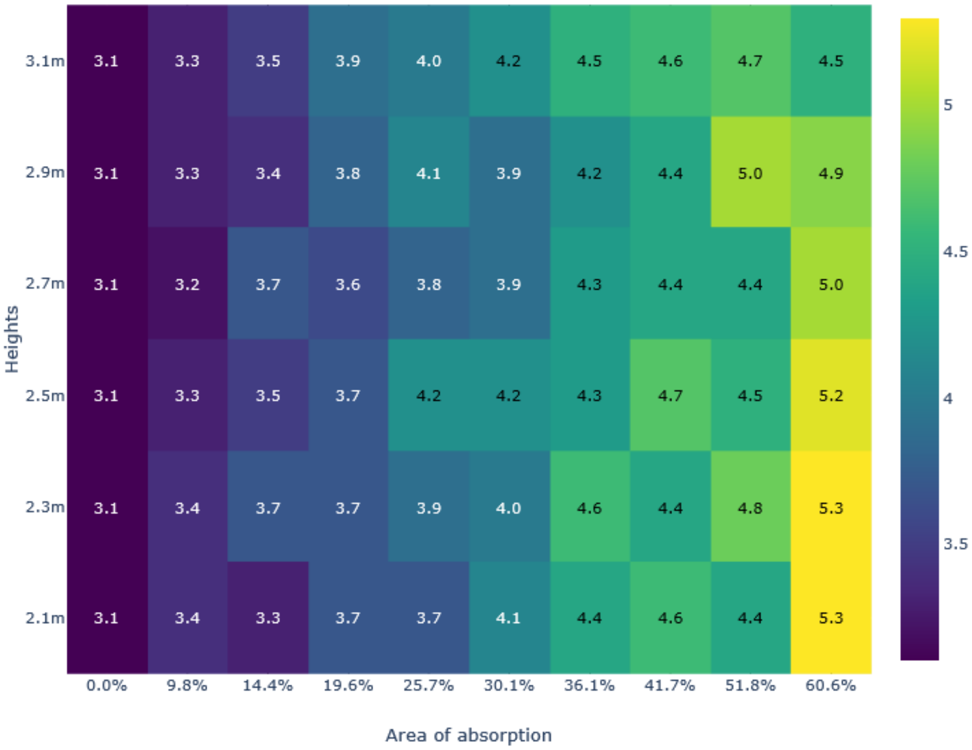

	0.0%	9.8%	14.4%	19.6%	25.7%	30.1%	36.1%	41.7%	51.8%	60.6%
3.1m	3.1	3.3	3.5	3.9	4.0	4.2	4.5	4.6	4.7	4.5
2.9m	3.1	3.3	3.4	3.8	4.1	3.9	4.2	4.4	5.0	4.9
2.7m	3.1	3.2	3.7	3.6	3.8	3.9	4.3	4.4	4.4	5.0
2.5m	3.1	3.3	3.5	3.7	4.2	4.2	4.3	4.7	4.5	5.2
2.3m	3.1	3.4	3.7	3.7	3.9	4.0	4.6	4.4	4.8	5.3
2.1m	3.1	3.4	3.3	3.7	3.7	4.1	4.4	4.6	4.4	5.3

Figure 47: *Matrix of* $D_{2,S}$

In both the matrices, some transitions across two immediate scenarios are substantial. For example, the r_D jump from 9.8% HR panels at 2.7m to r_D value at 14.4% and 19.6% panels at the same height form a sharp spike. Such inconsistencies seems likely to be a software error.

To gauge the efficiency of the HR panels, the same simulation was repeated with a traditional acoustic ceiling tile instead of the HR panel. Refer Appendix I for the full report of this study. The HR panel performs well in maintaining the reverberation time within the acceptable range in all the octave bands, since there is a good mix of low, mid, and high-frequency absorbers in the space. In the case of acoustic tiles, the reverberation time disproportionately deteriorates as the area percentage of the absorber increases, since the acoustic tiles have a substantial performance in the higher octaves. The acoustic tile does a better job of maintaining the r_D within the acceptable range in all the scenarios. Even with a 9.8% of acoustic tiles, the r_D in the presence of normal activity background noise @37dBA falls within the ISO's target value of 5m. However, in the case of HR panels, the r_D falls below 5m for 51.8% or more area percentage of the absorbers. This is because r_D is calculated from STI values which in turn is based on A-weighting standards that underestimate the annoyance caused by low frequencies (Pierre Jr et al. 2004). Hence, the HR panel which mainly focuses on the low - mid frequencies though being a broadband absorber, cannot outshine the performance of acoustic tile because the STI model is based on the A-weighting system. The HR panels are effective at minimizing $L_{p,A,S,4m}$ and are marginally better at improving the $D_{2,S}$ with increasing area of HR panels, compared to the same study with acoustic tiles.

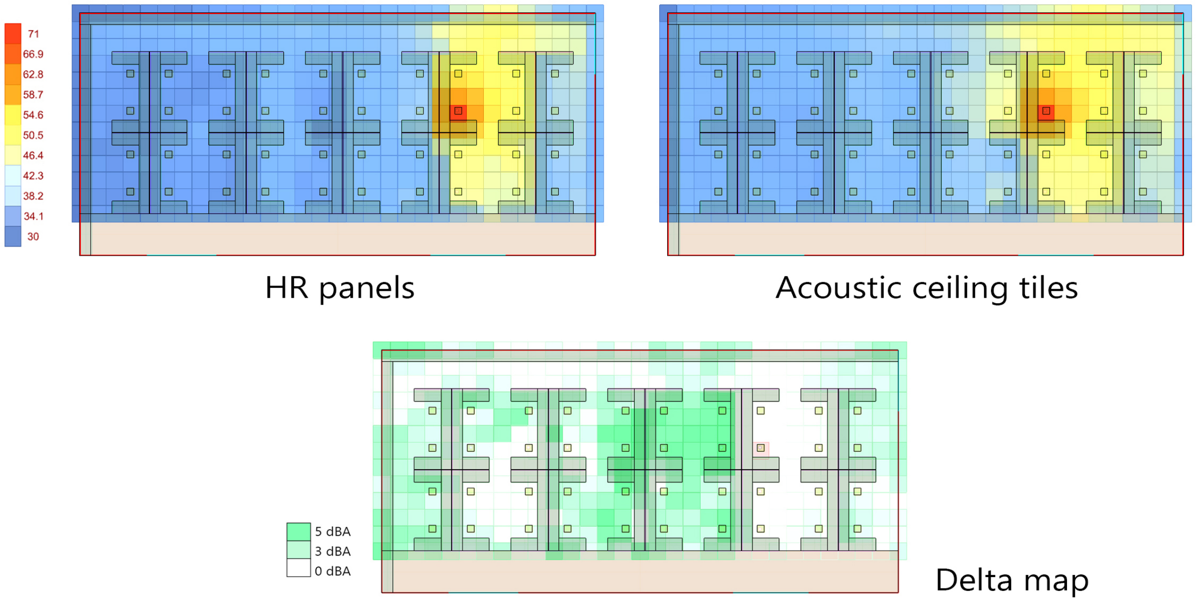

HR panels

Acoustic ceiling tiles

Delta map

Figure 48: *Sound energy distribution in the two scenarios of the layout and their delta map*

The sound energy distribution in both the cases (measured in dBA) is mapped out in figure 48. The lower end of the scale is limited to 30 dBA since values lower than that are not considered disturbing. Considering the fact that stark differences cannot be noticed with the heat-map color-scale, a delta map is plotted from the difference in their energies. In the delta map the white color depicts the zero difference zone, while green depicts the highest difference. The largest green zones are observed in the workstation bays right next to the speaker, with a difference of almost 5dBA. This shows that the HR panels are efficient at limiting the sound propagation, when compared to acoustic tiles.

5.6 Study 2 - Benchmarking with conventional offices

In the CBE Berkeley's occupant satisfaction survey (refer section 2.2) done to compare the workplace productivity in the LEED-rated and the conventional offices, the results show that cubicle-styled traditional office layout with high partitions acoustically performs better than an open office with low partitions. To test this interpretation in the open office model, a conventional workspace style was modeled in the same simple layout by enclosing the workstations on three sides by partition walls. Typically, the low partition height in open offices is maintained within the range 1.2m - 1.4m from the floor level to allow visual connectivity. In the cubicle-styled layout, a 1.7m tall partition wall made of foamy infill with fabric encasing surrounds a workstation on all the three sides. Though such a layout is not preferred, it can achieve good acoustics by hindering speech propagation in the space. The aim is to use the results from this study as a benchmark to achieve good acoustics in open offices with low partition walls.

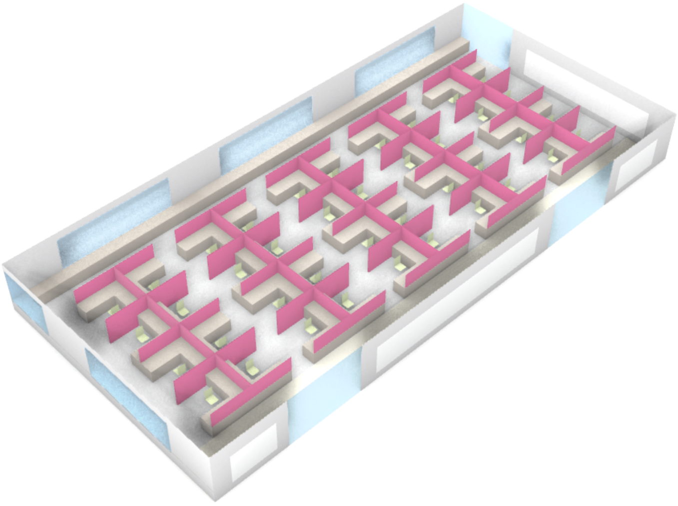

Figure 49: *Model of a cubicle-styled traditional office layout*

The same matrix technique was used in this study - scenarios of different panel distributions at varying heights are incorporated in the cubicle-style layout for acoustic simulation. A full report of this study is given in appendix I. To obtain the best performing scenarios, Pareto front analysis was performed. The fitness criteria utilized are to minimize the area of absorptive panels (and indirectly the cost), to minimize the r_D (ISO's target is $r_D \leq 5$) and to maximize the $D_{2,S}$ (ISO's target is $D_{2,S} \geq 7$). These three fitness functions are plotted on the three axes of a

3D graph and each 2D section of the 3D graph is given in figure 50. The green region marked in these sections correspond to the ISO's target values for the single-number parameters essential for achieving good acoustics (refer table 1). A gradient is applied for the area of absorption axis, because it is a subjective choice to minimize the cost invested in the HR panels. The red dots in these sections point out the Pareto frontier scenarios, and this set is considered favorable to all the fitness functions used. Within this set a few of the scenarios which lie within or in the vicinity of the green region are selected as candidate scenarios.

Apart from distraction distance and spatial decay rate, ISO suggests other single-number parameters to measure the acoustic quality of an open office. For the candidate scenarios, a spider chart with axes representing the single-number parameters recommended by the ISO is depicted in figure 51. The different value ranges of these parameters are modulated to a 1 - 5 spider plot scale. This conversion is given in Appendix I. The green region in the center of each chart delineates the values that fall within the ISO's benchmark.

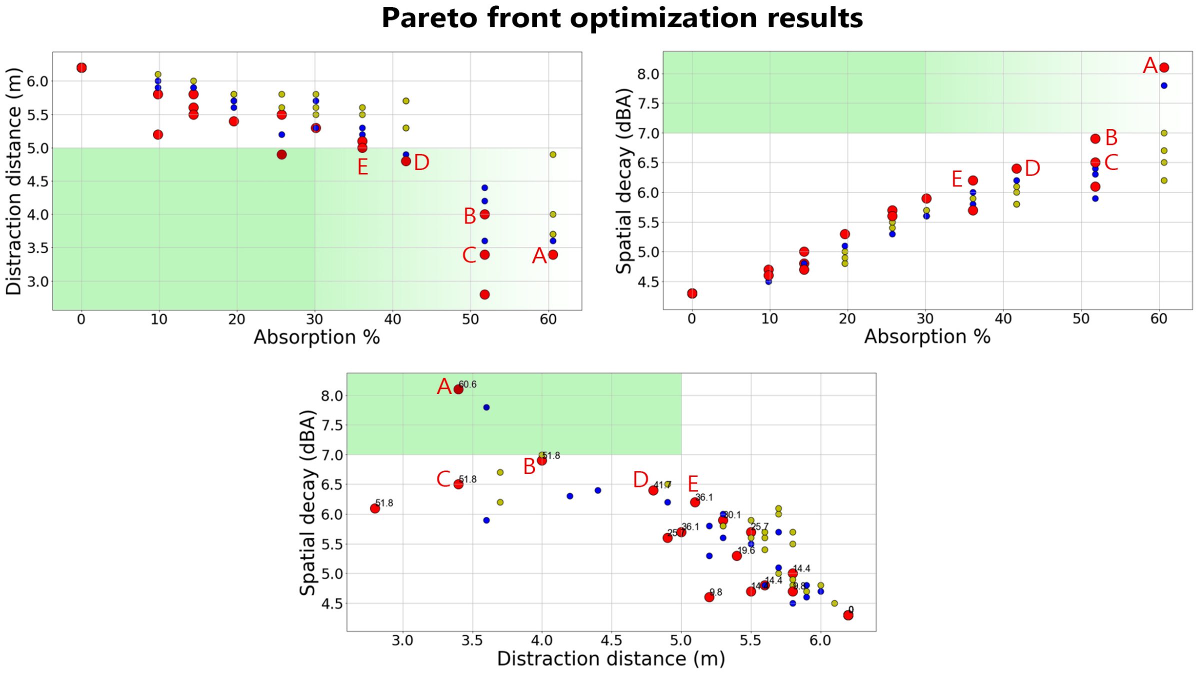

Figure 50: *Pareto front sections*

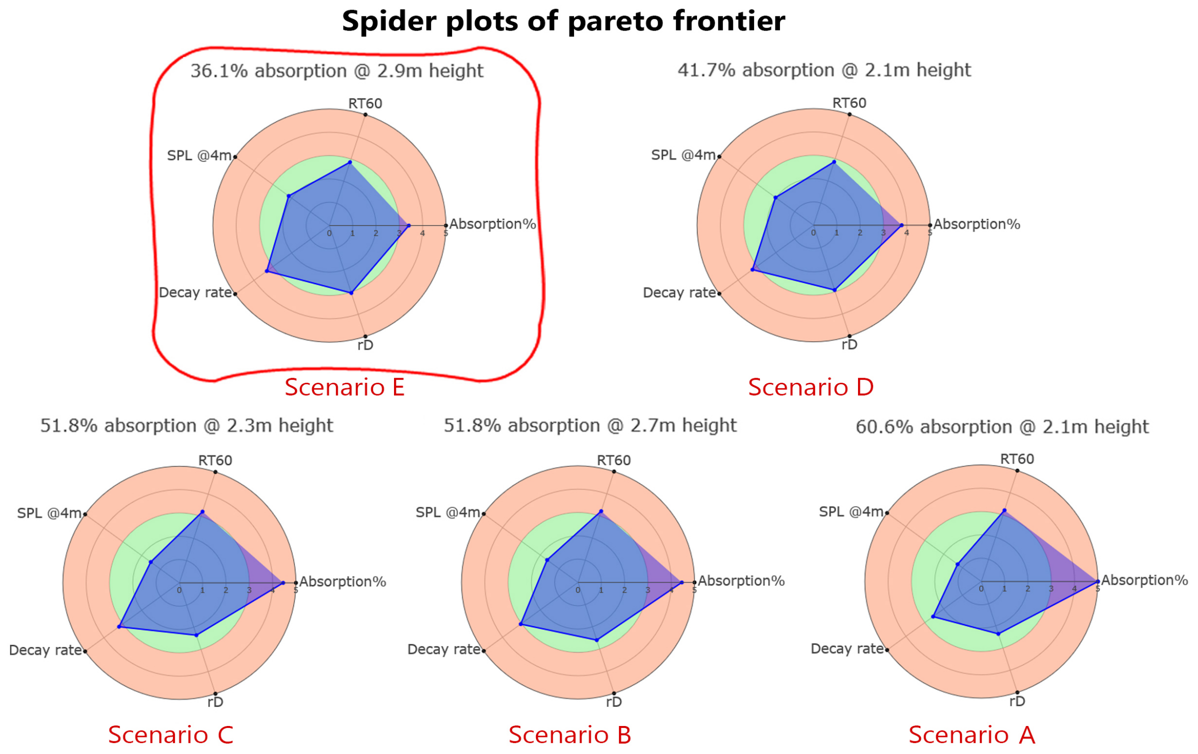

Figure 51: *Spider plot analysis of the candidate scenarios in the Pareto frontier*

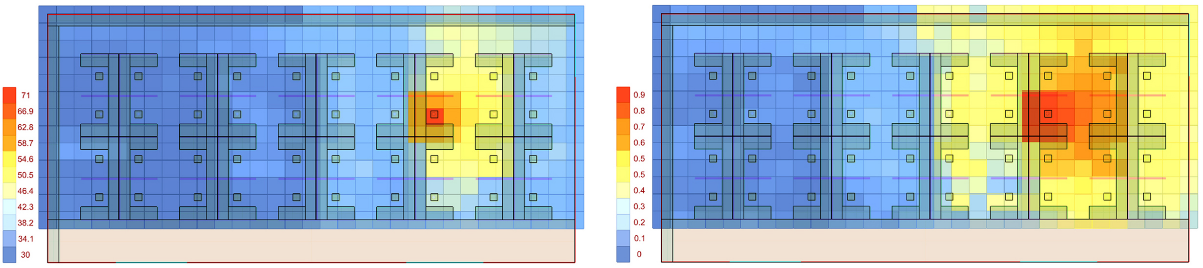

SPL A-weighted overlay

STI @Normal activity bg noise (37dBA) overlay

Figure 52: *Scenario E - Spatial sound distribution maps of the conventional layout*

From the spider plots (figure 51), it is clear that no scenario falls completely within the green zone. Improving one or some of the parameters curtails the others. Hence, some trade-offs must be made in choosing one scenario over the other candidate scenarios. The scenario E, which has 36.1% area of the ceiling covered with HR panels at the height of 2.9m from the floor level, is an interesting solution. Though the spatial decay is just outside of the target values set by the ISO, the other single number parameters show satisfactory results. Increasing the area of absorptive surfaces improves the spatial decay, but reduces the reverberation time in the open office well below the comfortable range. This is the case with scenario A, which has 60.6% area of the ceiling covered with HR panels. Such a high percentage might not be a feasible solution in terms of the cost invested in the panels. The same trends are observed in scenario B (51.8% HR panel absorbers @ 2.7m height) and scenario C (51.8% HR panel absorbers @ 2.3m height). A large area of absorption negatively impacts the reverberation time and increases the expenses. Between these two scenarios, there is a marginal difference in their decay rates caused by the location of the HR panels. Scenario D, which has 41.7% panel area coverage, has satisfactory single-number ratings, and has a similar acoustic response to that of scenario E (36.1%) except in the spatial decay parameter. This small difference could be seen as a trade-off with the cost of investment. Therefore, scenario E is a cost-effective solution that can achieve good acoustics. The best-case, Scenario E, among the other candidate solutions is highlighted in the figure 51.

5.7 Study 3 - Flat vs. Tilted HR panels

This study tests the efficiency of the ceiling-hung HR panels for two different orientations. The first case, flat ceiling-hung panels, has all the panels facing down towards the workstations. In the other case, the panels are angled to face the speakers or the chair locations. The tilted ceiling-hung panels are designed by pitching the flat panels along the center line. They form a "V" shape, and are anchored right above the partitions and the bays that separate two workstation rows. The height of the tilted panels is measured from the center of the panel. This study was done to observe how changing the way the speech sounds from the speaker are reflected can affect the room acoustics. These panels were modeled in the same layout as described in section 5.4. A set of simulations were run for each type of panel orientations and the results were recorded in the same matrix format.

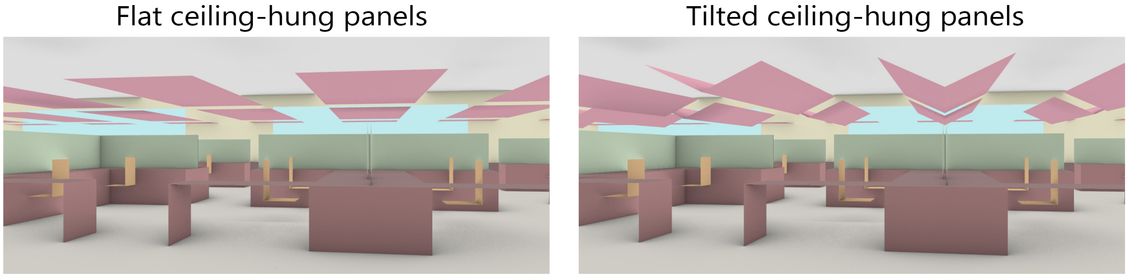

Figure 53: *Views of the open office with flat and tilted ceiling-hung HR panels*

Figure 56 shows the matrices of r_D in the presence of normal activity background noise @37dBA for each orientation. The flat HR panels can achieve the ISO's r_D target range for 51.8% or more area of absorption across all the heights. However, with minimum inclusion of tilted HR panels (i.e. 10% ceiling area), the r_D can be maintained within the acceptable range. The pitched panels focus the reflected sound waves back towards the speaker's workstation, and hence mitigating the propagation of the speech sounds to other workstations. The trends observed in the r_D matrix of the flat HR panels are already discussed in section 5.5. With tilted HR panels, there are no direct trends in r_D across the increasing area of absorption that correspond to all the panel heights. This is because, unlike with the flat panels, as the height of the pitched panels is increased, their surface normal changes with respect to a vector that connects the speaker to the panel's center. The dips observed in the r_D matrix of the tilted panels indicate the case when the surface normal aligns with the mentioned vector. In those cases, a large portion of the reflected sound waves is directed towards the speaker which improves the r_D value. In general, a larger area of HR panels at a low height forms the best-case in terms of r_D parameter.

Comparison between the $D_{2,S}$ matrices of flat and tilted HR panels are given in figure 57. The trends observed in both the matrices are similar since $D_{2,S}$ only factors in the amount and the location of absorbers, and the room geometry. With increasing area percentage of the HR panels, the spatial decay improves and this improvement is accelerated in lower panel heights. Though similar, the orientation of the absorbers makes a significant impact on the rate of improvement observed. The tilted panels show a higher rate of $D_{2,S}$ improvement across all the panel heights. This can be attributed to the sound containment quality of the pitched geometry.

Pareto front analysis is applied to the tilted HR panel set - scenarios of different panel distributions at varying heights. In the Pareto section between absorption % and the distraction distance (see figure 54), a lot more scenarios fall within the ISO's r_D target range, compared to the same Pareto section of flat HR panel distribution (given in Appendix I). However, none of the scenarios fall within the $D_{2,S}$ target range in the section between absorption % and spatial decay. Yet, the candidate scenarios marked is within 1dBA from the candidate solutions (not including scenario A) of the conventional style benchmark given in section 5.6. The $D_{2,S}$ value of the cost-effective solution (scenario E) discussed in the benchmarking study matches the $D_{2,S}$ value of scenario A marked in the Pareto sections of the tilted HR panel. Thus, the four scenarios marked and further explored in the spider plots are competent solutions.

The spider plots of the candidate scenarios (see figure 55) show the scenario's good performance in all the single-number parameters, except in the spatial decay parameter. Moving from scenario D (30.1% area of absorption @2.3m height) to scenario A (60.6% area of absorption @2.3m height), the distraction distance and spatial decay improve. However, there is a marginal decline in the reverberation time due to the increased amount of absorption in the space. Scenario B and scenario C with 51.8% and 41.7% area of absorption respectively, though slightly better than scenario D, are pricey options. Hence, scenario D is a cost-effective solution that can achieve good acoustics with some trade-offs. This best-case scenario is highlighted in the figure 55.

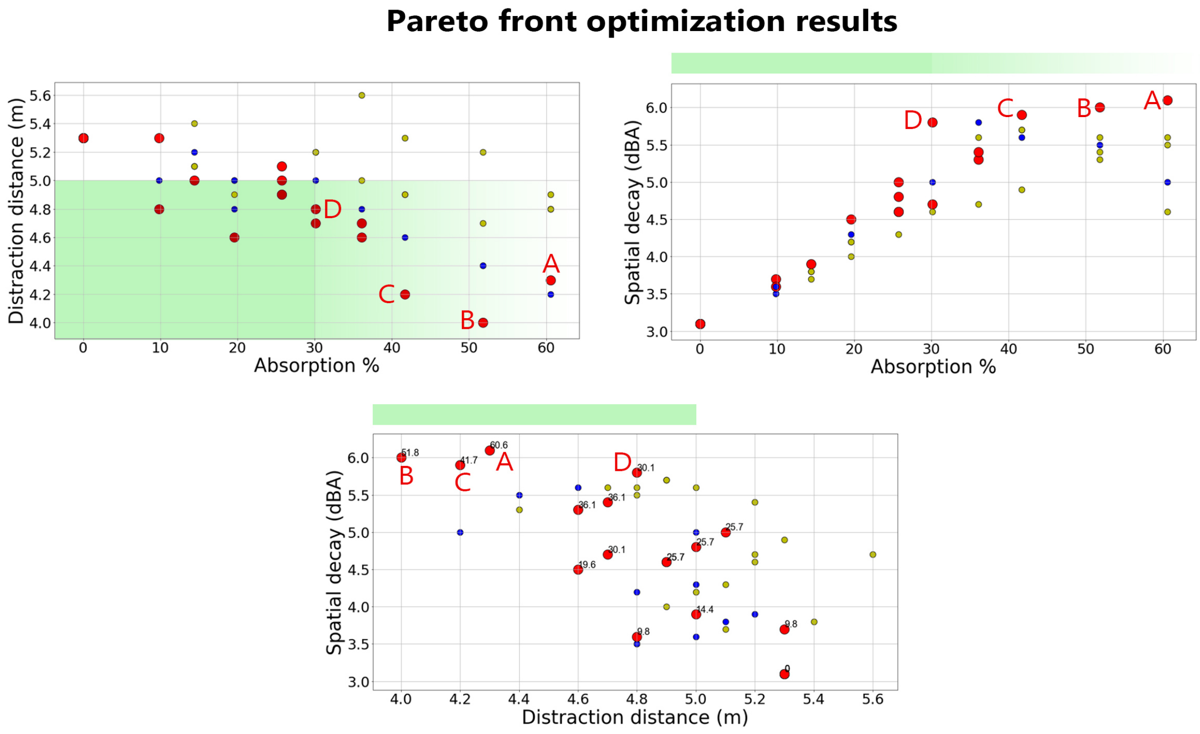

Figure 54: *Pareto front sections of tilted HR panel scenarios*

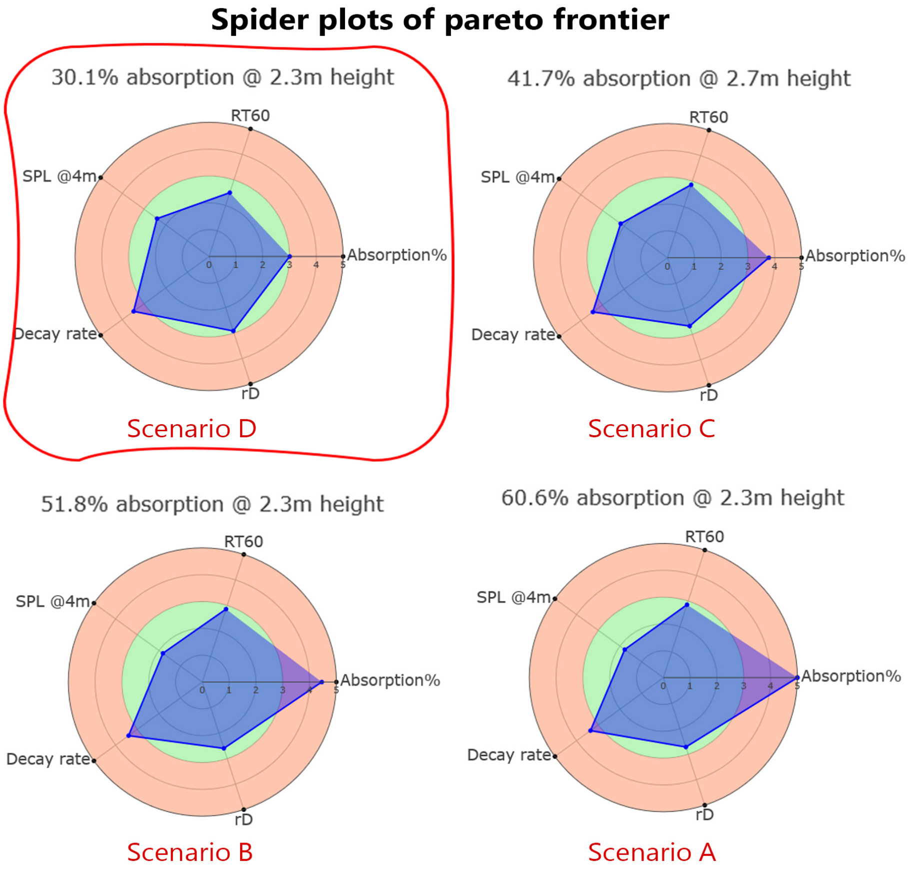

Figure 55: *Spider plot analysis of the candidate scenarios in the Pareto frontier*

Flat HR panel study

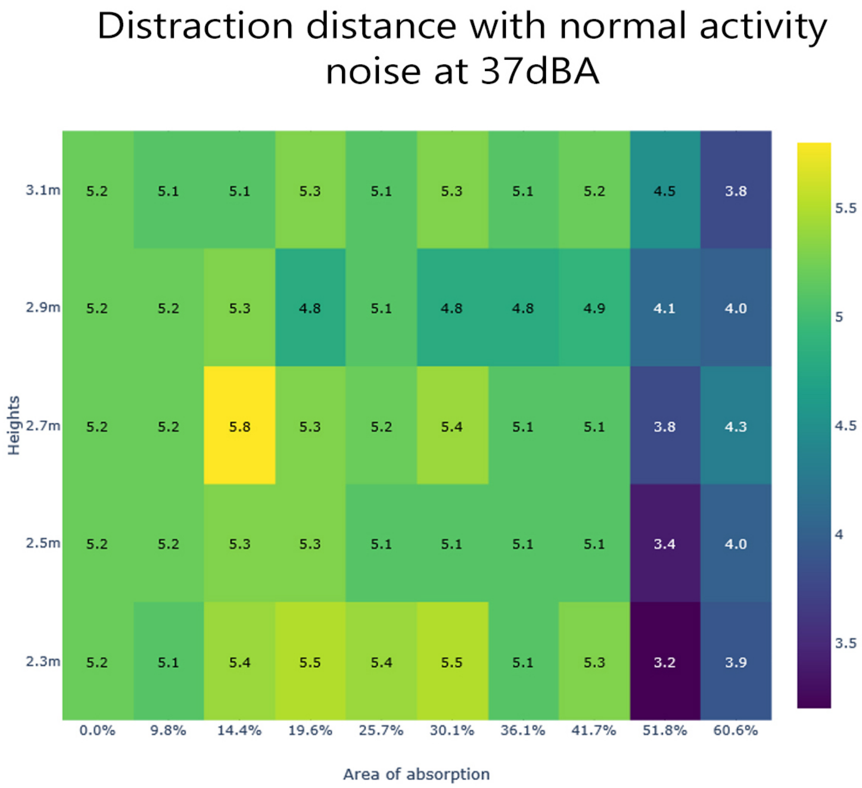

Tilted HR panel study

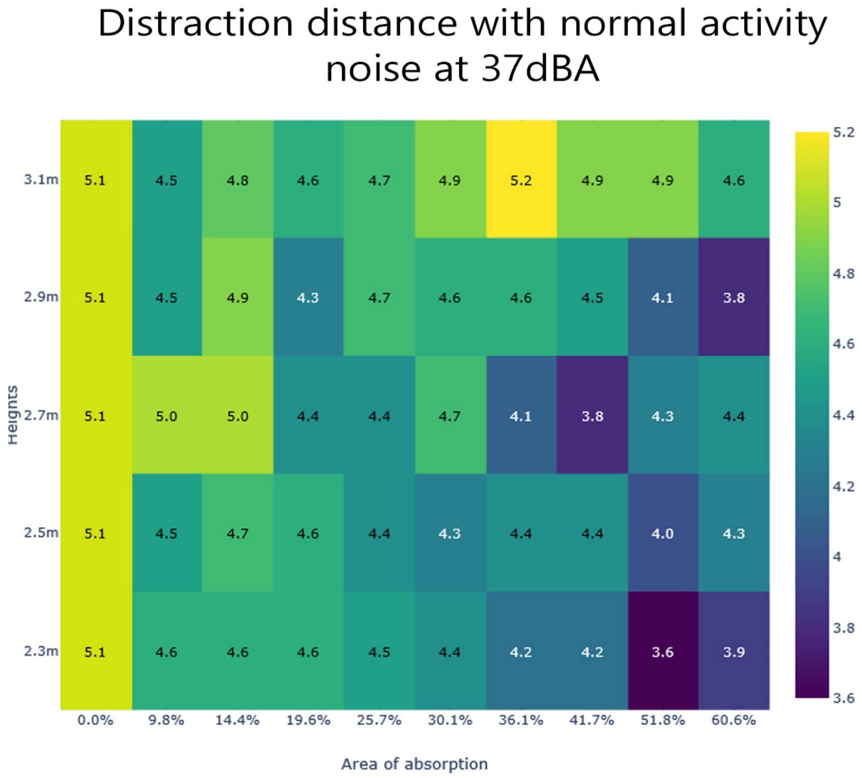

Figure 56: *Matrices of r_D of Flat and Tilted HR panels*

Flat HR panel study

Spatial decay rate ($D_{2,S}$)

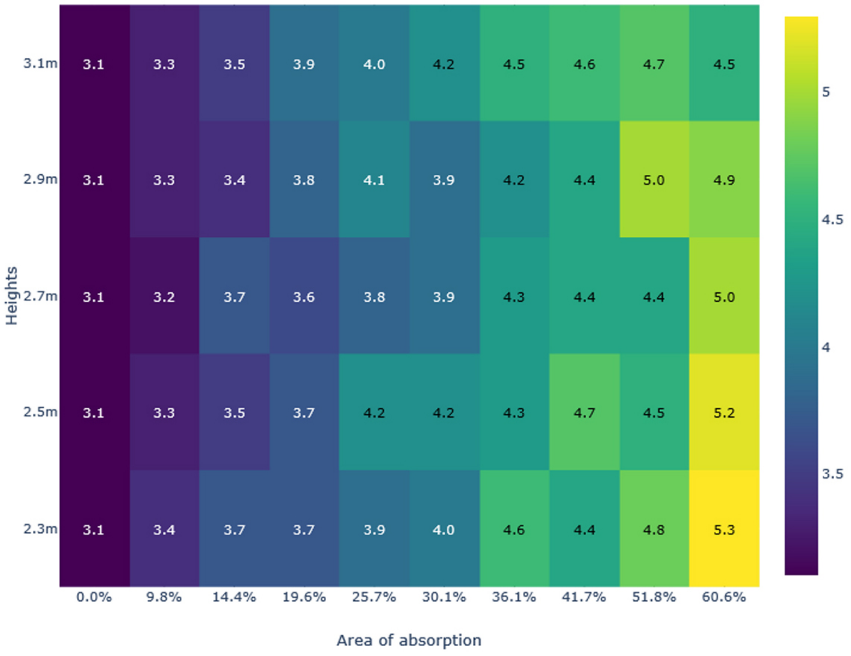

Heights	0.0%	9.8%	14.4%	19.6%	25.7%	30.1%	36.1%	41.7%	51.8%	60.6%
3.1m	3.1	3.3	3.5	3.9	4.0	4.2	4.5	4.6	4.7	4.5
2.9m	3.1	3.3	3.4	3.8	4.1	3.9	4.2	4.4	5.0	4.9
2.7m	3.1	3.2	3.7	3.6	3.8	3.9	4.3	4.4	4.4	5.0
2.5m	3.1	3.3	3.5	3.7	4.2	4.2	4.3	4.7	4.5	5.2
2.3m	3.1	3.4	3.7	3.7	3.9	4.0	4.6	4.4	4.8	5.3

Tilted HR panel study

Spatial decay rate ($D_{2,S}$)

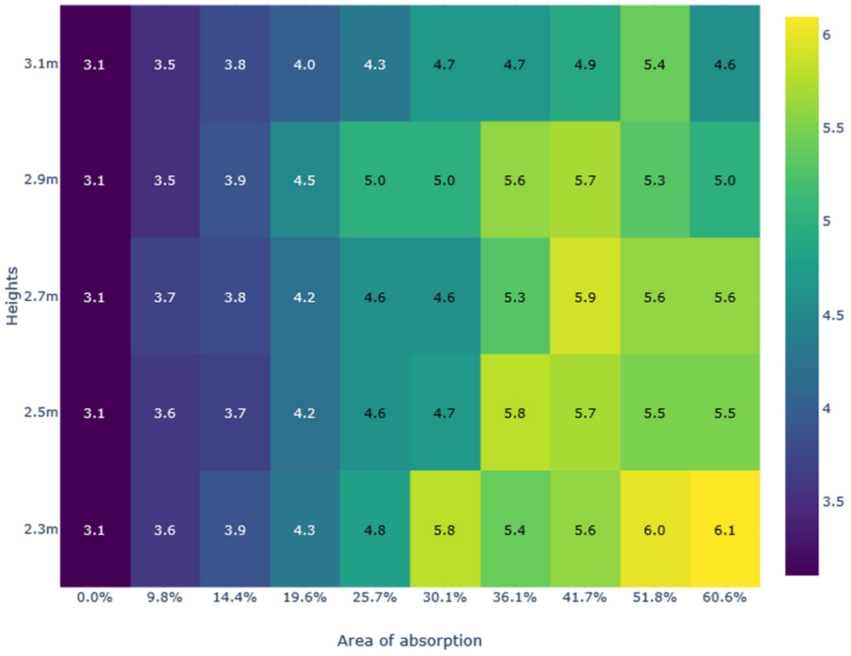

Heights	0.0%	9.8%	14.4%	19.6%	25.7%	30.1%	36.1%	41.7%	51.8%	60.6%
3.1m	3.1	3.5	3.8	4.0	4.3	4.7	4.7	4.9	5.4	4.6
2.9m	3.1	3.5	3.9	4.5	5.0	5.0	5.6	5.7	5.3	5.0
2.7m	3.1	3.7	3.8	4.2	4.6	4.6	5.3	5.9	5.6	5.6
2.5m	3.1	3.6	3.7	4.2	4.6	4.7	5.8	5.7	5.5	5.5
2.3m	3.1	3.6	3.9	4.3	4.8	5.8	5.4	5.6	6.0	6.1

Figure 57: *Matrices of* $D_{2,S}$ *of Flat and Tilted HR panels*

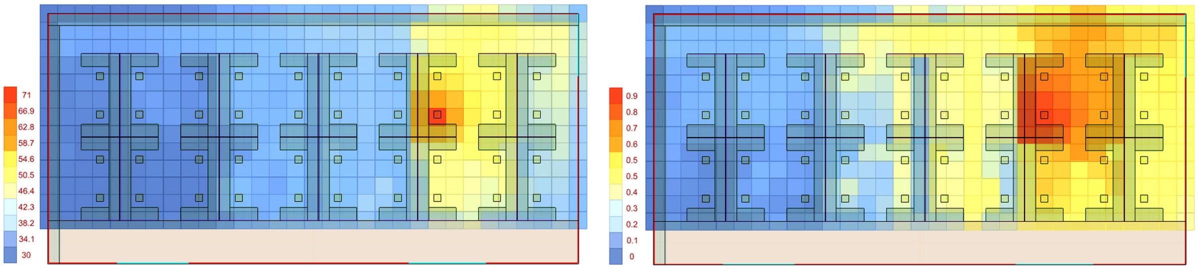

SPL A-weighted overlay

STI @Normal activity bg noise (37dBA) overlay

Figure 58: *Tilted HR panel - Detailed analysis of Scenario D - the SPL(A) and STI values are overlaid on the plan*

Figure 58 depicts the acoustical environment of scenario D where 30.1% area of the tilted HR panels are hung from the ceiling at a height of 2.3m from the floor level. Both the SPL and the STI overlays direct the attention to the sound focusing nature of the tilted panels within the bay of its origin. To portray the efficiency of tilted panels over flat panels, sound energy distribution in both the scenarios are given for comparison (see figure 59). It is clear that the tilted panels do a better job of containing the sound. The delta map shows the difference in the sound energies, and the green zone depicts the highest energy difference zone. The large green zone, two workstations away from the speaker, shows the tilted panel's efficacy in restricting the speech signals from affecting a lot more people. This is because the tilted panel reflects the sound back to the speaker instead of spreading it. The difference observed is almost 6.5dBA, which makes a significant difference in the acoustic quality in that zone.

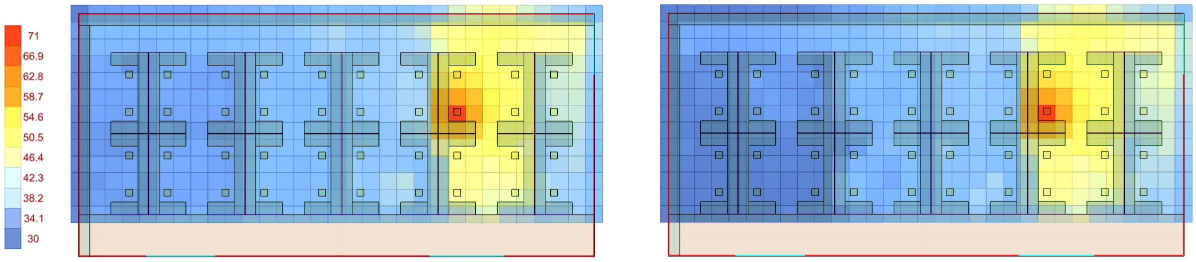

Flat HR panels

Tilted HR panels

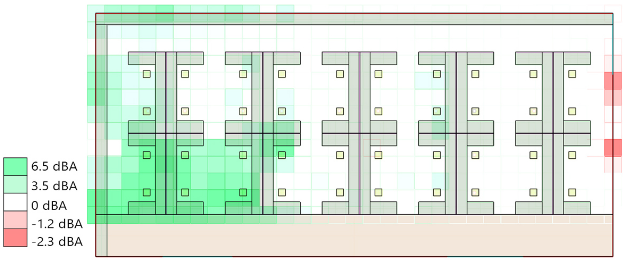

Delta map

Figure 59: *Comparative analysis - Flat HR panels covering 30.1% area of the ceiling at 2.3m high from the floor level*

5.8 Study 4 - Absorptive properties for the desk partitions

With the previous studies, the focus has been on containing the reflected sound waves from the speaker's workstation (see figure 34) using absorptive ceiling panels. This study was targeted at the absorptive properties of the desk partition. The desk partitions or screens play an important role in addressing the direct sound waves from the speaker. Thus, the question of how much absorption is suitable for partitions or screens becomes critical.

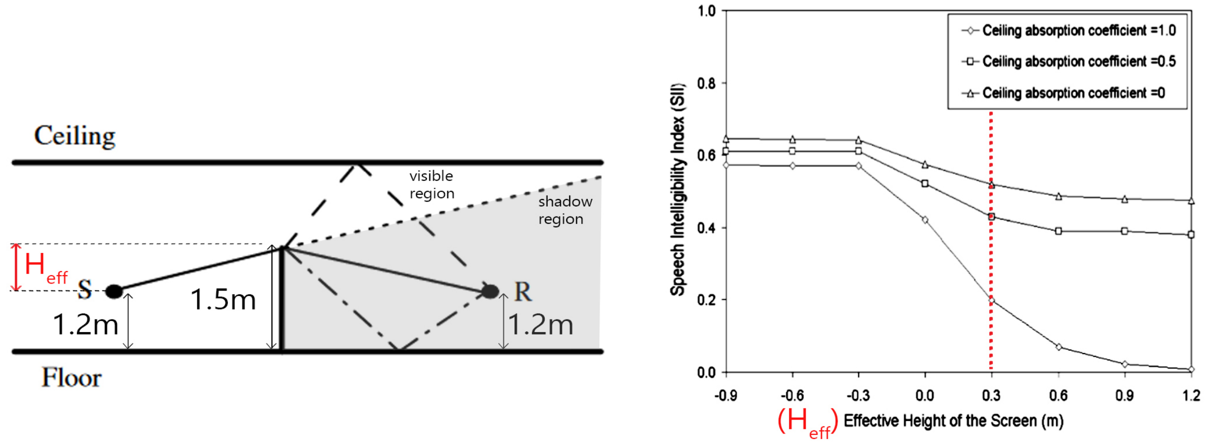

Figure 60: *Diffracted rays over the partition or screens and the effect of the height of the partition on the speech intelligibility at the receiver's position (Han & Mak 2008)*

For this study, the layout discussed in section 5.4 is used for the simulations. The desk partition's height is maintained at 1.5m, and the speaker and the receiver locations are at 1.2m from the floor level (see figure 60). The effective height of the partition, H_{eff} is defined as the difference between the heights of the partition and the speaker location. Figure 60 shows the effect of the height of partition on the speech intelligibility at the receiver's location. With increasing partition height, the amount of speech signal diffracted to the receiver's location is minimized. However, the values above 1.7m height of the partition are constant. Another factor that affects the diffracted signal at the receiver's location is the absorptive property of the ceiling panels. Increasing the absorption performance of the ceiling decreases the impact of reflected diffracted sound waves from the partition. In this study, H_{eff} of 0.3m, i.e. 1.5m high partition, and different HR panel distributions (as specified in section 5.4.2) at a height of 2.7m from the floor level, are used for the acoustic simulations.

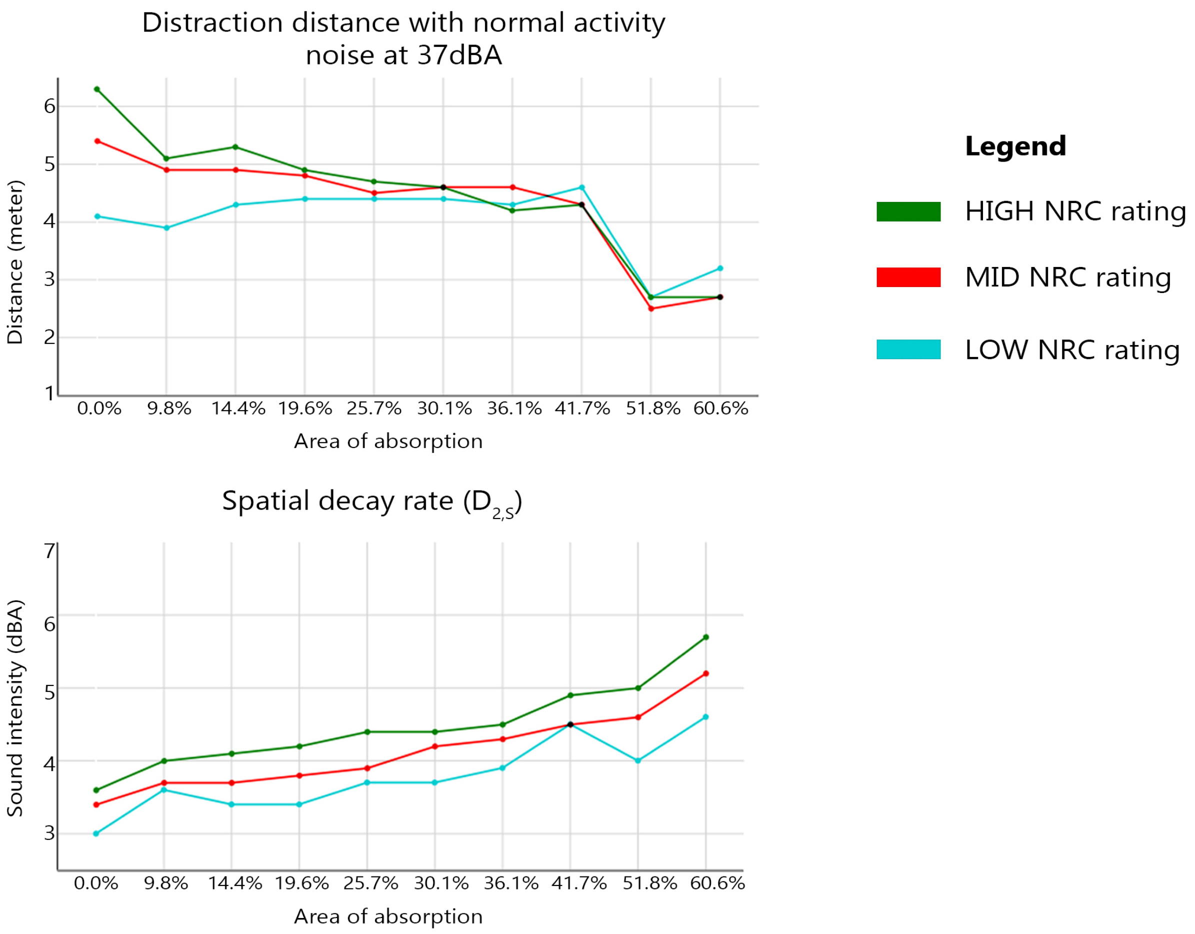

Figure 61: *r_D and $D_{2,S}$ graphs of three different NRC ratings applied to the desk partition material across increasing area of ceiling-hung HR panels*

The Noise Reduction Coefficient (NRC) rating of the desk partition material is varied for different sets of simulations to look for trends in the acoustic quality of the open office. Figure 61 shows the trends in r_D and $D_{2,S}$ for three different NRC rating materials. Low NRC rating material is preferred by r_D measured in 37dBA normal activity background noise. However, the same material is the least preferred in the view of $D_{2,S}$. Low absorptive partition material reflects most of the sound waves falling on it, thus increasing the reverberation time which helps in masking the speech signal but it does a bad job of minimizing the sound energy in the space (or maximizing the spatial decay). High NRC rating material decreases the r_D and maximizes the spatial decay with increasing area of ceiling absorption. In this case, instead of depending on the masking effect of the reverberation time, highly absorptive partition material removes the sound energy from the space, and hence improves the acoustic quality of the open office. The detailed report of this study and the absorption coefficients used are given in Appendix I.

Though these results show the overall impact of the desk partition's absorption on the single-number parameters, they are not representative of the acoustic environment in the space. Because the Pachyderm acoustic software does not have the edge diffraction feature. Hence, the results from this study might be different if edge diffraction or the diffracted rays are accounted for. Figure 62 shows the diffracted sound pressure distribution for a source strength of $Q_p = 1m^3/s$ and a 2m partition placed at 2m from the source which is at the origin. The sound pressure of the diffracted rays in the partition's shadow region is significant, though this is the region that is assumed to have zero sound pressure in the Pachyderm software. Although speech signals are of lower source strength than the one used in the example, the impact of edge diffraction is profound which is not incorporated in this study. But the aim of the study is to not determine the effective height of the partition walls that will reduce the amount of diffracted rays from reaching the next workstation. This study is about the absorptive quality of the partition walls for efficient absorption of direct sound waves. Though edge diffraction might have a role in these studies, the lack thereof might not change the trends observed in the single-number acoustic parameters.

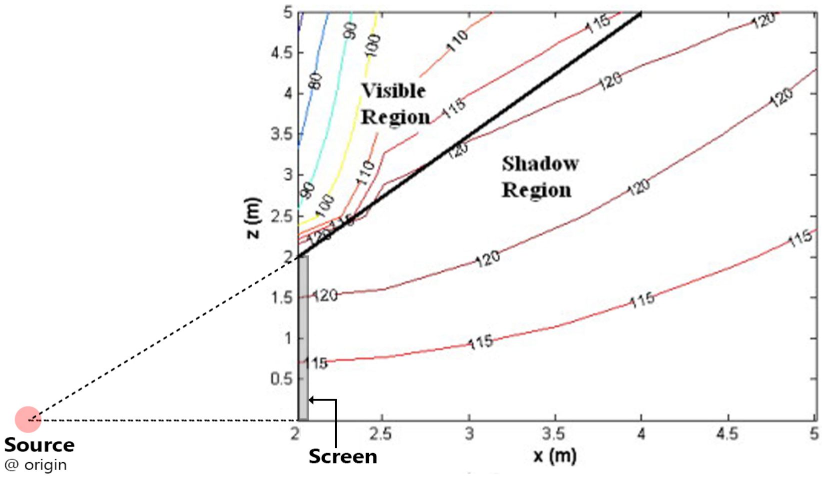

Figure 62: *Sound contours of diffracted sound energy (Han & Mak 2008)*

5.8.1 Materials for the desk partition

The same study was performed with four different desk partition materials, each with a good performance either in the low-mid or mid-high frequencies. The r_D and $D_{2,S}$ graphs are given in figure 63. And again, the trends in these graphs follow the observations made above. Glass has the lowest absorption performance while fabric encased foam infill material has the highest absorption performance among the samples used in this study. As mentioned above, a highly absorptive material, though not showing promising results in the r_D values, will help in improving the room acoustics. The hybrid combination of the low-mid frequency ceiling-hung HR panels and the mid-high-frequency fabric and foam partition will contribute positively towards the acoustical improvement in open offices.

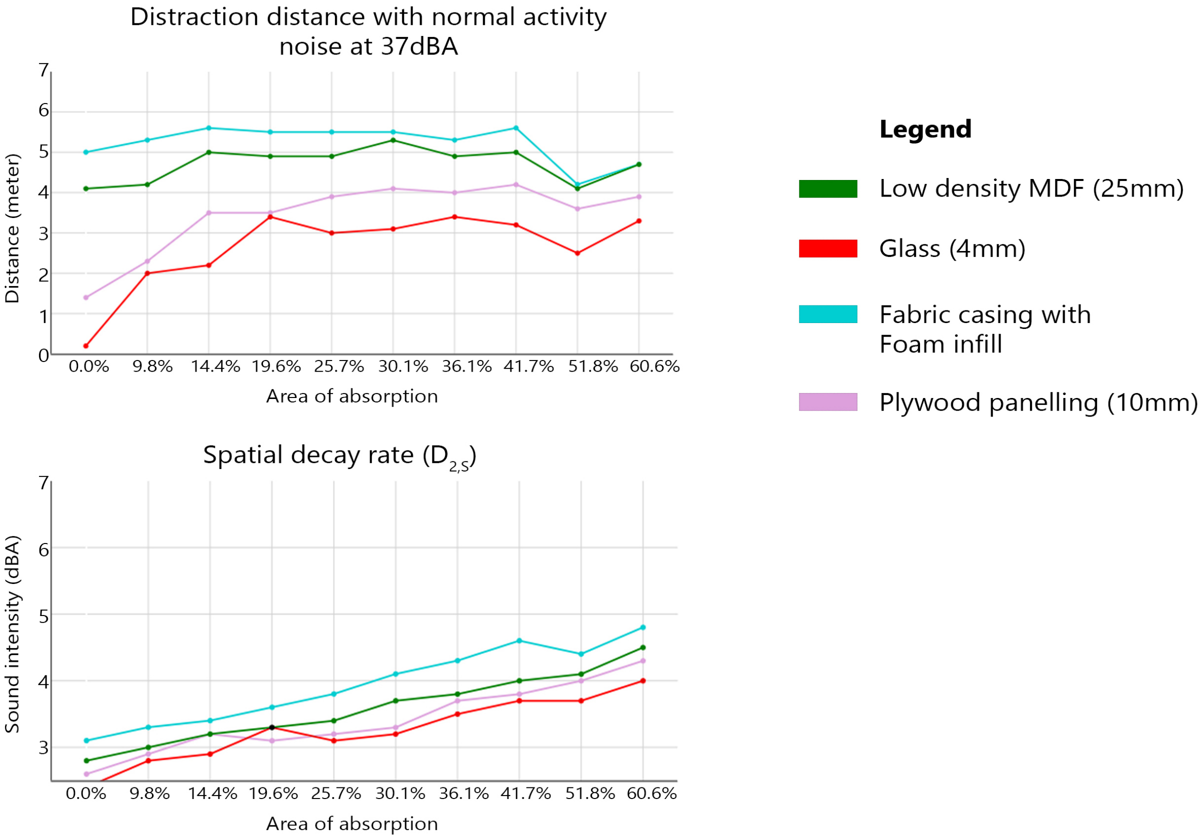

Figure 63: *r_D and $D_{2,S}$ graphs of four different desk partition materials tested across increasing area of ceiling-hung HR panels*

6 Open office case studies

The main takeaways from the studies are implemented in three open office layouts discussed in section 5.3.1. They are tested for their existing acoustic performance, and improvements using HR panels are suggested for each layout. These case studies are existing offices in the US and a representative section of the floor-plate is used in the simulations. The baseline scenario encompasses the existing conditions in the office space, including the materials used. The improvements to the office space are executed with two strategies - changing the desk partition material to fabric encased foam infill material, and replacing the acoustic ceiling tiles (ACT) with tilted HR panels.

6.1 Office layout 1

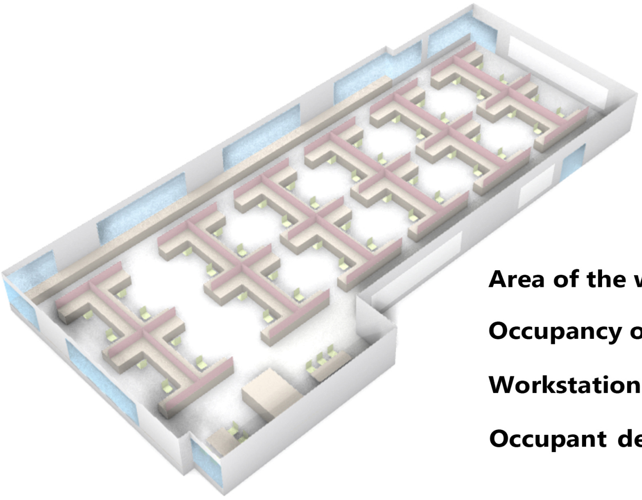

Area of the workstation area: 571.07 sqm

Occupancy of this work area: 60 people

Workstation area per person: 9.52 sqm/person

Occupant density: **10.5%**

Figure 64: *View of office layout 1 and its basic statistics*

Layout 1 is the simple office layout that was used in the studies given in section 5.4. To represent the existing conditions in this office space, further additions were made to this layout in this chapter - including changes to the surface material properties. This layout has a single main corridor that runs around the core of the building and connects the workstations to the main lobby and kitchen area. Meeting and conference rooms, on one end, isolate this workstation area from the public gathering spaces and provide visual privacy. On the other end, the collaboration area provides the disconnect from another similar workstation zone around the core. The work area is not densely populated and there is a sufficient buffer between the workstations. Mini enclosures are formed by the desk partitions promoting team spaces of 4 seats. This ensures worker collaboration and keeps in check the distraction caused to others.

6.1.1 Baseline scenario

Figure 65 shows the baseline scenario of office layout 1. The highlighted rectangles are acoustic ceiling tiles fixed to the ceiling over each workstation bay. The area of the tiles covers 64% of the workstation area. The desk partitions are made of metal panels and sit 0.6m above the table height. The spider chart is used as an acoustic rating system to compare the baseline scenario with the improvement scenarios. Each axis represents a single-number acoustic parameter – like distraction distance, reverberation time, spatial decay, and SPL at 4m from the speaker. ISO has set target values for these parameters in achieving good open office acoustics (refer table 1). The green zone marks the good acoustics zone. The baseline scenario achieves a good value on most of the parameters except the spatial decay parameter.

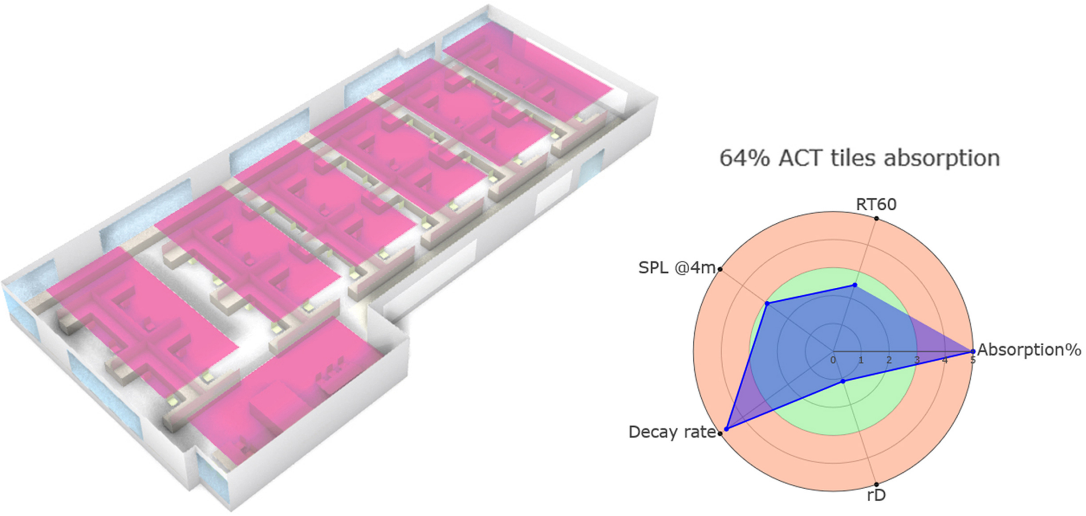

Figure 65: *View of the baseline scenario with highlighted acoustic ceiling tiles and its spider plot rating*

6.1.2 Improvements with HR panels

Two sets of improvements are performed on this layout. First, the desk partition height is increased to 1.5m (or 0.75m above the table height) and the material is switched to fabric encased foam infill. Second, the acoustic ceiling tiles are swapped with HR panels. To understand the optimum area of HR panels needed for this layout, 8 successively increasing area of HR panel distributions are used in constructing the height vs. area of absorption matrices (as discussed in section 5.5). The area of the panel distributions and the matrices are given in Appendix J. Pareto front analysis is applied on all the scenarios in the height vs. HR panel area matrix, given in figure 66. All the scenarios except for the 0% absorption fall within the ISO's target range for distraction distance, owing to the low occupant density and the large volume of the space. However, due to the same reasons, the target value of spatial decay is not met. Such a large space would require a substantial quantity of absorbers to achieve the target value. Still, the spatial decay values achieved by the candidate scenarios A and B are acceptable. The candidate scenarios are further explored through spider graph acoustic rating (refer figure 67).

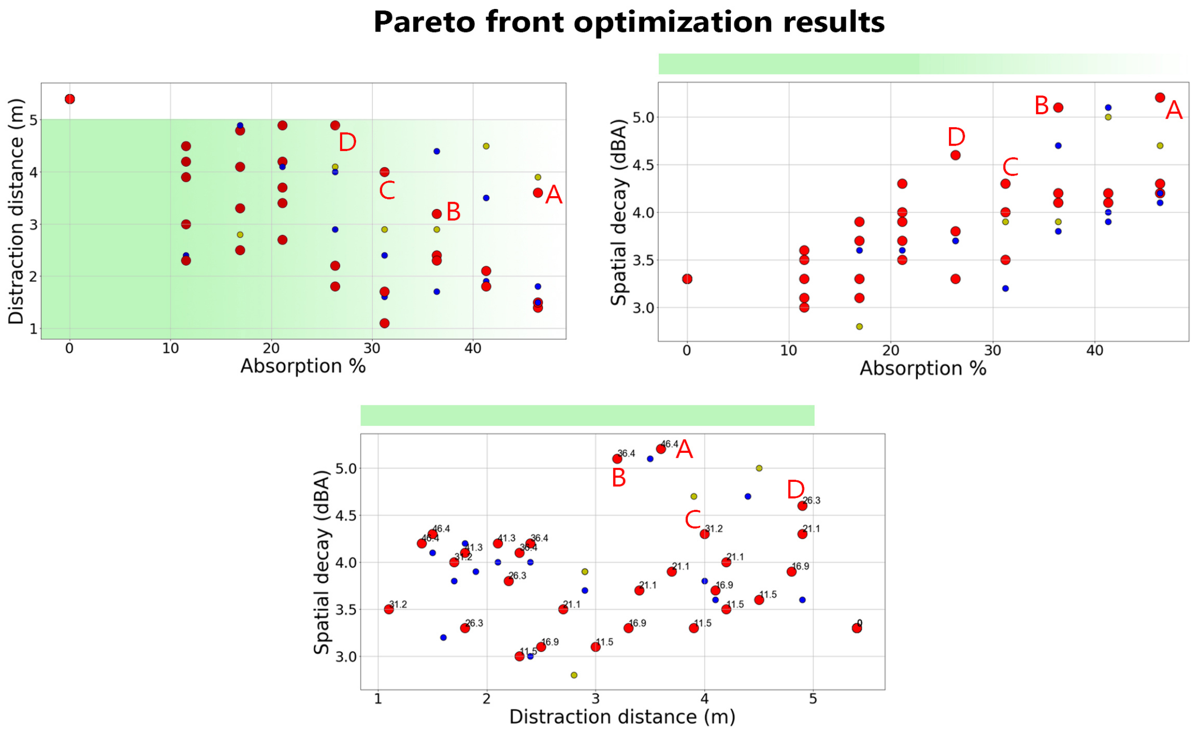

Figure 66: Pareto analysis of the different HR panel configurations

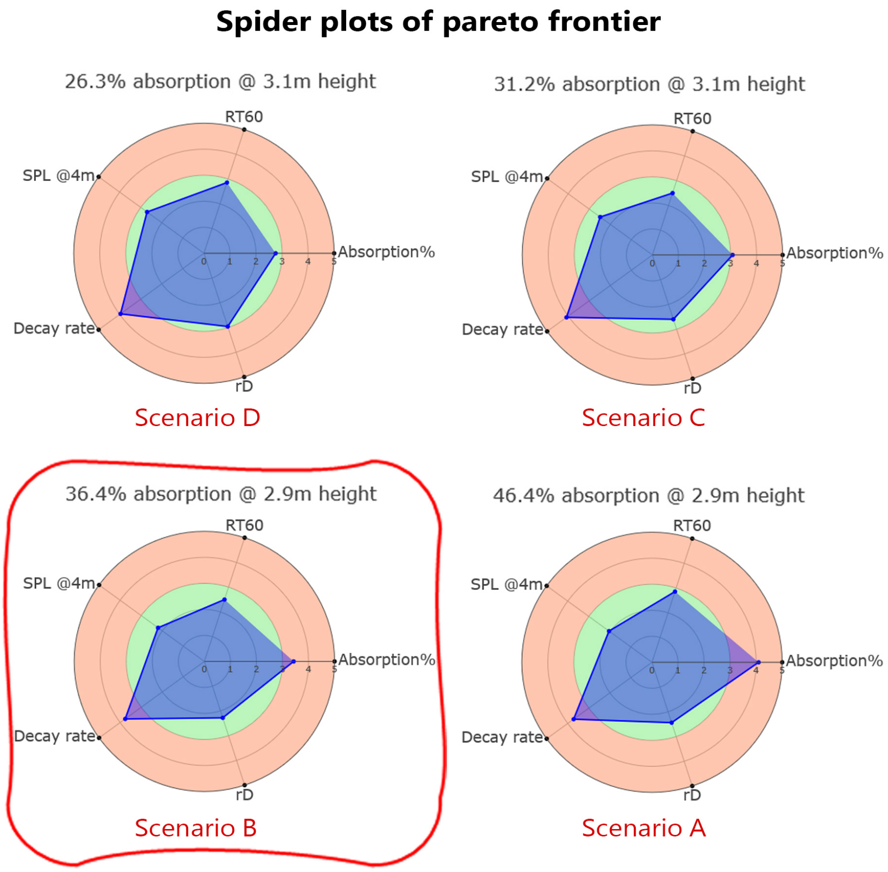

Figure 67: Spider plot analysis of the Pareto scenarios

Four different areas of absorption are in the candidate solution set - 26.3% (Scenario D), 31.2% (Scenario C), 36.4% (Scenario B), and 46.4% (Scenario A). All the scenarios have satisfactory values in each of the parameters except in spatial decay. The spatial decay improves with increasing area of absorption but both scenarios A (46.4%) and B (36.4%) exhibit similar spatial decay values. Scenario B is the most cost-effective scenario that can achieve good acoustics and hence is chosen as the best-case scenario. Figure 68 shows the layout's improved case with scenario B HR panel distribution.

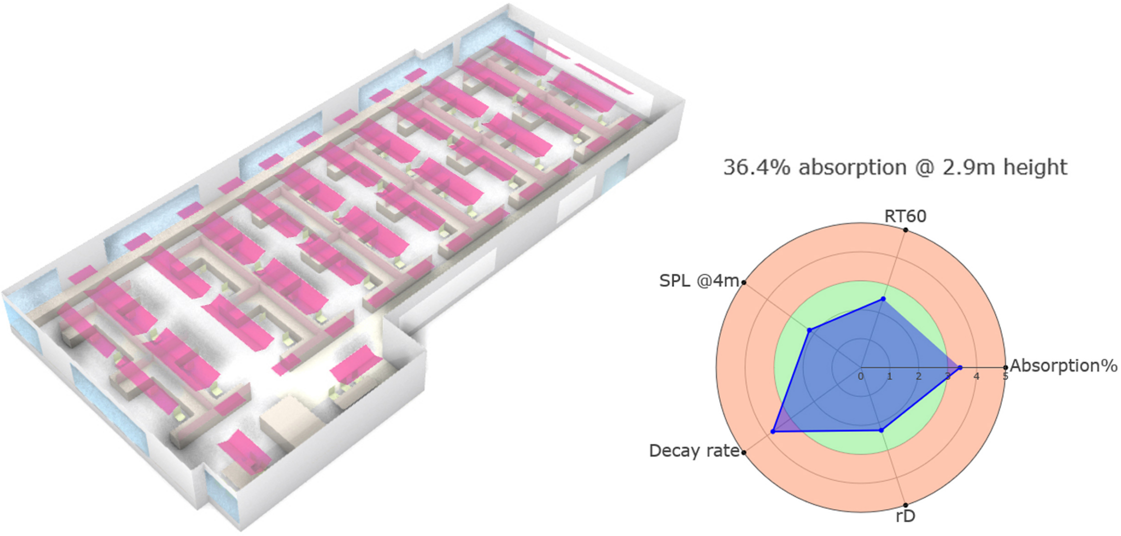

Figure 68: *View of the best-case scenario with highlighted HR panel configuration and its spider plot rating*

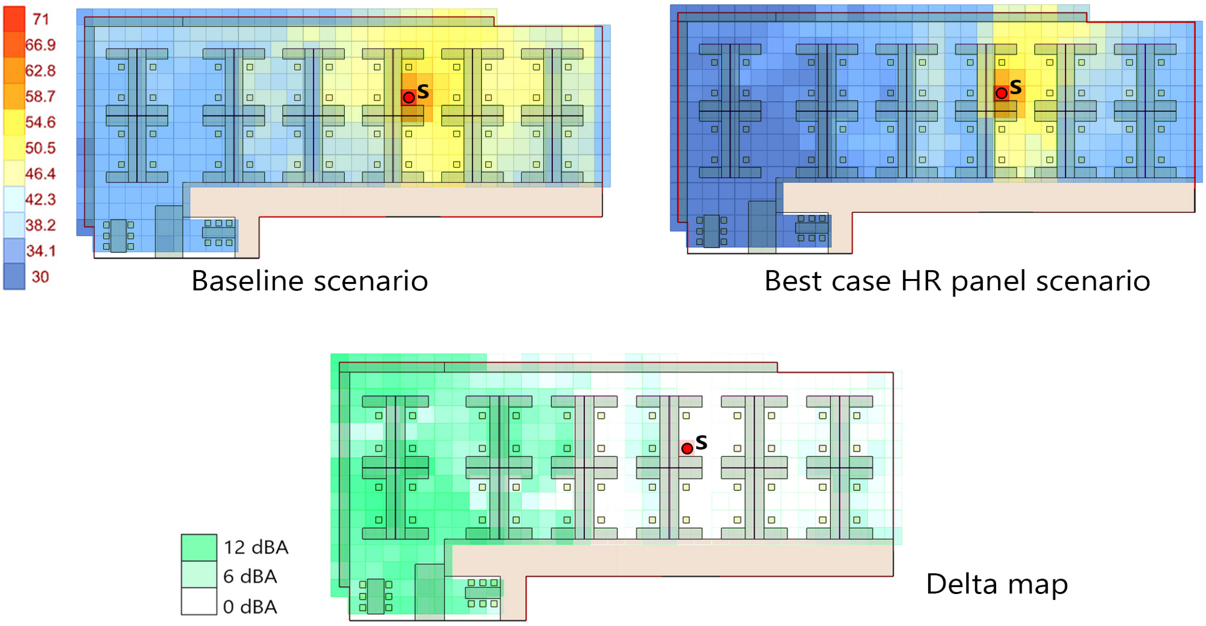

Baseline scenario

Best case HR panel scenario

Delta map

Figure 69: *Sound energy distribution in the baseline scenario and the best-case HR panel scenario and their delta map*

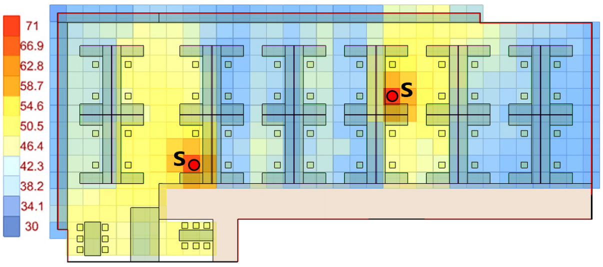

Two speakers

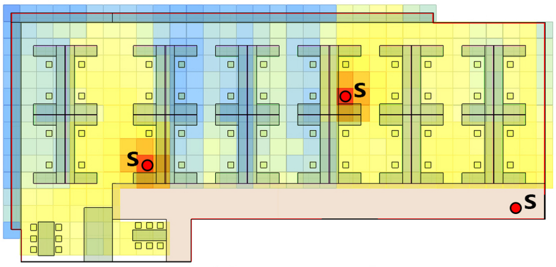

Three speakers

Figure 70: The best-case HR panel scenario with simultaneous speakers

Figure 69 shows the sound pressure distribution in the layout from a single source speaker for the two scenarios - the baseline case, and the improved case with HR panels. Even from the heat maps, it is clear that the best-case scenario performs well in containing the speech sounds. A delta map is produced from the energy differences between the two scenarios. The white zone depicts zero energy difference while green depicts the highest energy difference. A 10dBA improvement is achieved one workstation away from the speaker and up to 12dBA improvement at three workstations away. This is a very noticeable improvement at the receiver locations. For the same best-case scenario, simulations are generated for multiple speakers (given in figure 70). For two simultaneous speakers, there is a good acoustic screening effect observed at most of the employee locations in-between the sound sources. When a third speaker is introduced in the corridor space, the acoustic quality deteriorates because of the insufficient amount of absorption over the corridors.

6.2 Office layout 2

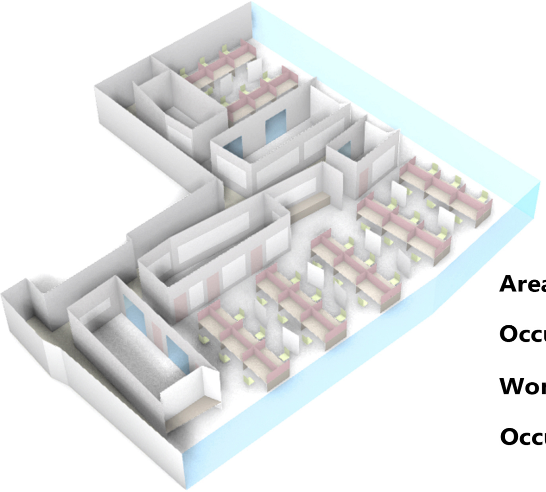

Area of the workstation area: 385.88 sqm

Occupancy of this work area: 42 people

Workstation area per person: 9.19 sqm/person

Occupant density: 10.9%

Figure 71: View of office layout 2 and its basic statistics

Layout 2 has two layers of circulation - the main public corridor that wraps around the core, and a semi-private corridor that wraps around the workstation area and connects it to the main corridor. Hence, there is sufficient visual privacy and acoustic isolation from the public spaces. In between the two corridors, focus rooms and collaboration spaces are nestled creating an acoustic buffer. The workstation area is split into smaller areas of 30-seating work spaces connected through a breakout area. The walls of the breakout area are lined with acoustic felt to contain the sound propagation between work areas. Within a work area, rows of workstations are separated by movable whiteboards to create some acoustic privacy. The proximity of workstations in this layout is much closer than layout 1, and hence the occupant density is slightly higher than layout 1.

6.2.1 Baseline scenario

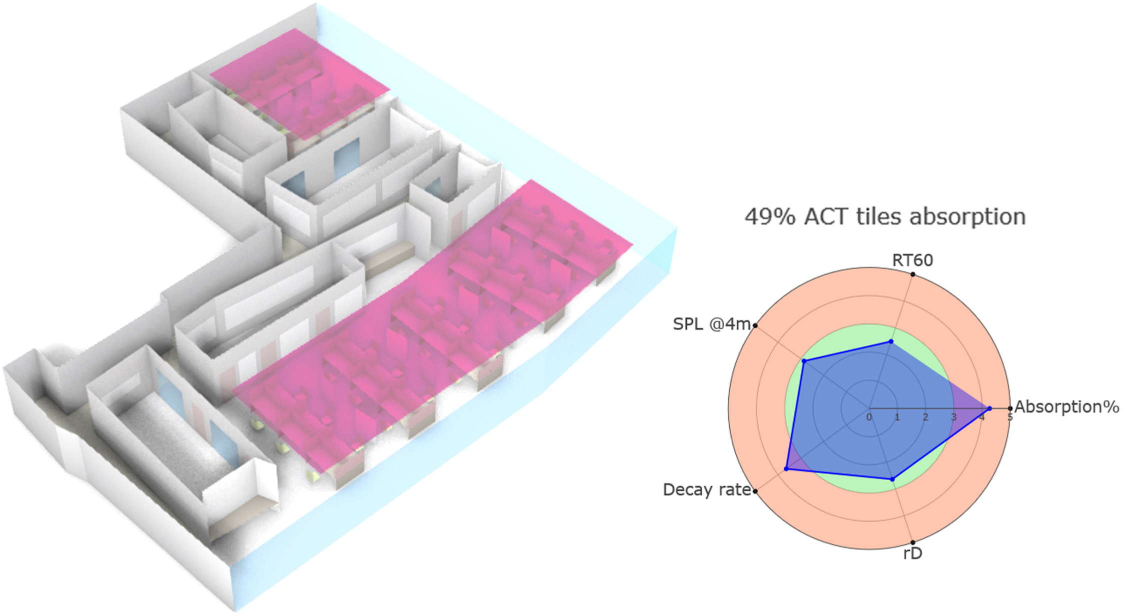

Figure 72: *View of the baseline scenario with highlighted acoustic ceiling tiles and its spider plot rating*

The baseline scenario of layout 2 is given in figure 72. The desk partitions are made of acoustic material with 0.45m of glass at the top. The highlighted rectangles are acoustic ceiling tiles at 2.3m from the floor level concealing the duct work and electrical wiring above. 49% of the workstation area is covered by the acoustic ceiling tiles. A band of painted gypsum ceiling runs along the perimeter in plane with the rectangular tiled area. This low-height false ceiling over the workstation zone works well in maintaining the acoustic parameters within the ISO's target range except for the spatial decay parameter, as depicted in the spider chart.

6.2.2 Improvements with HR panels

Again, two sets of improvements are performed on this layout. The height of the desk partition is maintained the same but the material of the whole partition is switched to fabric encased foam infill. A successively increasing area of HR panel distributions is designed to study the optimum area of tilted HR panel absorbers. The same height vs. area of absorption matrices are used for studying the trends and each scenario from this matrix is ranked using Pareto front sorting. The area of the panel distributions and the matrices are given in Appendix J. In the Pareto front results (see figure 73), approximately one-fourth of the scenarios fall within the ISO's target range for distraction distance. This portion is lesser than the one observed in layout 1 and can be attributed to the increased occupant density in layout 2. For the same reason, the spatial decay values of the candidate scenarios are marginally higher than the values attained in the improved layout 1. Though these values do not fall within the ISO's target range, they are acceptable. The candidate scenarios are further explored through spider graph acoustic rating (refer figure 74).

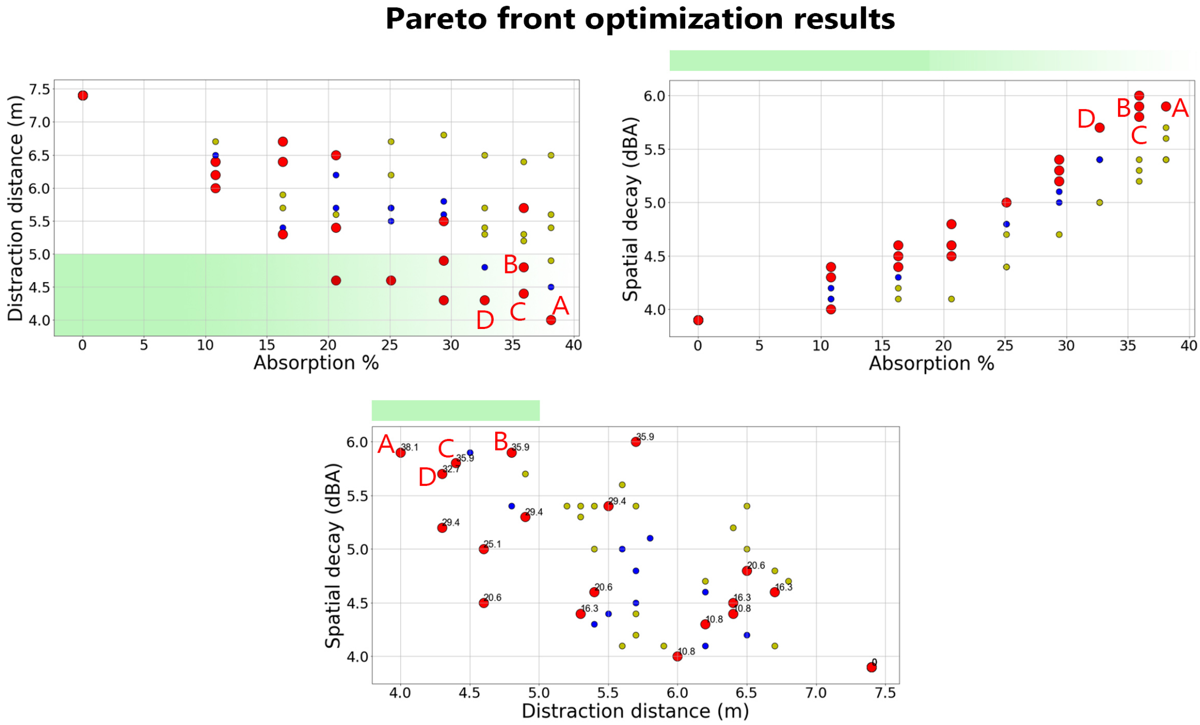

Figure 73: *Pareto analysis of the different HR panel configurations*

Three different areas of absorption are in the candidate solution set - 32.7% (Scenario D), 35.9% @2.1m height from the floor (Scenario C), 35.9% @2.3m height from the floor (Scenario B), and 38.1% (Scenario A). All the scenarios have satisfactory values in each of the parameters except in spatial decay. The spatial decay improves with increasing area of absorption, but both the scenarios A (38.1%) and B (35.9%) exhibit similar spatial decay values. Scenario B is the best-case scenario because the HR panels are hung at 2.3m from the floor which emulates the baseline scenario. Also, in the other scenarios, the panels are placed at 2.1m height from the floor level which is not permissible as per the standards given in the IBC. Figure 75 shows the layout's improved case with scenario B HR panel distribution.

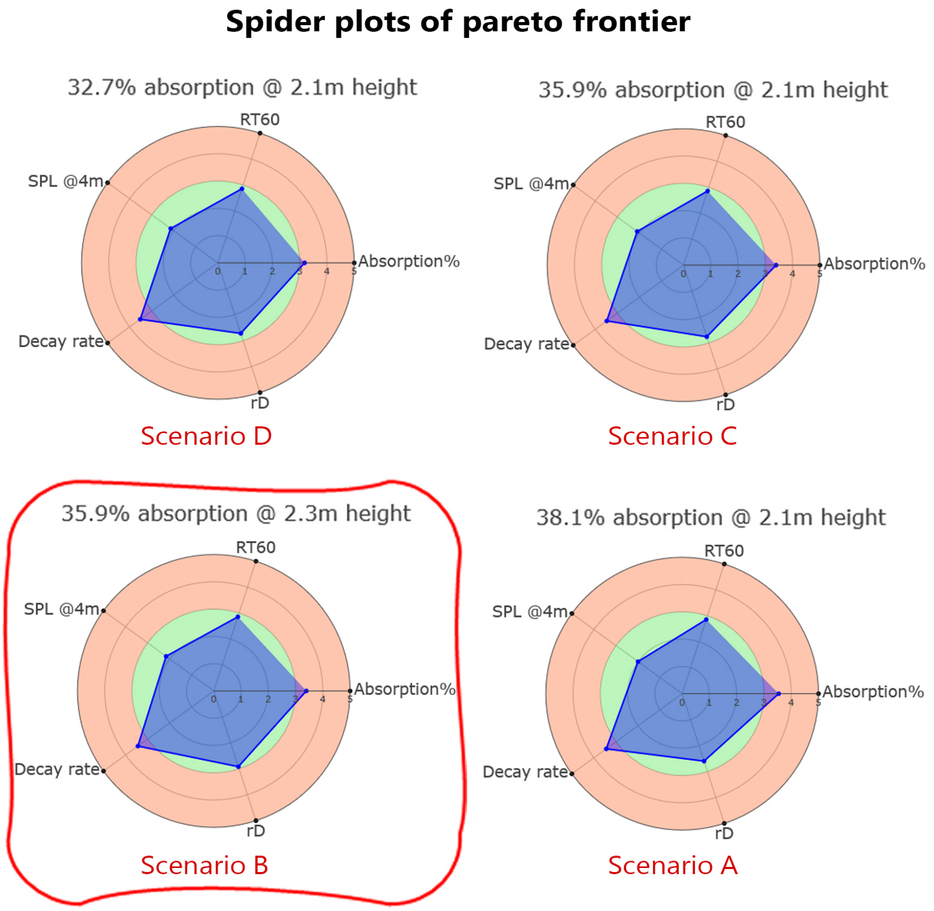

Figure 74: *Spider plot analysis of the Pareto scenarios*

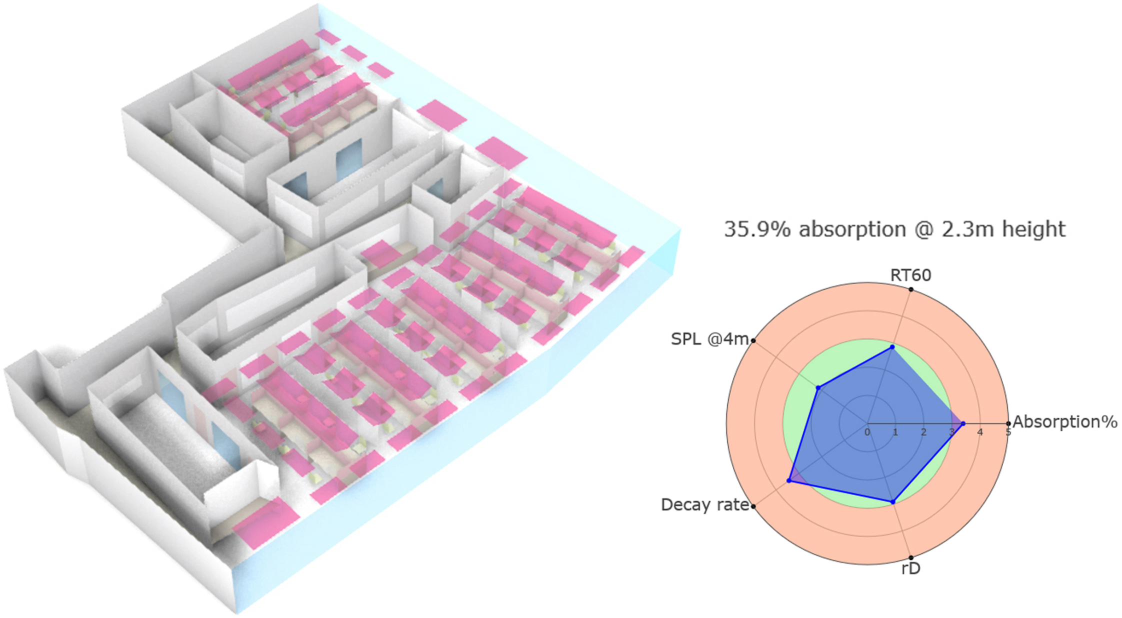

Figure 75: *View of the best-case scenario with highlighted HR panel configuration and its spider plot rating*

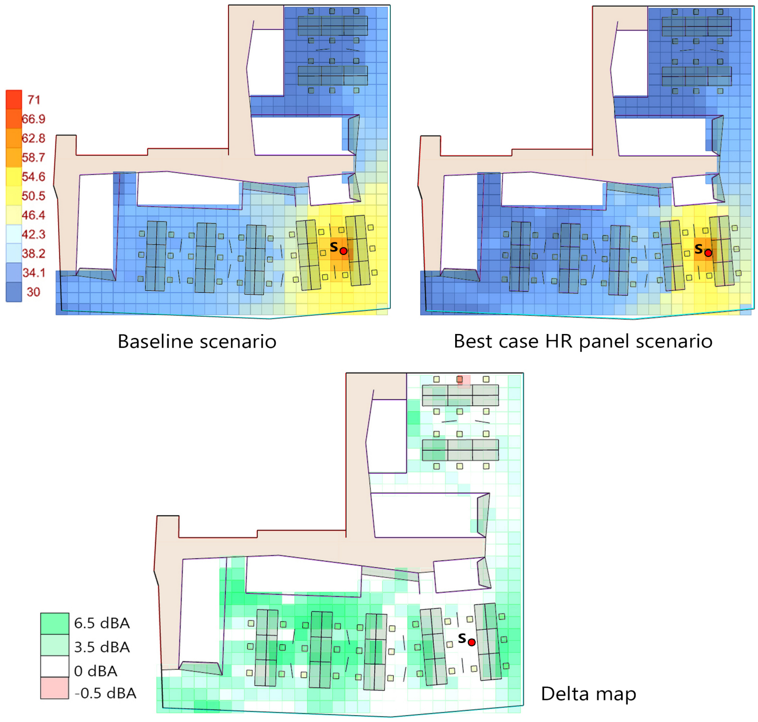

Baseline scenario

Best case HR panel scenario

Delta map

Figure 76: *Sound energy distribution in the baseline scenario and the best-case HR panel scenario and their delta map*

The sound pressure distribution in the layout from a single source speaker is compared between the two scenarios - the baseline case, and the improved case with HR panels. The best-case scenario performs well in containing the speech sounds from propagating to other workstations, compared to the baseline scenario. This is highlighted in the delta map which shows the energy differences between the two. Green zones, which marks the highest energy difference, are observed one workstation bay away from the speaker with an SPL drop of up to 6.5dBA. The area that is two workstations away from the speaker is completely shielded from the intruding speech sounds. This layout has sufficient buffer spaces so that speech originating from one work zone does not percolate into the adjoining workspace. This holds even when there are two simultaneous speakers in each work zone (figure 77). The design of this open office hinders the easy propagation of sounds to other zones. When a third speaker is introduced in the corridors, the acoustic quality in the work zones does not deteriorate much due to sufficient screening.

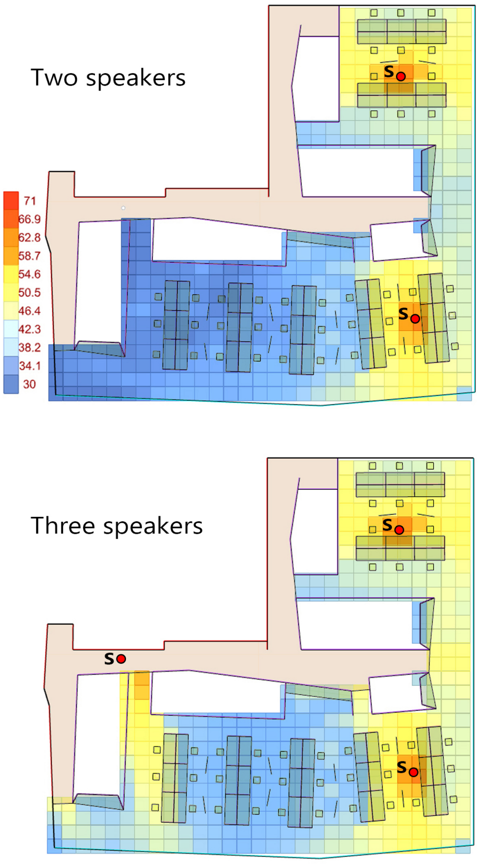

Two speakers

Three speakers

Figure 77: *Multiple speakers*

6.3 Office layout 3

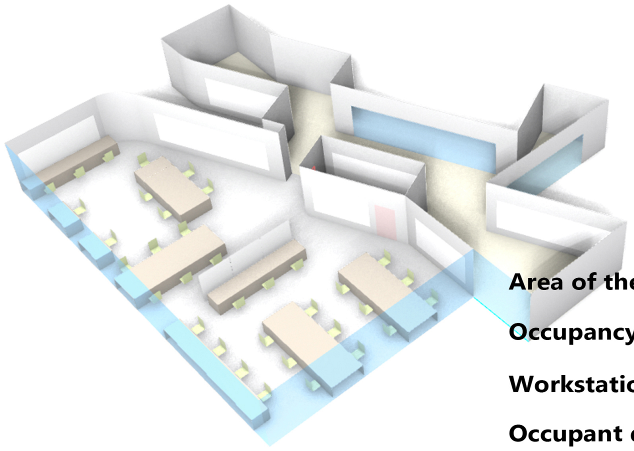

Area of the workstation area: 198.12 sqm

Occupancy of this work area: 35 people

Workstation area per person: 5.66 sqm/person

Occupant density: 17.7%

Figure 78: *View of office layout 3 and its basic statistics*

In layout 3, there are two types of work spaces - collaborative work space and private work zones. The private work zone is separated from the rest of the circulation area with just one entry point. Hence, it is visually and acoustically isolated from the public spaces. Pockets of collaborative work space branch out from the circulation area. The conference and meeting rooms are centralized for access from multiple private work zones while focus and phone rooms are localized and they create an acoustic buffer between the private work zone and the main circulation area. Within the private work zone, groups of 3 to 6 workstations are grouped together without any desk partitions between them. In comparison to the previous case studies, the occupant density is significantly higher.

6.3.1 Baseline scenario

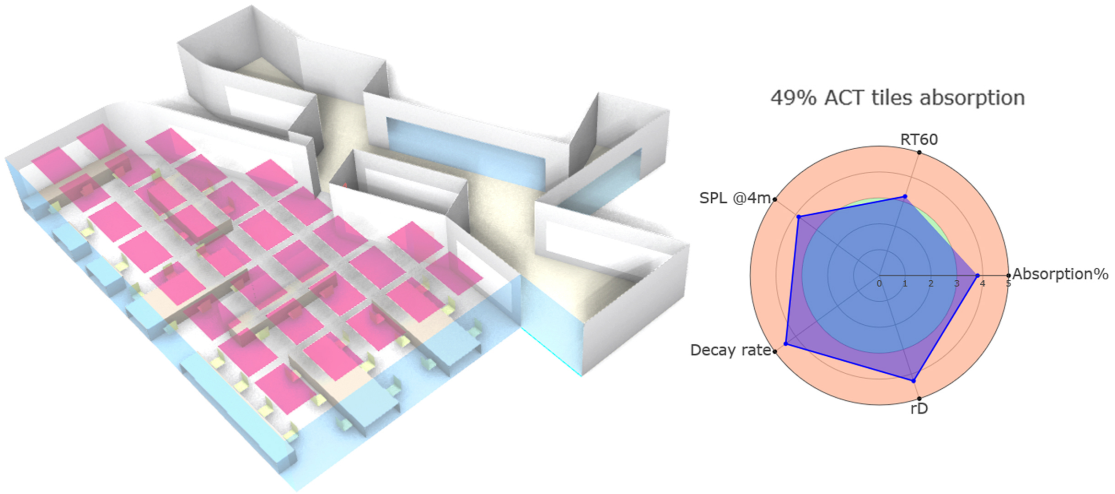

Figure 79: *View of the baseline scenario with highlighted acoustic ceiling tiles and its spider plot*

The baseline scenario of layout 3 is shown in figure 79. The highlighted rectangles are porous ceiling tiles adhered to the ceiling, and the duct work and electrical wiring run below these absorbers. 49% of the workstation area is covered by the acoustic ceiling tiles. Apart from these absorbers, there are no other absorptive surfaces in the space – no desk partitions or acoustic liners on the walls. And with the occupant density of the space, all the acoustic parameters fall outside of the ISO's target range as depicted in the spider chart.

6.3.2 Improvements with HR panels

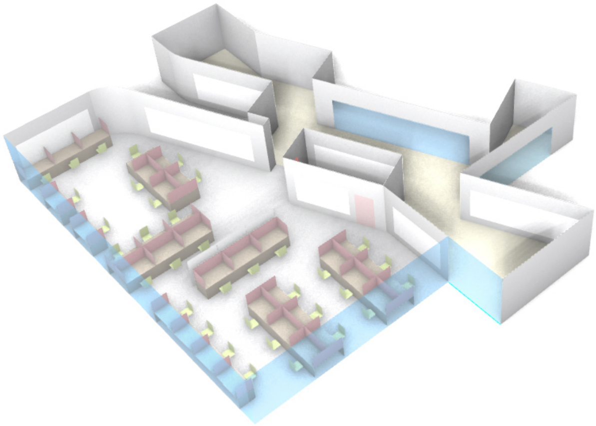

Figure 80: *Desk partitions are included to improve the sound attenuation in the open office layout 3*

Two sets of improvements are performed on this layout. First, desk partitions of height 0.6m made of fabric encased foam infill are included to improve the sound attenuation in the space (see figure 80). Second, different tilted HR panel distributions of successively increasing in area are designed to study the optimum area of absorption required for improving the acoustics. The same height vs. area of absorption matrices are used for studying the trends, and each scenario from this matrix is ranked using Pareto front sorting. The area of the panel distributions and the matrices are given in Appendix J. In the Pareto front results as shown in the charts (see figure 81), none of the solutions fall within the good acoustics zone (green area). This can be attributed to the higher occupant density compared to the other two layouts. For the same reason, the spatial decay values of the candidate scenarios are marginally higher than the values observed in the improved Layout 2 and Layout 1. Hence, the higher the occupant density, larger is the spatial decay (positive influence), and larger is the distraction distance (negative influence). Though none of the candidate solutions fall within the ISO's target range, solution A is an acceptable scenario.

The spider chart acoustic rating of all the candidate solutions are given in figure 82. The candidate solution set include 36.3% @2.1m height from the floor (Scenario D), 40.6% @2.1m height (Scenario C), 40.6% @2.3m height (Scenario B), and 46% @2.3m height (Scenario A). All the scenarios have satisfactory values in each of the parameters, except in distraction distance. Both the spatial decay and the distraction distance improve with increasing area of absorption. So, scenario A which has 46% area of HR panels at 2.3m height from the floor level has a better rating than the acoustic rating achieved in the baseline case. Though the area of coverage of the absorbers in scenario A and in the baseline case are similar, scenario A is preferred as it performs well in all the acoustic parameters except in distraction distance.

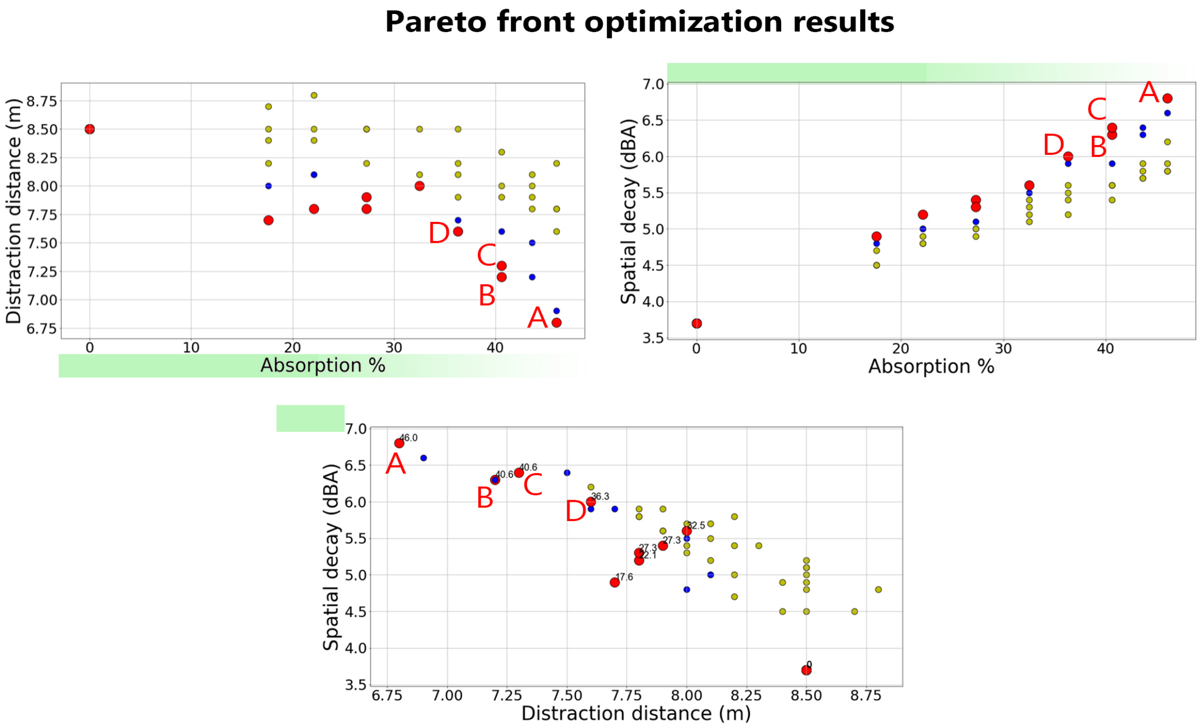

Figure 81: Pareto analysis of the different HR panel configurations

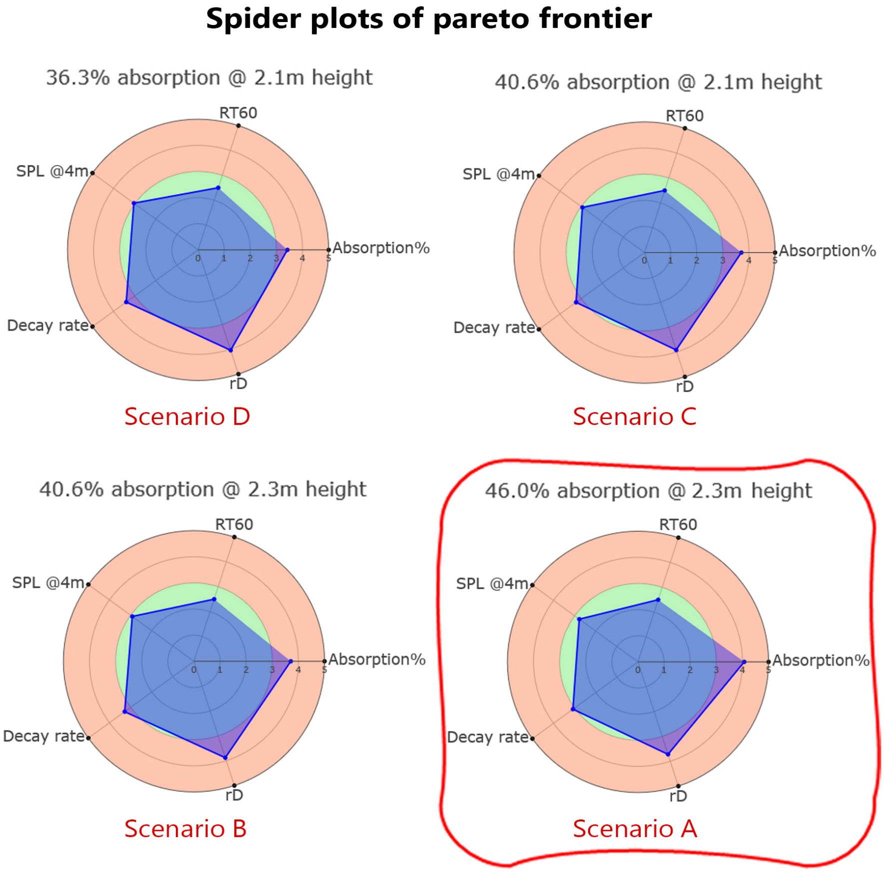

Figure 82: Spider plot analysis of the Pareto scenarios

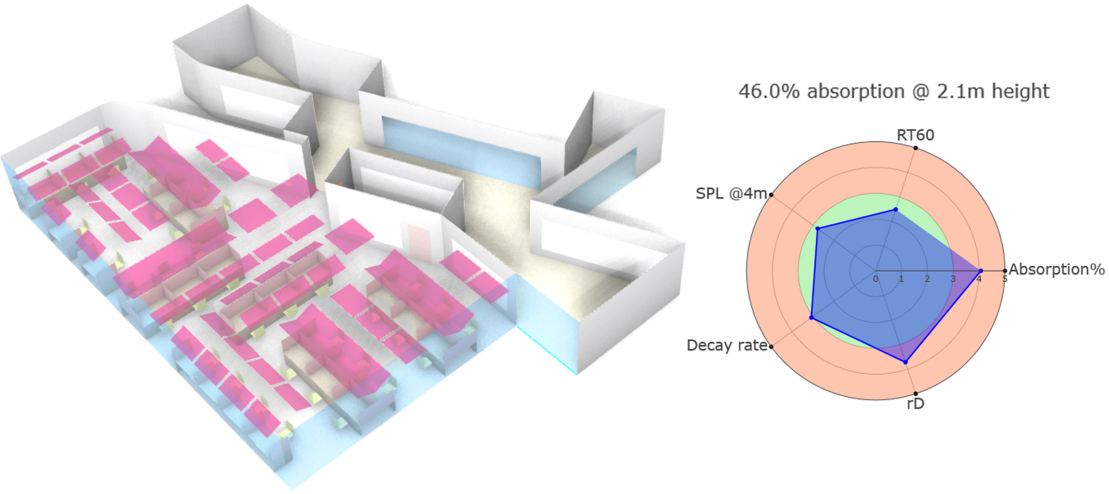

Figure 83: *View of the best-case scenario with highlighted HR panel configuration and its spider plot rating*

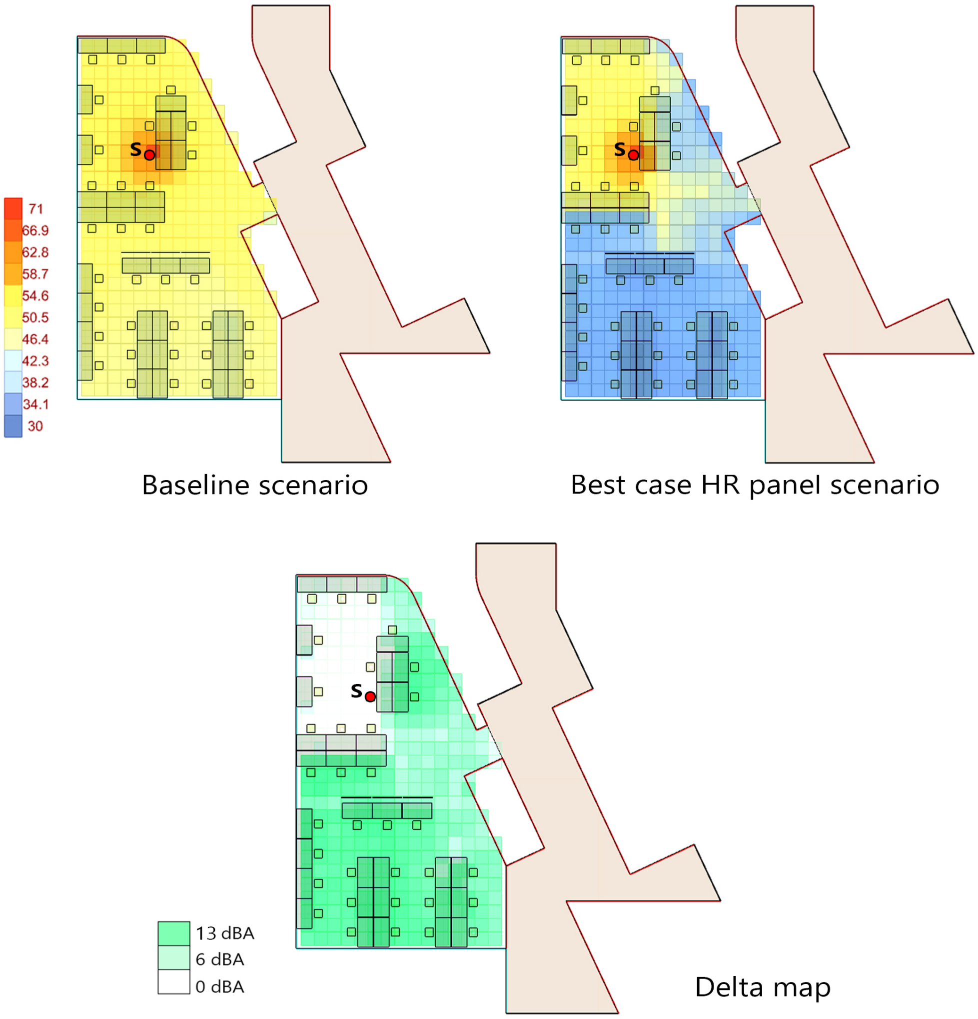

Figure 84: *Sound energy distribution in the baseline scenario and the best-case HR panel scenario and their delta map*

The sound pressure distribution in the layout from a single source speaker is compared between the two scenarios - the baseline case, and the improved case with HR panels and desk partitions. In the baseline scenario, due to the lack of sufficient absorbers in the space, the sound intensity does not reduce to the comfort levels (depicted by shades of blue in the sound distribution map). In the improved scenario with tilted HR panels, the speech sounds are contained well. The combination of the tilted panels and the desk partitions help in limiting the propagation of sound to the next set of workstations. However, compared to the other two layouts, the number of people affected by a single speaker is more because of the higher occupant density in this layout. The energy difference between the two scenarios is plotted in the delta map in which the green zone depicts the highest energy difference. Apart from a couple of workstations around the speaker, the rest of the workstations are sufficiently shielded and an SPL drop of up to 13dBA is observed. This is a noticeable difference, as noticeable as not having to sit next to a printer. However, if there are two simultaneous speakers in the improved scenario of this workspace, most of the employees fall in the distraction zone as they are all closely placed (see figure 85). Hence, in the design of the open office, careful consideration of the occupant density, along with the location and amount of absorption, is necessary to ensure an acoustically comfortable workspace.

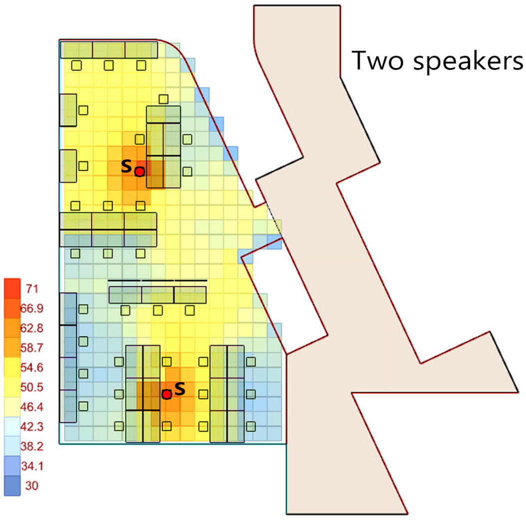

Figure 85: *The best-case HR panel scenario with simultaneous speakers*

6.4 Observations

All the three case studies have different occupant densities and different workplace geometries. Though the geometry of the space plays a role in highlighting certain room modes, the ray-tracing model does not account for the standing waves and hence the geometrical contribution to the acoustic comfort was not determined. The occupant density has an impact on the acoustic comfort - higher the occupant density, larger is the spatial decay (positive influence) and larger is the distraction distance (negative influence). Moving from layout 1 to layout 3, the occupant density increases and the distraction distance of the best-case scenarios migrates from good zone to the bad, while the spatial decay rate exhibits the opposite trend. Hence, to achieve optimal acoustics in an open office, the occupant density will have to be carefully considered. Apart from the occupant density, the arrangement of the workstations is also important. Moving from layout 1 to layout 3, the segmentation of the work space intensified. In layout 1, the work area was one large block of open space while in layout 2, the work zone was split into two portions connected through a breakout area. In layout 3, the private work zone is an enclosed space with one entry point. Comparing the spatial sound distribution quality of the case studies, layout 2 performs well in restricting the speech sound propagation in the space. Even with simultaneous multiple speakers in the space, the other employees are sufficiently screened. This can be attributed to the acoustic buffer created by the segmentation of the workspace.

Other than the physical design aspects of an open office, the arrangement, location, and orientation of the ceiling absorbers impact the acoustics of the office. All the improvement scenarios with HR panels perform better than the baseline scenario with acoustic ceiling tiles. This can be attributed to a combination of variables - the type of absorber, its arrangement, and its orientation with respect to the workstations. In the improvement scenario the HR panels, which are low to mid-frequency broadband absorbers, are equally distributed over the workstations and are tilted to face the speakers rather than face down. This combination works well in absorbing the speech signals and in containing the sound from propagating to other workstations. Improvement of up to 12 or 13dBA is possible with the tilted HR panel configuration, compared to the baseline scenario with flat porous tiles. This is a noticeable drop in the spatial sound intensity – as noticeable as not having to sit next to a printer.

7 Application Considerations - Materials and Fabrication

7.1 Recycled objects as resonators

Empty plastic bottles (PET bottles) resemble a Helmholtz resonator. The mouth of the bottle acts as the neck of a resonator when left open. Though a wide range of frequencies could not be targeted with these standard-sized bottles, they could be retrofitted to achieve the desired results. A mouthpiece with embedded neck could be fabricated with varying neck lengths to attach to these standard-sized bottles (refer fig 86). This system acts as a resonator with an embedded neck (as described above) and the length of the neck determines the frequency at which the bottle-resonator performs its best. This mouthpiece could also be designed as a conical neck or a perforated neck plate to achieve a variation in the sound frequencies absorbed.

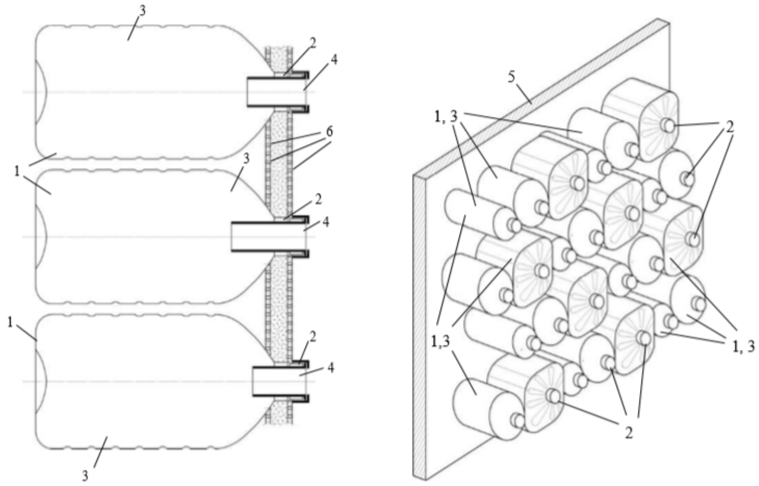

Figure 86: *Recycled plastic bottles as a resonator absorber (Fesina et al. 2017)*

Scrap wood can be used to mill out a resonator. A resonator made of wood has an added advantage of being a diffusive surface as well. Figure 87 shows a resonator array made of scrap wood. The varying heights of the wood make it a diffuser and the milled out resonator cavity makes it absorptive in the low-frequency. The natural voids between the wood resonators act as a quarter-wave resonator (a simple pipe or a tube resonator closed at one end). This broadens the absorption bandwidth of the resonator system. In the same system, another cavity connecting all the milled out cavities is attached to the back end of this system. Hence, now each resonator, has two connected cavities of air providing the spring effect (called a dual Helmholtz resonator). This improves the sound absorption of the resonator panel.

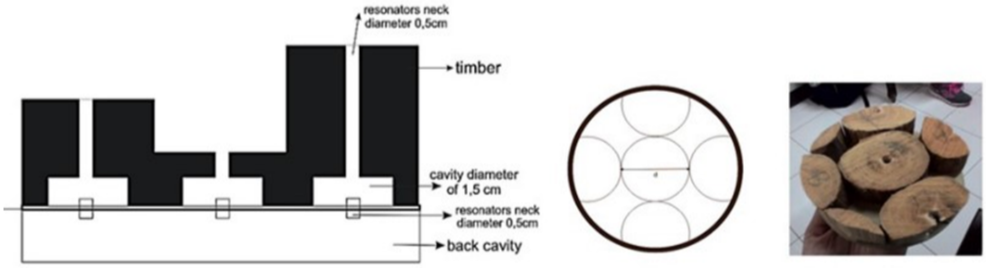

(a) (b) (c)

Figure 87: *Scrap wood diffuser and absorber (Romadhona et al. 2017)*

7.2 Acoustic metamaterials

With the advent of 3D printing technology, more complex geometry for controlling, directing, and manipulating sound waves can be fabricated - called acoustic metamaterials. The precision and customization of geometry achieved with 3D printing have introduced sub-wavelength resonators, whose thickness are smaller than the wavelength of sound. Sub-wavelength resonators have pioneered developments in compact broadband variants of Helmholtz resonators. An example is depicted in figure 88. It is a spiral metamaterial that is capable of achieving perfect absorption at the resonant frequency. The sound waves are damped in the long winding path embedded with this structure through visco-thermal losses. A panel comprising of coplanar and coiled tubes effectively absorbs low-frequency sound with a thickness of less than one percent of wavelength (Cai et al. 2014).

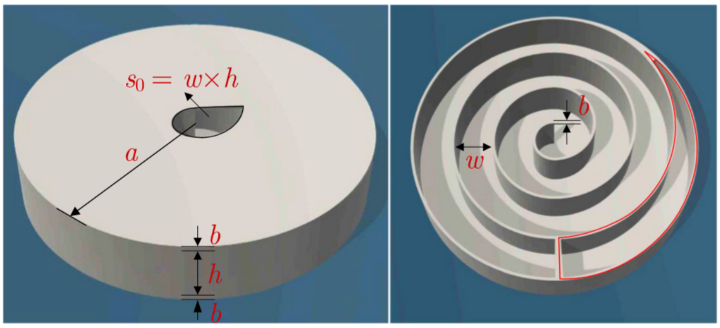

Figure 88: *Spiral sub-wavelength resonator (Huang et al. 2019)*

A traditional Helmholtz resonator's cavity is quite bulky for attenuating low frequencies and has a narrow bandwidth of absorption. And a panel composed of multiple such resonators would be deep and wide which might make their wide application impractical. A sub-wavelength resonator inspired by the dual Helmholtz resonator construct, and made possible by 3D printing, is given in figure 89. The neck and the first cavity chamber in this split-ring resonator are folded in within the larger cavity, thus saving space without compromising its efficiency. The absorption performance of this resonator and a classical Helmholtz resonator of the same resonant frequency is compared in figure 90.

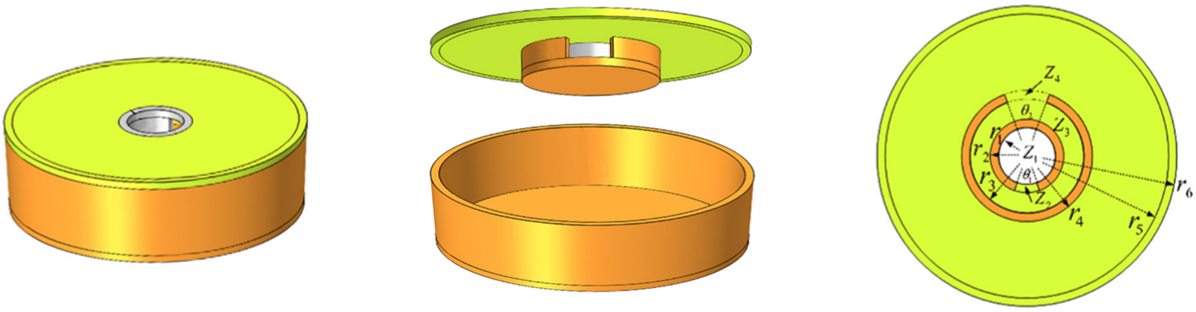

(a) Exterior view (b) Exploded view (c) Cross-sectional view

Figure 89: *Sub-wavelength acoustic resonator with split ring neck (Yuan et al. 2019)*

The overall height of the split ring neck resonator designed to achieve the resonant frequency of 196Hz is 22mm and a width of 36mm (Yuan et al. 2019). The width of the classical Helmholtz resonator used for comparison is maintained the same. However, to achieve a similar resonant frequency, the neck length is set to 86mm and the cavity depth is 30mm (overall height is 116mm). Hence, for the same resonant frequency, the split ring neck has a better absorption coefficient and a wider bandwidth of absorption at less than one-fifth of the overall height of the classical Helmholtz resonator. Thus, the sub-wavelength resonators prove to be highly beneficial in the design and fabrication of a sound absorptive panel composed of resonators. The resonator's performance can be made broader with the inclusion of a thin lossy medium which further improves the visco-thermal losses (Lee et al. 2019).

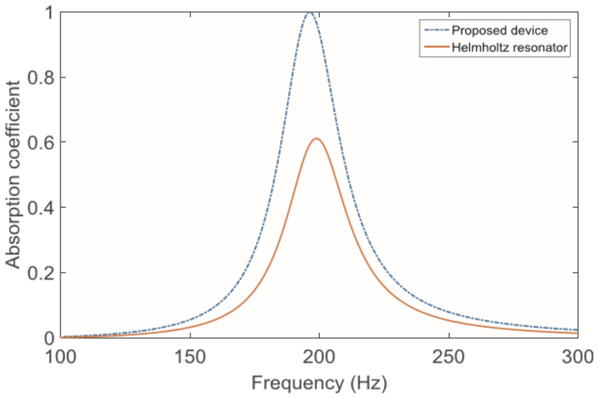

Figure 90: *Absorption performance comparison between the split ring neck resonator and a classical Helmholtz resonator (Yuan et al. 2019)*

8 Experimentation

To validate the absorption performance of a HR panel obtained analytically, experiments were conducted in an impedance tube setup. ASTM standard test method for impedance and absorption of acoustical materials using two microphones was executed for this experimentation. Though the reverberation room method is an apt method for testing the HR panel's sound absorptive properties, the timeline of this research, fabrication funding, and force of nature (COVID-19 pandemic) thwarted the efforts. The impedance tube method will not be able to test the absorption performance of the whole HR panel discussed in section 4.7 but rather test smaller sections of it. And the results from the impedance tube experiment is only for normal incidence of sound and not for the diffuse sound field which is usually the case in open offices.

The impedance tube method is quite straightforward. A rectangular or circular tube is enclosed on either end with a source and a resonator panel sample backed by a metal plate. A broadband source produces sound waves that are made planar in the long tube. Microphones are inserted into the walls of the tube to record the forward and backward planar waves to measure the loss in the sound pressure level in the returning waves. The entire setup is made airtight to prevent any leaks and the metal backing plate ensures that the forward planar waves are not transmitted outside. For this research, an impedance tube was custom made to fit the size and shape of the sample and its frequency requirements. The impedance tube was built in collaboration with the Department of Physics at the Central Washington University.

8.1 Construction of the impedance tube

A square cross-section is chosen for the body of the impedance tube to snugly fit the sample piece within it. The walls of the impedance tube are made from 3/4" (0.019m) Medium density overlay (MDO) board and finished with a smooth coating on the interior side to make them non-porous. The interior edge length is 0.2m - derived from a basic working frequency range (F_l to F_u) for this research. The relationship is edge length $< 0.5 * c/F_u$ and accordingly, to have the working frequency flexibility up to 850Hz and to maximize the sample size, the edge length is fixed at 0.2m. Figure 92 shows the construction details of the impedance tube. The length of the main tube is 1.2m long of which 0.6m (or three times the edge length) is the minimum spacing requirement between the source and the microphones to allow for the sound waves to develop into planar waves. The minimum spacing requirement between the microphones and the HR sample (an asymmetrical sample) is two times the edge length. Factoring in all these minimum requirements, the length of the tube is kept at 1.2m. A smaller length extension is fabricated with the same edge length to house thick samples so as not to disrupt the minimum spacing requirements. The tube's ends were equipped with flanges to connect to the tube to the different components of the setup. The tube is closed on one end with a metal backing plate of 0.02m to reflect back all the on-coming planar waves.

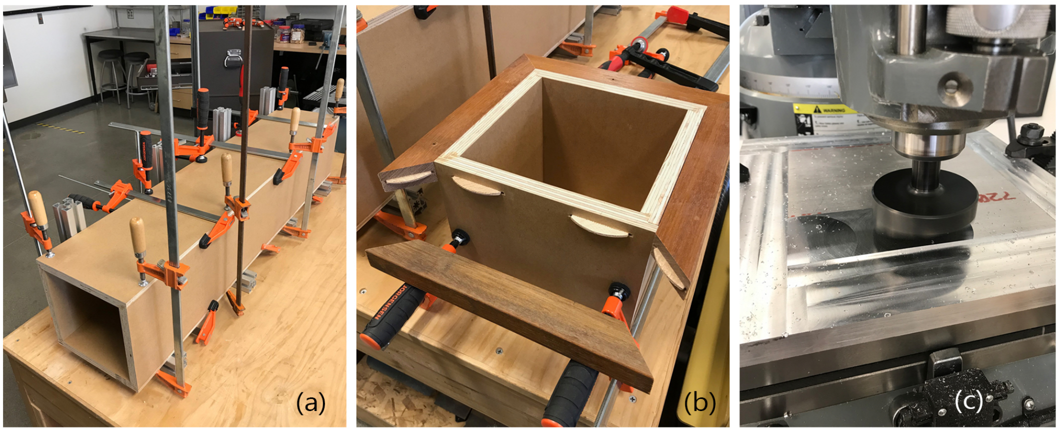

Figure 91: *Impedance tube: (a) Square cross-section tube; (b) Flanges at the ends of the tube; (c) Metal backing plate*

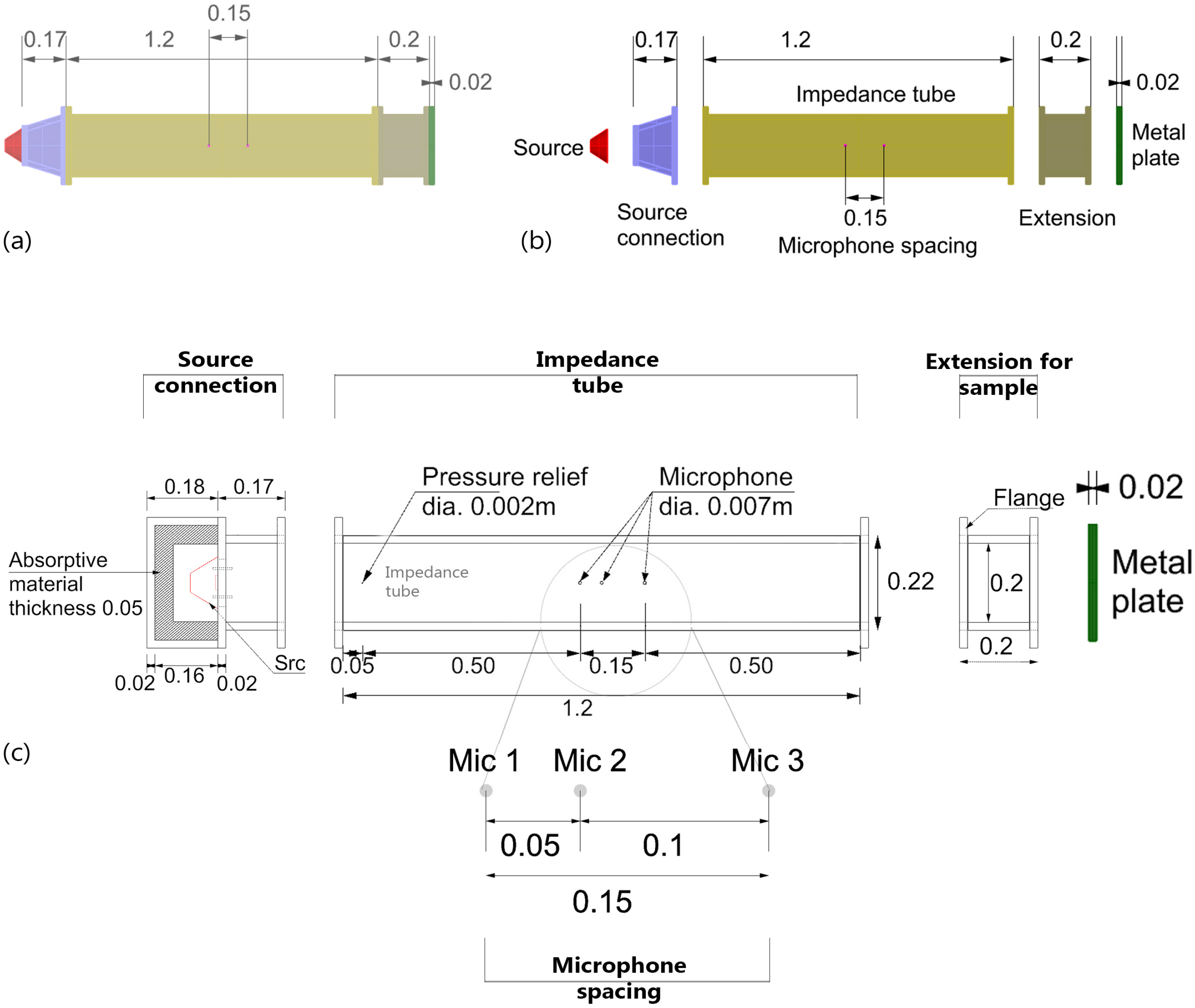

Figure 92: *Constructional details of the impedance tube: (a) Conceptual impedance tube setup; (b) Different components of the impedance tube; (c) Detailed section with dimensions*

8.1.1 Source and its adapter

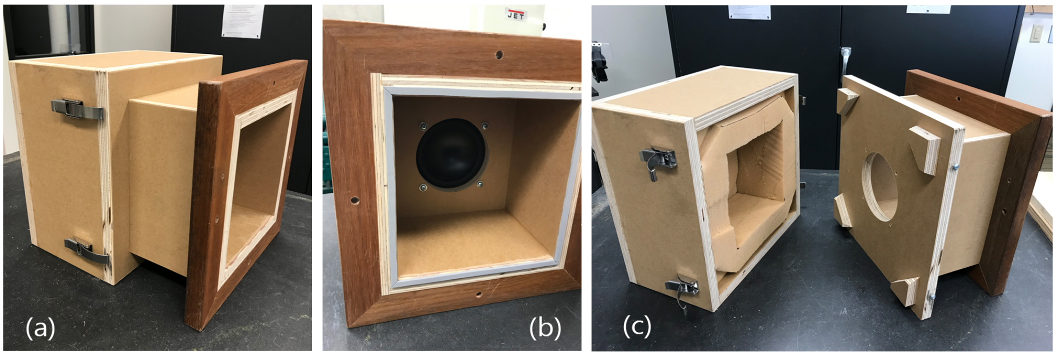

Figure 93: *Source connection: (a) View of the source adapter; (b) The adapter's flanges and the thin foam lining around the edges; (c) Foam filled source enclosure*

The source is separated from the main impedance tube to reduce the structure-borne sound excitation in the tube. The source adapter has a thin foam lining around the edge of the inner tube for isolation purposes. The source chosen for this experiment is Dayton Audio ND140-8 5-1/4" driver (0.133m diameter). It has an extended range from 54 Hz to 8 kHz performance. Since it is a direct radiator, it needs an enclosure filled with absorptive material to ensure the air-tightness of the tube. The source has an additional extension of about 0.17m (distance from the source location to the adapter's flanges) to further aid in the development of planar waves. A 0.002m hole is drilled into the main tube closer to the source as a pressure relief.

8.1.2 Microphones and their spacing

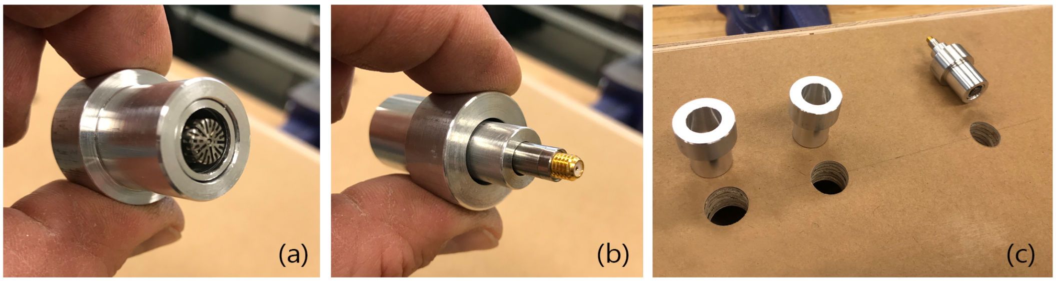

Figure 94: *Microphone holder: (a) Front view of the microphone head and its holder; (b) Rear view showing the electrical connection of the microphone; (c) Microphone locations on the main tube*

Typically, two microphones are used in this experiment method and the spacing between the microphones plays a major part in setting the lower limit of the working frequency range. The microphone spacing also affects the quality of the results. Hence, in this impedance tube, three microphones are used to favor both high-frequency and low-frequency measurements. The maximum microphone spacing is limited to 80% of the upper limit of the working frequency range. Therefore, the distance between the extreme microphones is 0.15m, and the third one is placed at one-third distance from the microphone closest to the source. GRAS 46BD 1/4” (0.007m diameter) microphones are used.

8.1.3 HR panel samples

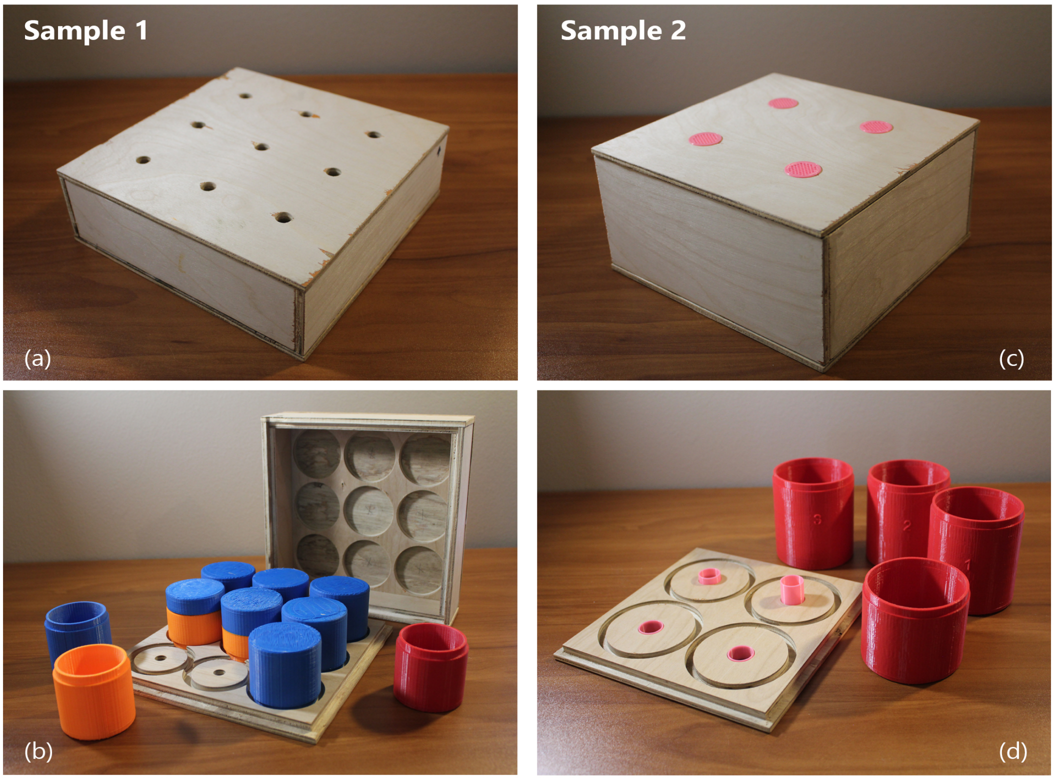

Figure 95: *Panel samples: (a) Mid frequency sample 1; (b) Interior view of sample 1; (c) Low-frequency sample 2; (d) Interior view of sample 2 showing the neck extensions into the cavity*

Two sample pieces were fabricated for the experiment - Sample 1 has resonators working in the mid frequencies, and Sample 2 has large resonators for low frequencies. The resonators were 3D printed and the encasing box was milled out of plywood. In both the samples, the resonators are embedded into the top and bottom plywood plates through friction, which ensures air-tightness and also allows for interchangeability. The top plates are removable to allow the switching of resonators. In sample 1, the resonators are sized to achieve peak absorption at mid frequencies and the necks are drilled into the 1/2” (0.013m) top plate. The relatively small size of the resonators allows nine resonators to be fitted within a 0.2m x 0.2m panel. The resonators are replaceable in this sample. In one iteration all the resonators are identical, to validate the correctness of the resonant frequency calculation. In another iteration just one resonator is replaced with a dissimilar resonator, to validate the mutual interaction between varying resonators. Since Kim’s mutual impedance equation (Eqn. 4.15) does not account for the arrangement of the resonators, the dissimilar resonator in the sample panel is moved around to verify the impact of arrangement on the absorption performance of the array.

Sample 2 is built to test a low-frequency panel, and requires resonators with bigger cavities. Compared to sample 1, sample 2 has a lesser number of resonators, and is deeper to accommodate the low-frequency resonators. In this simple the resonators are attached to the top plate without any neck attachments, to verify the analytical formulas. In the next iteration hollow-neck attachments are inserted into the neck to model the embedded resonator type (discussed in section 3.3), which further reduces the resonant frequencies. In the final iteration the hollow-neck attachments are swapped with perforated neck attachments of the same length (discussed in section 3.4), which should widen the bandwidth of absorption. All the cases are compared to analyze the changes in the absorption performance, as predicted in the analytical results.

8.1.4 Completed impedance tube setup

Figure 96: *View of the completed impedance tube setup*

Figure 96 shows the completed impedance tube setup ready for calibration. All the flanges used for connecting the different components are maintained at the same height and hence are used as supports to prop up the setup. The possible areas of error accumulation in this setup include air leaks around joints, gaps between the tube and the mounted sample, increased pressure in the tube after sample mounting which might disrupt the microphone measurements, and structural vibrations from the source during the measurements.

8.2 Experiment's results

The experiment's results were recorded using the LabVIEW software and post-processed in MATLAB. On the recorded data, Fast Fourier Transformation (FFT) and transfer functions were applied to convert the electrical measurements into absorption performance curves. Further details of this process can be found in the ASTM standards.

8.2.1 Experiment set 1

In set 1, two configurations of sample 1 were measured. In the first configuration, all the resonators were identical, while in the second configuration one of the resonators was replaced with a dissimilar resonator. This was done to measure the difference that one dissimilar resonator can make. The results are given in figure 97. The red line shows the results from analytical predictions and the blue line denotes the experimentation results.

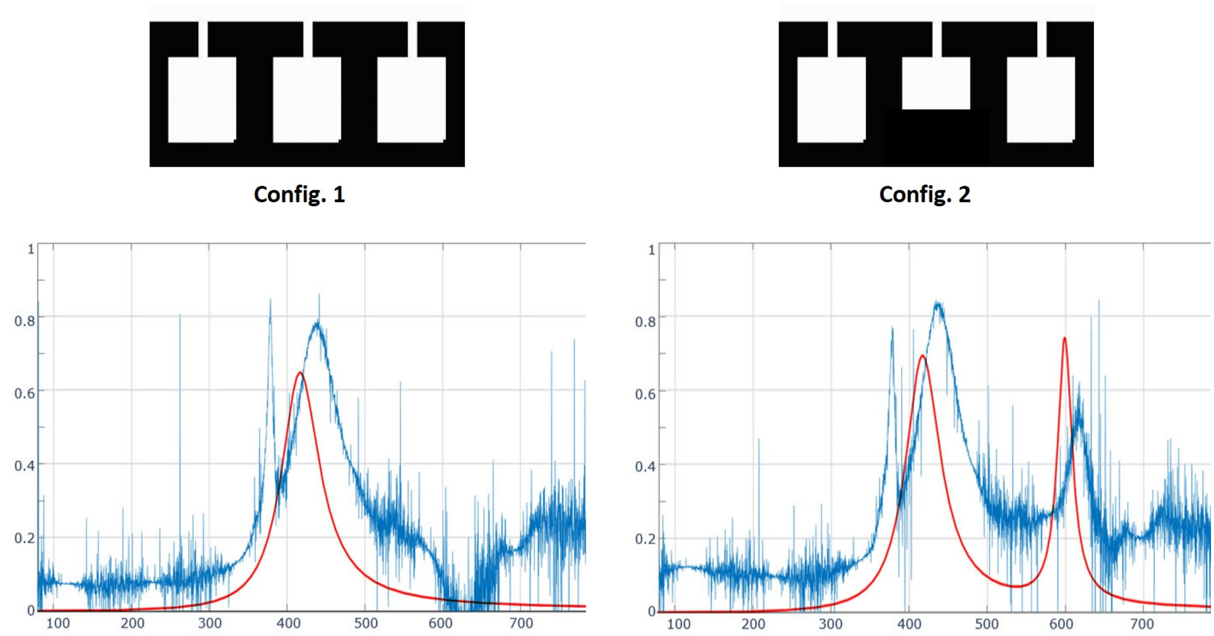

Figure 97: *The configurations used in experiment set 1 and their corresponding absorption performances–overlapped experiment results and analytical predictions*

Overall, there is a good agreement between the analytical predictions and the experiment results. A shift is observed between the two results, which could have been due to imperfections in the fabrication and the placement of the sample in the impedance tube. The measured values are also slightly higher than the predicted values which might be because of the absorptive properties of the sample's top plate. In the configuration 1, there is just one prominent spike in the absorption performance curve because all the resonators are identical. In the configuration 2, with just one dissimilar resonator, another spike corresponding to the resonant frequency of the dissimilar resonator is observed. However, the height of that spike is not as high as the prediction. The mutual interaction between the resonators can be observed in the valley between the two spikes. The experiment results show a better mutual interaction than the predicted behavior.

8.2.2 Experiment set 2

In set 2, three configurations by changing the relative position of the dissimilar resonator in sample 1 were measured to observe the variations induced by the arrangement of resonators. The results are given in figure 98. The red line shows the results from the analytical predictions, and the blue, green, and brown lines correspond to configurations 1, 2, and 3, respectively. Figure 98 shows the overlapped performances of configuration 1 and 2, and all the configurations. There is a marginal difference between the absorption performances of the three configurations.

Hence, Kim's mutual impedance equation (Eqn. 4.15), which does not account for the arrangement of the resonators, is a reasonable abstraction to calculate the absorption performance of an array of resonators. However, sufficient experimentation would have to be done on a larger panel of resonators to confirm the independence of the mutual impedance equation from the relative positions of the resonators.

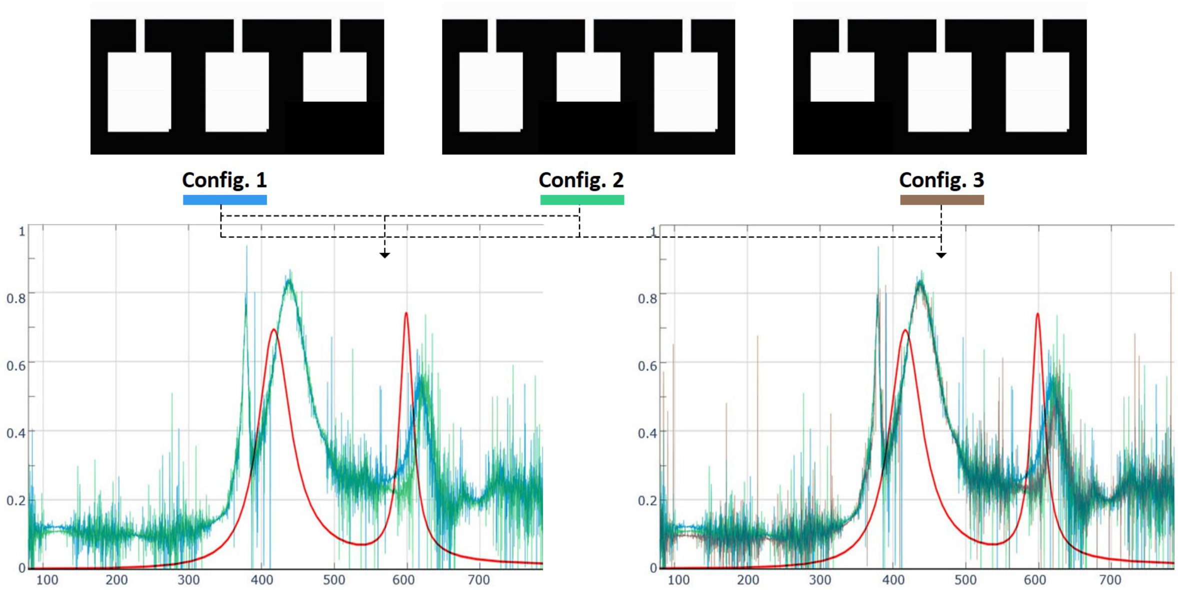

Figure 98: *The configurations used in experiment set 2, and the overlapped absorption performances of configuration 1 and 2, and all the configurations*

8.2.3 Experiment set 3

This set uses the sample 2 to test the efficiency and the accuracy in the predicted performances of embedded neck resonators. Hollow 3D printed necks of varying lengths can be inserted into the top plate of the sample without changing the resonators. Accordingly, the configuration 1 does not have any embedded necks (thus, a simple resonator geometry) and the configuration 2 has hollow-necks embedded into the resonators to compare the performances of both. Figure 99 shows the experiment results of both the configurations overlaid with the results from the analytical predictions (depicted through red lines). In configuration 1, though there are four resonators, the resonant frequencies are clumped together to form two spikes in the performance graph. These spikes are between 330Hz - 400Hz. While in configuration 2, the embedded necks lower the resonant frequencies of the resonators to below 350 Hz. And four prominent spikes can be observed in its performance graph as the lengths of the embedded necks are all different. The 200Hz spike corresponds to the resonator with the longest embedded neck.

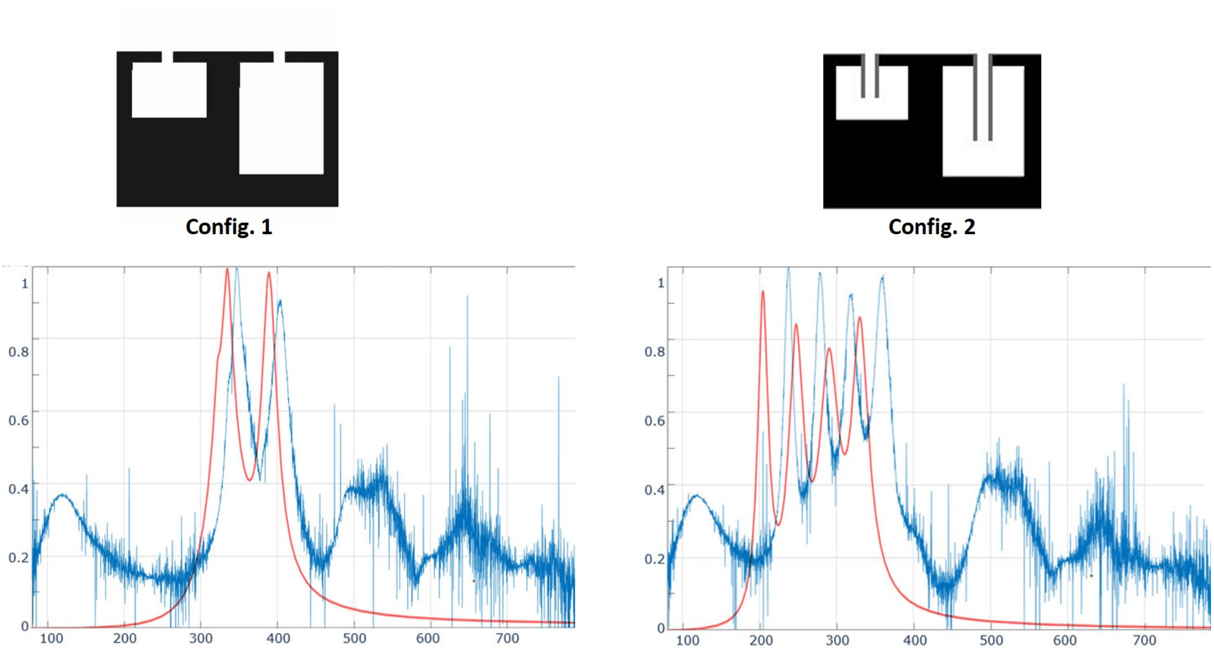

Figure 99: *The configurations used in experiment set 3 and their corresponding absorption performances–overlapped experiment results and analytical predictions*

Again, a shift is observed between the experiment results and the analytical predictions. In configuration 1, the shift is small, and could be due to imprecision in its fabrication. However, the shift observed in configuration 2 is relatively large and could be due to a combination of inaccuracies in fabrication and abstractions used in the analytical formulas. Also, the peak absorption values in the experiment results are higher than the predicted peak values.

8.2.4 Experiment set 4

In set 4, two variants of the embedded necks are explored in the sample 2. In configuration 1, hollow-necks are embedded into the resonators and in the other configuration, the hollow-necks are replaced with neck perforations of the same length to model additional resistance in the necks. The neck perforations have 48 cylindrical voids of diameter 2mm that run throughout the length of the embedded neck. Hence, the neck perforations are 48% porous and are completely 3D printed. Figure 100 shows the comparison between the performances of the two neck variants. In configuration 1, the resonant frequencies of the resonators are predicted to be in the range 200Hz - 330Hz, but the experiment results exhibit a range of 230Hz - 360Hz. This 30Hz shift could be due to error accumulation in fabrication or in the abstractions used in the analytical formulas. In configuration 2, the predicted resonant frequencies fall in the range of 150Hz - 250Hz and it matches well with the experiment results. The analytical formulas used are precise in the predictions. Although the resonant frequencies match, the peak values are lower in the experiment results in comparison to the predictions. This could be due to imperfections in the 3D printing of the neck perforations, as the size of the pores in the opening is small.

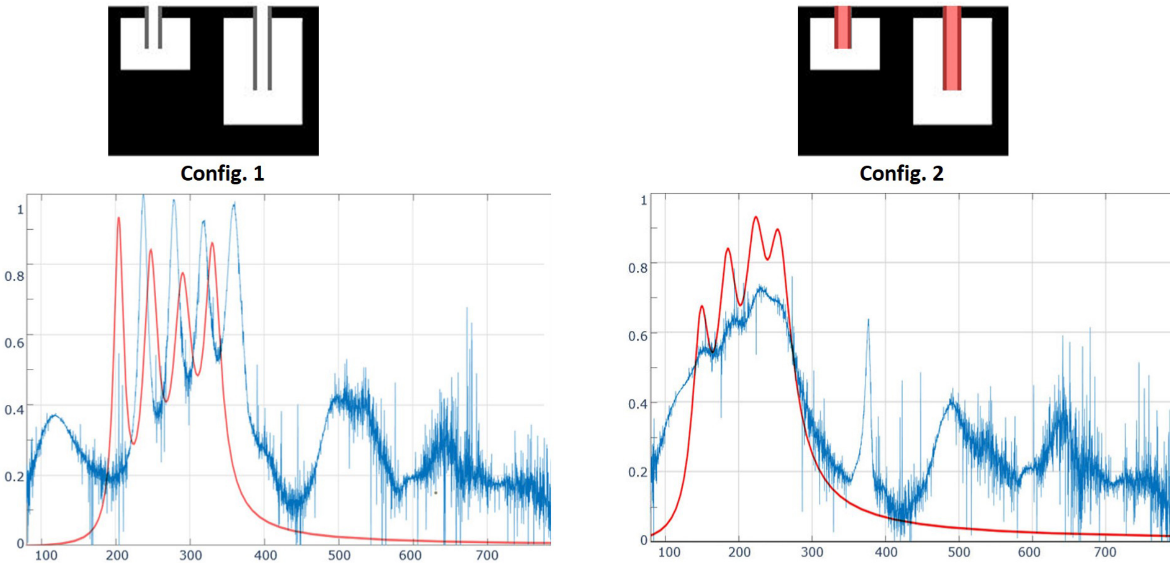

Figure 100: *The configurations used in experiment set 4 and their corresponding absorption performances–overlapped experiment results and analytical predictions*

The neck perforations (or additional resistance in the necks) have a two-fold advantage - they lower the resonant frequencies and improve the absorption performance in the valleys between the resonant peaks. However, due to fabrication constraints, the resonant peaks are not prominent in the experiment results. But, improvements in the valleys are noticeable in the configuration 2 graph in figure 100.

8.2.5 Limitations

Overall, the experiment results agree well with the analytical predictions. However, it should be noted that at the time of this thesis publication, the calibration of the impedance tube was incomplete. The calibration and the phase correction of the microphones are done with an absorptive foam wedge on one end of the tube instead of the reflective metal plate. In our calibration step, the foam wedge was not sufficiently absorptive and hence caused low-frequency roll-off and messiness in the frequency range above 900Hz. So, this step was skipped in all the measurements taken. But these experimental results are reliable as the microphones used are precise and have a very low offset percentage. Therefore, there will not be a large deviation from these results and the calibrated results.

Another consistent limitation observed in the experiment results is a sharp projection around 380Hz. This could have been caused by the resonance of the impedance tube itself, which acts as a quarter-wave resonator. The sharp projection should be eliminated by an appropriately executed calibration step. In general, the calibration step helps in removing the environment-dependent inconsistencies–the resonance of the impedance tube and the phase differences in the microphones. The calibration step will be re-worked and added to the measurements for the upcoming research paper publications.

9 Conclusions and discussion

Through this research, the potential application of Helmholtz Resonators in an open office is explored. Resonator panels are a “healthier” and a ”competent” solution for improving the open office acoustics. The major driving forces in the resonator panel design are to reduce the annoyance caused by the low frequencies and the intruding speech signals. And the panel’s application in room acoustic simulations proved to be beneficial, compared to acoustic ceiling tiles.

In the Helmholtz Resonator scale, the basic resonator geometry and a couple of simple modifications to that geometry were analyzed through analytical methods. With these geometries, resonators were designed to specifically attenuate the frequencies important for speech intelligibility. Resonators designed for the low frequencies were large and they take up a lot of space. However, acoustic metamaterials, made possible through 3D printing, have complex resonator geometry that is more compact and can achieve perfect absorption in low frequencies. Such complex geometries do not have an existing analytical method to derive their absorption performance. Still, they can be studied using Finite Element Analysis (FEA) simulations.

In the array of resonators scale, the coupling effect between the resonators gave the resonator panel a competitive advantage over porous absorbers. Various parameters of the panel design were varied to study their impact on the panel’s absorption performance. The spacing between the resonators is an important parameter that controls the positive impact of mutual interaction between the resonators. And with large low-frequency resonators in the panel, the compactness and the absorption performance of the panel diminishes. However, replacing the traditional resonators with the more advanced sub-wavelength resonators might solve this problem.

In the room-scale, geometrical acoustic simulations were run for studying the effectiveness of HR panels in the open offices. Three case studies were chosen to compare the results from its baseline case and from an improved case with HR panels. Tilted ceiling-hung HR panels attained good acoustics for a smaller absorption area coverage, compared to the acoustic ceiling tiles used in the baseline case. However, these results are not representative of the actual situation as the simulation models do not factor in edge diffraction, sound interference, or room modes. Studying the trends helped focus on the location optimization of the absorbers in the open office.

The experimentation helped to bridge the results from analytical predictions and physical testing, and to understand the limitations in both the procedures. Though the reverberation chamber method would have provided a thorough understanding of the panel’s behavior in room conditions, the impedance tube method helped test out a number of iterations of the samples with minimum fabrication and calibration of the setup. The results from an impedance tube experiment can help in calibrating an FEA model when analyzing complex resonator geometry.

Though the resonator panel designed in this project is bulky and might not prove to be practical, it provides a starting point to analyze the usefulness of Helmholtz Resonators in room acoustics. Instead of having the resonators in a ceiling-hung panel, these could even be integrated into the ceiling slab design or in the partition walls, and could become an integral aspect for improving room acoustics.

9.1 Future work

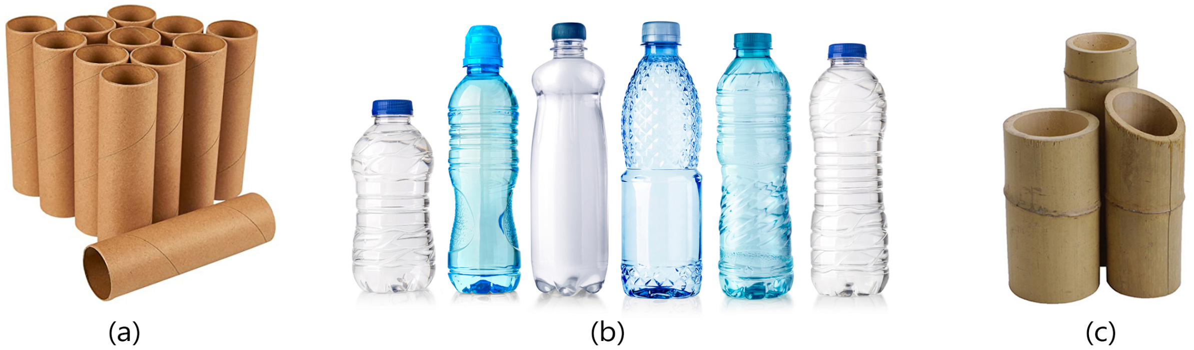

Figure 101: *Resonators from everyday objects: (a) Cardboard tubes; (b) Plastic bottles; (c) Bamboo shoots*

The next steps in continuing this research would be targeted towards complex resonator geometry that is more compact and broadband in their performance, like the sub-wavelength resonators discussed in section 7.2. Hence, a shift towards FEA simulations is required as the boundaries of existing analytical models have been met in this research. On the array scale, an in-depth study on the impact of the resonator arrangement on the absorption performance of the HR panel is of interest.

Figure 101 shows some of the recyclable objects (plastic bottles and cardboard tubes), and naturally occurring material like bamboo shoots that can be used as resonators. They might prove to be more eco-friendly and carbon-neutral, compared to other synthetic materials, for fabricating the resonators. Further research would have to be conducted to bolster the application and advantages of these materials as efficient resonators.

Application of resonator panels in spaces other than open offices is an interesting direction. Since the resonators are relatively dust-free compared to porous absorbers, they could be used in sensitive rooms in a hospital. Research on integrating them into building components - like partition walls or ceiling slabs - could provide novel ways in designing spaces for acoustic comfort.

10 Appendices

10.1 Symbols and Properties of air

Table 2: *Properties of air*

Symbol	**Value**	**Property**	**Units**
ρ_0	1.205	Density of air	$< kg/m^3 >$
c	343	Speed of sound in air	$< m/s >$
μ	1.88 x 10ˆ-5	Dynamic viscosity of air	$< Ns/m^2 >$
ν	1.5 x 10ˆ-5	Kinematic viscosity of air	$< m^2/s >$
γ	1.4	Ratio of specific heats	$< - >$
K	0.026	Coefficient of thermal conductivity	$< W/mK >$
C_p	1010	Specific heat capacity at constant pressure	$< J/kgK >$
P_0	101325	Atmospheric pressure	$< Pa >$
Pr	0.71	Prandtl number for air	$< - >$

Table 3: *Symbols and its units*

Symbol	**Definition**	**Units**
f	Frequency	$< Hz$ or $1/s >$
ω	Angular frequency	$< Hz$ or $1/s >$
k	Wavenumber	$< 1/m >$
r	Radius of the neck opening	$< m >$
l	Length of the neck	$< m >$
l'	corrected length of the neck	$< m >$
S_n	Surface area of the neck opening	$< m^2 >$
M_n	Acoustic mass of the neck	$< kg/m^2 >$
R	Radius of the cavity	$< m >$
L_c	Length of the cavity	$< m >$
S_c	Surface area of the cavity	$< m^2 >$
V_c	Volume of the cavity	$< m^3 >$

10.2 Appendix A - Cylindrical resonator (Johansson & Kleiner 2001)

Resonator body mass, M_b, mass correction derived by Panton and Miller,

$$M_b = \frac{\rho_0 L_c}{3}\left(\frac{Sn}{Sc}\right)$$

where L_c is the length of the cavity.

Resonator neck mass, M_n,

$$M_n = \rho_0(l + \Delta l')$$

where $\Delta l'$ is the sum of $l'_{inner} = 0.509r$ and $l'_{outer} = 0.68r$

Neck resistance, R_n

$$R_n = \frac{l}{r}\frac{\sqrt{2\mu_{eff}\rho_0\omega}}{\pi r^2} + \frac{2\sqrt{2\mu_0\rho_0\omega}}{\pi r^2} + \frac{2\pi\rho_0 f^2}{c}$$

$$\mu_{eff} = \mu_0\left(1 + (\gamma - 1)\sqrt{\frac{K}{\mu_0 C_p}}\right)^2$$

where K is the coefficient of thermal conductivity, C_p is the specific heat capacity at constant pressure, and γ is the ratio of specific heats.

The first two terms in R_n are the viscous losses in the neck (as cited by Ingard). The first one accounts for the loss to the neck's boundary wall while the second one is for the neck's ends. The final term is the radiation loss in the neck.

Impedance:

$$Z_n = R_n + j\omega M_n$$

$$Z_c = j\omega M_b - j\frac{1}{\omega C_b} \qquad C_b = \frac{V_c}{\rho_0 c^2 S_n}$$

where C_b is the stiffness of the spring.

10.3 Appendix B - Square cavity resonator (Kim et al. 2003)

Impedance for a square cavity, Z_c,

$$Z_c = -j\frac{\rho_0 c^2 S_n}{\omega V_c}$$

where S_n is the area of the neck and V_c is the volume of the cavity.

Acoustic mass of a perforated neck panel (Cox & d'Antonio 2016),

$$m = \rho_0\left[l + 2\delta r + \sqrt{\frac{8\nu}{\omega}}\left(1 + \frac{l}{2r}\right)\right]$$

The reactance term and the length correction,

$$X_m = \omega m \quad ; \qquad \delta = \frac{8}{3\pi} \approx 0.85$$

Impedance of the neck,

$$Z_{hole} = Z_{rad} + \rho_0 \frac{l}{r}\sqrt{8\nu\omega} + j\omega\rho_0 \left(\frac{8}{3\pi}r + 2\sqrt{\frac{8\nu}{\omega}}\right) + j\omega\rho_0 l \left(1 + \frac{\sqrt{\frac{8\nu}{\omega}}}{2r}\right)$$

where l, r are the length, and the radius of the neck, respectively. Z_{rad} is the radiation impedance.

$$Z_{rad} \approx \frac{1}{2}\rho_0 c(ka)^2 + j\omega\rho_0 \frac{8}{3\pi}a \quad ; \qquad if(kr) << 1$$

Average spatial impedance, Z, is given by

$$Z_{HR} = Z_c + Z_{hole}; \qquad Z = \frac{Z_{HR}}{\varepsilon}; \quad \varepsilon = \frac{S_n}{S_c}$$

10.4 Appendix C - Embedded neck resonator (Huang et al. 2019)

Viscous wave number, k_v,

$$k_v^2 = -j\omega\frac{\rho_0}{\eta}$$

$$\Psi_v = \frac{J_2(k_v r)}{J_0(k_v r)}$$

Thermal wave number, k_h,

$$k_h^2 = -j\omega\frac{\rho_0 C_p}{K}$$

$$\Psi_h = \frac{J_2(k_h r)}{J_0(k_h r)}$$

where r and l are the radius and the length of the neck, respectively, C_p is the specific heat capacity at constant pressure, and K is the thermal conductivity.

Complex wave number, k_c,

$$k_c^2 = k_0^2\left(\frac{\gamma - (\gamma - 1)\Psi_h}{\Psi_v}\right)$$

Complex air density, ρ_c,

$$\rho_c = \frac{\rho_0}{\Psi_v}$$

Complex speed of sound, c_c,

$$c_c = \frac{\omega}{k_c}$$

Acoustic impedance of the embedded neck, Z_n,

$$Z_n = -\rho_0 c_0 \frac{\left(2jsin\left(\frac{k_c l}{2}\right)\right)}{\sqrt{(\gamma - (\gamma - 1)\Psi_h)\Psi_v}}$$

For a short neck, the acoustic impedance of the neck can be simplified as,

$$Z_n = \frac{-j\rho_0 \omega l}{\Psi_v}$$

Acoustic impedance of the chamber, Z_c,

$$Z_c = \frac{-jS_n \rho_c c_c^2}{\omega V_c}$$

where $V_c =$ (Vol. of cavity - Vol. of embedded neck), ρ_c and c_c are the complex density and speed of sound.

Total acoustic impedance, Z_{HR},

$$Z_{HR} = Z_n + Z_c + 2\sqrt{2\omega\rho_0\eta} + j\omega\rho_0\delta_i \quad ; \qquad Z = \left(\frac{S_c}{S_n}\right) Z_{HR}$$

where δ_i is the acoustic mass end correction,

$$\delta_i = (1 + (1 - 1.25\varepsilon)) \times \frac{8r}{3\pi}$$

$$\varepsilon = \frac{r}{R}$$

10.5 Appendix D - Conical neck resonator (Vigran 2004)

Outer neck radius, r_i, and inner neck radius, r_o, where $r_o > r_i$
Impedance at r_i, Z_a,

$$Z_a = 1 - \frac{2J_1(2kr_i)}{2kr_i} + j\frac{2S_1(2kr_i)}{2kr_i}$$

Impedance at r_o, Z_b,

$$Z_b = 1 - \frac{2J_1(2kr_o)}{2kr_o} + j\frac{2S_1(2kr_o)}{2kr_o}$$

where J_1 and S_1 are the Bessel and Struve function of order 1.

The input impedance is given by, Z_i,

$$Z_i = \frac{A_2 e^{-jkx_1} + B_2 e^{jkx_1}}{U_1 x_1}; \qquad x_1 = \frac{r_i l}{r_o - r_i}; \qquad x_2 = \frac{r_o l}{r_o - r_i}$$

where A_2, B_2, and U_1 are amplitudes derived from the matrix below,

$$P = \begin{bmatrix} e^{-jkx_1} & e^{jkx_1} & Z_0 Z_a x_1 & 0 \\ (1+jkx_1)e^{-jkx_1} & (1-jkx_1)e^{jkx_1} & -jZ_0 k x_1^2 & 0 \\ (1+jkx_2)e^{-jkx_2} & (1-jkx_2)e^{jkx_2} & 0 & -jZ_0 k x_2^2 \\ e^{-jkx_2} & e^{jkx_2} & 0 & -Z_0 Z_b x_2 \end{bmatrix}$$

$$q = \begin{bmatrix} A_2 \\ B_2 \\ U_1 \\ U_2 \end{bmatrix} \qquad R = \begin{bmatrix} 2x_1 cos(kx_1) \\ 0 \\ 0 \\ 0 \end{bmatrix}$$

Solving P∗q = R, the amplitudes can be derived.

10.6 Appendix E - Effect of Fitness function

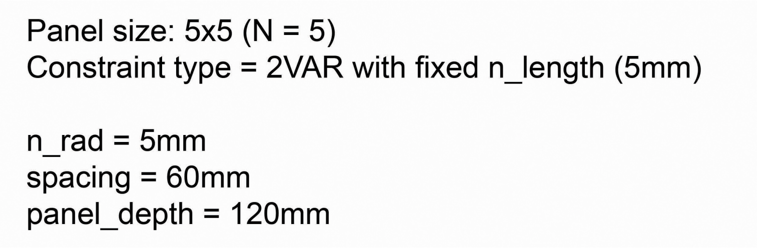

Panel size: 5x5 (N = 5)
Constraint type = 2VAR with fixed n_length (5mm)

n_rad = 5mm
spacing = 60mm
panel_depth = 120mm

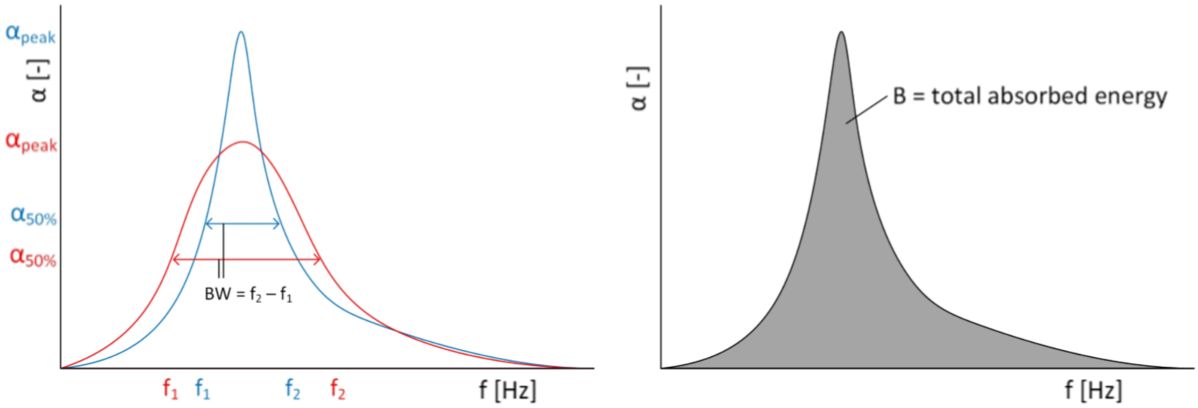

Figure 102: *Fitness functions used for the evolutionary solver (Gommer 2016)*

Bandwidth (f = 0.7)

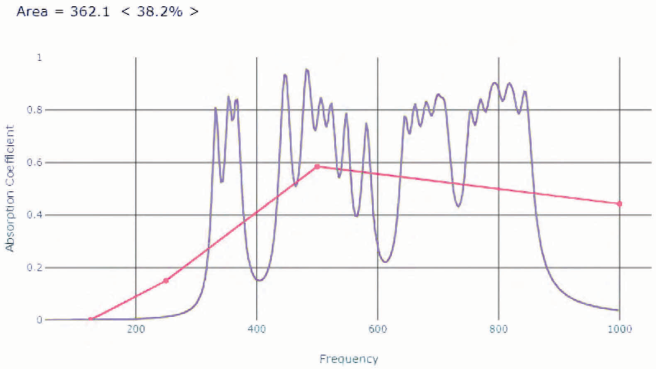

Area under the curve

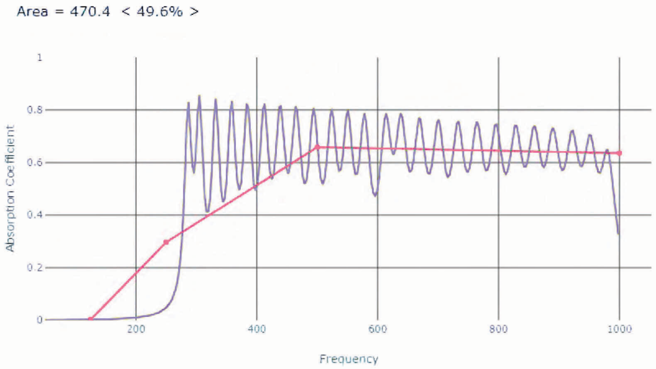

Combination (f = 0.7)

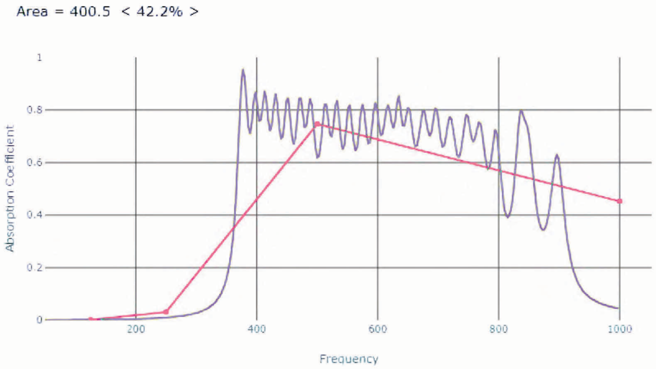

Bandwidth (f = 0.8)

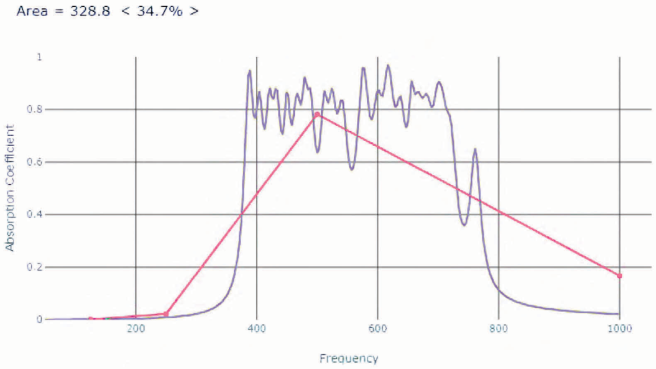

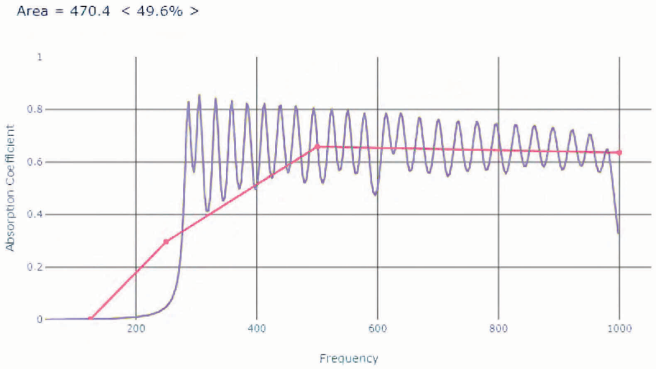

Combination (f = 0.8)

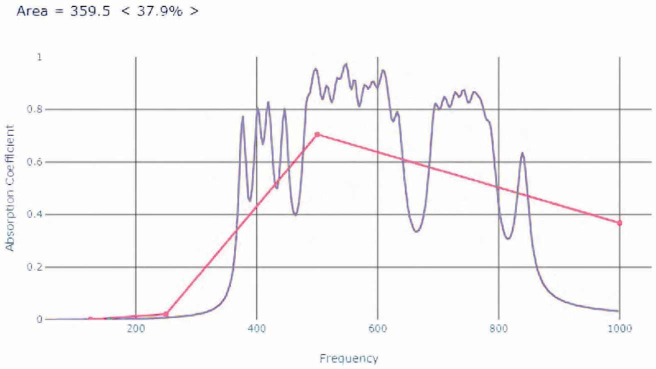

Bandwidth (f = 0.9)

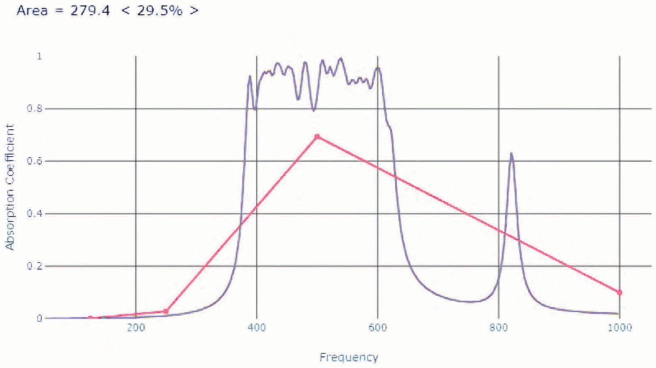

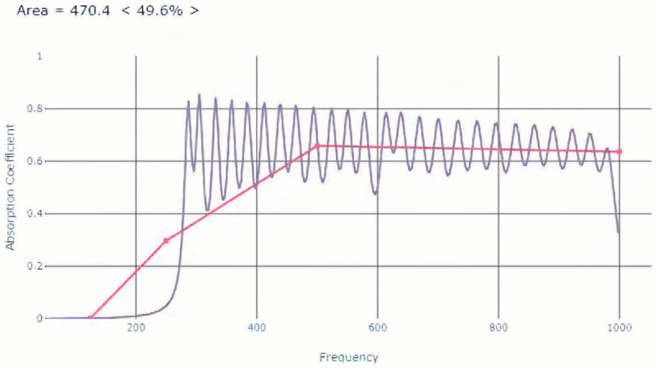

Combination (f = 0.9)

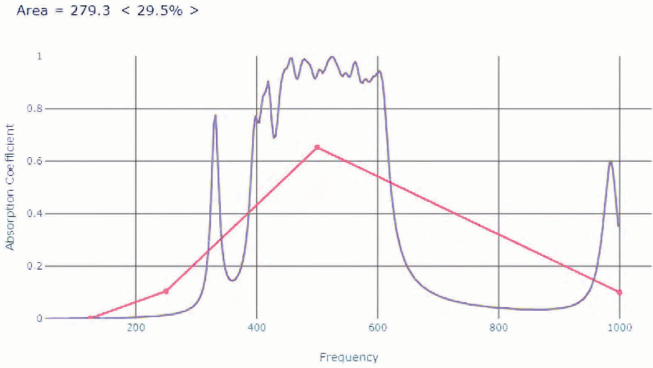

10.7 Appendix F - Panel studies by varying the fixed variables

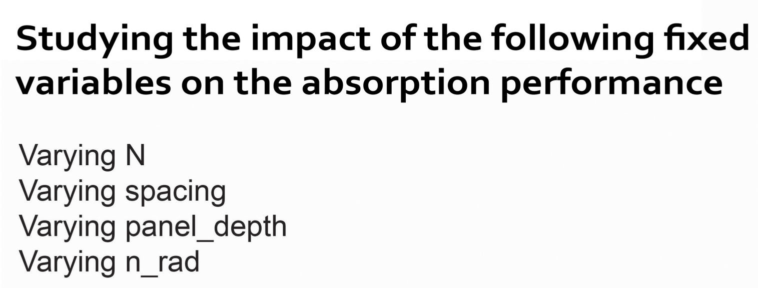

Studying the impact of the following fixed variables on the absorption performance

Varying N
Varying spacing
Varying panel_depth
Varying n_rad

CONSTRAINT TYPE	FREE VARIABLES	FIXED VARIABLES	DEPENDENCIES
 Different HR lengths *<'diff_HR_lengths'>* SEARCH - 150 generations 100 population per gen	3 free variables - n_length, c_depth, c_radius	4 fixed variables - N, spacing, n_rad, panel_depth	0 dependency but constraint_check n_length + c_depth <= panel_depth
 Different HR lengths *<'const_n_length'>* SEARCH - 100 generations 100 population per gen	2 free variables - c_depth, c_radius	5 fixed variables - N, spacing, n_rad, n_length, panel_depth	
 Constant HR lengths *<'const_HR_lengths'>* SEARCH - 100 generations 100 population per gen	2 free variables - n_length, c_radius	4 fixed variables - N, spacing, n_rad, panel_depth	1 dependency - c_depth = panel_depth - n_length
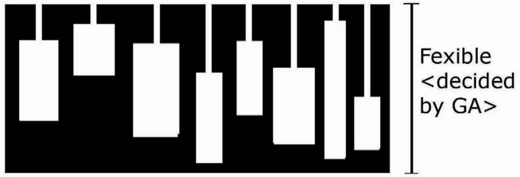 No constraint *<'no_constraint'>* SEARCH - 300 generations	4 free variables - n_length, c_depth, c_radius, panel_depth	3 fixed variables - N, spacing, n_rad	

Varying N

3 VAR - different HR lengths

n_rad = 5mm
spacing = 60mm
panel_depth = 120mm
fitness func = curve area

N = 3

Area = 391.4 < 41.3% >

41.3%

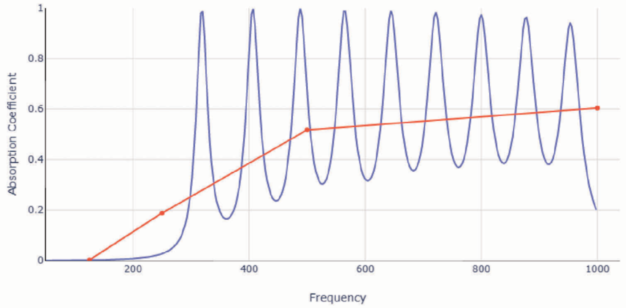

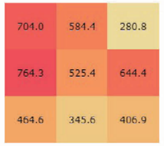

704.0	584.4	280.8
764.3	525.4	644.4
464.6	345.6	406.9

N = 4

Area = 394.6 < 41.6% >

41.6%

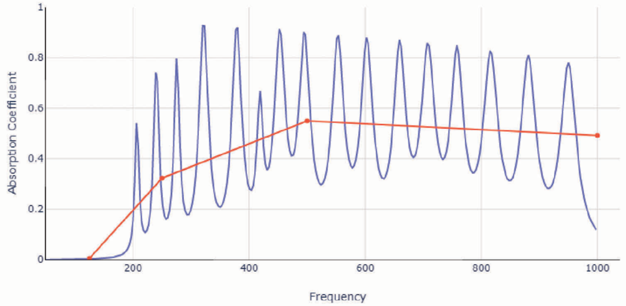

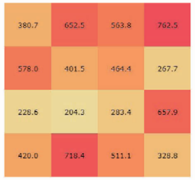

380.7	652.5	563.8	762.5
578.0	401.5	464.4	267.7
228.6	204.3	283.4	657.9
420.0	718.4	511.1	328.8

N = 5

Area = 349.1 < 36.8% >

36.8%

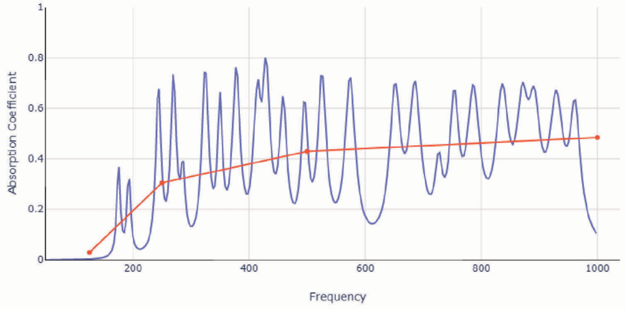

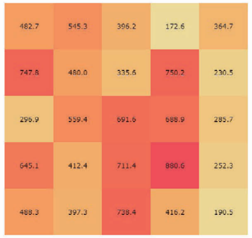

482.7	545.3	396.2	172.6	364.7
747.8	480.0	335.6	750.2	230.5
296.9	559.4	691.6	688.9	285.7
645.1	412.4	711.4	880.6	252.3
488.3	397.3	738.4	416.2	190.5

2 VAR - constant neck lengths

n_rad = 5mm
spacing = 60mm
panel_depth = 120mm
n_length = 5mm
fitness func = curve area

N = 3

Area = 390.4 < 41.2% >

41.2%

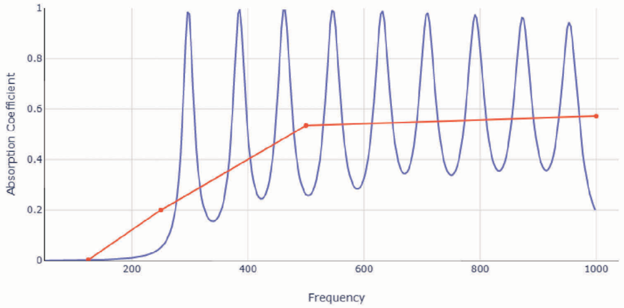

515.3	387.8	329.9
763.0	700.9	450.9
265.3	638.1	575.2

N = 4

Area = 449.8 < 47.5% >

47.5%

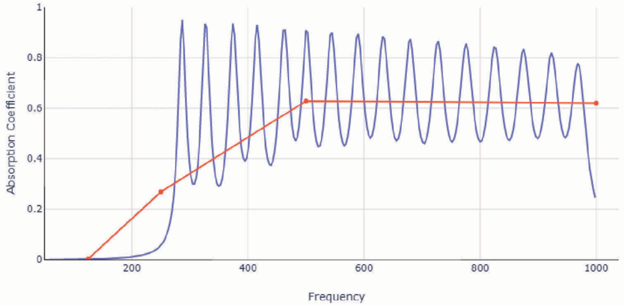

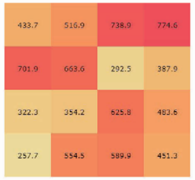

433.7	516.9	738.9	774.6
701.9	663.6	292.5	387.9
322.3	354.2	625.8	483.6
257.7	554.5	589.9	451.3

N = 5

Area = 472.8 < 49.9% >

49.9%

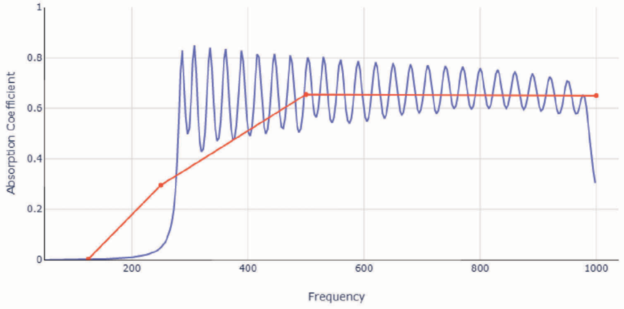

451.9	622.1	313.4	407.5	293.2
375.4	333.6	508.4	554.5	484.6
713.5	690.2	534.6	276.8	418.8
576.8	760.3	360.2	667.3	737.0
644.9	781.8	257.7	598.6	462.7

Varying N

3 VAR - different HR lengths

n_rad = 5mm
spacing = 60mm
panel_depth = 120mm
fitness func = curve area

N = 6

Area = 399.9 < 42.2% >

42.2%

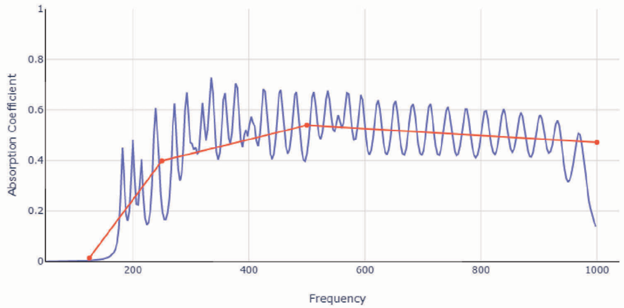

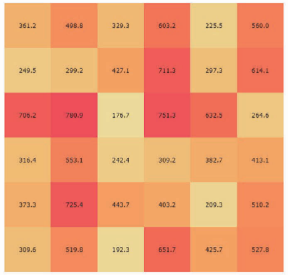

361.2	498.8	329.3	603.2	225.5	560.0
249.5	299.2	427.1	711.3	297.3	614.1
706.2	780.9	176.7	751.3	632.5	264.6
316.4	553.1	242.4	309.2	382.7	413.1
373.3	725.4	443.7	403.2	209.3	510.2
309.6	519.8	192.3	651.7	425.7	527.8

N = 7

Area = 397.4 < 41.9% >

41.9%

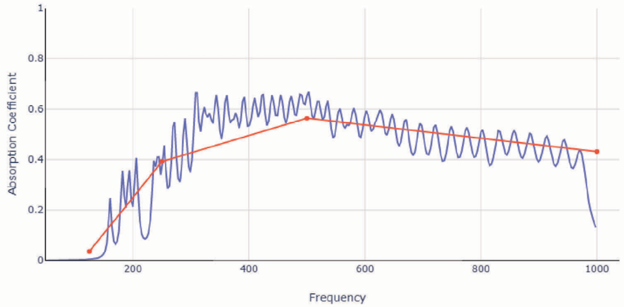

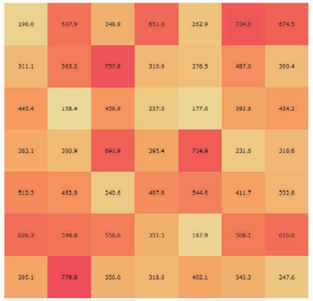

198.0	607.9	348.9	651.0	262.9	734.0	674.5
311.1	563.2	757.8	310.6	276.5	487.0	300.4
445.4	158.4	459.9	237.0	177.6	392.8	434.2
383.1	300.9	691.9	395.4	714.9	231.6	318.6
512.3	482.8	240.6	497.9	544.6	411.7	332.8
626.3	598.8	550.6	351.5	187.9	568.1	616.0
395.1	779.8	356.0	318.0	402.1	343.2	247.6

N = 8

Area = 359.5 < 37.9% >

37.9%

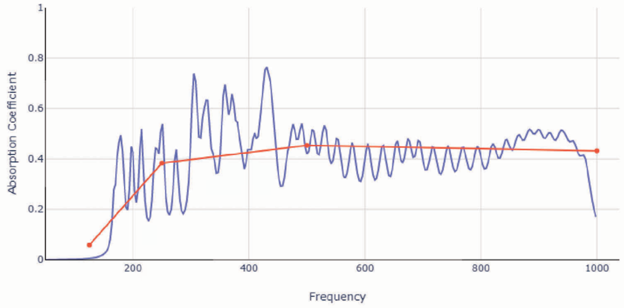

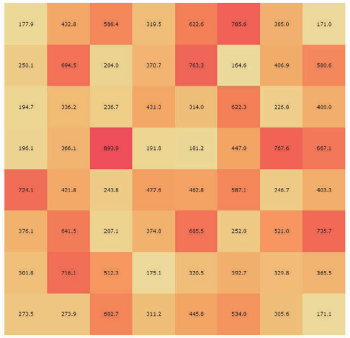

177.9	432.8	588.4	319.5	622.6	785.6	385.0	171.0
250.1	694.5	204.0	370.7	763.3	164.6	406.9	580.6
194.7	336.2	236.7	431.3	314.0	622.3	226.8	400.0
196.1	366.1	893.9	191.8	181.2	447.0	767.6	667.1
724.1	421.8	243.8	477.6	462.8	587.1	246.7	403.3
376.1	641.5	207.1	374.8	685.5	252.0	521.0	735.7
301.8	716.1	512.3	175.1	320.5	392.7	329.8	365.5
273.5	273.9	602.7	311.2	445.8	534.0	305.6	171.1

2 VAR - constant neck lengths

n_rad = 5mm
spacing = 60mm
panel_depth = 120mm
n_length = 5mm
fitness func = curve area

N = 6

Area = 459.2 < 48.4% >

48.4%

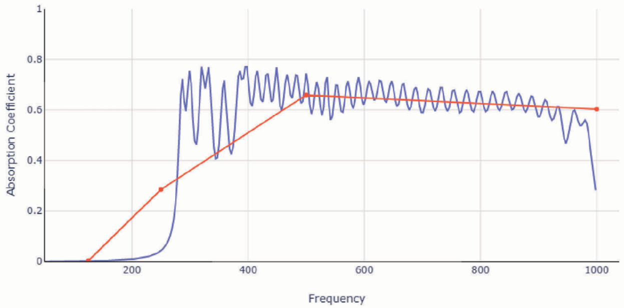

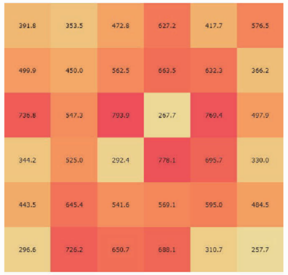

391.8	353.5	472.8	627.2	417.7	576.5
499.9	450.0	562.5	663.5	632.3	366.2
736.8	547.3	793.9	267.7	769.4	497.9
344.2	525.0	292.4	778.1	695.7	330.0
443.5	645.4	541.6	569.1	595.0	484.5
296.6	726.2	650.7	688.1	310.7	257.7

N = 7

Area = 478.4 < 50.5% >

50.5%

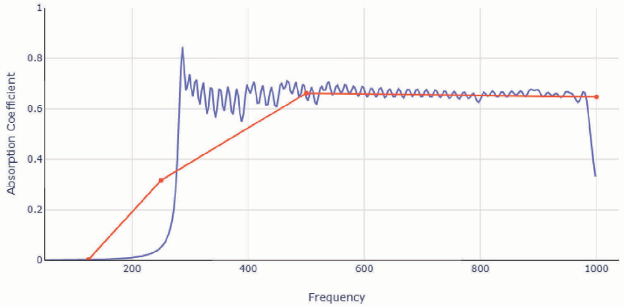

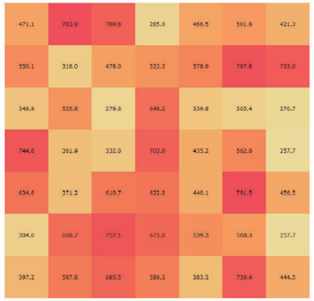

471.1	783.9	709.8	285.0	466.5	501.8	421.3
550.1	316.0	478.0	522.3	578.6	767.8	733.0
348.9	525.8	279.6	648.2	339.8	305.4	270.7
744.6	361.9	332.0	703.0	435.2	562.8	257.7
634.6	371.2	610.7	622.8	440.1	781.5	456.5
304.6	660.7	757.1	673.0	539.3	500.3	257.7
397.2	597.8	685.5	589.3	383.3	720.4	444.5

N = 8

Area = 476.4 < 50.3% >

50.3%

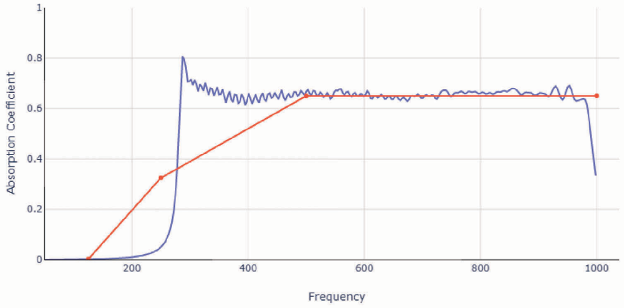

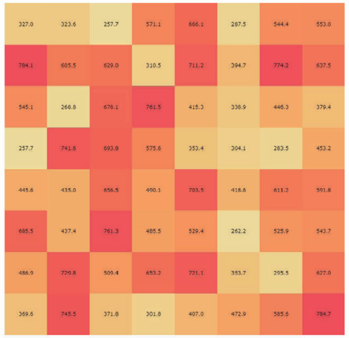

327.0	323.6	257.7	571.1	666.1	287.5	544.4	553.0
784.1	605.5	629.0	310.5	711.2	394.7	774.2	637.5
545.1	268.8	678.1	761.5	415.3	338.9	446.3	379.4
257.7	741.6	693.8	575.6	353.4	304.1	283.5	453.2
445.6	435.0	656.5	490.1	703.5	418.6	611.2	591.8
685.5	437.4	761.3	485.5	529.4	262.2	525.9	543.7
486.9	729.8	509.4	653.2	721.1	353.7	295.5	627.0
369.6	745.5	371.8	301.8	407.0	472.9	585.6	784.7

2 VAR - constant HR length

n_rad = 5mm
spacing = 60mm
panel_depth = 120mm
fitness func = curve area

23.2%

N = 3

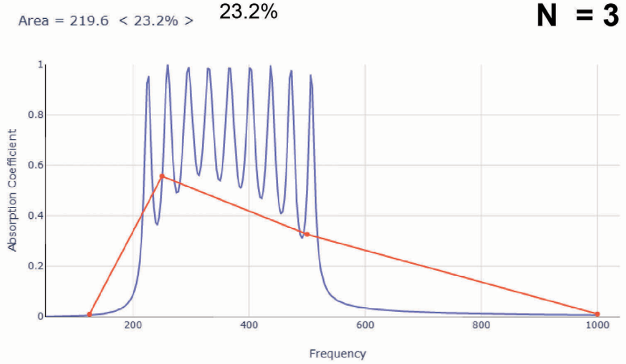

350.4	628.9	238.2
461.9	402.2	263.8
304.4	533.5	212.0

25.8%

N = 4

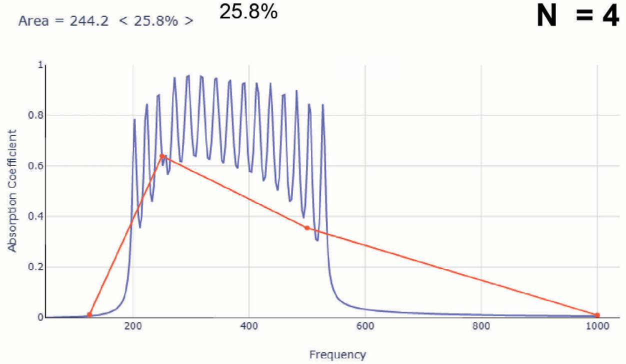

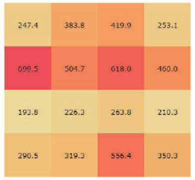

247.4	383.8	419.9	253.1
699.5	504.7	618.0	460.0
193.8	226.3	263.8	210.3
290.5	319.3	556.4	350.3

25.8%

N = 5

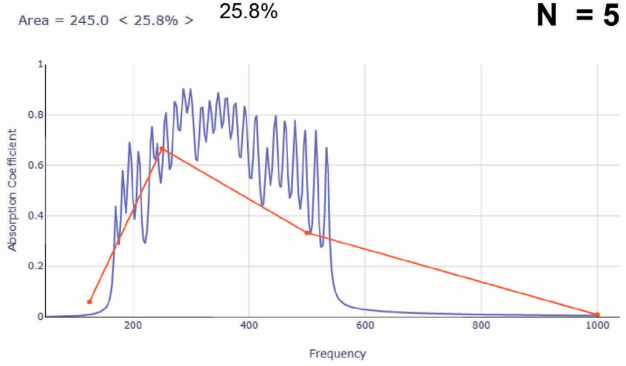

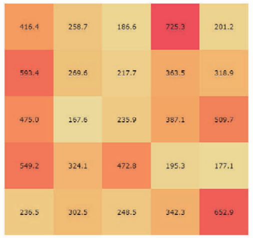

416.4	258.7	186.6	725.3	201.2
593.4	269.6	217.7	363.5	318.9
475.0	167.6	235.9	387.1	509.7
549.2	324.1	472.8	195.3	177.1
236.5	302.5	248.5	342.3	652.9

No constraint

n_rad = 5mm
spacing = 60mm
fitness func = curve area

37.0%

N = 3

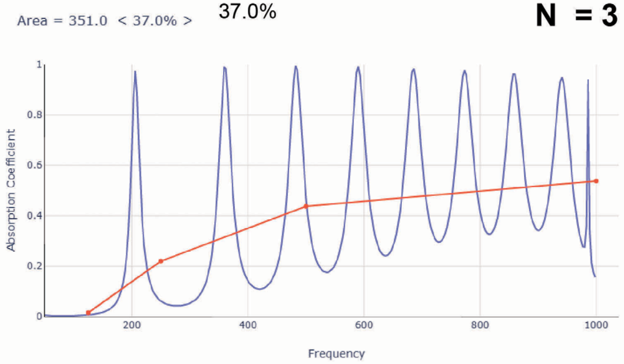

754.1	34.7	199.5
311.8	689.4	403.0
624.1	483.6	556.2

34.4%

N = 4

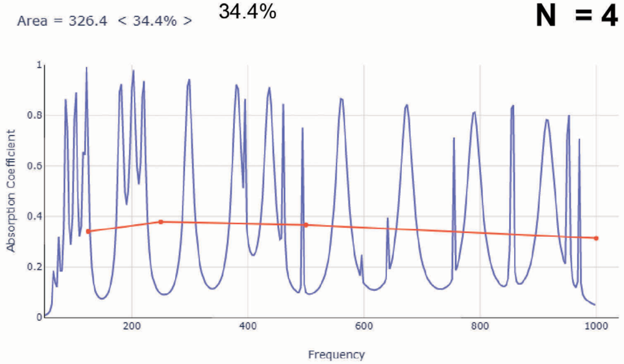

733.8	327.7	266.6	547.4
198.0	463.1	153.4	254.1
636.2	176.9	98.2	79.7
130.7	111.5	369.4	67.7

30.5%

N = 5

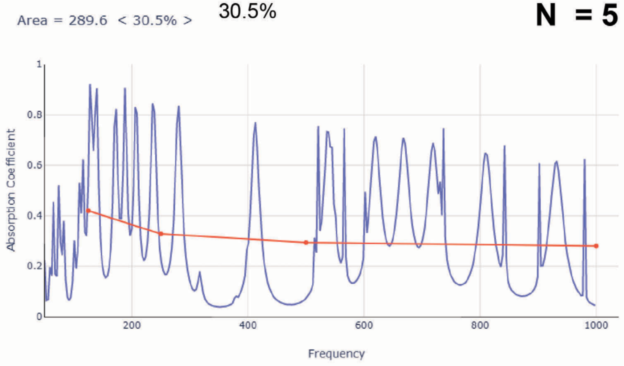

133.1	227.0	129.0	745.7	170.3
317.0	127.3	362.5	254.5	144.0
104.5	446.5	68.6	154.7	81.7
543.6	506.2	52.2	652.6	216.7
592.1	86.4	65.0	91.0	224.8

2 VAR - constant HR length

n_rad = 5mm
spacing = 60mm
panel_depth = 120mm
fitness func = curve area

26.0% **N = 6**

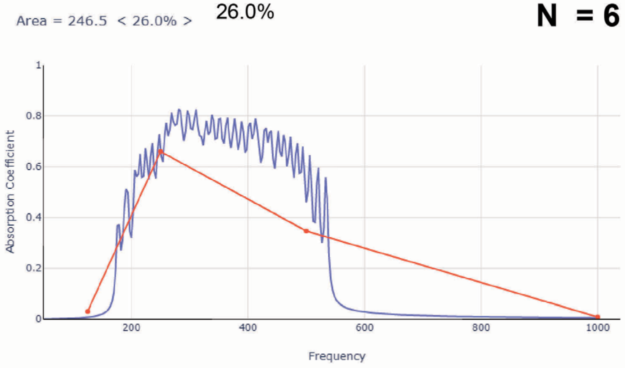

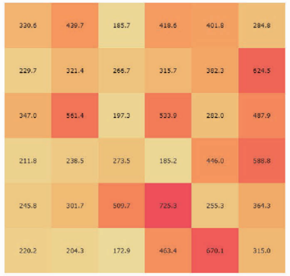

330.6	439.7	185.7	418.6	401.8	284.8
229.7	321.4	266.7	315.7	382.3	624.5
347.0	561.4	197.3	533.9	282.0	487.9
211.8	238.5	273.5	185.2	446.0	588.8
245.8	301.7	509.7	725.3	255.3	364.3
220.2	204.3	172.9	463.4	670.1	315.0

26.2% **N = 7**

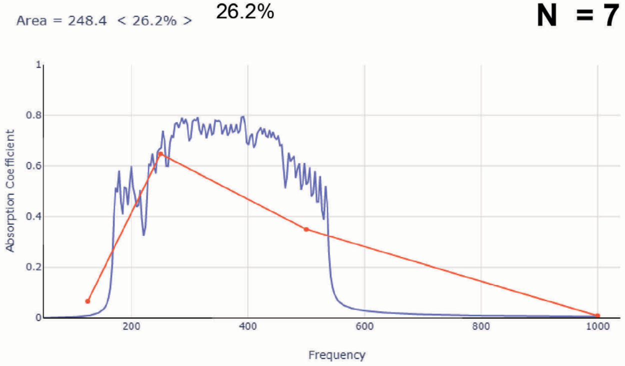

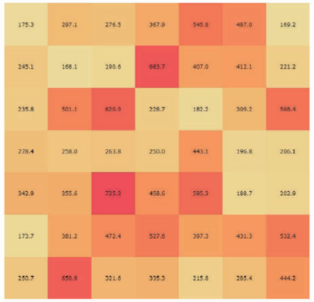

175.3	297.1	276.5	367.9	545.8	487.0	169.2
245.1	168.1	190.6	683.7	407.0	412.1	221.2
235.8	501.1	620.9	228.7	182.2	309.2	568.4
278.4	258.0	263.8	250.0	443.1	196.8	206.1
342.9	355.6	725.3	458.6	595.3	188.7	202.9
173.7	381.2	472.4	527.6	397.3	431.3	532.4
250.7	650.9	321.6	335.3	215.8	285.4	444.2

26.4% **N = 8**

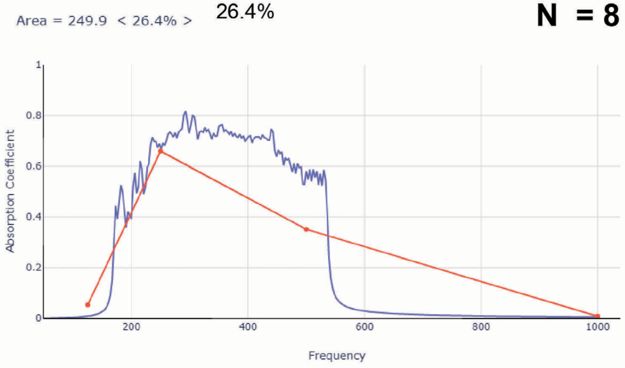

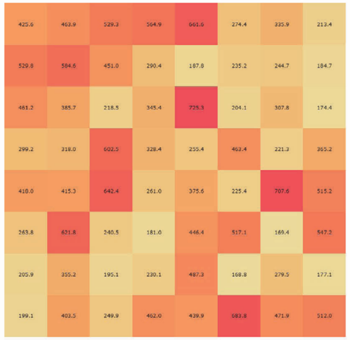

425.6	463.9	529.3	564.9	661.6	274.4	335.9	213.4
529.8	584.6	451.0	290.4	187.8	235.2	244.7	184.7
461.2	385.7	218.5	345.4	725.3	204.1	307.8	174.4
299.2	318.0	602.5	328.4	255.4	463.4	221.3	365.2
418.0	415.3	642.4	261.0	375.6	225.4	707.6	515.2
263.8	621.8	240.5	181.0	446.4	517.1	169.4	547.2
205.9	355.2	195.1	230.1	487.3	168.8	279.5	177.1
199.1	403.5	249.9	462.0	439.9	683.8	471.9	512.0

No constraint

n_rad = 5mm
spacing = 60mm
fitness func = curve area

20.3% **N = 6**

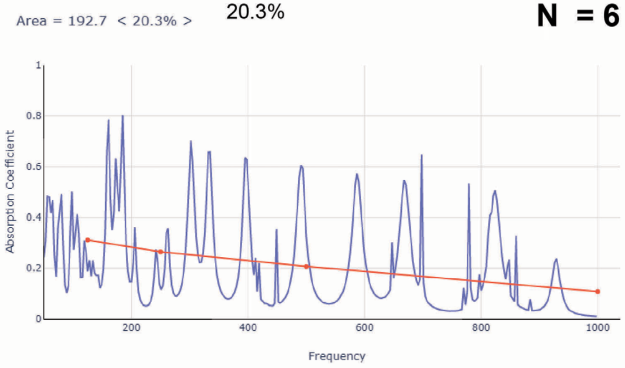

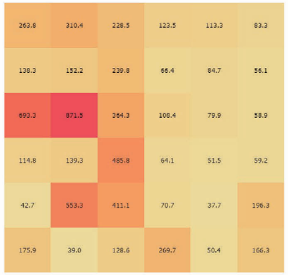

263.8	310.4	228.5	123.5	113.3	83.3
138.3	152.2	239.8	66.4	84.7	56.1
693.3	871.5	364.3	108.4	79.9	58.9
114.8	139.3	485.8	64.1	51.5	59.2
42.7	553.3	411.1	70.7	37.7	196.3
175.9	39.0	128.6	269.7	50.4	166.3

19.5% **N = 7**

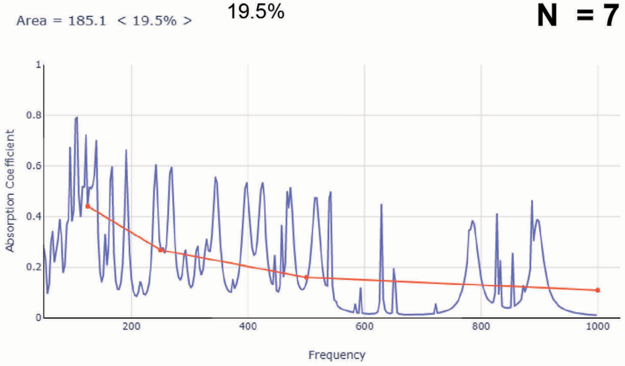

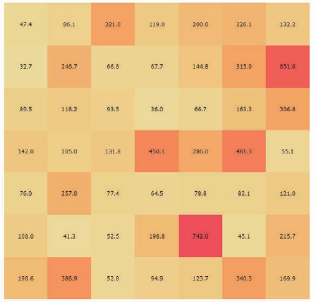

47.4	86.1	321.0	119.0	200.6	226.1	132.2
32.7	246.7	66.6	67.7	144.8	315.9	651.6
89.5	116.2	93.5	36.0	66.7	163.3	306.6
142.0	105.0	131.8	450.1	286.0	481.3	55.1
76.0	257.0	77.4	64.5	78.8	82.1	121.0
108.0	41.3	52.5	198.8	742.0	45.1	215.7
198.6	386.9	52.8	94.9	123.7	340.3	169.9

16.2% **N = 8**

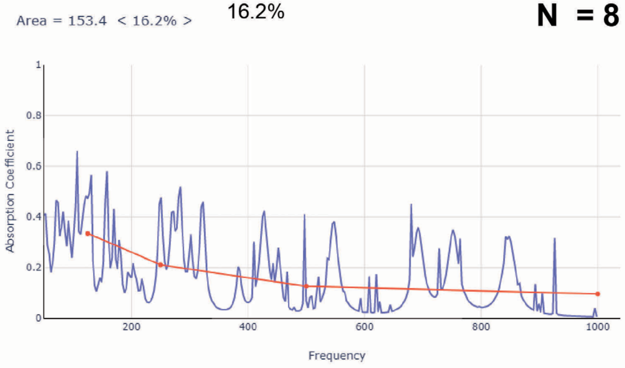

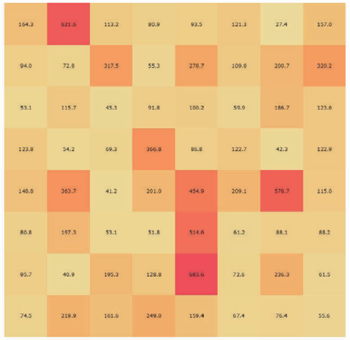

164.3	621.6	113.2	80.9	93.5	121.3	27.4	157.0
94.0	72.8	317.5	55.3	278.7	109.8	200.7	320.2
53.1	115.7	45.3	91.8	100.2	59.9	186.7	123.6
123.8	54.2	69.3	366.8	86.8	122.7	42.3	122.9
148.8	363.7	41.2	201.0	454.9	209.1	578.7	115.0
80.8	197.3	53.1	51.8	514.6	61.2	88.1	88.2
95.7	40.9	195.3	128.8	683.6	72.6	236.3	61.5
74.5	219.9	161.6	249.0	159.4	67.4	76.4	55.6

Varying spacing

N = 5 (5x5 panel)
n_rad = 5mm
panel_depth = 120mm
fitness func = curve area

3 VAR - different HR lengths

Area = 390.1 < 41.2% >

41.2%

spacing = 50mm

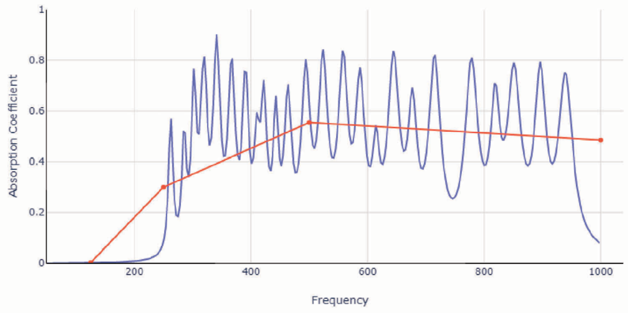

632.5	340.9	416.1	507.4	769.8
396.9	474.1	321.2	325.5	710.7
588.7	260.2	390.1	558.3	301.9
431.5	660.4	528.7	443.0	474.7
326.8	286.9	783.0	833.8	616.0

Area = 421.9 < 44.5% >

44.5%

spacing = 60mm

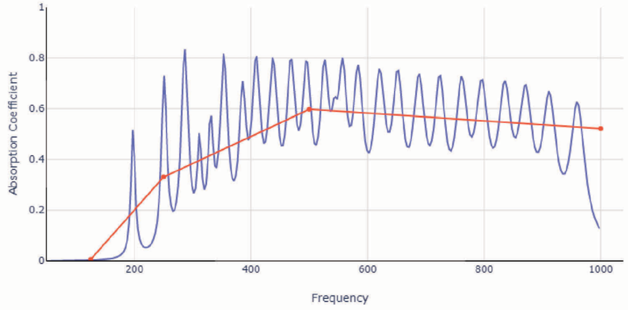

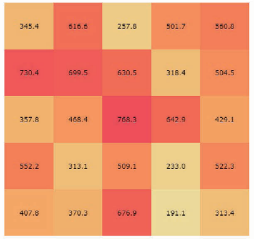

345.4	616.6	257.8	501.7	560.8
730.4	699.5	630.5	318.4	504.5
357.8	468.4	768.3	642.9	429.1
552.2	313.1	509.1	233.0	522.3
407.8	370.3	676.9	191.1	313.4

Area = 395.6 < 41.7% >

41.7%

spacing = 70mm

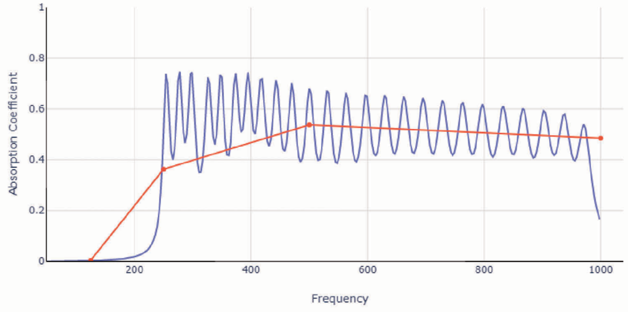

341.1	750.3	352.5	458.2	485.5
561.3	318.9	416.2	460.4	587.4
640.9	256.3	408.1	536.2	378.9
326.1	695.8	617.1	511.5	723.8
240.9	777.3	669.1	279.1	223.1

N = 5 (5x5 panel)
n_rad = 5mm
panel_depth = 120mm
n_length = 5mm
fitness func = curve area

2 VAR - constant neck lengths

Area = 528.8 < 55.8% >

55.8%

spacing = 50mm

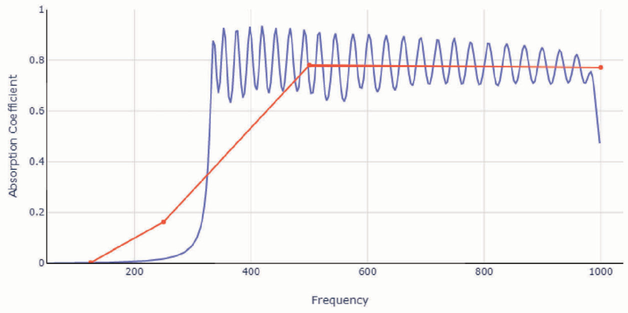

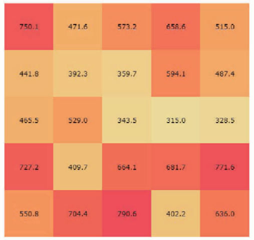

750.1	471.6	573.2	658.6	515.0
441.8	392.3	359.7	594.1	487.4
465.5	529.0	343.5	315.0	328.5
727.2	409.7	664.1	681.7	771.6
550.8	704.4	790.6	402.2	636.0

Area = 472.6 < 49.9% >

49.9%

spacing = 60mm

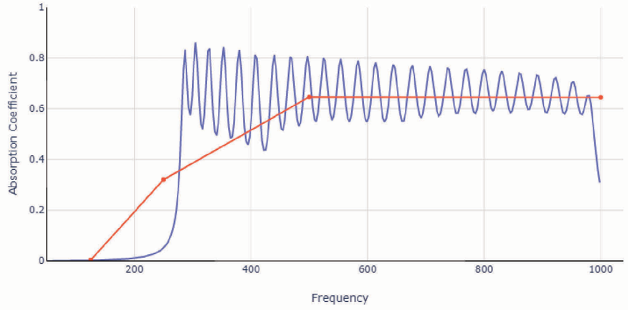

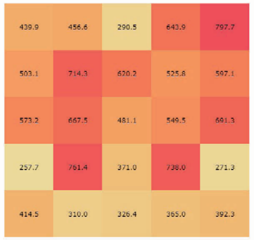

439.9	456.6	290.5	643.9	797.7
503.1	714.3	620.2	525.8	597.1
573.2	667.5	481.1	549.5	691.3
257.7	761.4	371.0	738.0	271.3
414.5	310.0	326.4	365.0	392.3

Area = 402.9 < 42.5% >

42.5%

spacing = 70mm

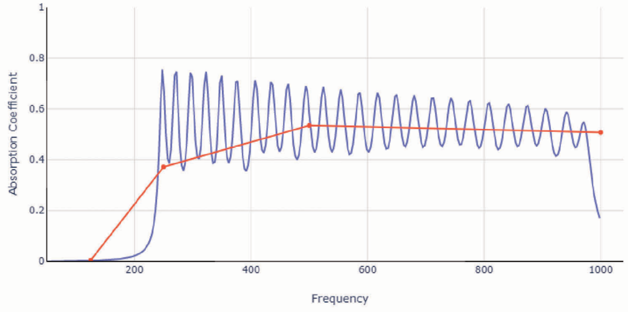

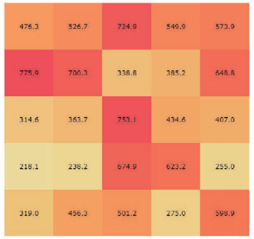

476.3	526.7	724.9	549.9	573.9
775.9	700.3	338.8	385.2	648.8
314.6	363.7	753.1	434.6	407.0
218.1	238.2	674.9	623.2	255.0
319.0	456.3	501.2	275.0	598.9

Varying spacing

3 VAR - different HR lengths

N = 5 (5x5 panel)
n_rad = 5mm
panel_depth = 120mm
fitness func = curve area

Area = 297.7 < 31.4% >

31.4%

spacing = 80mm

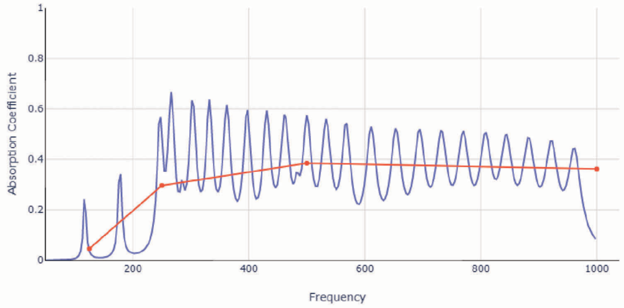

282.4	172.0	255.9	589.7	488.7
424.8	480.3	707.8	651.0	383.2
372.1	619.2	528.6	768.8	115.7
436.0	292.4	678.1	345.1	560.6
738.3	496.7	218.4	225.7	300.1

Area = 280.0 < 29.5% >

29.5%

spacing = 90mm

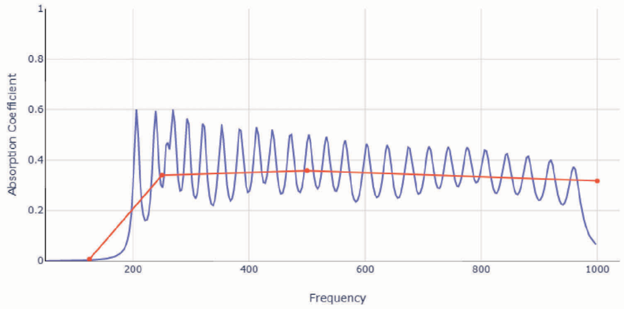

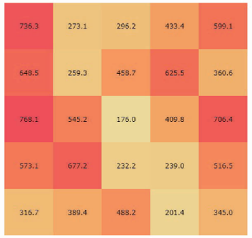

736.3	273.1	296.2	433.4	599.1
648.5	259.3	458.7	625.5	360.6
768.1	545.2	176.0	409.8	706.4
573.1	677.2	232.2	239.0	516.5
316.7	389.4	488.2	201.4	345.0

2 VAR - constant neck lengths

N = 5 (5x5 panel)
n_rad = 5mm
panel_depth = 120mm
n_length = 5mm
fitness func = curve area

Area = 340.7 < 35.9% >

35.9%

spacing = 80mm

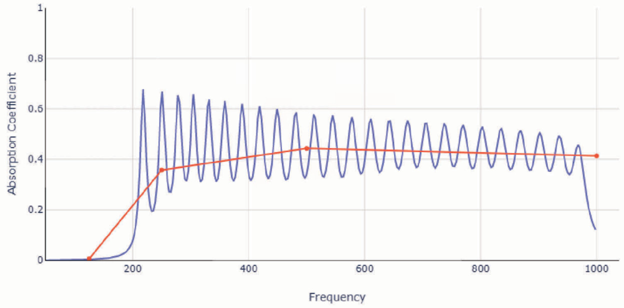

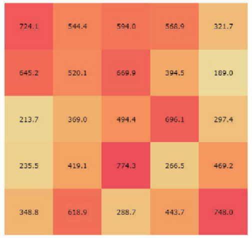

724.1	544.4	594.0	568.9	321.7
645.2	520.1	669.9	394.5	189.0
213.7	369.0	494.4	696.1	297.4
235.5	419.1	774.3	266.5	469.2
348.8	618.9	288.7	443.7	748.0

Area = 288.9 < 30.5% >

30.5%

spacing = 90mm

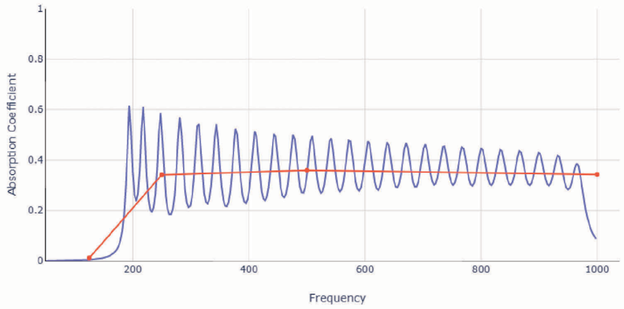

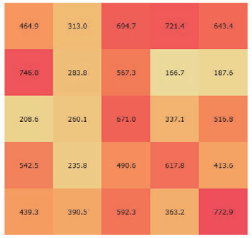

464.9	313.0	694.7	721.4	643.4
746.0	283.8	567.3	166.7	187.6
208.6	260.1	671.0	337.1	516.8
542.5	235.8	490.6	617.8	413.6
439.3	390.5	592.3	363.2	772.9

2 VAR - constant HR length

N = 5 (5x5 panel)
n_rad = 5mm
panel_depth = 120mm
fitness func = curve area

28.7%

spacing = 50mm

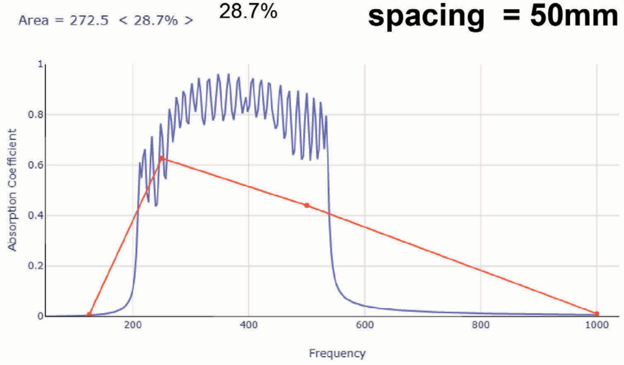

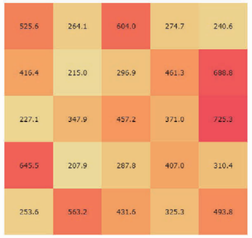

525.6	264.1	604.0	274.7	240.6
416.4	215.0	296.9	461.3	688.8
227.1	347.9	457.2	371.0	725.3
645.5	207.9	287.8	407.0	310.4
253.6	563.2	431.6	325.3	493.8

23.4%

spacing = 60mm

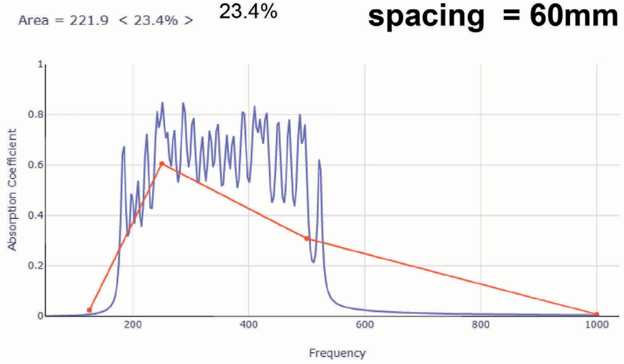

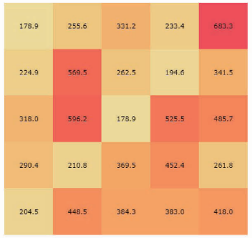

178.9	255.6	331.2	233.4	683.3
224.9	569.5	262.5	194.6	341.5
318.0	596.2	178.9	525.5	485.7
290.4	210.8	369.5	452.4	261.8
204.5	448.5	384.3	383.0	418.0

24.7%

spacing = 70mm

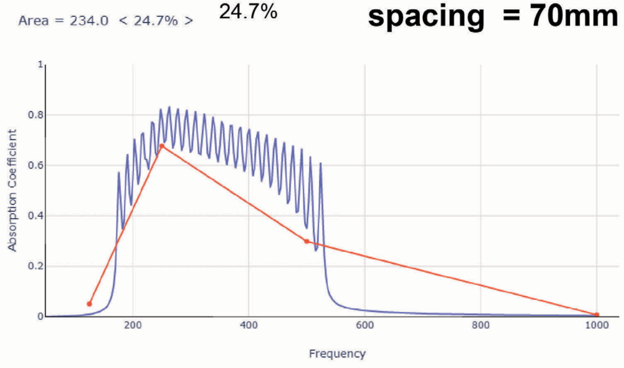

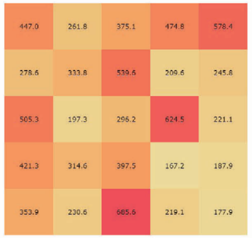

447.0	261.8	375.1	474.8	578.4
278.6	333.8	539.6	209.6	245.8
505.3	197.3	296.2	624.5	221.1
421.3	314.6	397.5	167.2	187.9
353.9	230.6	685.6	219.1	177.9

No constraint

N = 5 (5x5 panel)
n_rad = 5mm
fitness func = curve area

32.8%

spacing = 50mm

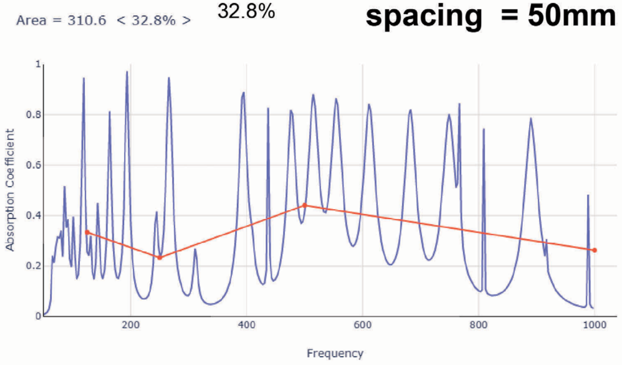

218.5	138.2	69.0	167.7	95.3
244.4	84.9	315.9	74.7	617.3
90.7	409.9	725.7	474.2	356.9
79.0	591.8	446.6	266.2	154.1
426.6	127.7	106.0	514.3	152.5

28.5%

spacing = 60mm

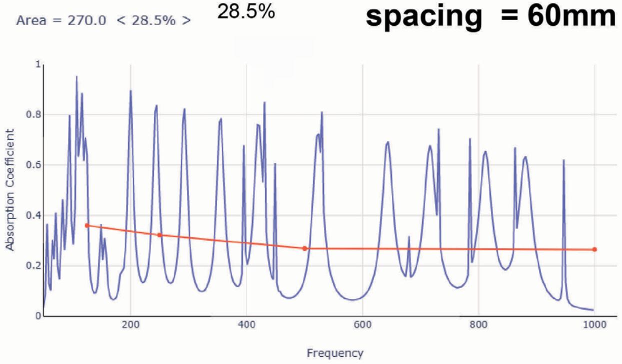

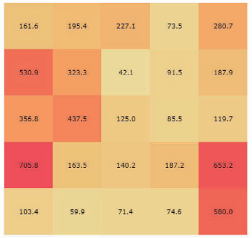

161.6	195.4	227.1	73.5	280.7
530.9	323.3	42.1	91.5	187.9
356.8	437.5	125.0	85.5	119.7
705.8	163.5	140.2	187.2	653.2
103.4	59.9	71.4	74.6	580.0

22.6%

spacing = 70mm

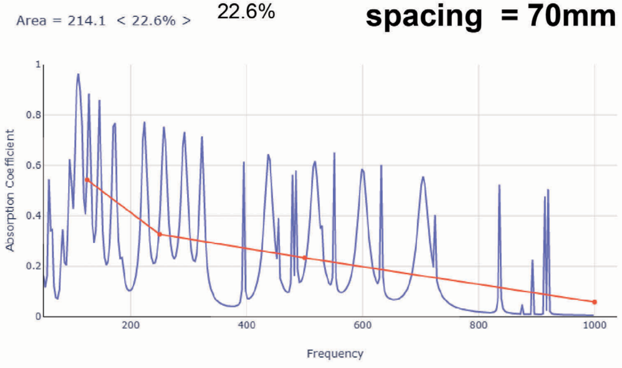

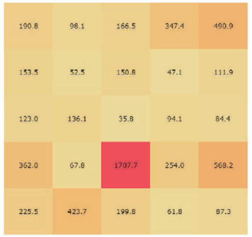

190.8	98.1	166.5	347.4	490.9
153.5	52.5	150.8	47.1	111.9
123.0	136.1	35.8	94.1	84.4
362.0	67.8	1707.7	254.0	568.2
225.5	423.7	199.8	61.8	87.3

2 VAR - constant HR length

N = 5 (5x5 panel)
n_rad = 5mm
panel_depth = 120mm
fitness func = curve area

Area = 204.0 < 21.5% >

21.5%

spacing = 80mm

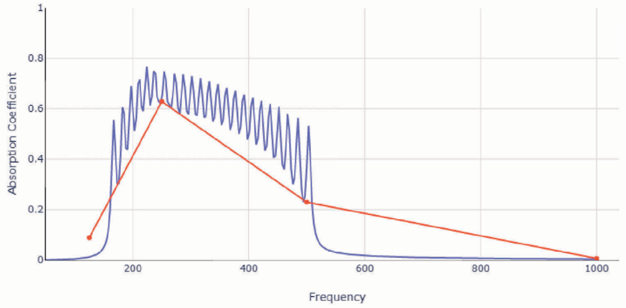

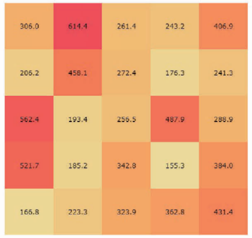

306.0	614.4	261.4	243.2	406.9
206.2	458.1	272.4	176.3	241.3
562.4	193.4	256.5	487.9	288.9
521.7	185.2	342.8	155.3	384.0
166.8	223.3	323.9	362.8	431.4

Area = 189.3 < 20.0% >

20.0%

spacing = 90mm

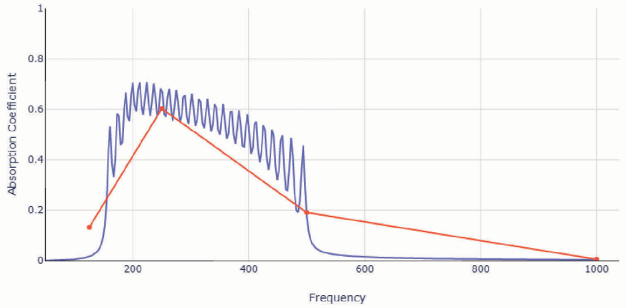

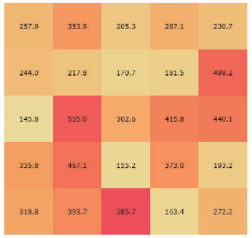

257.9	353.9	205.3	287.1	230.7
244.0	217.8	170.7	181.5	498.2
145.8	535.0	302.6	415.8	440.1
335.8	467.1	155.2	373.0	193.2
318.8	393.7	585.7	163.4	272.2

No constraint

N = 5 (5x5 panel)
n_rad = 5mm
fitness func = curve area

Area = 199.8 < 21.1% >

21.1%

spacing = 80mm

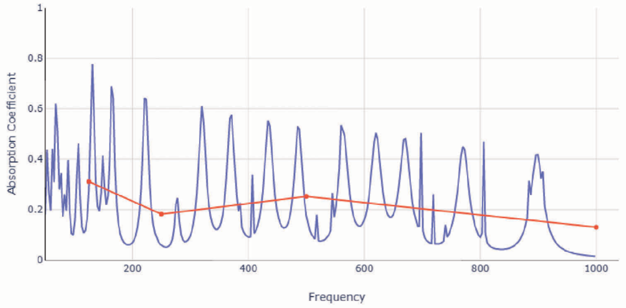

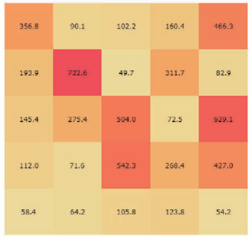

356.8	90.1	102.2	160.4	466.3
193.9	722.6	49.7	311.7	82.9
145.4	275.4	504.0	72.5	629.1
112.0	71.6	542.3	268.4	427.0
58.4	64.2	105.8	123.8	54.2

Area = 145.3 < 15.3% >

15.3%

spacing = 90mm

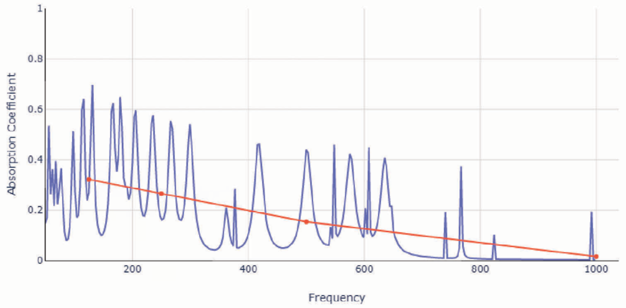

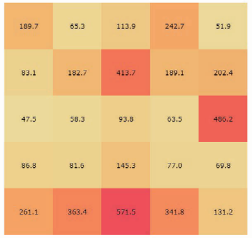

189.7	65.3	113.9	242.7	51.9
83.1	182.7	413.7	189.1	202.4
47.5	58.3	93.8	63.5	486.2
86.8	81.6	145.3	77.0	69.8
261.1	363.4	571.5	341.8	131.2

Varying panel_depth

N = 5 (5x5 panel)
n_rad = 5mm
spacing = 60mm
fitness func = curve area

3 VAR - different HR lengths

42.4%

panel_depth = 80mm

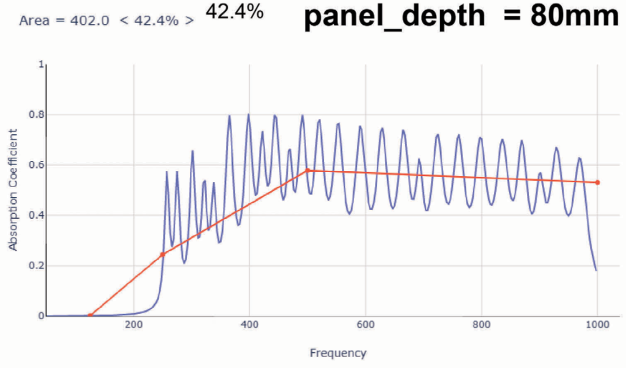

436.0	594.1	636.3	243.3	554.5
456.2	781.6	516.3	778.0	833.8
382.7	317.1	490.6	340.9	437.8
277.8	262.0	304.9	386.8	680.0
323.4	445.5	665.2	661.9	763.7

38.5%

panel_depth = 120mm

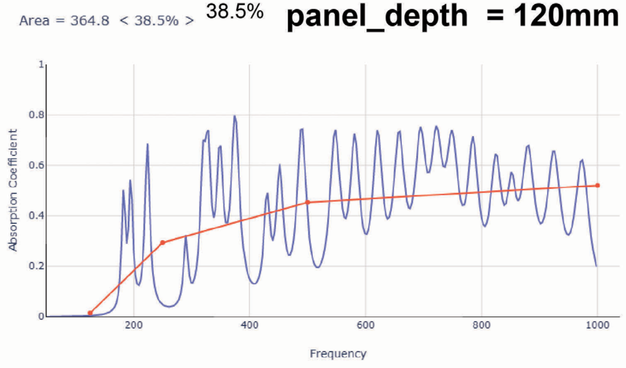

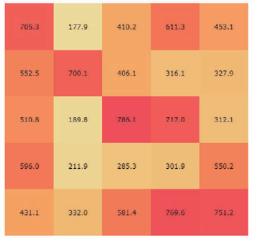

705.3	177.9	410.2	611.3	453.1
552.5	700.1	406.1	316.1	327.9
510.8	189.8	786.1	717.0	312.1
596.0	211.9	285.3	301.9	550.2
431.1	332.0	581.4	769.6	751.2

41.0%

panel_depth = 160mm

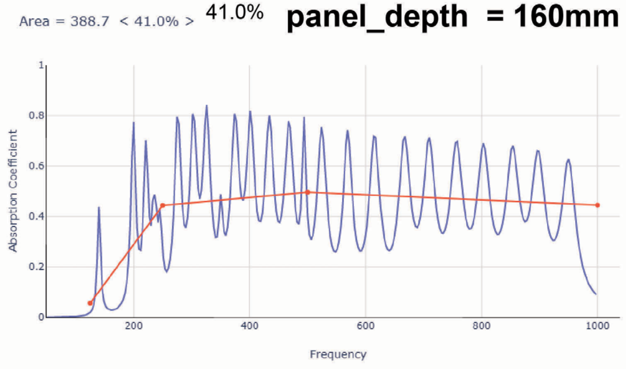

459.1	241.0	291.4	524.0	719.3
551.2	685.2	611.1	372.5	404.9
139.5	760.7	381.2	271.5	635.0
323.6	209.4	650.6	241.3	190.8
356.9	586.6	240.1	250.9	519.6

2 VAR - constant neck lengths

N = 5 (5x5 panel)
n_rad = 5mm
spacing = 60mm
n_length = 5mm
fitness func = curve area

48.0%

panel_depth = 80mm

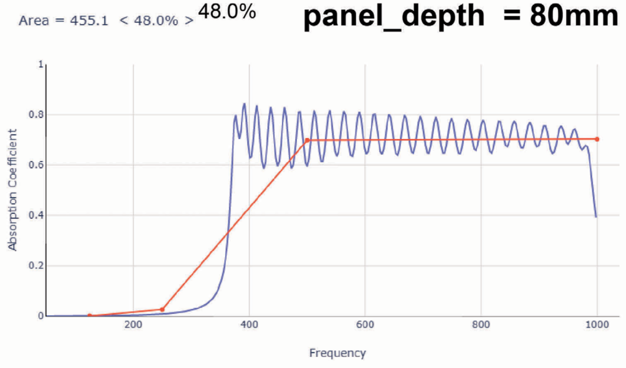

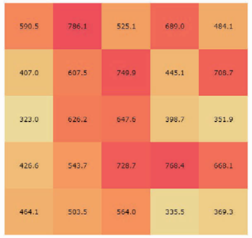

590.5	786.1	525.1	689.0	484.1
407.0	607.5	749.9	445.1	708.7
323.0	626.2	647.6	398.7	351.9
426.6	543.7	728.7	768.4	668.1
464.1	503.5	564.0	335.5	369.3

49.6%

panel_depth = 120mm

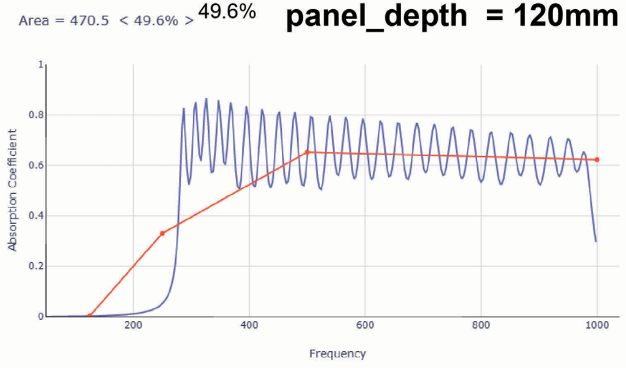

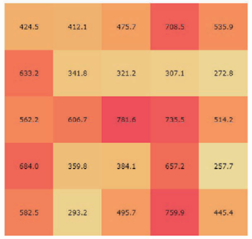

424.5	412.1	475.7	708.5	535.9
633.2	341.8	321.2	307.1	272.8
562.2	606.7	781.6	735.5	514.2
684.0	359.8	384.1	657.2	257.7
582.5	293.2	495.7	759.9	445.4

50.5%

panel_depth = 160mm

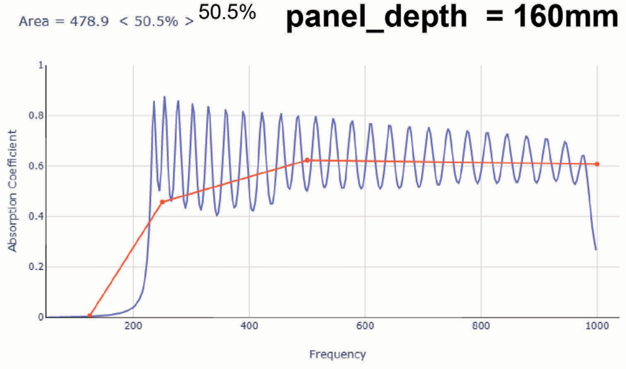

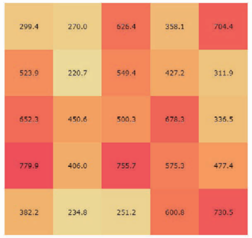

299.4	270.0	626.4	358.1	704.4
523.9	220.7	549.4	427.2	311.9
652.3	450.6	500.3	678.3	336.5
779.9	406.0	755.7	575.3	477.4
382.2	234.8	251.2	600.8	730.5

Varying panel_depth

N = 5 (5x5 panel)
n_rad = 5mm
spacing = 60mm
fitness func = curve area

3 VAR - different HR lengths

Area = 357.5 < 37.7% > 37.7% **panel_depth = 200mm**

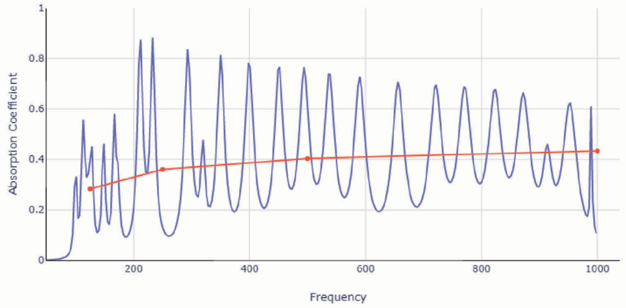

452.1	318.2	112.5	484.7	118.1
583.7	534.8	843.2	173.7	700.1
323.5	146.7	414.1	243.0	341.5
171.9	762.4	203.4	662.0	263.1
125.1	100.3	621.8	130.1	389.4

2 VAR - constant neck lengths

N = 5 (5x5 panel)
n_rad = 5mm
spacing = 60mm
n_length = 5mm
fitness func = curve area

Area = 474.6 < 50.1% > 50.1% **panel_depth = 200mm**

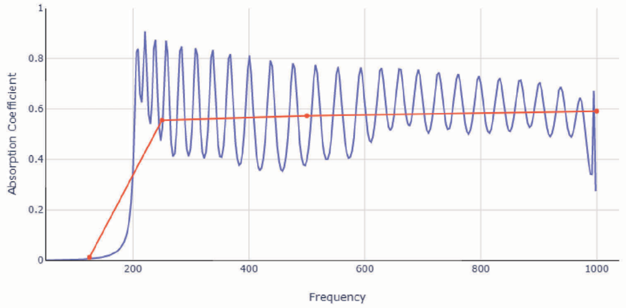

722.0	369.8	217.8	512.8	669.0
696.1	344.4	256.7	456.9	200.4
302.9	402.7	250.6	614.2	750.0
284.1	588.4	317.5	427.7	776.4
230.1	537.8	641.5	562.0	486.1

2 VAR - constant HR length

N = 5 (5x5 panel)
n_rad = 5mm
spacing = 60mm
fitness func = curve area

Area = 332.6 < 35.1% > 35.1%

panel_depth = 80mm

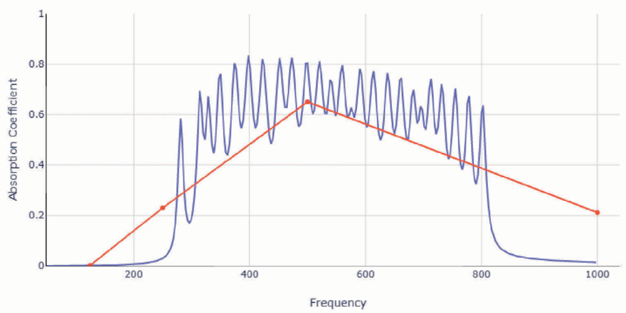

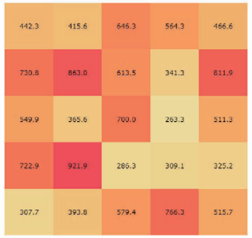

442.3	415.6	646.3	564.3	466.6
730.8	863.0	613.5	341.3	811.9
549.9	365.6	700.0	263.3	511.3
722.9	921.9	286.3	309.1	325.2
307.7	393.8	579.4	766.3	515.7

Area = 263.2 < 27.8% > 27.8%

panel_depth = 120mm

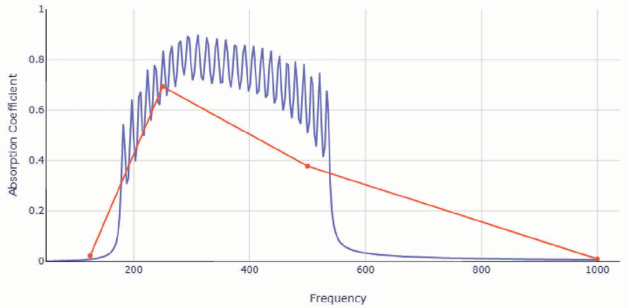

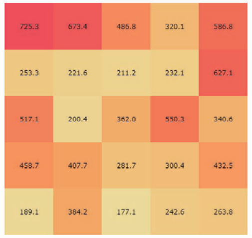

725.3	673.4	486.8	320.1	586.8
253.3	221.6	211.2	232.1	627.1
517.1	200.4	362.0	550.3	340.6
458.7	407.7	281.7	300.4	432.5
189.1	384.2	177.1	242.6	263.8

Area = 197.3 < 20.8% > 20.8%

panel_depth = 160mm

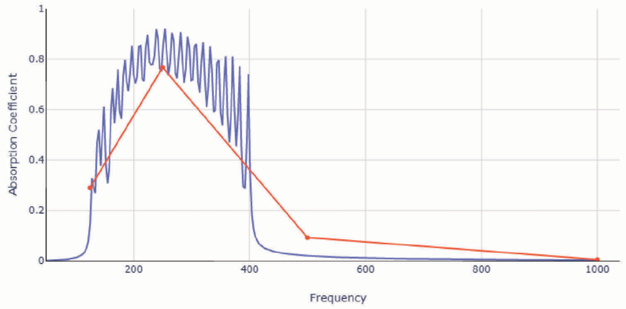

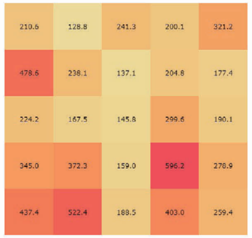

210.6	128.8	241.3	200.1	321.2
478.6	238.1	137.1	204.8	177.4
224.2	167.5	145.8	299.6	190.1
345.0	372.3	159.0	596.2	278.9
437.4	522.4	188.5	403.0	259.4

No constraint

N = 5 (5x5 panel)
n_rad = 5mm
spacing = 60mm
fitness func = curve area

Area = 244.3 < 25.8% > 25.8%

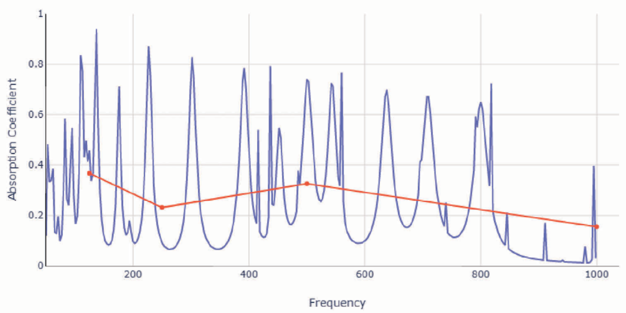

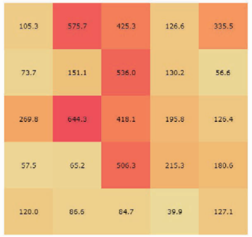

105.3	575.7	425.3	126.6	335.5
73.7	151.1	536.0	130.2	56.6
269.8	644.3	418.1	195.8	126.4
57.5	65.2	506.3	215.3	180.6
120.0	86.6	84.7	39.9	127.1

2 VAR - constant HR length

N = 5 (5x5 panel)
n_rad = 5mm
spacing = 60mm
fitness func = curve area

Area = 166.5 < 17.6% > 17.6% **panel_depth = 200mm**

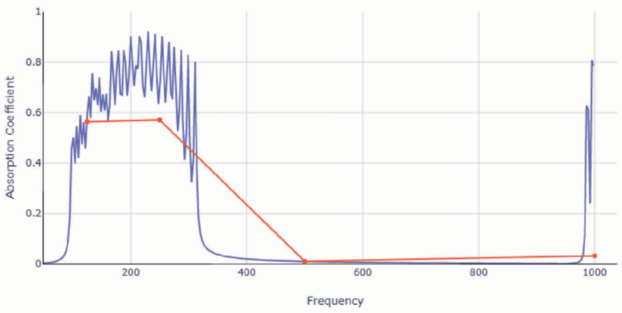

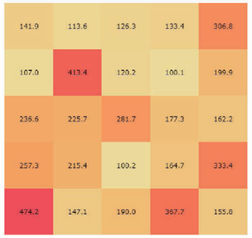

141.9	113.6	126.3	133.4	306.8
107.0	413.4	120.2	100.1	199.9
236.6	225.7	281.7	177.3	162.2
257.3	215.4	100.2	164.7	333.4
474.2	147.1	190.0	367.7	155.8

Varying neck radius

3 VAR - different HR lengths

N = 5 (5x5 panel)
spacing = 60mm
panel_depth = 120mm
fitness func = curve area

29.2%

n_rad = 3mm

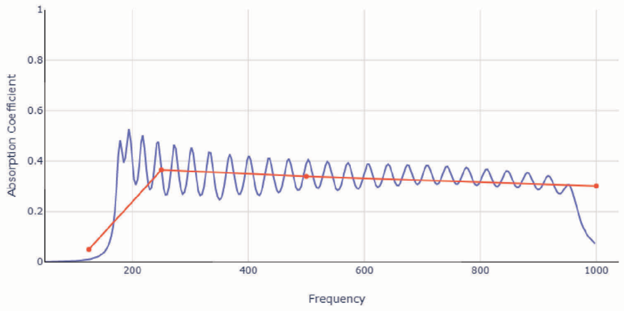

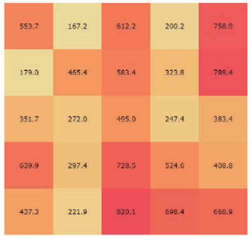

553.7	167.2	612.2	200.2	758.9
179.0	465.4	583.4	323.8	789.4
351.7	272.0	495.0	247.4	383.4
639.9	297.4	728.5	524.6	408.8
437.3	221.9	820.1	698.4	668.9

33.3%

n_rad = 4mm

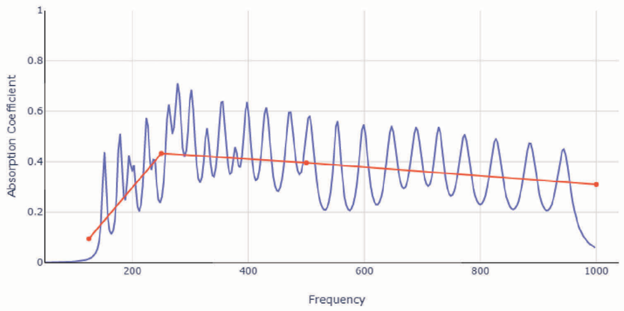

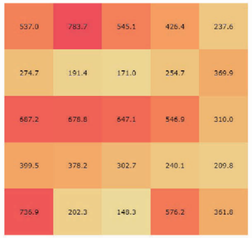

537.0	783.7	545.1	426.4	237.6
274.7	191.4	171.0	254.7	369.9
687.2	678.8	647.1	546.9	310.0
399.5	378.2	302.7	240.1	209.8
736.9	202.3	148.3	576.2	361.8

47.4%

n_rad = 5mm

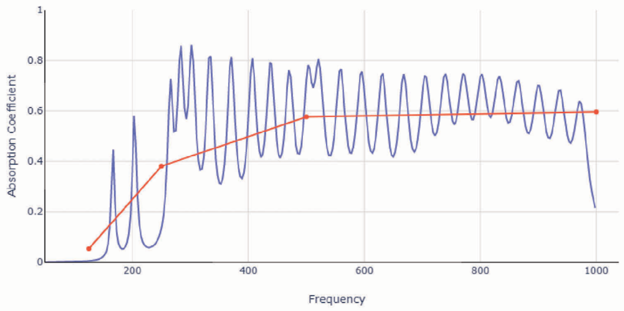

597.8	488.8	269.9	778.1	721.8
649.5	195.6	401.3	324.7	750.3
470.2	255.6	245.5	567.7	163.5
377.3	297.6	352.1	539.4	628.2
694.2	433.3	578.9	429.0	670.8

2 VAR - constant neck lengths

N = 5 (5x5 panel)
spacing = 60mm
panel_depth = 120mm
n_length = 5mm
fitness func = curve area

29.4%

n_rad = 3mm

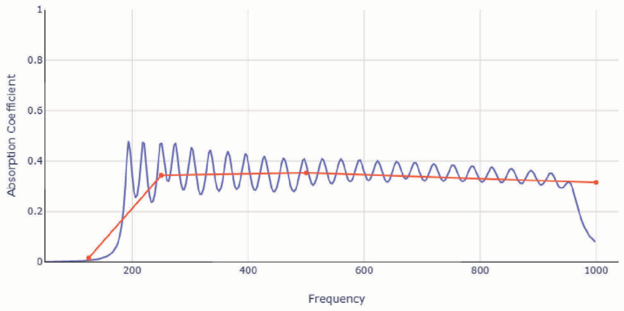

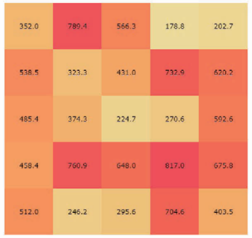

352.0	789.4	566.3	178.8	202.7
538.5	323.3	431.0	732.9	620.2
485.4	374.3	224.7	270.6	592.6
458.4	760.9	648.0	817.0	675.8
512.0	246.2	295.6	704.6	403.5

41.1%

n_rad = 4mm

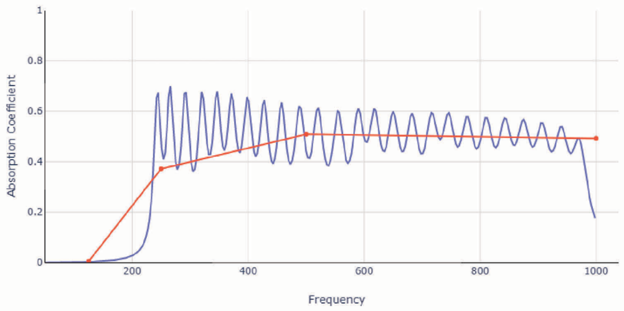

774.9	343.9	800.1	241.2	644.2
469.3	568.2	518.3	618.4	722.3
407.2	748.0	542.2	308.9	670.7
439.9	259.2	413.3	373.1	595.3
696.8	280.3	493.6	321.3	220.5

49.6%

n_rad = 5mm

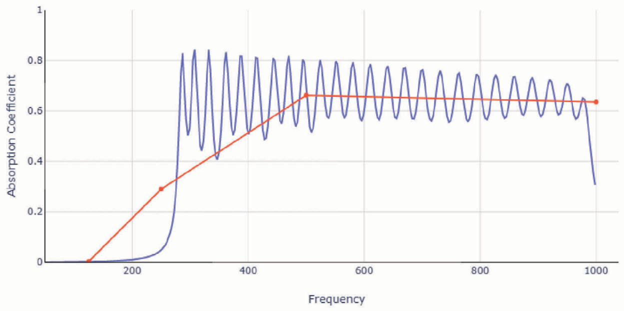

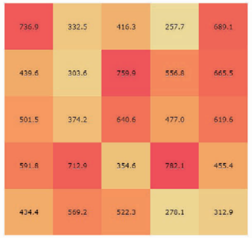

736.9	332.5	416.3	257.7	689.1
439.6	303.6	759.9	556.8	665.5
501.5	374.2	640.6	477.0	619.6
591.8	712.9	354.6	782.1	455.4
434.4	569.2	522.3	278.1	312.9

Varying neck radius

N = 5 (5x5 panel)
spacing = 60mm
panel_depth = 120mm
fitness func = curve area

3 VAR - different HR lengths

Area = 457.2 < 48.2% > 48.2%

n_rad = 6mm

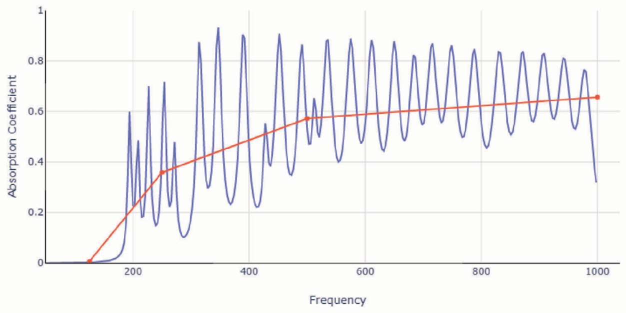

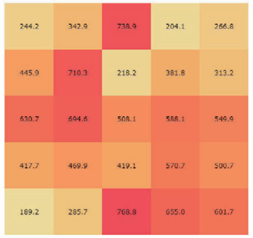

244.2	342.9	738.9	204.1	266.8
445.9	710.3	218.2	381.8	313.2
630.7	694.6	508.1	588.1	549.9
417.7	469.9	419.1	570.7	500.7
189.2	285.7	768.8	655.0	601.7

Area = 428.4 < 45.2% > 45.2%

n_rad = 7mm

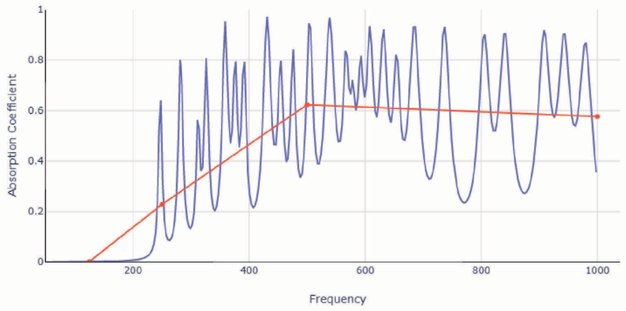

671.0	651.6	592.2	548.7	555.0
310.7	732.2	756.8	559.7	375.4
551.8	265.8	303.0	240.6	574.0
446.0	416.7	530.1	604.7	500.7
377.0	460.9	335.9	767.3	379.1

2 VAR - constant neck lengths

N = 5 (5x5 panel)
spacing = 60mm
panel_depth = 120mm
n_length = 5mm
fitness func = curve area

Area = 518.9 < 54.7% > 54.7%

n_rad = 6mm

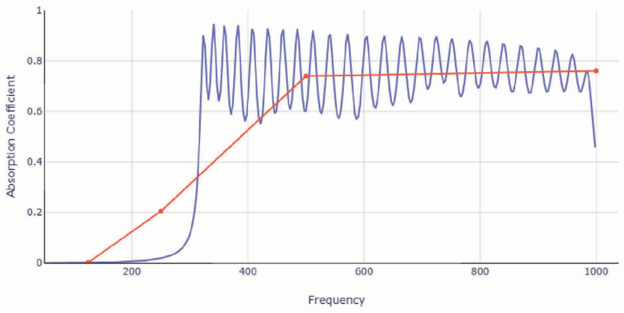

596.9	398.2	309.3	327.0	706.0
383.7	336.6	446.2	748.8	472.5
577.3	419.6	641.1	767.9	291.4
489.9	434.0	535.1	727.3	512.4
619.3	692.5	556.4	350.8	662.6

Area = 534.3 < 56.4% > 56.4%

n_rad = 7mm

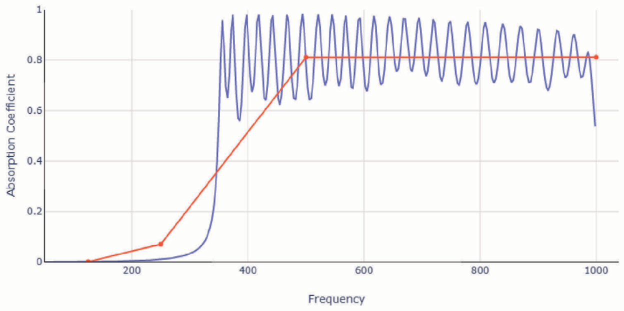

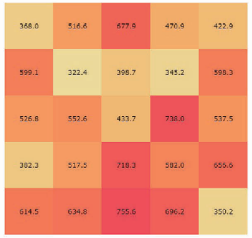

368.0	516.6	677.9	470.9	422.9
599.1	322.4	398.7	345.2	598.3
526.8	552.6	433.7	738.0	537.5
382.3	517.5	718.3	582.0	656.6
614.5	634.8	755.6	696.2	350.2

2 VAR - constant HR length

N = 5 (5x5 panel)
spacing = 60mm
panel_depth = 120mm
fitness func = curve area

Area = 178.8 < 18.9% > 18.9%

n_rad = 3mm

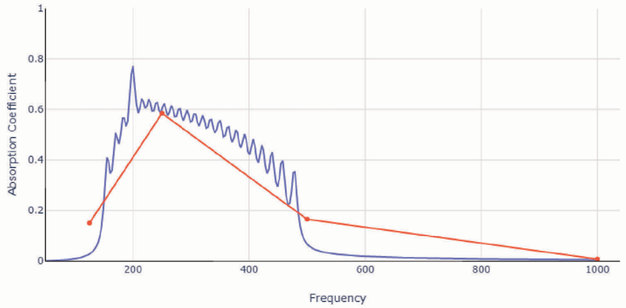

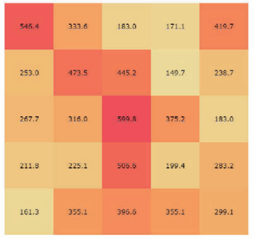

546.4	333.6	183.0	171.1	419.7
253.0	473.5	445.2	149.7	238.7
267.7	316.0	599.8	375.2	183.0
211.8	225.1	506.6	199.4	283.2
161.3	355.1	396.6	355.1	299.1

Area = 227.8 < 24.0% > 24.0%

n_rad = 4mm

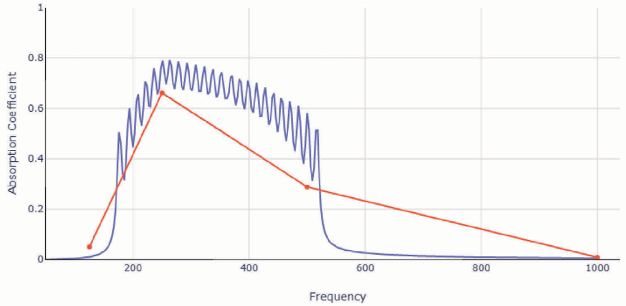

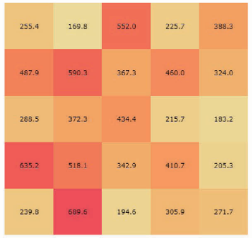

255.4	169.8	552.0	225.7	388.3
487.9	590.3	367.3	460.0	324.0
288.5	372.3	434.4	215.7	183.2
635.2	518.1	342.9	410.7	205.3
239.8	689.6	194.6	305.9	271.7

Area = 259.2 < 27.3% > 27.3%

n_rad = 5mm

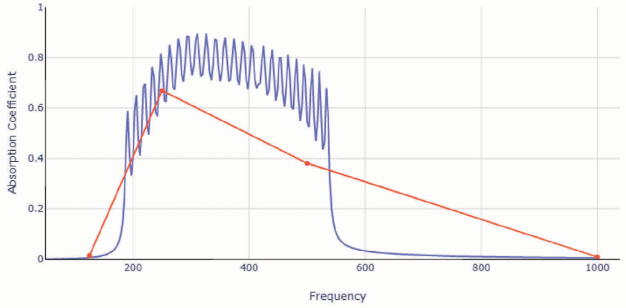

241.5	590.2	263.8	319.0	431.1
252.6	207.7	630.2	463.8	437.5
675.2	299.6	554.4	281.1	725.3
382.2	230.3	360.2	219.1	521.8
405.5	195.8	183.9	491.7	339.2

No constraint

N = 5 (5x5 panel)
spacing = 60mm
fitness func = curve area

Area = 137.6 < 14.5% > 14.5%

n_rad = 3mm

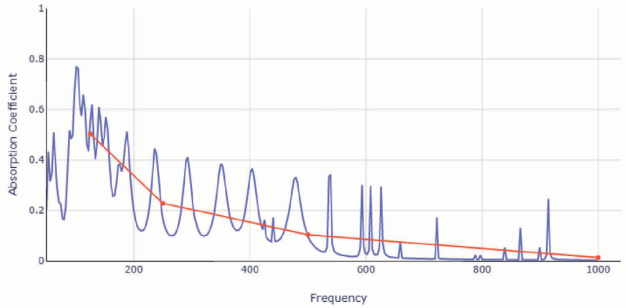

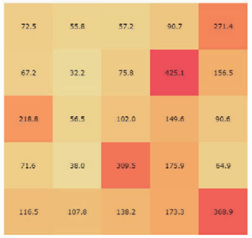

72.5	55.8	57.2	90.7	271.4
67.2	32.2	75.8	425.1	156.5
218.8	56.5	102.0	149.6	90.6
71.6	38.0	309.5	175.9	64.9
116.5	107.8	138.2	173.3	368.9

Area = 183.4 < 19.3% > 19.3%

n_rad = 4mm

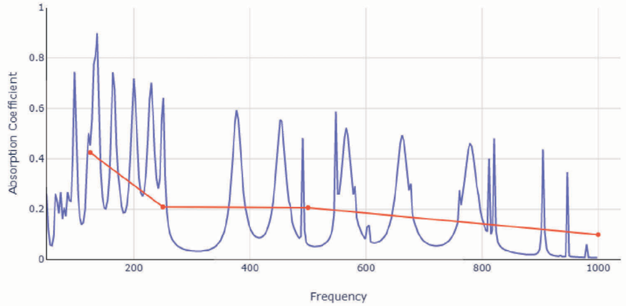

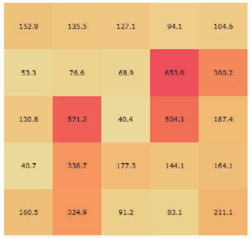

152.9	135.5	127.1	94.1	104.6
53.3	76.6	68.9	653.9	390.2
130.8	571.2	40.4	504.1	187.4
40.7	338.7	177.3	144.1	164.1
160.5	324.9	91.2	83.1	211.1

Area = 257.1 < 27.1% > 27.1%

n_rad = 5mm

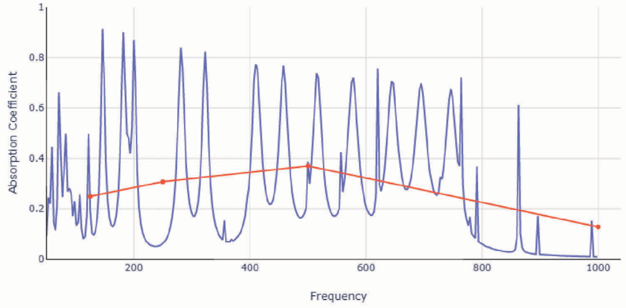

147.8	108.7	83.1	403.7	85.0
254.4	93.7	180.9	29.4	191.6
47.7	454.6	57.0	319.3	91.1
536.1	633.7	61.2	239.7	99.4
156.5	479.6	77.8	349.8	564.1

2 VAR - constant HR length

N = 5 (5x5 panel)
spacing = 60mm
panel_depth = 120mm
fitness func = curve area

n_rad = 6mm

Area = 254.5 < 26.8% > 26.8%

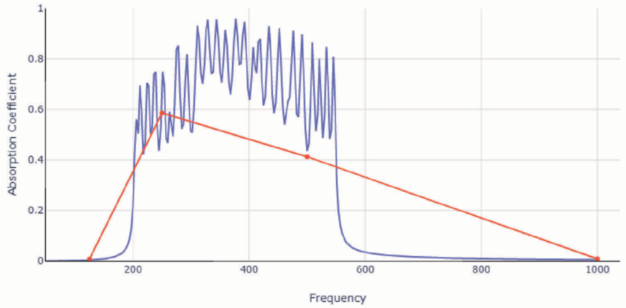

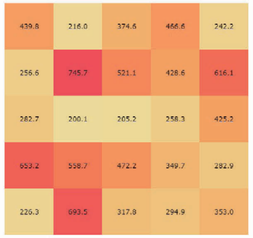

439.8	216.0	374.6	466.6	242.2
256.6	745.7	521.1	428.6	616.1
282.7	200.1	205.2	258.3	425.2
653.2	558.7	472.2	349.7	282.9
226.3	693.5	317.8	294.9	353.0

n_rad = 7mm

Area = 252.1 < 26.6% > 26.6%

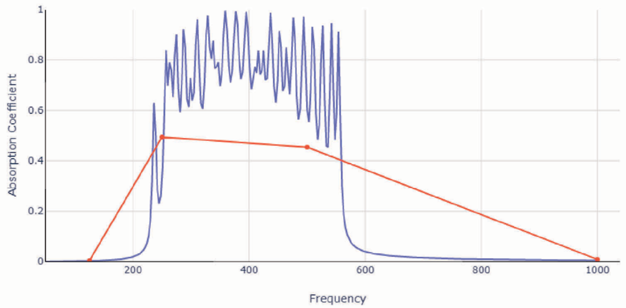

254.9	287.8	290.8	497.5	332.6
756.3	547.5	301.4	404.0	700.9
592.0	339.0	508.3	325.1	368.9
422.8	641.2	269.7	244.0	434.5
431.7	344.6	258.8	483.9	228.9

No constraint

N = 5 (5x5 panel)
spacing = 60mm
fitness func = curve area

n_rad = 6mm

Area = 282.0 < 29.8% > 29.8%

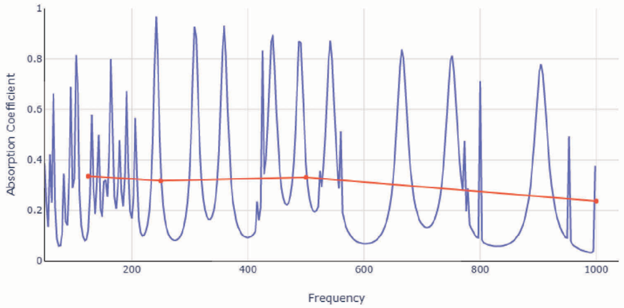

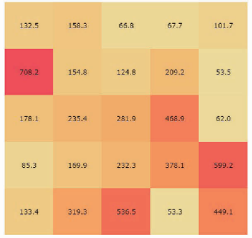

132.5	158.3	66.8	67.7	101.7
708.2	154.8	124.8	209.2	53.5
178.1	235.4	281.9	468.9	62.0
85.3	169.9	232.3	378.1	599.2
133.4	319.3	536.5	53.3	449.1

n_rad = 7mm

Area = 303.8 < 32.0% > 32.0%

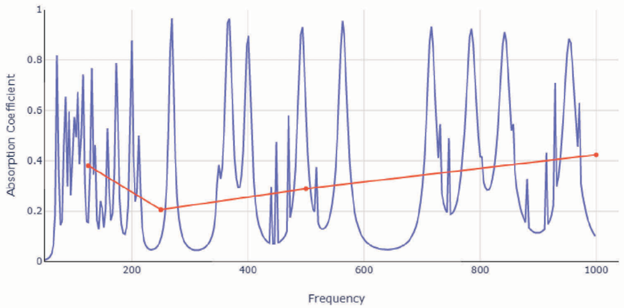

115.0	357.6	108.2	76.6	150.5
104.5	170.8	220.7	92.6	666.0
734.7	161.3	348.1	79.7	623.3
173.7	95.3	210.4	123.3	257.2
330.4	420.5	485.5	630.4	147.5

10.8 Appendix G - Helmholtz resonator's performance calculator

An interface was built using python in Jupyter notebook and libraries, such as Plotly and ipywidgets. Plotly is a python library for generating interactive graphs and charts. Ipywidgets is used for receiving user inputs in the form of text or option from a list of choices. Figure 104 shows the interface to compute the sound absorption of different geometrical configurations of Helmholtz resonators. The calculator is built on the formulas discussed in section 3.3 for the various resonator designs. The user is expected to choose a type of resonator geometry and feed the geometry values in the given text boxes. As the user changes these geometry values, the resonant frequency and the sectional representation of the resonator are automatically updated. The user also has the option to choose one of the additional neck resistances as discussed in section 3.4. The "Generate graph" button produces the absorption performance curve of the resonator over the frequency range specified in the code. Performance comparison can be made between a resonator with and without the additional resistance.

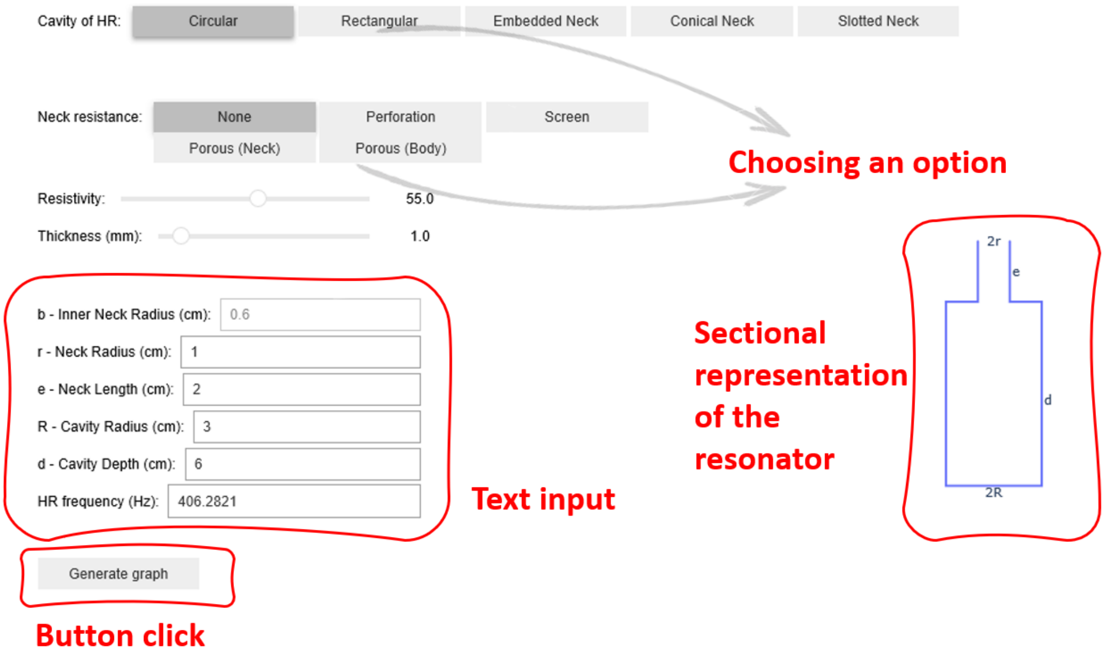

Resistivity: 55.0
Thickness (mm): 1.0

b - Inner Neck Radius (cm): 0.6
r - Neck Radius (cm): 1
e - Neck Length (cm): 2
R - Cavity Radius (cm): 3
d - Cavity Depth (cm): 6
HR frequency (Hz): 406.2821

Choosing an option

Sectional representation of the resonator

Text input

Button click

Figure 103: *Inputs required to run the calculator*

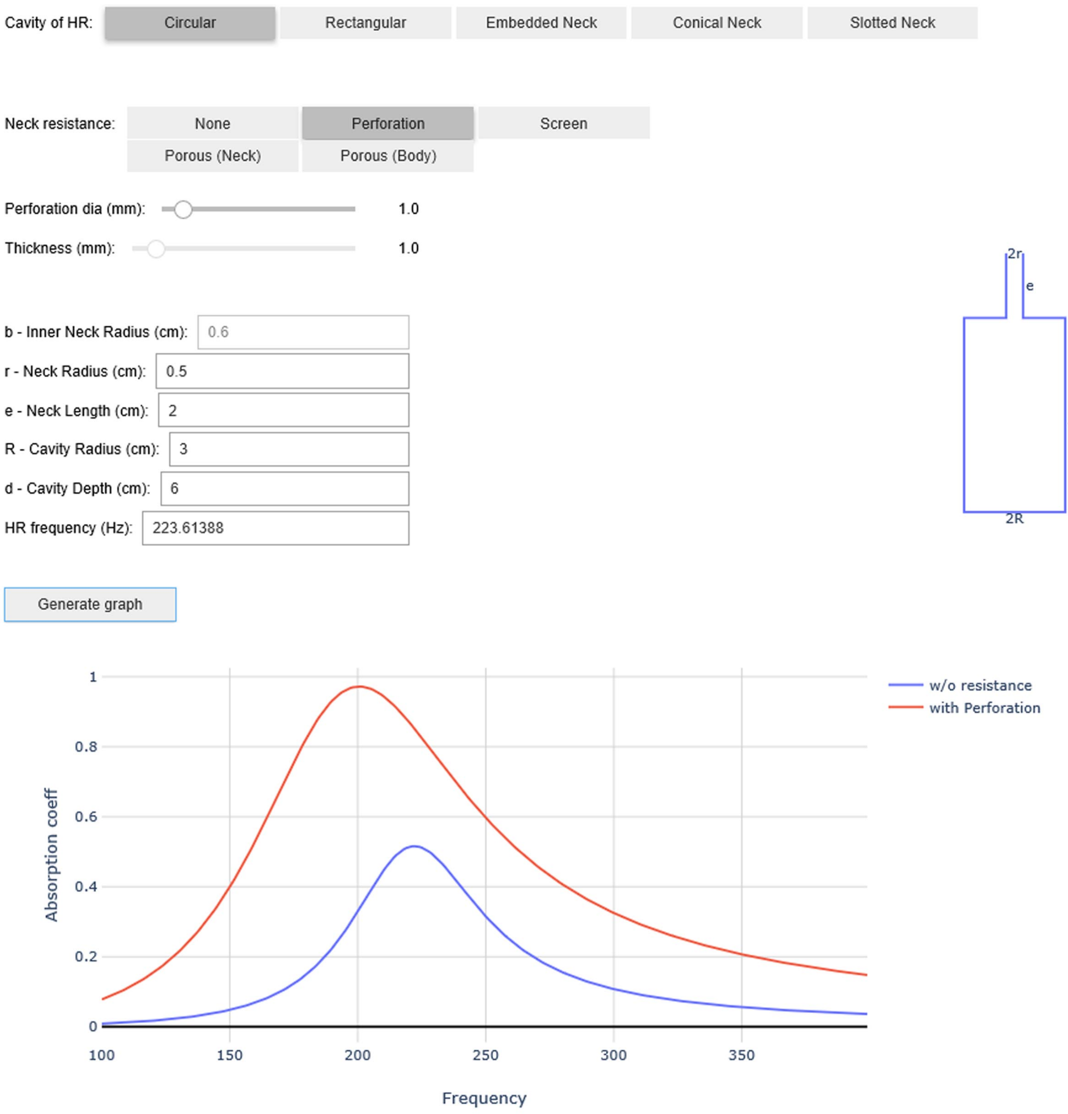

Cavity of HR: Circular

Neck resistance: Perforation

Perforation dia (mm): 1.0

Thickness (mm): 1.0

b - Inner Neck Radius (cm): 0.6

r - Neck Radius (cm): 0.5

e - Neck Length (cm): 2

R - Cavity Radius (cm): 3

d - Cavity Depth (cm): 6

HR frequency (Hz): 223.61388

Figure 104: *Interface for calculating the sound absorption of different kinds of Helmholtz resonators*

10.9 Appendix H - Semi-automated resonator array calculator

A simple interface was built to semi-automate the process of the resonator array design which requires minimum input from the user. The user is expected to provide the bandwidth of absorption that they are interested in and the closeness of the resonance peaks (refer figure 106). This decides the number of resonators in the panels and their resonant frequencies. The user can choose a panel type composed of one out of the three cases discussed in section 4.2 - Cylindrical cavity, Square cavity, and Embedded neck cylindrical cavity (refer figure 107) and control the panel's depth. Based on the resonator geometry, the user can also specify the neck length for maintaining it constant. The neck radius and spacing between the resonators are fixed variables and are defined in the python code.

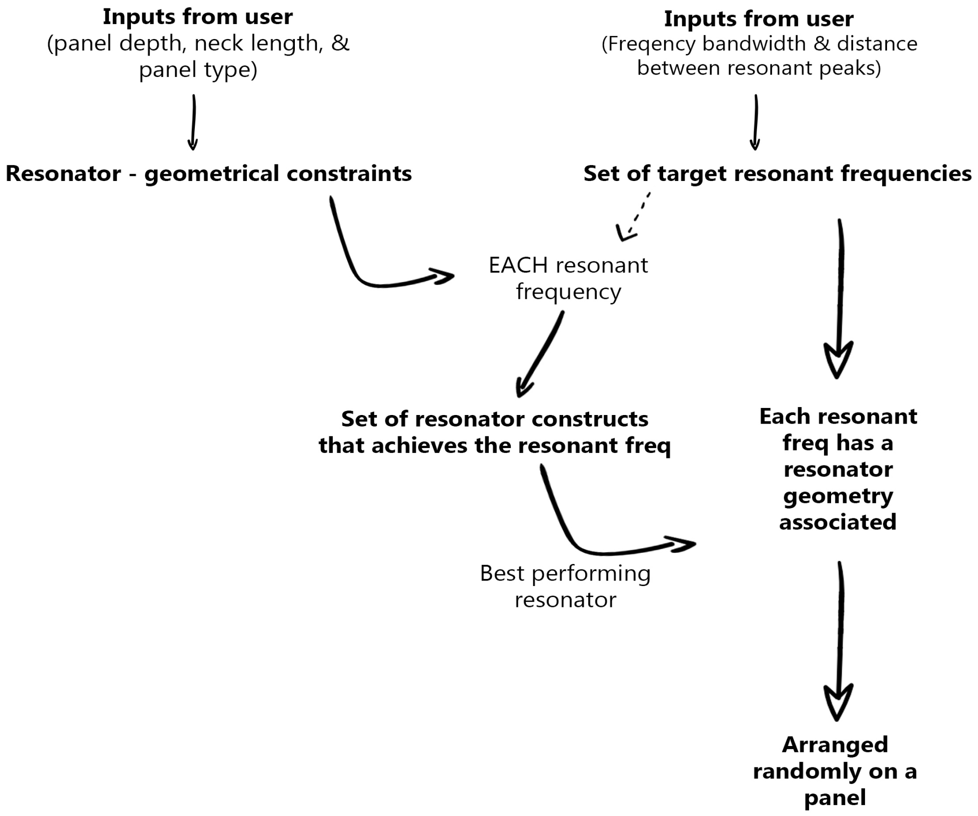

Figure 105: Flow-chart of the algorithm used

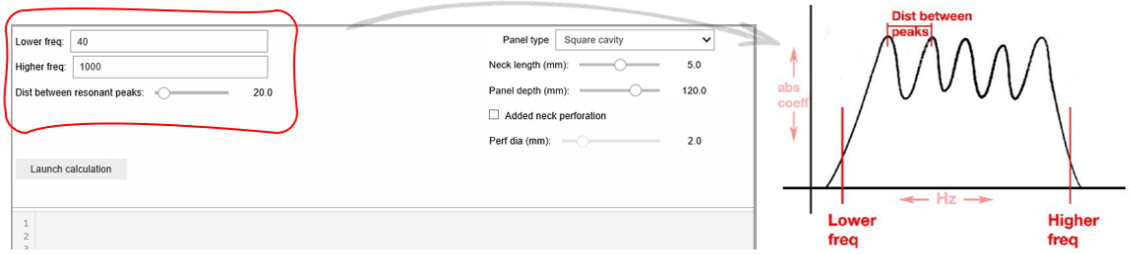

Lower freq: 40
Higher freq: 1000
Dist between resonant peaks: 20.0
Panel type: Square cavity
Neck length (mm): 5.0
Panel depth (mm): 120.0
☐ Added neck perforation
Perf dia (mm): 2.0

Figure 106: Inputs: Frequency bandwidth and the closeness of the resonant frequencies

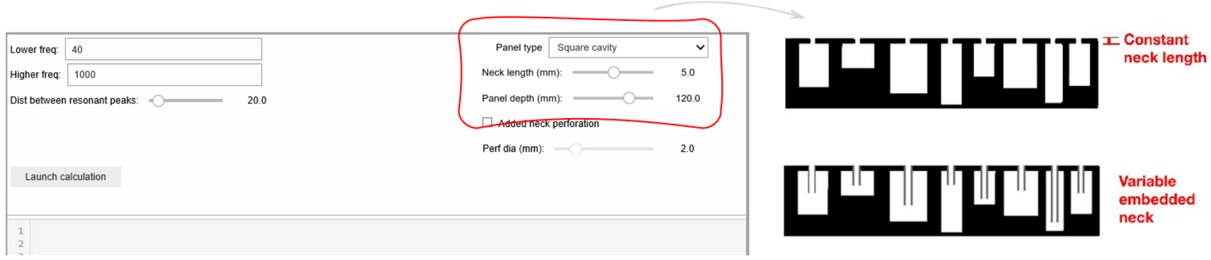

Lower freq: 40
Higher freq: 1000
Dist between resonant peaks: 20.0
Panel type: Square cavity
Neck length (mm): 5.0
Panel depth (mm): 120.0
☐ Added neck perforation
Perf dia (mm): 2.0

Figure 107: Input: Panel type

Additional neck resistance to improve the absorption performance can be added by checking the box in the interface (refer figure 108). Currently, the additional resistance is provided in the form of perforated neck plates. The user can specify the pore size of the perforations.

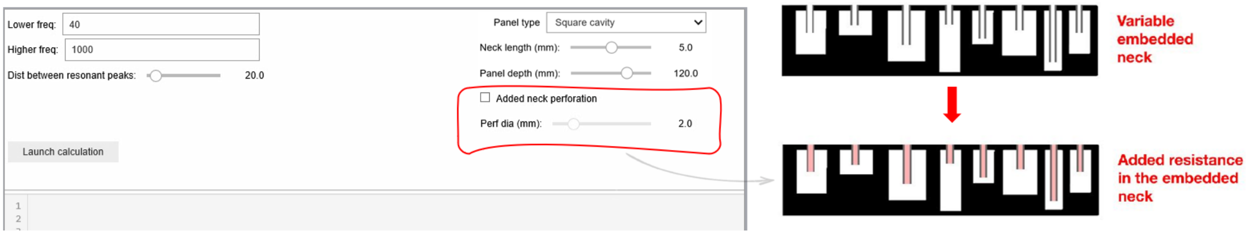

Lower freq: 40
Higher freq: 1000
Dist between resonant peaks: 20.0
Panel type: Square cavity
Neck length (mm): 5.0
Panel depth (mm): 120.0
☐ Added neck perforation
Perf dia (mm): 2.0

Figure 108: Checkbox to include additional neck resistance

10.10 Appendix I - Open office acoustic simulations

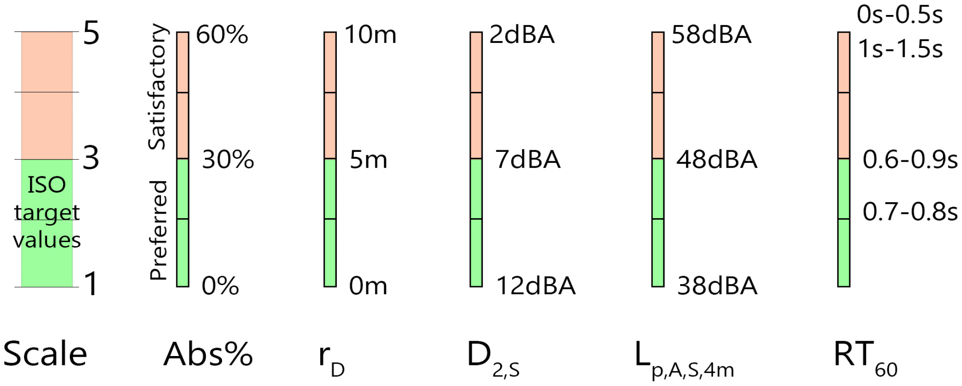

Figure 109: Conversion of single-number parameter ranges to polar scale metrics

Rhino element	Material	Absorption coefficients							
		63Hz	125Hz	250Hz	500Hz	1000Hz	2000Hz	4000Hz	8000Hz
Walls	2x13mm plasterboard on steel frame, 5cm mineral wool in the cavity, surface painted	0.17	0.15	0.1	0.06	0.04	0.04	0.05	0.06
Wall treatment	Fabric tiles	0.03	0.03	0.2	0.3	0.3	0.27	0.19	0.12
Windows	Large pane heavy glass	0.22	0.18	0.06	0.04	0.03	0.02	0.02	0.02
Flooring	Vinyl flooring	0.03	0.04	0.04	0.07	0.06	0.06	0.07	0.07
Corridor	6mm carpet on foam lining	0.03	0.03	0.09	0.25	0.31	0.33	0.44	0.44
Ceiling	Smooth concrete	0.01	0.01	0.01	0.02	0.02	0.02	0.05	0.04
Furniture	Wooden	0.12	0.12	0.12	0.13	0.13	0.1	0.1	0.1
Furn - Table	Wooden table top	0.1	0.15	0.19	0.22	0.39	0.38	0.3	0.25
Furn - Chair	Chair	0.15	0.22	0.28	0.32	0.35	0.32	0.28	0.22
Desk partition	Fabric + foam	0.04	0.19	0.3	0.36	0.52	0.79	0.86	0.73
Ceiling-hung panel	Helmholtz resonator panel	0.35	0.73	0.83	0.93	0.94	0.35	0.3	0.1

Figure 110: Absorption coefficients used in the Rhino model for the acoustic simulation

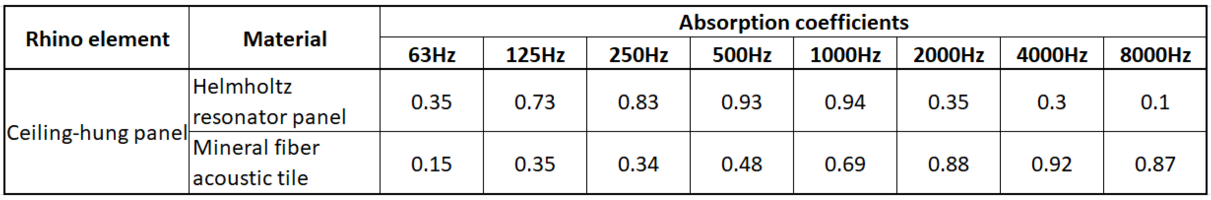

Rhino element	Material	Absorption coefficients							
		63Hz	125Hz	250Hz	500Hz	1000Hz	2000Hz	4000Hz	8000Hz
Ceiling-hung panel	Helmholtz resonator panel	0.35	0.73	0.83	0.93	0.94	0.35	0.3	0.1
	Mineral fiber acoustic tile	0.15	0.35	0.34	0.48	0.69	0.88	0.92	0.87

Figure 111: *Absorption coefficients used Study 1*

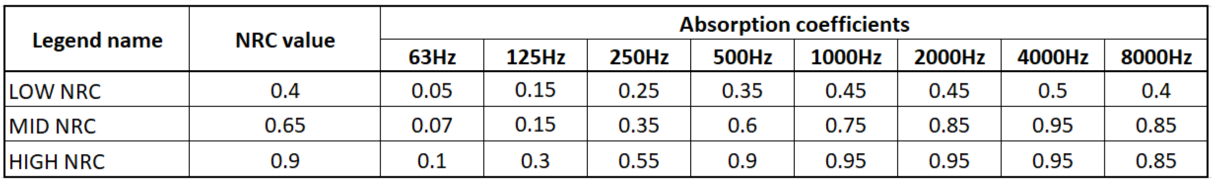

Legend name	NRC value	Absorption coefficients							
		63Hz	125Hz	250Hz	500Hz	1000Hz	2000Hz	4000Hz	8000Hz
LOW NRC	0.4	0.05	0.15	0.25	0.35	0.45	0.45	0.5	0.4
MID NRC	0.65	0.07	0.15	0.35	0.6	0.75	0.85	0.95	0.85
HIGH NRC	0.9	0.1	0.3	0.55	0.9	0.95	0.95	0.95	0.85

Figure 112: *Absorption coefficients used Study 4*

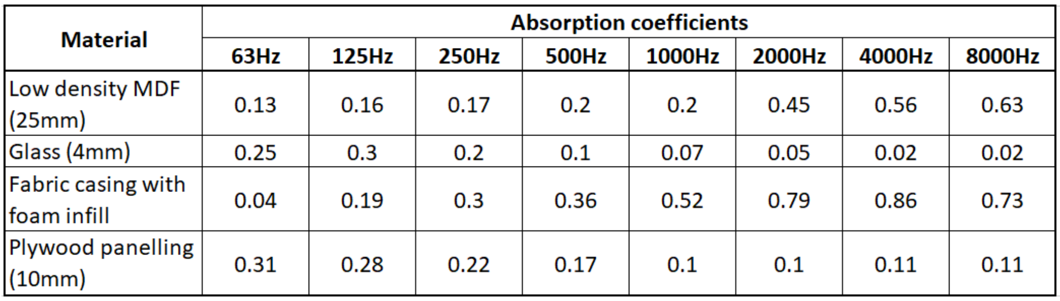

Material	Absorption coefficients							
	63Hz	125Hz	250Hz	500Hz	1000Hz	2000Hz	4000Hz	8000Hz
Low density MDF (25mm)	0.13	0.16	0.17	0.2	0.2	0.45	0.56	0.63
Glass (4mm)	0.25	0.3	0.2	0.1	0.07	0.05	0.02	0.02
Fabric casing with foam infill	0.04	0.19	0.3	0.36	0.52	0.79	0.86	0.73
Plywood panelling (10mm)	0.31	0.28	0.22	0.17	0.1	0.1	0.11	0.11

Figure 113: *Absorption coefficients used Study 4.b*

Study 1 - Efficiency of the HR panel

Helmholtz resonator panel study


Distraction distance with BG level of RC30


Distraction distance with normal activity noise at 37dBA


Distraction distance with background speech noise at 37dBA

Acsoutic tiles study

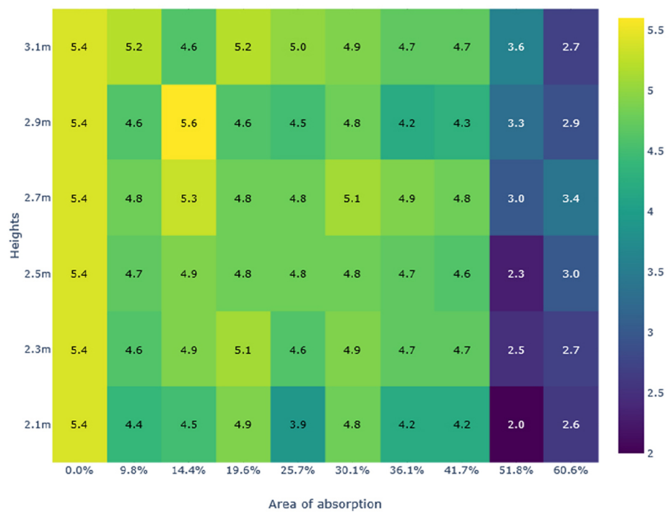
Distraction distance with BG level of RC30


Distraction distance with normal activity noise at 37dBA


Distraction distance with background speech noise at 37dBA

Study 1 - Efficiency of the HR panel

Helmholtz resonator panel study

Spatial decay rate ($D_{2,S}$)

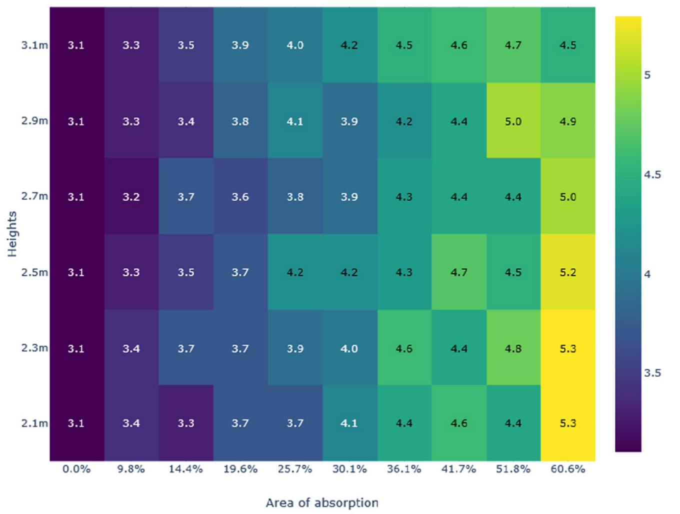

	0.0%	9.8%	14.4%	19.6%	25.7%	30.1%	36.1%	41.7%	51.8%	60.6%
3.1m	3.1	3.3	3.5	3.9	4.0	4.2	4.5	4.6	4.7	4.5
2.9m	3.1	3.3	3.4	3.8	4.1	3.9	4.2	4.4	5.0	4.9
2.7m	3.1	3.2	3.7	3.6	3.8	3.9	4.3	4.4	4.4	5.0
2.5m	3.1	3.3	3.5	3.7	4.2	4.2	4.3	4.7	4.5	5.2
2.3m	3.1	3.4	3.7	3.7	3.9	4.0	4.6	4.4	4.8	5.3
2.1m	3.1	3.4	3.3	3.7	3.7	4.1	4.4	4.6	4.4	5.3

SPL-A at 4m ($L_{p,A,S,4m}$)

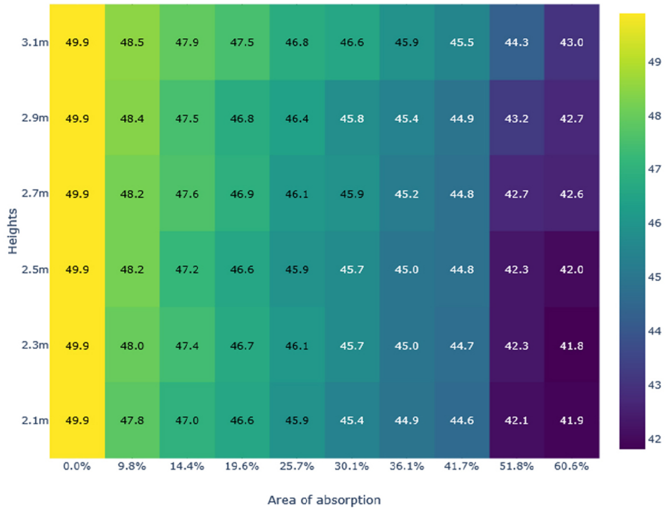

	0.0%	9.8%	14.4%	19.6%	25.7%	30.1%	36.1%	41.7%	51.8%	60.6%
3.1m	49.9	48.5	47.9	47.5	46.8	46.6	45.9	45.5	44.3	43.0
2.9m	49.9	48.4	47.5	46.8	46.4	45.8	45.4	44.9	43.2	42.7
2.7m	49.9	48.2	47.6	46.9	46.1	45.9	45.2	44.8	42.7	42.6
2.5m	49.9	48.2	47.2	46.6	45.9	45.7	45.0	44.8	42.3	42.0
2.3m	49.9	48.0	47.4	46.7	46.1	45.7	45.0	44.7	42.3	41.8
2.1m	49.9	47.8	47.0	46.6	45.9	45.4	44.9	44.6	42.1	41.9

Reverberation Time (RT_{60})

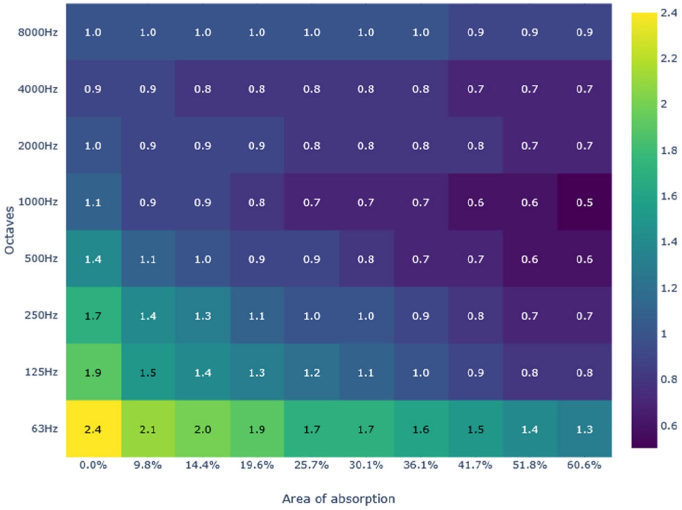

	0.0%	9.8%	14.4%	19.6%	25.7%	30.1%	36.1%	41.7%	51.8%	60.6%
8000Hz	1.0	1.0	1.0	1.0	1.0	1.0	1.0	0.9	0.9	0.9
4000Hz	0.9	0.9	0.8	0.8	0.8	0.8	0.8	0.7	0.7	0.7
2000Hz	1.0	0.9	0.9	0.9	0.8	0.8	0.8	0.8	0.7	0.7
1000Hz	1.1	0.9	0.9	0.8	0.7	0.7	0.7	0.6	0.6	0.5
500Hz	1.4	1.1	1.0	0.9	0.9	0.8	0.7	0.7	0.6	0.6
250Hz	1.7	1.4	1.3	1.1	1.0	1.0	0.9	0.8	0.7	0.7
125Hz	1.9	1.5	1.4	1.3	1.2	1.1	1.0	0.9	0.8	0.8
63Hz	2.4	2.1	2.0	1.9	1.7	1.7	1.6	1.5	1.4	1.3

Acsoutic tiles study

Spatial decay rate ($D_{2,S}$)

	0.0%	9.8%	14.4%	19.6%	25.7%	30.1%	36.1%	41.7%	51.8%	60.6%
3.1m	3.1	3.3	3.4	3.6	3.8	3.8	4.2	4.3	4.2	4.2
2.9m	3.1	3.3	3.4	3.5	3.6	4.0	3.9	4.2	4.3	4.5
2.7m	3.1	3.4	3.5	3.5	3.6	3.8	4.1	3.9	4.3	4.5
2.5m	3.1	3.3	3.4	3.6	3.8	3.9	4.0	4.2	4.4	5.0
2.3m	3.1	3.2	3.6	3.6	4.0	3.9	4.1	4.6	4.5	5.2
2.1m	3.1	3.4	3.5	3.9	3.7	3.8	4.2	4.4	4.6	5.1

SPL-A at 4m ($L_{p,A,S,4m}$)

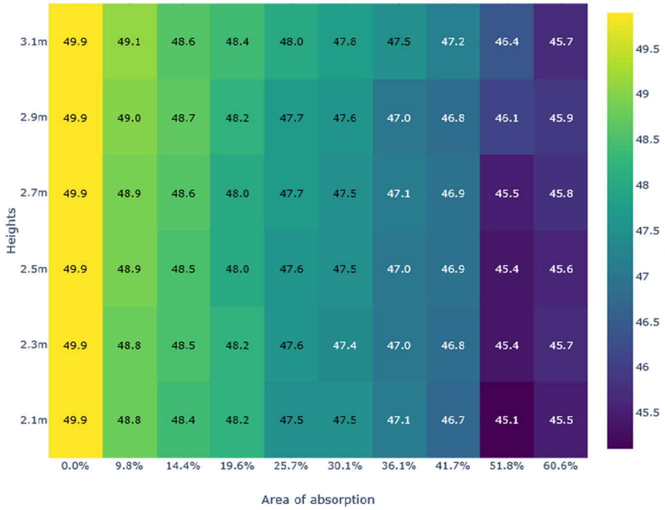

	0.0%	9.8%	14.4%	19.6%	25.7%	30.1%	36.1%	41.7%	51.8%	60.6%
3.1m	49.9	49.1	48.6	48.4	48.0	47.8	47.5	47.2	46.4	45.7
2.9m	49.9	49.0	48.7	48.2	47.7	47.6	47.0	46.8	46.1	45.9
2.7m	49.9	48.9	48.6	48.0	47.7	47.5	47.1	46.9	45.5	45.8
2.5m	49.9	48.9	48.5	48.0	47.6	47.5	47.0	46.9	45.4	45.6
2.3m	49.9	48.8	48.5	48.2	47.6	47.4	47.0	46.8	45.4	45.7
2.1m	49.9	48.8	48.4	48.2	47.5	47.5	47.1	46.7	45.1	45.5

Reverberation Time (RT_{60})

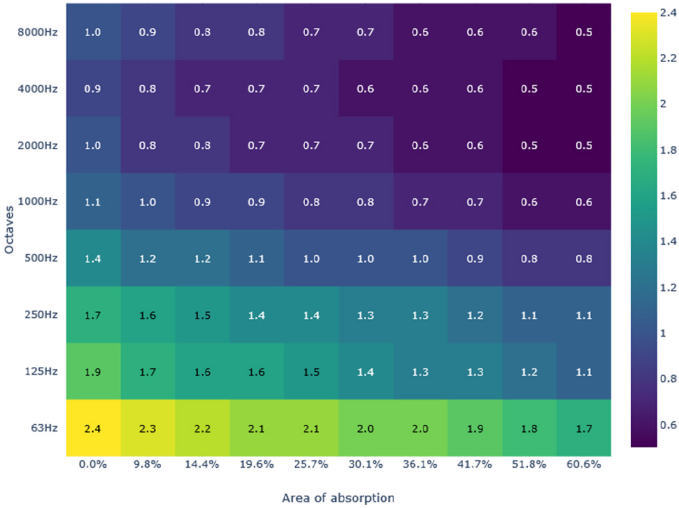

	0.0%	9.8%	14.4%	19.6%	25.7%	30.1%	36.1%	41.7%	51.8%	60.6%
8000Hz	1.0	0.9	0.8	0.8	0.7	0.7	0.6	0.6	0.6	0.5
4000Hz	0.9	0.8	0.7	0.7	0.7	0.6	0.6	0.6	0.5	0.5
2000Hz	1.0	0.8	0.8	0.7	0.7	0.7	0.6	0.6	0.5	0.5
1000Hz	1.1	1.0	0.9	0.9	0.8	0.8	0.7	0.7	0.6	0.6
500Hz	1.4	1.2	1.2	1.1	1.0	1.0	1.0	0.9	0.8	0.8
250Hz	1.7	1.6	1.5	1.4	1.4	1.3	1.3	1.2	1.1	1.1
125Hz	1.9	1.7	1.6	1.6	1.5	1.4	1.3	1.3	1.2	1.1
63Hz	2.4	2.3	2.2	2.1	2.1	2.0	2.0	1.9	1.8	1.7

Study 1 - Efficiency of the HR panel

Helmholtz resonator panel study – Pareto front results

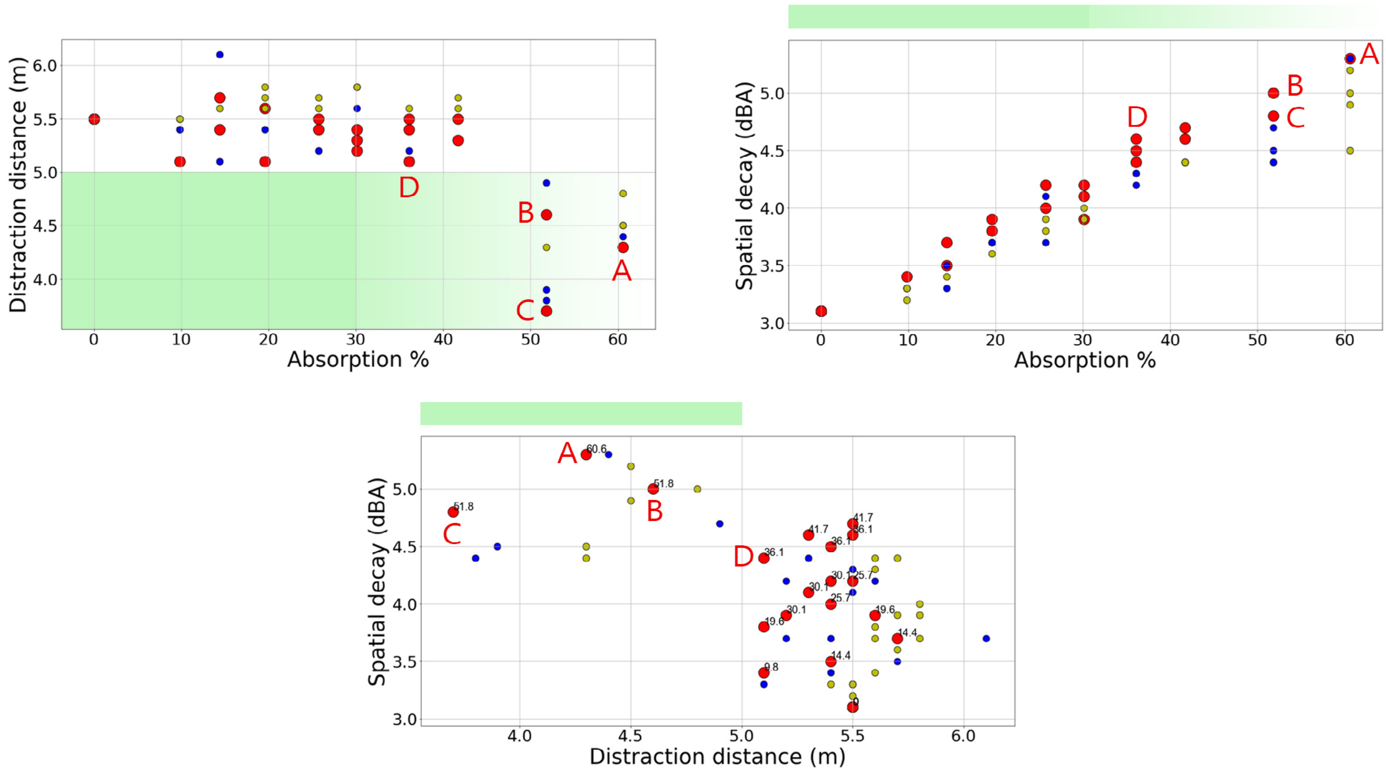

Spider plots of pareto frontier

36.1% absorption @ 2.1m height

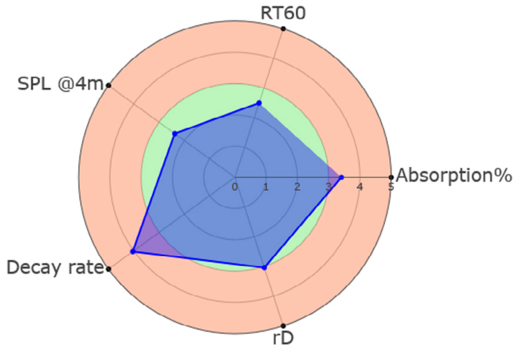

Scenario D

51.8% absorption @ 2.3m height

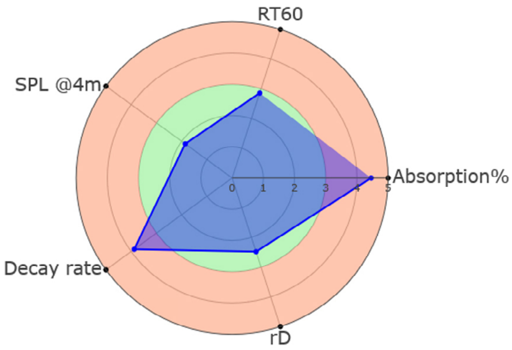

Scenario C

51.8% absorption @ 2.9m height

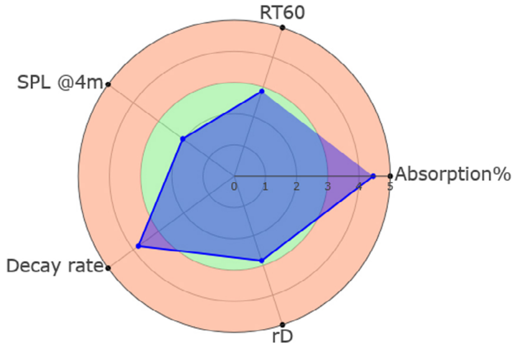

Scenario B

60.6% absorption @ 2.3m height

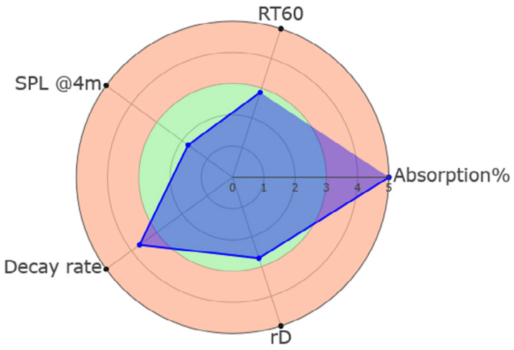

Scenario A

Study 1 - Efficiency of the HR panel

Acsoutic tiles panel study – Pareto front results

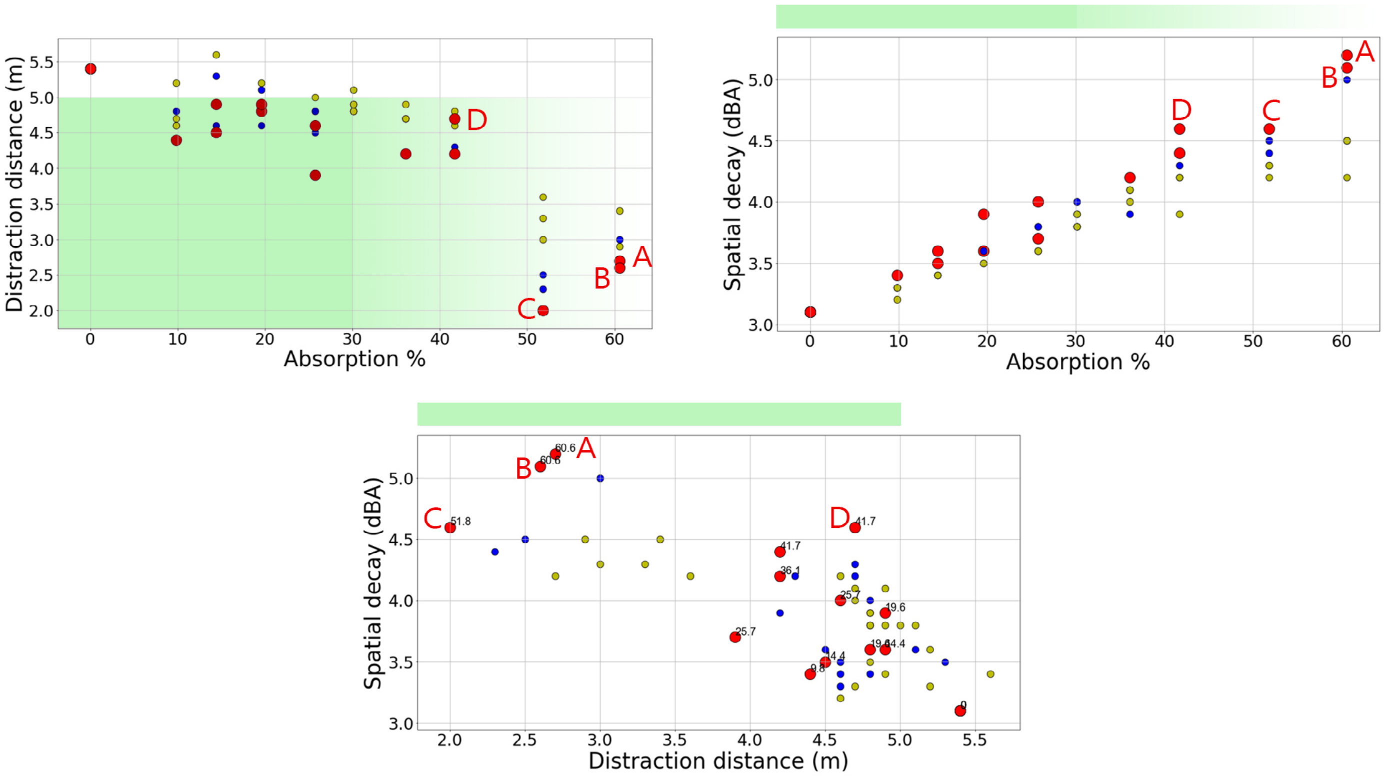

Spider plots of pareto frontier

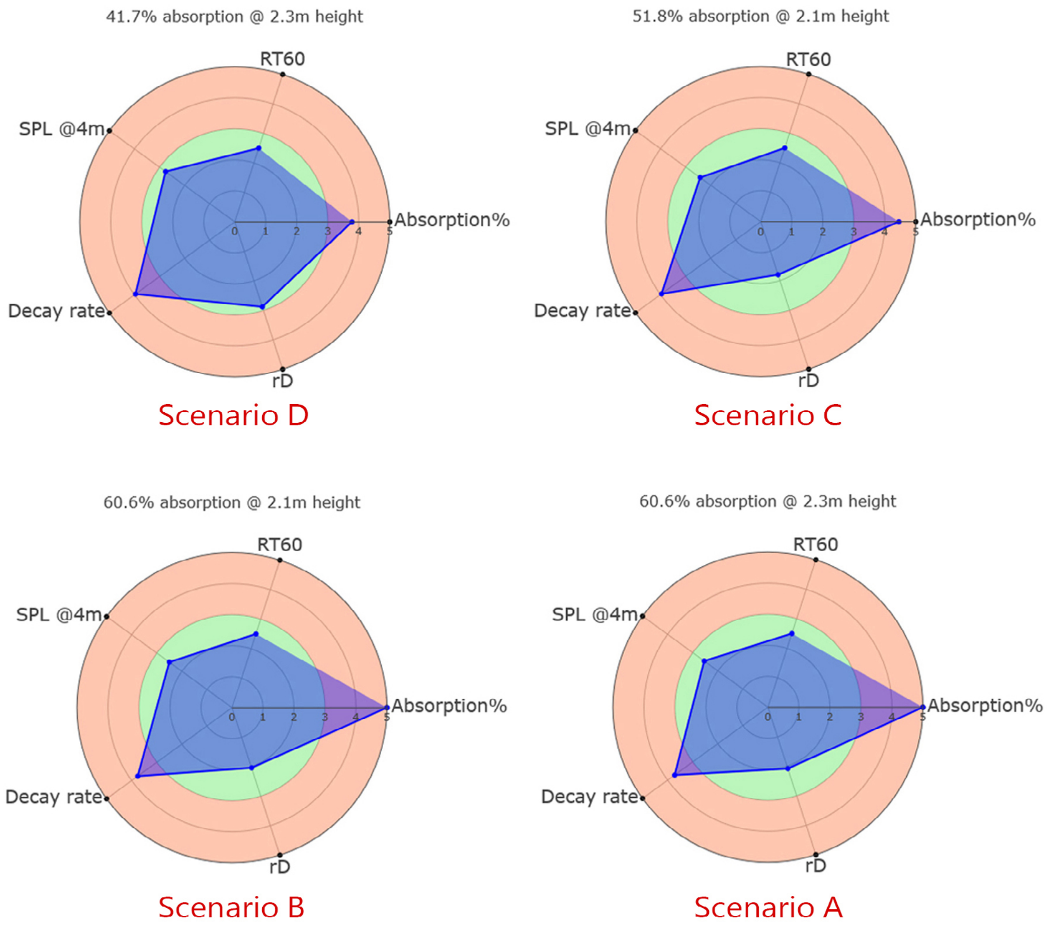

Study 2 - Benchmarking with conventional offices

Distraction distance with BG level of RC30

Distraction distance with normal activity noise at 37dBA

Distraction distance with background speech noise at 37dBA

Spatial decay rate ($D_{2,S}$)

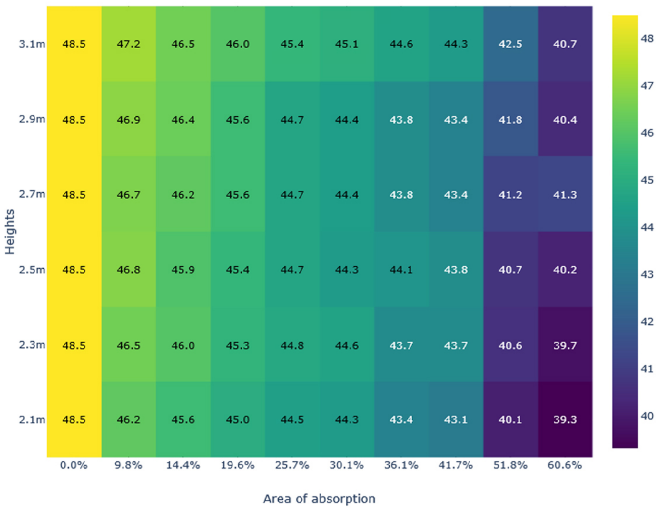

SPL-A at 4m ($L_{p,A,S,4m}$)

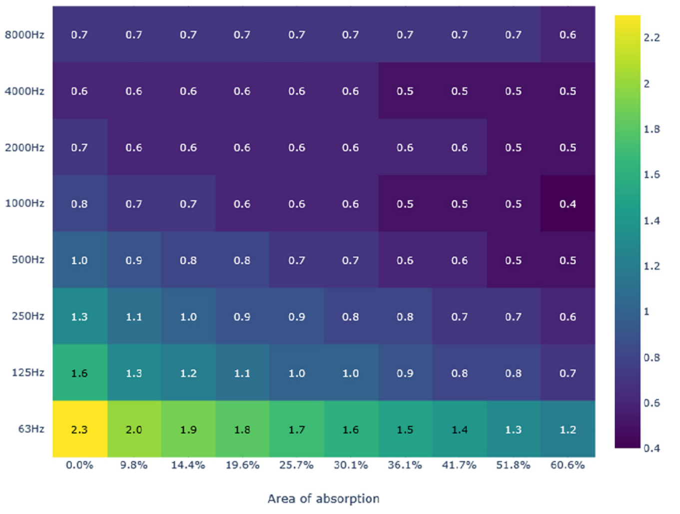

Reverberation Time (RT_{60})

Study 3 - Flat vs. Tilted HR panels

Flat HR panel study

Distraction distance with BG level of RC30

Heights	0.0%	9.8%	14.4%	19.6%	25.7%	30.1%	36.1%	41.7%	51.8%	60.6%
3.1m	5.5	5.4	5.4	5.6	5.4	5.6	5.4	5.5	4.9	4.3
2.9m	5.5	5.5	5.6	5.1	5.5	5.2	5.2	5.3	4.6	4.5
2.7m	5.5	5.5	6.1	5.7	5.6	5.8	5.6	5.6	4.3	4.8
2.5m	5.5	5.5	5.7	5.6	5.5	5.4	5.5	5.5	3.9	4.5
2.3m	5.5	5.4	5.7	5.8	5.7	5.8	5.5	5.7	3.7	4.3

Distraction distance with normal activity noise at 37dBA

Heights	0.0%	9.8%	14.4%	19.6%	25.7%	30.1%	36.1%	41.7%	51.8%	60.6%
3.1m	5.2	5.1	5.1	5.3	5.1	5.3	5.1	5.2	4.5	3.8
2.9m	5.2	5.2	5.3	4.8	5.1	4.8	4.8	4.9	4.1	4.0
2.7m	5.2	5.2	5.8	5.3	5.2	5.4	5.1	5.1	3.8	4.3
2.5m	5.2	5.2	5.3	5.3	5.1	5.1	5.1	5.1	3.4	4.0
2.3m	5.2	5.1	5.4	5.5	5.4	5.5	5.1	5.3	3.2	3.9

Distraction distance with background speech noise at 37dBA

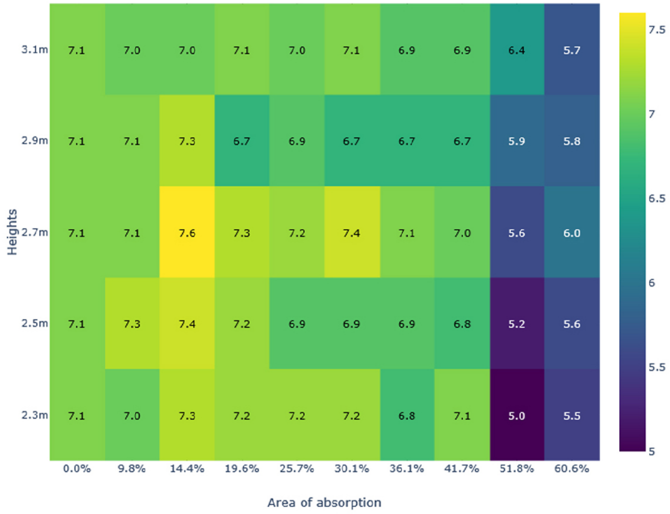

Heights	0.0%	9.8%	14.4%	19.6%	25.7%	30.1%	36.1%	41.7%	51.8%	60.6%
3.1m	7.1	7.0	7.0	7.1	7.0	7.1	6.9	6.9	6.4	5.7
2.9m	7.1	7.1	7.3	6.7	6.9	6.7	6.7	6.7	5.9	5.8
2.7m	7.1	7.1	7.6	7.3	7.2	7.4	7.1	7.0	5.6	6.0
2.5m	7.1	7.3	7.4	7.2	6.9	6.9	6.9	6.8	5.2	5.6
2.3m	7.1	7.0	7.3	7.2	7.2	7.2	6.8	7.1	5.0	5.5

Tilted HR panel study

Distraction distance with BG level of RC30

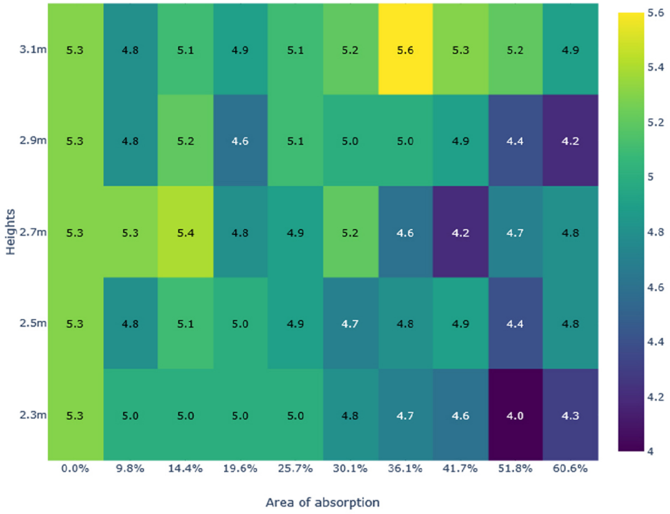

Heights	0.0%	9.8%	14.4%	19.6%	25.7%	30.1%	36.1%	41.7%	51.8%	60.6%
3.1m	5.3	4.8	5.1	4.9	5.1	5.2	5.6	5.3	5.2	4.9
2.9m	5.3	4.8	5.2	4.6	5.1	5.0	5.0	4.9	4.4	4.2
2.7m	5.3	5.3	5.4	4.8	4.9	5.2	4.6	4.2	4.7	4.8
2.5m	5.3	4.8	5.1	5.0	4.9	4.7	4.8	4.9	4.4	4.8
2.3m	5.3	5.0	5.0	5.0	5.0	4.8	4.7	4.6	4.0	4.3

Distraction distance with normal activity noise at 37dBA

Heights	0.0%	9.8%	14.4%	19.6%	25.7%	30.1%	36.1%	41.7%	51.8%	60.6%
3.1m	5.1	4.5	4.8	4.6	4.7	4.9	5.2	4.9	4.9	4.6
2.9m	5.1	4.5	4.9	4.3	4.7	4.6	4.6	4.5	4.1	3.8
2.7m	5.1	5.0	5.0	4.4	4.4	4.7	4.1	3.8	4.3	4.4
2.5m	5.1	4.5	4.7	4.6	4.4	4.3	4.4	4.4	4.0	4.3
2.3m	5.1	4.6	4.6	4.6	4.5	4.4	4.2	4.2	3.6	3.9

Distraction distance with background speech noise at 37dBA

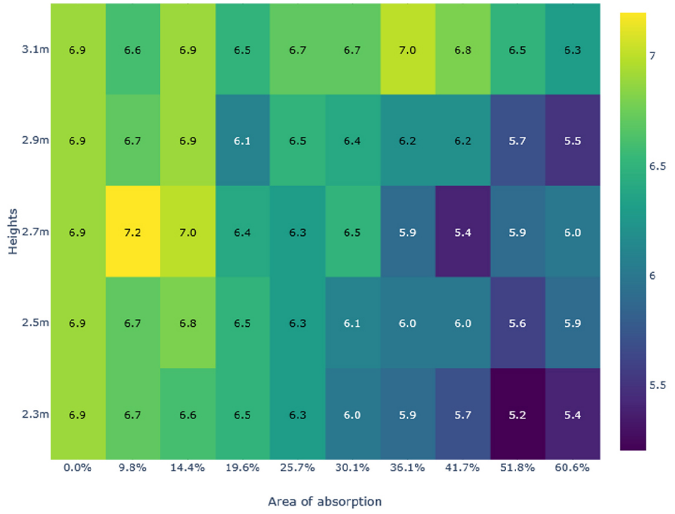

Heights	0.0%	9.8%	14.4%	19.6%	25.7%	30.1%	36.1%	41.7%	51.8%	60.6%
3.1m	6.9	6.6	6.9	6.5	6.7	6.7	7.0	6.8	6.5	6.3
2.9m	6.9	6.7	6.9	6.1	6.5	6.4	6.2	6.2	5.7	5.5
2.7m	6.9	7.2	7.0	6.4	6.3	6.5	5.9	5.4	5.9	6.0
2.5m	6.9	6.7	6.8	6.5	6.3	6.1	6.0	6.0	5.6	5.9
2.3m	6.9	6.7	6.6	6.5	6.3	6.0	5.9	5.7	5.2	5.4

Study 3 - Flat vs. Tilted HR panels

Flat HR panel study

Spatial decay rate ($D_{2,S}$)

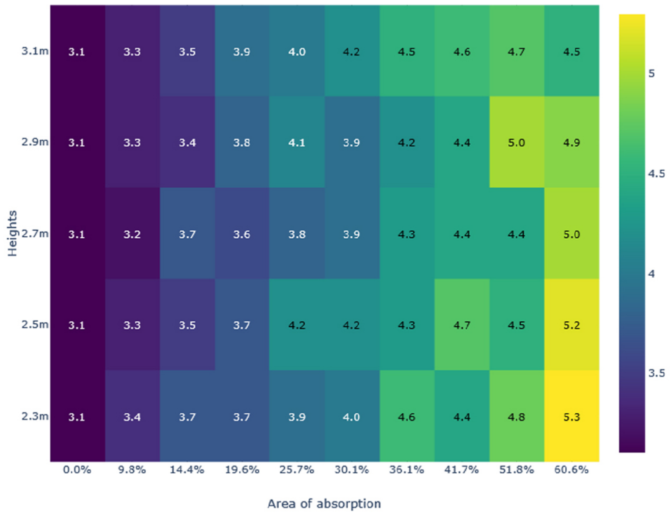

Heights	0.0%	9.8%	14.4%	19.6%	25.7%	30.1%	36.1%	41.7%	51.8%	60.6%
3.1m	3.1	3.3	3.5	3.9	4.0	4.2	4.5	4.6	4.7	4.5
2.9m	3.1	3.3	3.4	3.8	4.1	3.9	4.2	4.4	5.0	4.9
2.7m	3.1	3.2	3.7	3.6	3.8	3.9	4.3	4.4	4.4	5.0
2.5m	3.1	3.3	3.5	3.7	4.2	4.2	4.3	4.7	4.5	5.2
2.3m	3.1	3.4	3.7	3.7	3.9	4.0	4.6	4.4	4.8	5.3

SPL-A at 4m ($L_{p,A,S,4m}$)

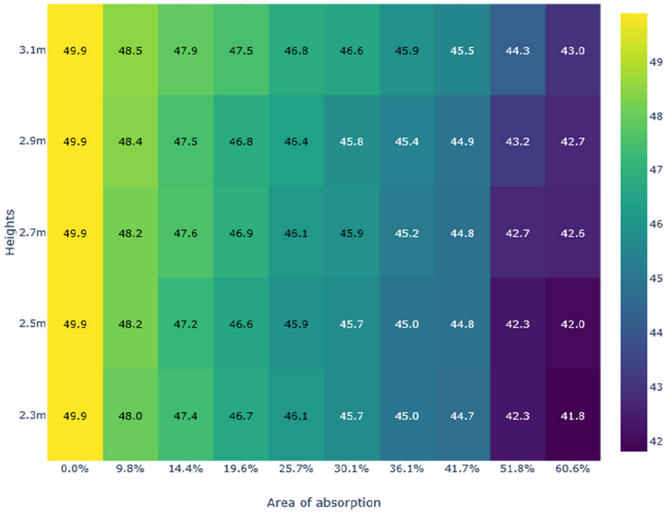

Heights	0.0%	9.8%	14.4%	19.6%	25.7%	30.1%	36.1%	41.7%	51.8%	60.6%
3.1m	49.9	48.5	47.9	47.5	46.8	46.6	45.9	45.5	44.3	43.0
2.9m	49.9	48.4	47.5	46.8	46.4	45.8	45.4	44.9	43.2	42.7
2.7m	49.9	48.2	47.6	46.9	46.1	45.9	45.2	44.8	42.7	42.6
2.5m	49.9	48.2	47.2	46.6	45.9	45.7	45.0	44.8	42.3	42.0
2.3m	49.9	48.0	47.4	46.7	46.1	45.7	45.0	44.7	42.3	41.8

Reverberation Time (RT_{60})

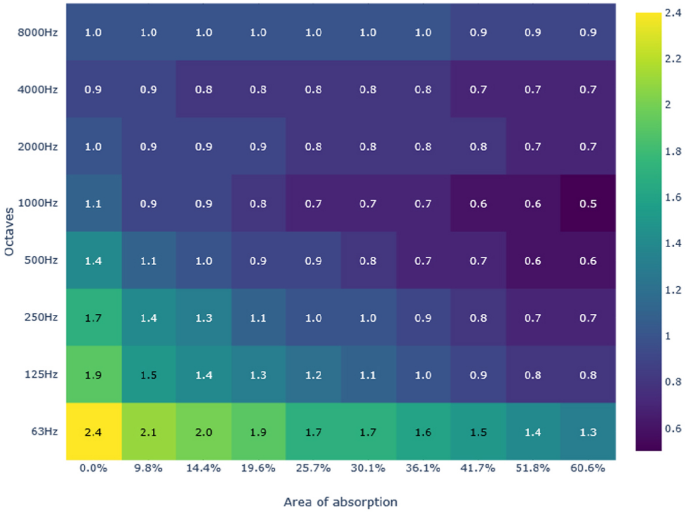

Octaves	0.0%	9.8%	14.4%	19.6%	25.7%	30.1%	36.1%	41.7%	51.8%	60.6%
8000Hz	1.0	1.0	1.0	1.0	1.0	1.0	1.0	0.9	0.9	0.9
4000Hz	0.9	0.9	0.8	0.8	0.8	0.8	0.8	0.7	0.7	0.7
2000Hz	1.0	0.9	0.9	0.9	0.8	0.8	0.8	0.8	0.7	0.7
1000Hz	1.1	0.9	0.9	0.8	0.7	0.7	0.7	0.6	0.6	0.5
500Hz	1.4	1.1	1.0	0.9	0.9	0.8	0.7	0.7	0.6	0.6
250Hz	1.7	1.4	1.3	1.1	1.0	1.0	0.9	0.8	0.7	0.7
125Hz	1.9	1.5	1.4	1.3	1.2	1.1	1.0	0.9	0.8	0.8
63Hz	2.4	2.1	2.0	1.9	1.7	1.7	1.6	1.5	1.4	1.3

Tilted HR panel study

Spatial decay rate ($D_{2,S}$)

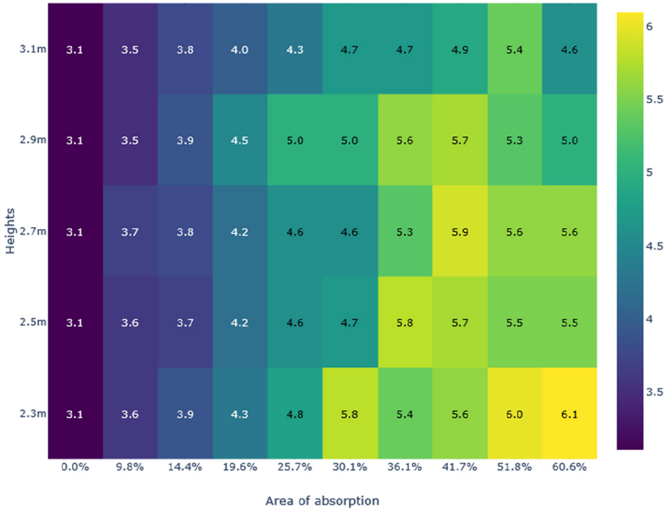

Heights	0.0%	9.8%	14.4%	19.6%	25.7%	30.1%	36.1%	41.7%	51.8%	60.6%
3.1m	3.1	3.5	3.8	4.0	4.3	4.7	4.7	4.9	5.4	4.6
2.9m	3.1	3.5	3.9	4.5	5.0	5.0	5.6	5.7	5.3	5.0
2.7m	3.1	3.7	3.8	4.2	4.6	4.6	5.3	5.9	5.6	5.6
2.5m	3.1	3.6	3.7	4.2	4.6	4.7	5.8	5.7	5.5	5.5
2.3m	3.1	3.6	3.9	4.3	4.8	5.8	5.4	5.6	6.0	6.1

SPL-A at 4m ($L_{p,A,S,4m}$)

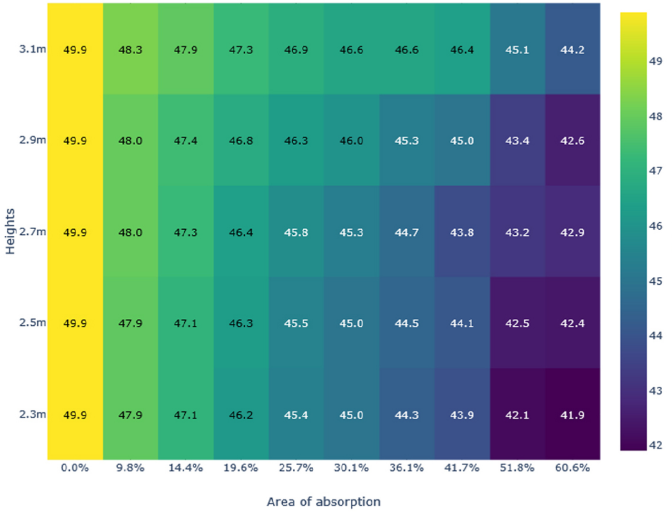

Heights	0.0%	9.8%	14.4%	19.6%	25.7%	30.1%	36.1%	41.7%	51.8%	60.6%
3.1m	49.9	48.3	47.9	47.3	46.9	46.6	46.6	46.4	45.1	44.2
2.9m	49.9	48.0	47.4	46.8	46.3	46.0	45.3	45.0	43.4	42.6
2.7m	49.9	48.0	47.3	46.4	45.8	45.3	44.7	43.8	43.2	42.9
2.5m	49.9	47.9	47.1	46.3	45.5	45.0	44.5	44.1	42.5	42.4
2.3m	49.9	47.9	47.1	46.2	45.4	45.0	44.3	43.9	42.1	41.9

Reverberation Time (RT_{60})

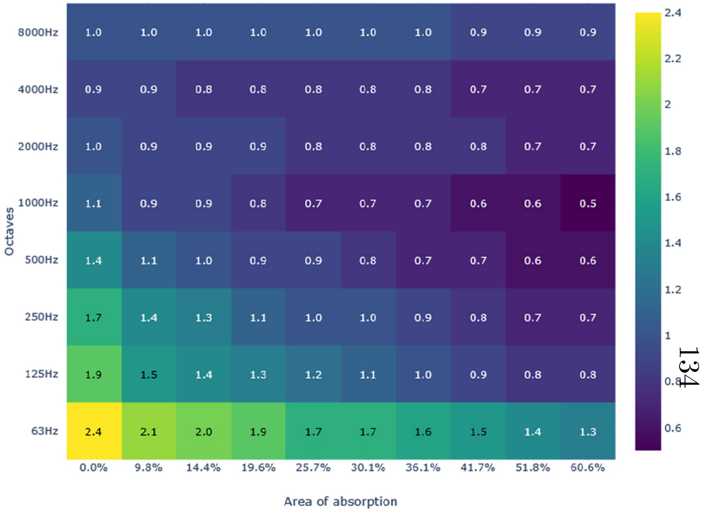

Octaves	0.0%	9.8%	14.4%	19.6%	25.7%	30.1%	36.1%	41.7%	51.8%	60.6%
8000Hz	1.0	1.0	1.0	1.0	1.0	1.0	1.0	0.9	0.9	0.9
4000Hz	0.9	0.9	0.8	0.8	0.8	0.8	0.8	0.7	0.7	0.7
2000Hz	1.0	0.9	0.9	0.9	0.8	0.8	0.8	0.8	0.7	0.7
1000Hz	1.1	0.9	0.9	0.8	0.7	0.7	0.7	0.6	0.6	0.5
500Hz	1.4	1.1	1.0	0.9	0.9	0.8	0.7	0.7	0.6	0.6
250Hz	1.7	1.4	1.3	1.1	1.0	1.0	0.9	0.8	0.7	0.7
125Hz	1.9	1.5	1.4	1.3	1.2	1.1	1.0	0.9	0.8	0.8
63Hz	2.4	2.1	2.0	1.9	1.7	1.7	1.6	1.5	1.4	1.3

Study 3 - Flat vs. Tilted HR panels

Flat HR panel study – Pareto front results

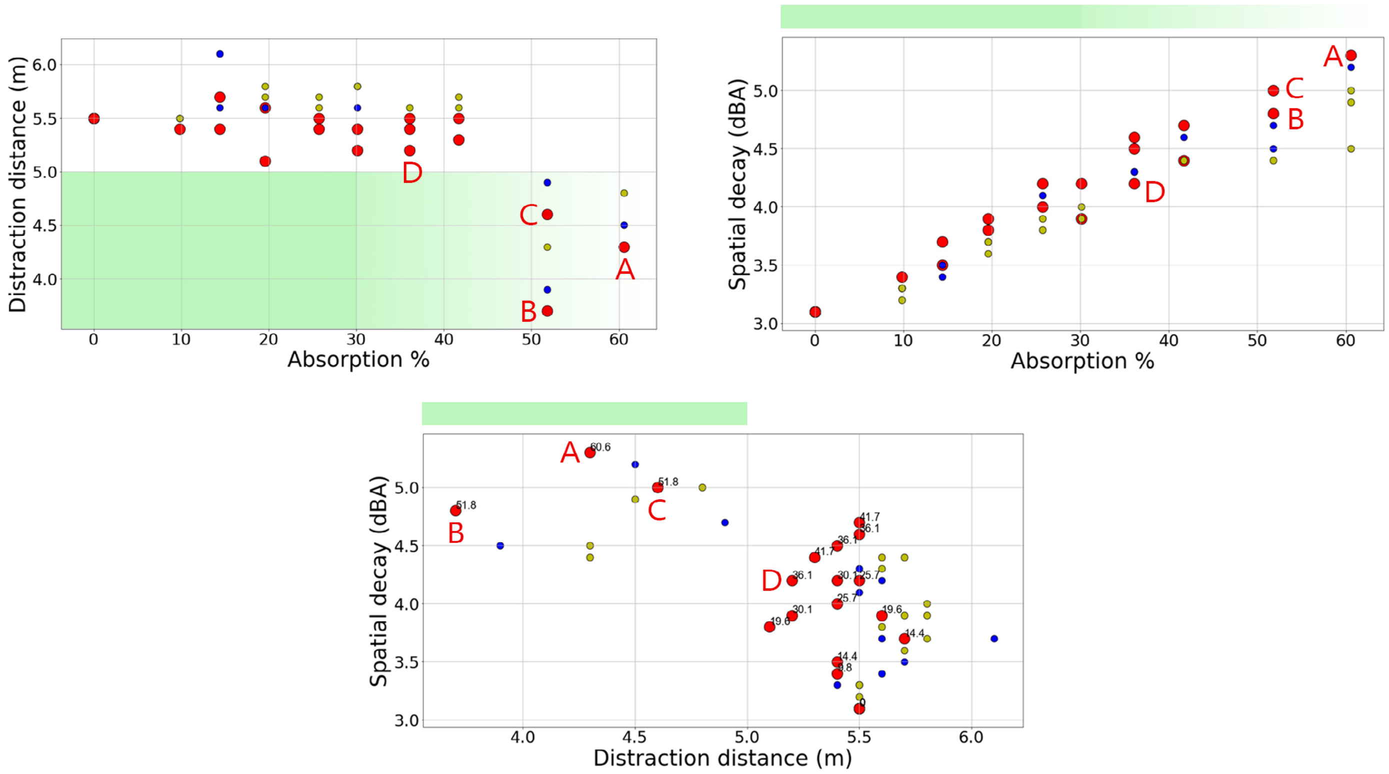

Spider plots of pareto frontier

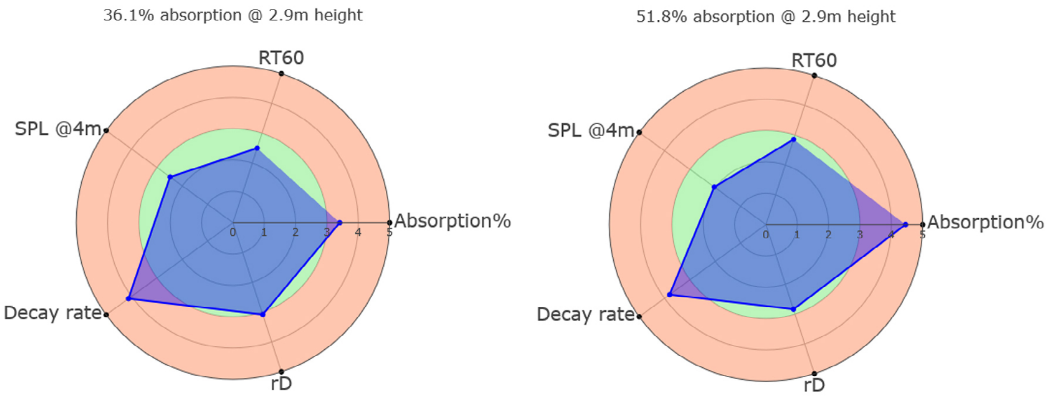

Scenario D

Scenario C

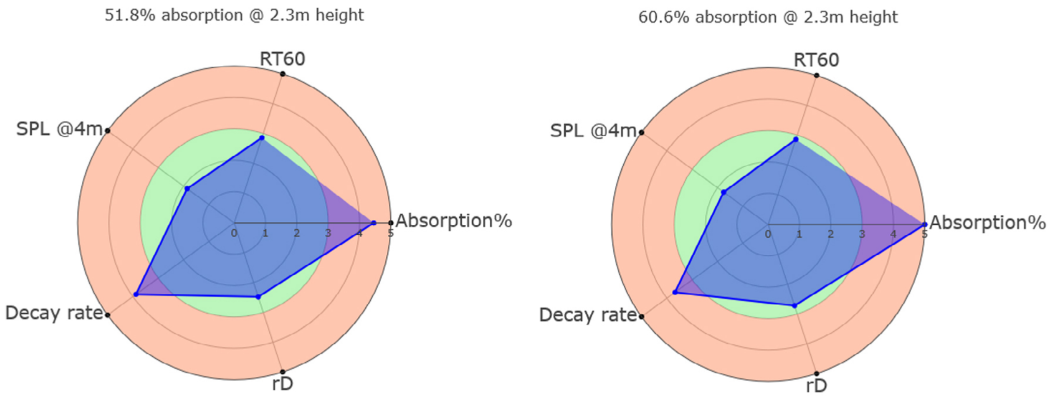

Scenario B

Scenario A

Study 4 - NRC ratings for the desk paritions

Panels @2.4m

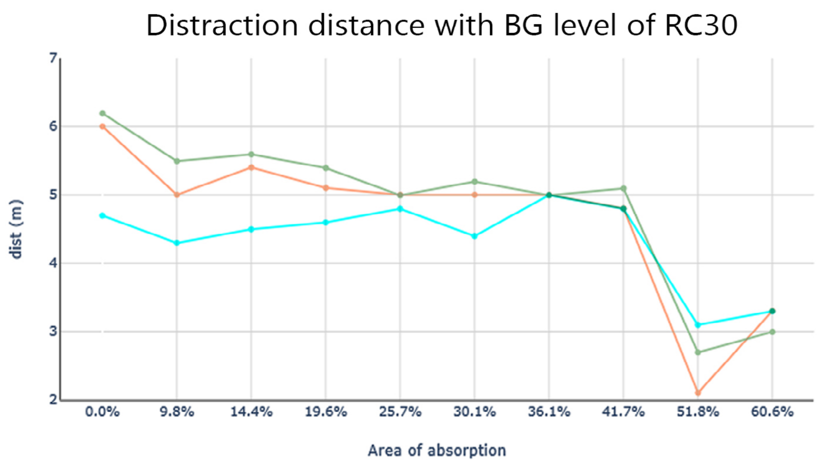

Distraction distance with BG level of RC30

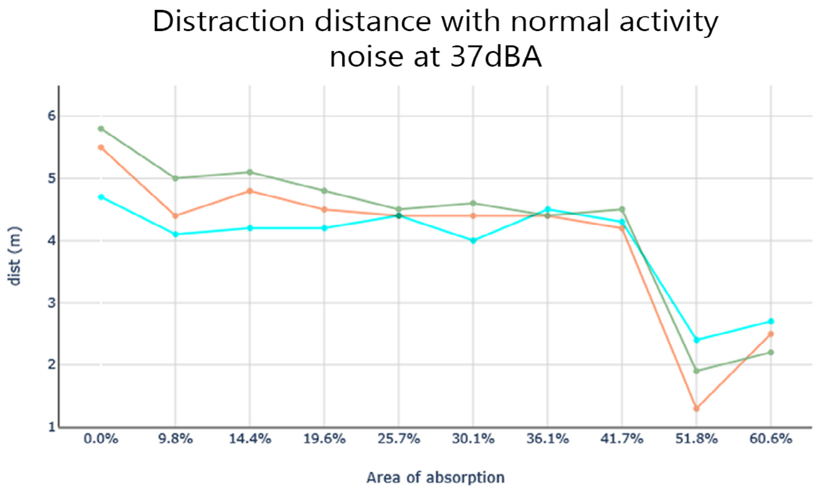

Distraction distance with normal activity noise at 37dBA

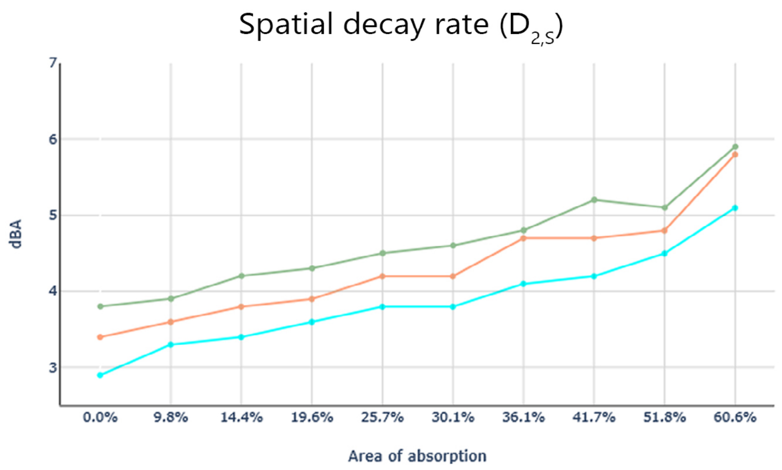

Spatial decay rate ($D_{2,S}$)

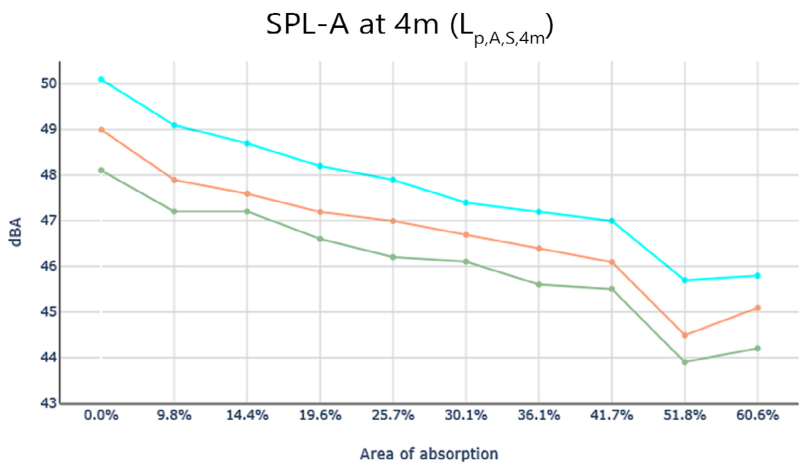

SPL-A at 4m ($L_{p,A,S,4m}$)

Legend

🟩 HIGH NRC rating

🟧 MID NRC rating

🟦 LOW NRC rating

Study 4 - NRC ratings for the desk paritions

Panels @2.7m

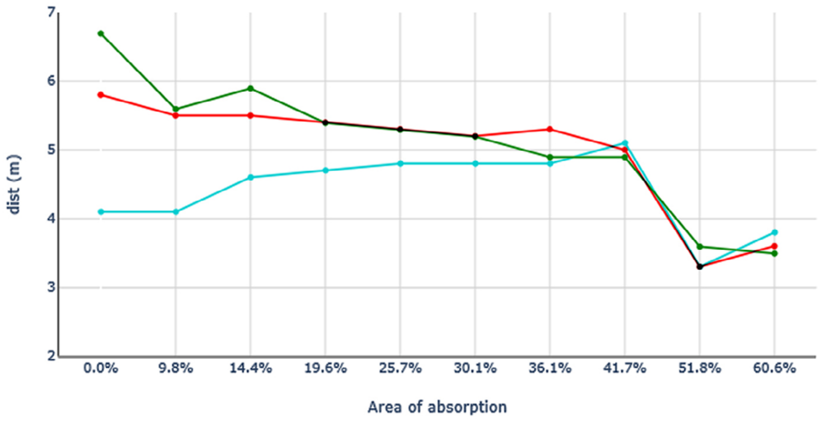
Distraction distance with BG level of RC30

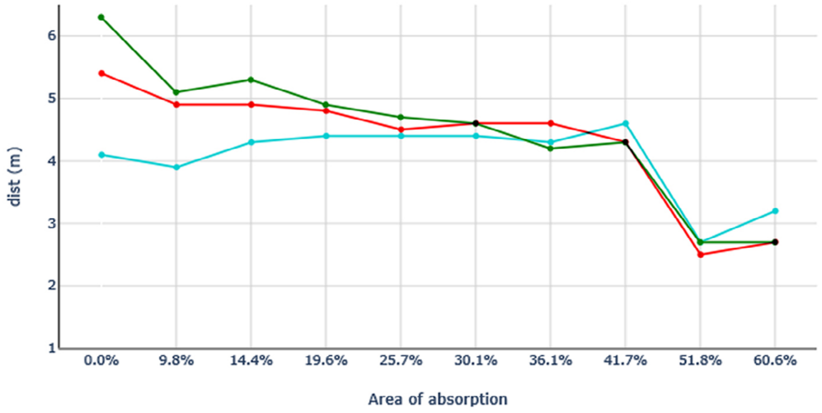
Distraction distance with normal activity noise at 37dBA

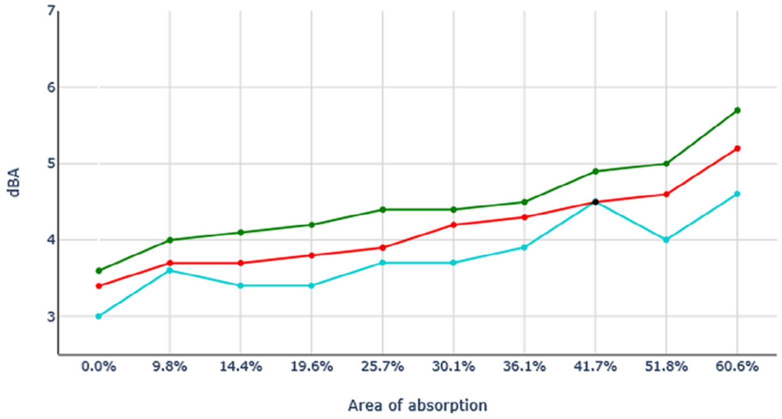
Spatial decay rate ($D_{2,S}$)

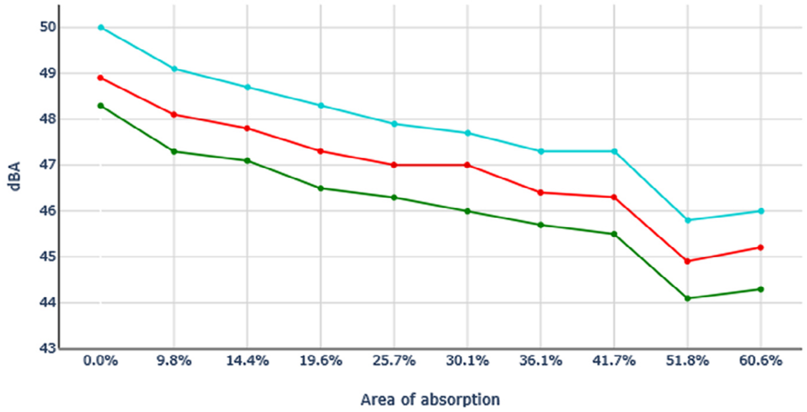
SPL-A at 4m ($L_{p,A,S,4m}$)

Legend

🟩 HIGH NRC rating

🟥 MID NRC rating

🟦 LOW NRC rating

Study 4.b - Materials for the desk paritions

Panels @2.4m

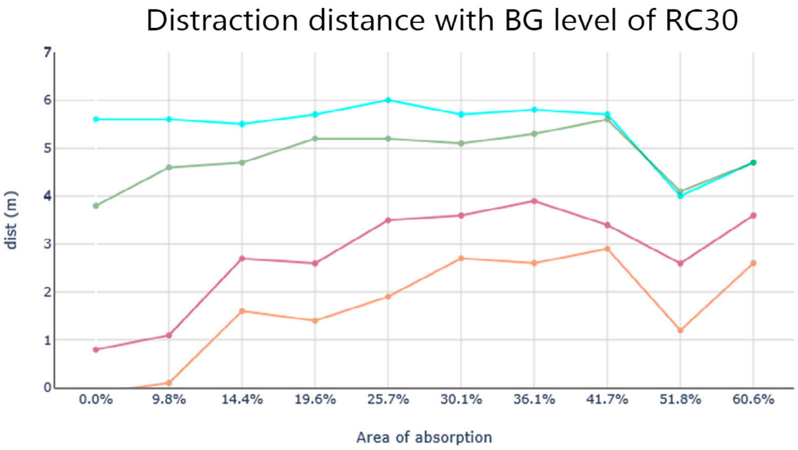
Distraction distance with BG level of RC30

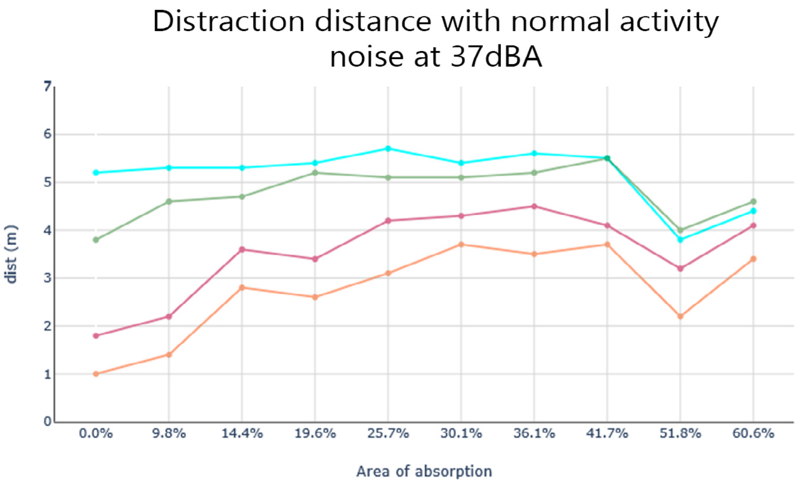
Distraction distance with normal activity noise at 37dBA

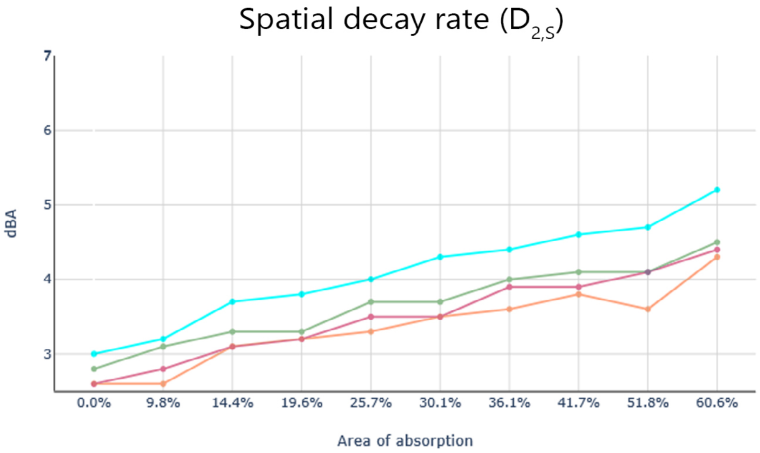
Spatial decay rate ($D_{2,S}$)

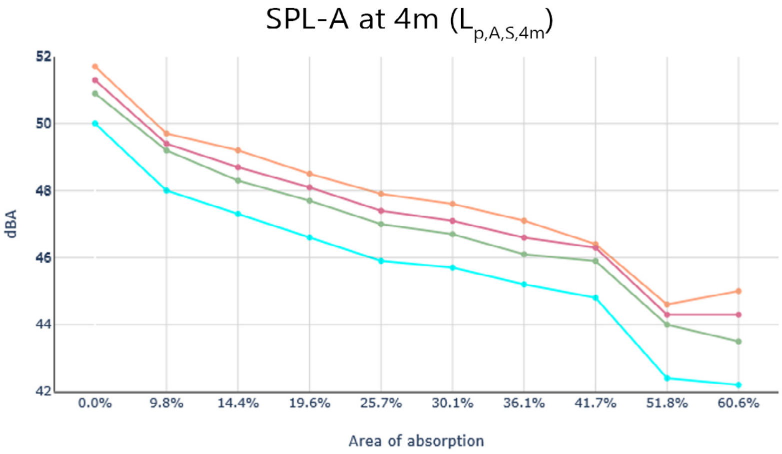
SPL-A at 4m ($L_{p,A,S,4m}$)

Legend

🟩 Low density MDF (25mm)

🟧 Glass (4mm)

🟦 Fabric casing with Foam infill

🟪 Plywood panelling (10mm)

Study 4.b - Materials for the desk paritions

Panels @2.7m

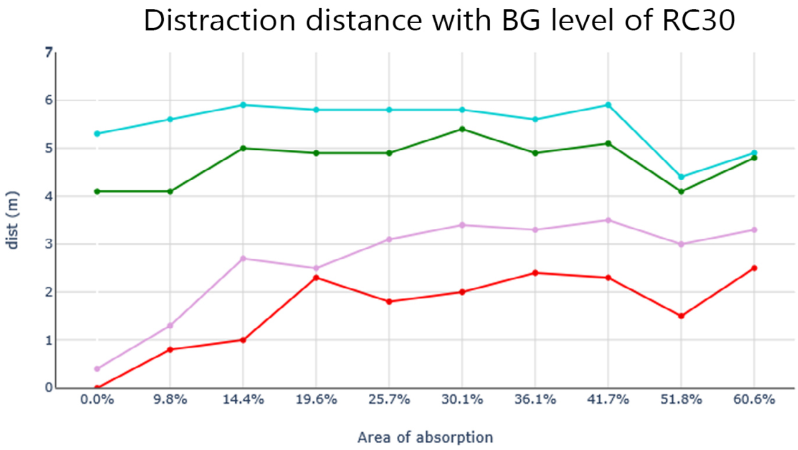
Distraction distance with BG level of RC30

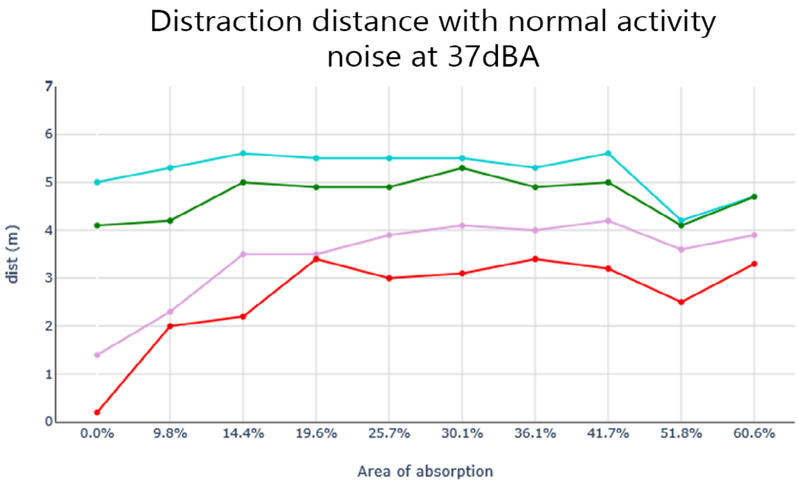
Distraction distance with normal activity noise at 37dBA

Legend

🟩 Low density MDF (25mm)

🟥 Glass (4mm)

🟦 Fabric casing with Foam infill

🟪 Plywood panelling (10mm)

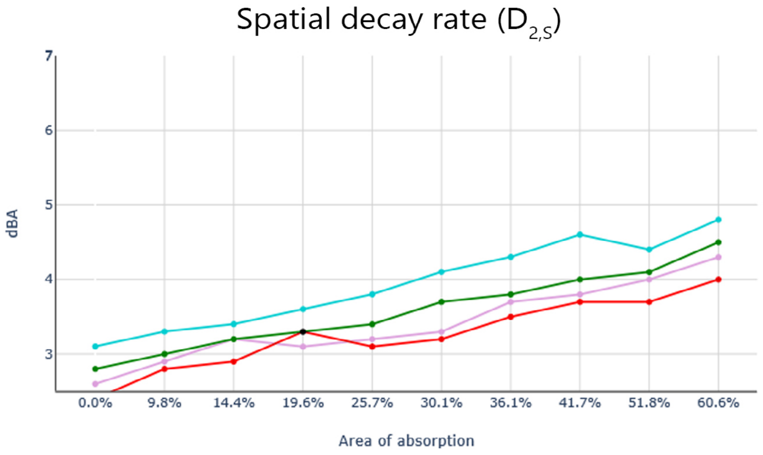
Spatial decay rate ($D_{2,S}$)

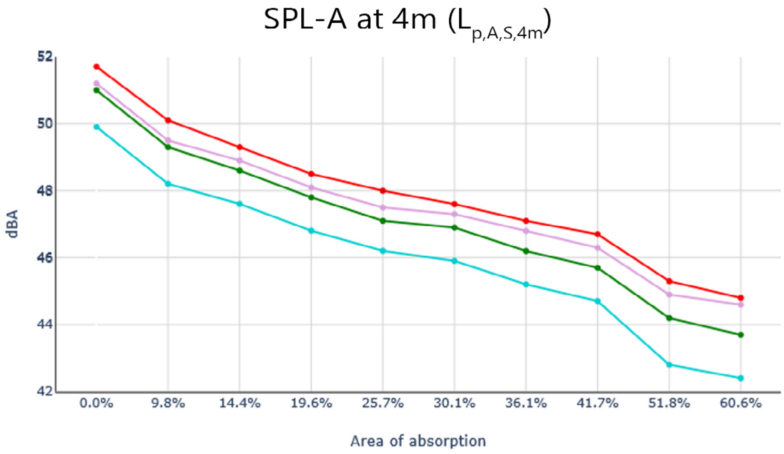
SPL-A at 4m ($L_{p,A,S,4m}$)

10.11 Appendix J - Case study layout simulations

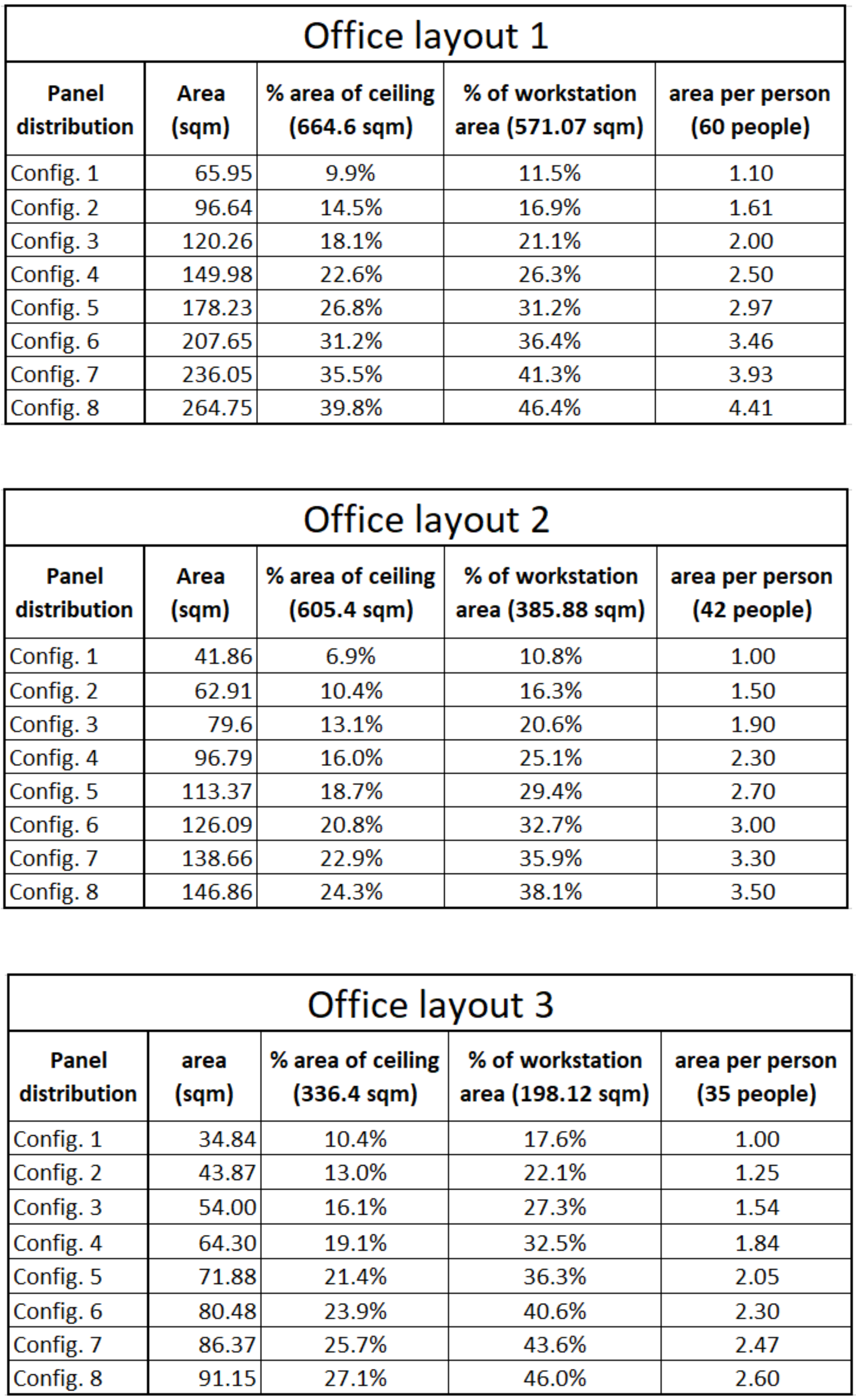

Office layout 1				
Panel distribution	**Area (sqm)**	**% area of ceiling (664.6 sqm)**	**% of workstation area (571.07 sqm)**	**area per person (60 people)**
Config. 1	65.95	9.9%	11.5%	1.10
Config. 2	96.64	14.5%	16.9%	1.61
Config. 3	120.26	18.1%	21.1%	2.00
Config. 4	149.98	22.6%	26.3%	2.50
Config. 5	178.23	26.8%	31.2%	2.97
Config. 6	207.65	31.2%	36.4%	3.46
Config. 7	236.05	35.5%	41.3%	3.93
Config. 8	264.75	39.8%	46.4%	4.41

Office layout 2				
Panel distribution	**Area (sqm)**	**% area of ceiling (605.4 sqm)**	**% of workstation area (385.88 sqm)**	**area per person (42 people)**
Config. 1	41.86	6.9%	10.8%	1.00
Config. 2	62.91	10.4%	16.3%	1.50
Config. 3	79.6	13.1%	20.6%	1.90
Config. 4	96.79	16.0%	25.1%	2.30
Config. 5	113.37	18.7%	29.4%	2.70
Config. 6	126.09	20.8%	32.7%	3.00
Config. 7	138.66	22.9%	35.9%	3.30
Config. 8	146.86	24.3%	38.1%	3.50

Office layout 3				
Panel distribution	**area (sqm)**	**% area of ceiling (336.4 sqm)**	**% of workstation area (198.12 sqm)**	**area per person (35 people)**
Config. 1	34.84	10.4%	17.6%	1.00
Config. 2	43.87	13.0%	22.1%	1.25
Config. 3	54.00	16.1%	27.3%	1.54
Config. 4	64.30	19.1%	32.5%	1.84
Config. 5	71.88	21.4%	36.3%	2.05
Config. 6	80.48	23.9%	40.6%	2.30
Config. 7	86.37	25.7%	43.6%	2.47
Config. 8	91.15	27.1%	46.0%	2.60

Figure 114: *Area statistics of the panel configurations used in all the three office layouts*

Case Study - Office Layout 1

Distraction distance with BG level of RC30

Distraction distance with normal activity noise at 37dBA

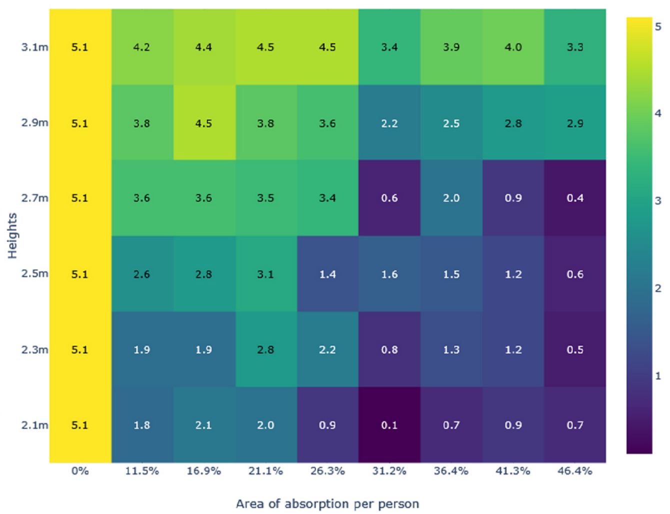

Distraction distance with background speech noise at 37dBA

Spatial decay rate ($D_{2,S}$)

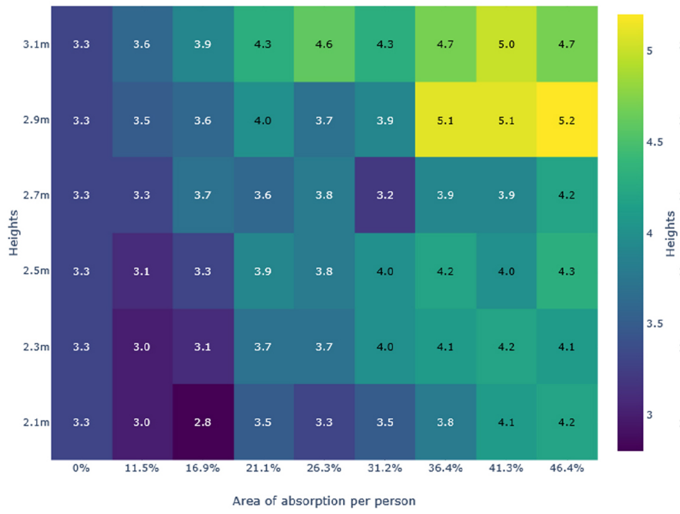

SPL-A at 4m ($L_{p,A,S,4m}$)

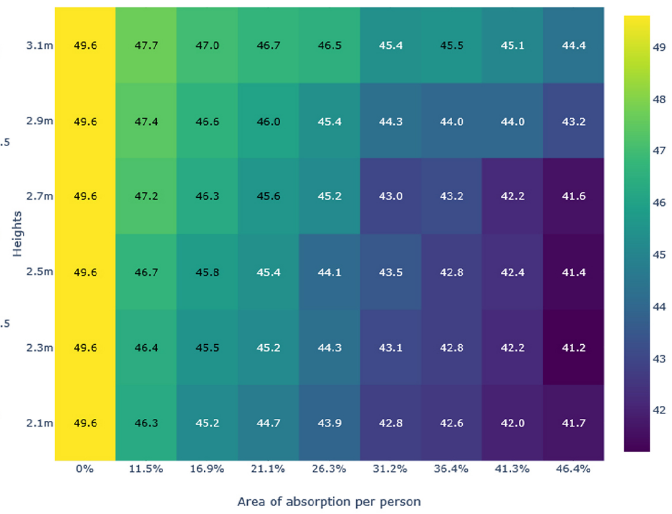

Reverberation Time (RT_{60})

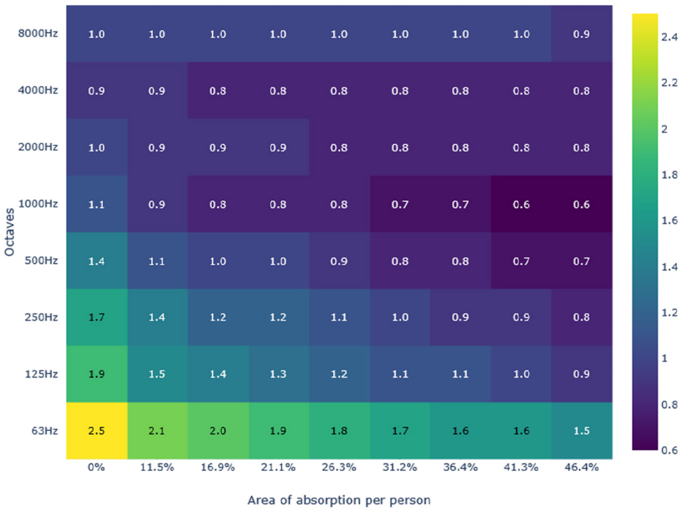

Case Study - Office Layout 2

Distraction distance with BG level of RC30

Heights	0%	10.8%	16.3%	20.6%	25.1%	29.4%	32.7%	35.9%	38.1%
3.1m	7.4	6.4	6.7	6.5	6.7	6.8	6.5	6.4	6.5
2.9m	7.4	6.7	6.4	6.2	6.2	5.8	5.7	5.7	5.6
2.7m	7.4	6.2	5.7	5.7	5.5	5.6	5.4	5.2	5.4
2.5m	7.4	6.0	5.9	5.6	5.7	5.5	5.3	5.3	4.9
2.3m	7.4	6.5	5.4	5.4	5.7	4.9	4.8	4.8	4.5
2.1m	7.4	6.2	5.3	4.6	4.6	4.3	4.3	4.4	4.0

Distraction distance with normal activity noise at 37dBA

Heights	0%	10.8%	16.3%	20.6%	25.1%	29.4%	32.7%	35.9%	38.1%
3.1m	6.7	5.8	6.1	5.9	6.1	6.0	5.9	5.8	5.9
2.9m	6.7	6.1	5.8	5.5	5.6	5.2	5.1	5.2	5.0
2.7m	6.7	5.6	5.1	5.1	4.8	4.9	4.7	4.6	4.7
2.5m	6.7	5.4	5.2	4.9	5.0	5.0	4.8	4.7	4.4
2.3m	6.7	6.0	4.7	4.7	5.1	4.4	4.2	4.3	4.0
2.1m	6.7	5.6	4.7	4.0	4.1	3.8	3.7	3.8	3.4

Distraction distance with background speech noise at 37dBA

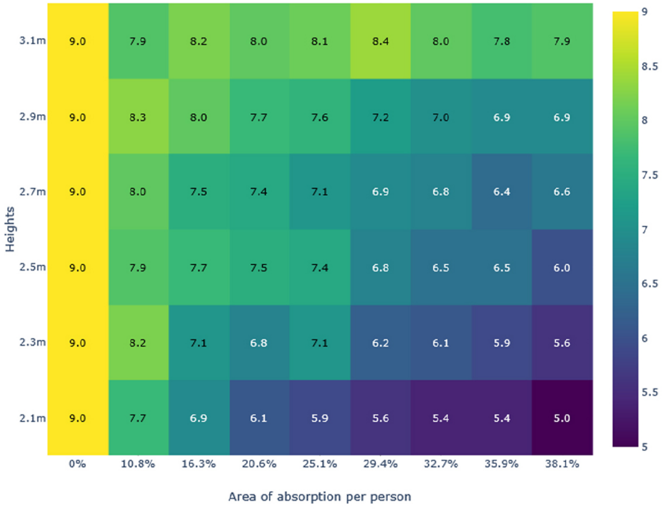

Heights	0%	10.8%	16.3%	20.6%	25.1%	29.4%	32.7%	35.9%	38.1%
3.1m	9.0	7.9	8.2	8.0	8.1	8.4	8.0	7.8	7.9
2.9m	9.0	8.3	8.0	7.7	7.6	7.2	7.0	6.9	6.9
2.7m	9.0	8.0	7.5	7.4	7.1	6.9	6.8	6.4	6.6
2.5m	9.0	7.9	7.7	7.5	7.4	6.8	6.5	6.5	6.0
2.3m	9.0	8.2	7.1	6.8	7.1	6.2	6.1	5.9	5.6
2.1m	9.0	7.7	6.9	6.1	5.9	5.6	5.4	5.4	5.0

Spatial decay rate ($D_{2,S}$)

Heights	0%	10.8%	16.3%	20.6%	25.1%	29.4%	32.7%	35.9%	38.1%
3.1m	3.9	4.4	4.6	4.8	4.8	4.7	5.0	5.2	5.4
2.9m	3.9	4.1	4.5	4.6	4.7	5.1	5.4	6.0	5.6
2.7m	3.9	4.1	4.2	4.5	4.4	5.0	5.0	5.4	5.4
2.5m	3.9	4.0	4.1	4.1	4.4	5.4	5.4	5.3	5.7
2.3m	3.9	4.2	4.3	4.6	4.8	5.3	5.4	5.9	5.9
2.1m	3.9	4.3	4.4	4.5	5.0	5.2	5.7	5.8	5.9

SPL-A at 4m ($L_{p,A,S,4m}$)

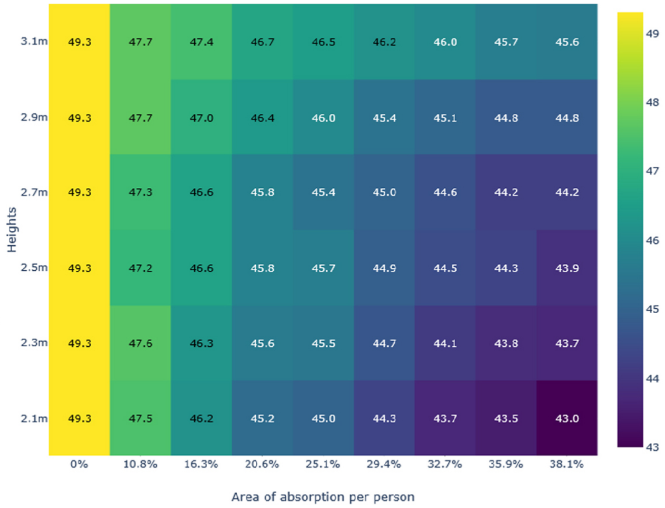

Heights	0%	10.8%	16.3%	20.6%	25.1%	29.4%	32.7%	35.9%	38.1%
3.1m	49.3	47.7	47.4	46.7	46.5	46.2	46.0	45.7	45.6
2.9m	49.3	47.7	47.0	46.4	46.0	45.4	45.1	44.8	44.8
2.7m	49.3	47.3	46.6	45.8	45.4	45.0	44.6	44.2	44.2
2.5m	49.3	47.2	46.6	45.8	45.7	44.9	44.5	44.3	43.9
2.3m	49.3	47.6	46.3	45.6	45.5	44.7	44.1	43.8	43.7
2.1m	49.3	47.5	46.2	45.2	45.0	44.3	43.7	43.5	43.0

Reverberation Time (RT_{60})

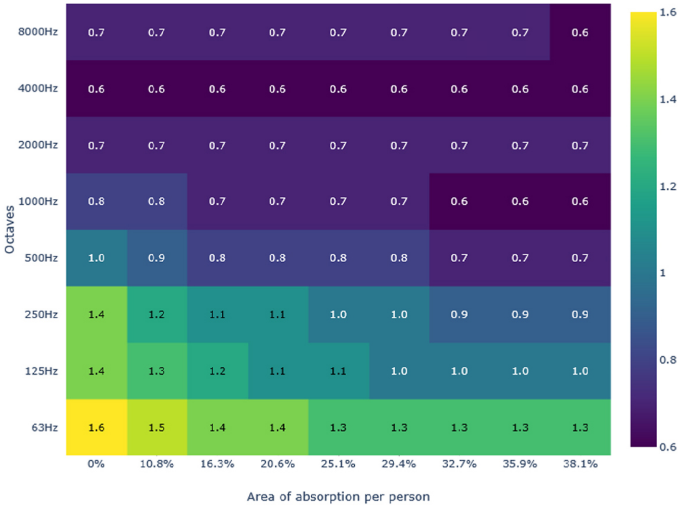

Octaves	0%	10.8%	16.3%	20.6%	25.1%	29.4%	32.7%	35.9%	38.1%
8000Hz	0.7	0.7	0.7	0.7	0.7	0.7	0.7	0.7	0.6
4000Hz	0.6	0.6	0.6	0.6	0.6	0.6	0.6	0.6	0.6
2000Hz	0.7	0.7	0.7	0.7	0.7	0.7	0.7	0.7	0.7
1000Hz	0.8	0.8	0.7	0.7	0.7	0.7	0.6	0.6	0.6
500Hz	1.0	0.9	0.8	0.8	0.8	0.8	0.7	0.7	0.7
250Hz	1.4	1.2	1.1	1.1	1.0	1.0	0.9	0.9	0.9
125Hz	1.4	1.3	1.2	1.1	1.1	1.0	1.0	1.0	1.0
63Hz	1.6	1.5	1.4	1.4	1.3	1.3	1.3	1.3	1.3

Case Study - Office Layout 3

Distraction distance with BG level of RC30

Heights	0%	17.6%	22.1%	27.3%	32.5%	36.3%	40.6%	43.6%	46.0%
3.1m	8.5	8.7	8.8	8.5	8.5	8.5	8.3	8.1	8.2
2.9m	8.5	8.4	8.5	8.5	8.1	8.2	8.0	7.9	7.6
2.7m	8.5	8.5	8.4	8.5	8.0	8.1	7.9	7.8	7.8
2.5m	8.5	8.2	8.1	8.2	8.0	7.9	7.6	8.0	7.8
2.3m	8.5	8.0	8.1	7.9	8.0	7.7	7.2	7.2	6.9
2.1m	8.5	7.7	7.8	7.8	8.0	7.6	7.3	7.5	6.8

Distraction distance with normal activity noise at 37dBA

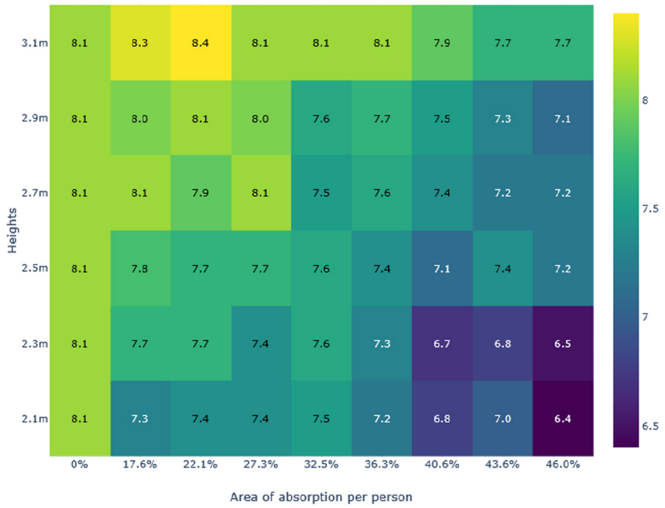

Heights	0%	17.6%	22.1%	27.3%	32.5%	36.3%	40.6%	43.6%	46.0%
3.1m	8.1	8.3	8.4	8.1	8.1	8.1	7.9	7.7	7.7
2.9m	8.1	8.0	8.1	8.0	7.6	7.7	7.5	7.3	7.1
2.7m	8.1	8.1	7.9	8.1	7.5	7.6	7.4	7.2	7.2
2.5m	8.1	7.8	7.7	7.7	7.6	7.4	7.1	7.4	7.2
2.3m	8.1	7.7	7.7	7.4	7.6	7.3	6.7	6.8	6.5
2.1m	8.1	7.3	7.4	7.4	7.5	7.2	6.8	7.0	6.4

Distraction distance with background speech noise at 37dBA

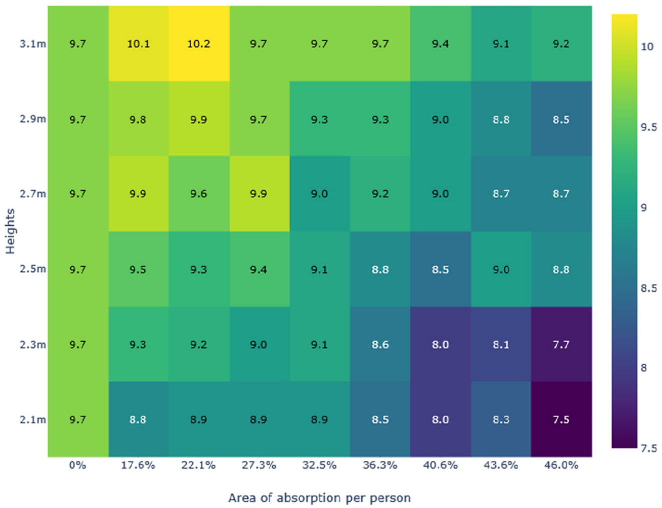

Heights	0%	17.6%	22.1%	27.3%	32.5%	36.3%	40.6%	43.6%	46.0%
3.1m	9.7	10.1	10.2	9.7	9.7	9.7	9.4	9.1	9.2
2.9m	9.7	9.8	9.9	9.7	9.3	9.3	9.0	8.8	8.5
2.7m	9.7	9.9	9.6	9.9	9.0	9.2	9.0	8.7	8.7
2.5m	9.7	9.5	9.3	9.4	9.1	8.8	8.5	9.0	8.8
2.3m	9.7	9.3	9.2	9.0	9.1	8.6	8.0	8.1	7.7
2.1m	9.7	8.8	8.9	8.9	8.9	8.5	8.0	8.3	7.5

Spatial decay rate ($D_{2,S}$)

Heights	0%	17.6%	22.1%	27.3%	32.5%	36.3%	40.6%	43.6%	46.0%
3.1m	3.7	4.5	4.8	5.1	5.1	5.2	5.4	5.7	5.8
2.9m	3.7	4.5	4.8	5.0	5.2	5.4	5.6	5.9	6.2
2.7m	3.7	4.5	4.9	4.9	5.4	5.5	5.6	5.8	5.9
2.5m	3.7	4.7	5.0	5.0	5.3	5.6	5.9	5.7	5.8
2.3m	3.7	4.8	5.0	5.4	5.5	5.9	6.3	6.3	6.6
2.1m	3.7	4.9	5.2	5.3	5.6	6.0	6.4	6.4	6.8

SPL-A at 4m ($L_{p,A,S,4m}$)

Heights	0%	17.6%	22.1%	27.3%	32.5%	36.3%	40.6%	43.6%	46.0%
3.1m	52.1	50.5	50.2	49.6	49.4	49.2	49.0	48.8	48.5
2.9m	52.1	50.2	49.8	49.3	48.7	48.6	48.4	48.0	47.7
2.7m	52.1	50.1	49.6	49.1	48.6	48.4	48.0	47.7	47.6
2.5m	52.1	50.0	49.5	48.9	48.6	48.2	47.8	47.8	47.6
2.3m	52.1	49.9	49.5	48.8	48.6	48.3	47.6	47.3	47.0
2.1m	52.1	49.8	49.5	48.7	48.5	48.2	47.7	47.5	46.9

Reverberation Time (RT_{60})

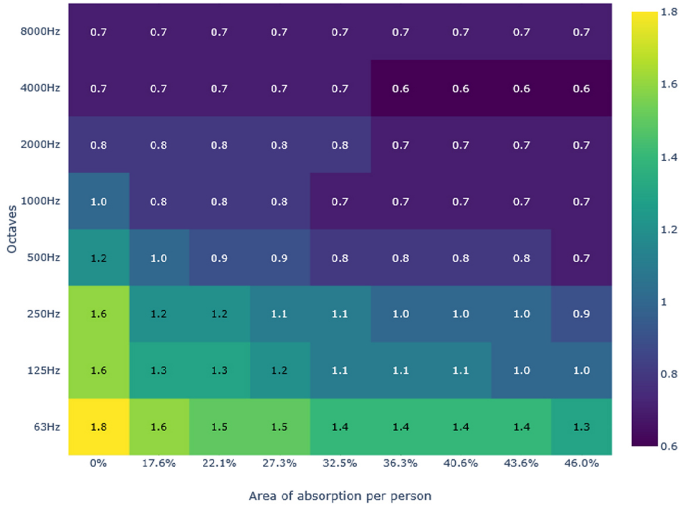

Octaves	0%	17.6%	22.1%	27.3%	32.5%	36.3%	40.6%	43.6%	46.0%
8000Hz	0.7	0.7	0.7	0.7	0.7	0.7	0.7	0.7	0.7
4000Hz	0.7	0.7	0.7	0.7	0.7	0.6	0.6	0.6	0.6
2000Hz	0.8	0.8	0.8	0.8	0.8	0.7	0.7	0.7	0.7
1000Hz	1.0	0.8	0.8	0.8	0.7	0.7	0.7	0.7	0.7
500Hz	1.2	1.0	0.9	0.9	0.8	0.8	0.8	0.8	0.7
250Hz	1.6	1.2	1.2	1.1	1.1	1.0	1.0	1.0	0.9
125Hz	1.6	1.3	1.3	1.2	1.1	1.1	1.1	1.0	1.0
63Hz	1.8	1.6	1.5	1.5	1.4	1.4	1.4	1.4	1.3

References

Abbaszadeh, S., Zagreus, L., Lehrer, D. & Huizenga, C. (2006), 'Occupant satisfaction with indoor environmental quality in green buildings'.

Atalla, N. & Sgard, F. (2007), 'Modeling of perforated plates and screens using rigid frame porous models', *Journal of sound and vibration* **303**(1-2), 195–208.

Bradley, J. (2004), *Acoustical design for open-plan offices*, Institute for Research in Construction, National Research Council of Canada.

Bradley, J. S. (2003), 'The acoustical design of conventional open plan offices', *Canadian Acoustics* **31**(2), 23–31.

Brennan, A., Chugh, J. S. & Kline, T. (2002), 'Traditional versus open office design: A longitudinal field study', *Environment and behavior* **34**(3), 279–299.

Cai, X., Guo, Q., Hu, G. & Yang, J. (2014), 'Ultrathin low-frequency sound absorbing panels based on coplanar spiral tubes or coplanar helmholtz resonators', *Applied Physics Letters* **105**(12), 121901.

Carvalho De Sousa, A., Deckers, E., Claeys, C. & Desmet, W. (2019), 'Parallel assembly of acoustic resonators to obtain narrow-band unity sound absorption peaks below 1000 hz', *http://www.icedyn.net/* .

Chazot, J.-D. & Guyader, J.-L. (2007), 'Prediction of transmission loss of double panels with a patch-mobility method', *The Journal of the Acoustical Society of America* **121**(1), 267–278.

Chenzhi, C. & Mak, C. M. (2018), 'Noise attenuation capacity of a helmholtz resonator', *Advances in Engineering Software* **116**, 60–66.

Cox, T. & d'Antonio, P. (2016), *Acoustic absorbers and diffusers: theory, design and application*, Crc Press.

Davidsson, F. (2016), 'Generating and understanding speech'.
URL: *https://www.vubp.cz/konference/2016/prezentace/sound-offices-and-people-davidsson.pdf*

Deb, K. (2001), *Multi-objective optimization using evolutionary algorithms*, Vol. 16, John Wiley & Sons.

Delle Macchie, S., Secchi, S. & Cellai, G. (2018), 'Acoustic issues in open plan offices: A typological analysis', *Buildings* **8**(11), 161.

Ebissou, A., Parizet, E. & Chevret, P. (2015), 'Use of the speech transmission index for the assessment of sound annoyance in open-plan offices', *Applied Acoustics* **88**, 90–95.

Fesina, M. I., Krasnov, A. V. & Gorina, L. N. (2017), ‘On different engineering ideas of eco-designer resource-saving studies of effective sound-absorbing substances and noise-reducing constructions’, *Procedia Engineering* **176**, 150–158.

Fuchs, H. V. (2013), *Applied Acoustics: Concepts, Absorbers, and Silencers for Acoustical Comfort and Noise Control: Alternative Solutions-Innovative Tools-Practical Examples*, Springer Science & Business Media.

Fuchs, H., Zha, X., Zhou, X. & Drotleff, H. (2001), ‘Creating low-noise environments in communication rooms’, *Applied Acoustics* **62**(12), 1375–1396.

Gommer, B. (2016), ‘Resistance in helmholtz resonators: Exploring the potential of sound absorption created by additive manufacturing’.

Griffin, S., Lane, S. A. & Huybrechts, S. (2000), ‘Coupled helmholtz resonators for acoustic attenuation’, *J. Vib. Acoust.* **123**(1), 11–17.

Haapakangas, A., Hongisto, V., Eerola, M. & Kuusisto, T. (2017), ‘Distraction distance and perceived disturbance by noise—an analysis of 21 open-plan offices’, *The Journal of the Acoustical Society of America* **141**(1), 127–136.

Han, N. & Mak, C. M. (2008), ‘A further study of a mathematical model for a screen in open-plan offices’, *Applied acoustics* **69**(11), 1114–1119.

Hodgson, M. (2011), ‘Evaluation and control of acoustical environments in ’green’(sustainable) office buildings’, *Canadian Acoustics* **39**(1), 11–21.

Huang, S., Fang, X., Wang, X., Assouar, B., Cheng, Q. & Li, Y. (2019), ‘Acoustic perfect absorbers via helmholtz resonators with embedded apertures’, *The Journal of the Acoustical Society of America* **145**(1), 254–262.

Ingard, U. (1953), ‘On the theory and design of acoustic resonators’, *The Journal of the acoustical society of America* **25**(6), 1037–1061.

ISO 3382-3 (2012), ‘Acoustics - Measurement of room acoustic parameters - Part 3: Open-plan offices’.

Johansson, T. A. & Kleiner, M. (2001), ‘Theory and experiments on the coupling of two helmholtz resonators’, *The Journal of the Acoustical Society of America* **110**(3), 1315–1328.

Jordan, V. L. (1947), ‘The application of helmholtz resonators to sound-absorbing structures’, *The Journal of the Acoustical Society of America* **19**(6), 972–981.

Keränen, J., Virjonen, P., Elorza, D. O. & Hongisto, V. (2008), ‘Design of room acoustics for open offices’, *SJWEH Supplements* (4), 46–49.

Kim, S., Kim, Y.-H. & Jang, J.-H. (2006), 'A theoretical model to predict the low-frequency sound absorption of a helmholtz resonator array', *The Journal of the Acoustical Society of America* **119**(4), 1933–1936.

Kim, S.-R., Kim, M.-S., Kim, Y.-H. & Kim, Y.-W. (2003), Absorptive characteristics of resonator panel for low frequency noise control, and its applications, *in* 'inter-Noise 2003', Inter-noise.

Kim, Y.-H. (2010), *Sound propagation: an impedance based approach*, John Wiley & Sons.

Komkin, A., Mironov, M. & Bykov, A. (2017), 'Sound absorption by a helmholtz resonator', *Acoustical Physics* **63**(4), 385–392.

Kuttruff, H. (2016), *Room acoustics*, Crc Press.

Lee, T., Nomura, T. & Iizuka, H. (2019), 'Damped resonance for broadband acoustic absorption in one-port and two-port systems', *Scientific reports* **9**(1), 1–11.

Lee, Y. S. & Kim, S.-K. (2008), 'Indoor environmental quality in leed-certified buildings in the us', *Journal of Asian Architecture and Building Engineering* **7**(2), 293–300.

Leventhall, H. G. et al. (2004), 'Low frequency noise and annoyance', *Noise and Health* **6**(23), 59.

Maennel, M., Forssén, J. & Van der Aa, B. (2013), Improving the acoustic performance of low noise road surfaces using resonators, *in* 'Proceedings of Meetings on Acoustics ICA2013', Vol. 19, Acoustical Society of America, p. 040036.

Meissner, M. (2004), 'The response of helmholtz resonator to external excitation. part i: Acoustically induced resonance', *Archives of Acoustics* **29**(1).

Nilsson, E. & Hellström, B. (2010), 'Nt technical report'.

Pawlaczyk-łuszczyńska, M., Dudarewicz, A., Waszkowska, M. & Śliwińska-kowalska, M. (2003), 'Assessment of annoyance from low frequency and broadband noises', *Int J Occup Environ Med* **16**, 337–43.

Pieren, R. (2012), 'Sound absorption modeling of thin woven fabrics backed by an air cavity', *Textile Research Journal* **82**(9), 864–874.

Pierre Jr, R. L. S., Maguire, D. J. & Automotive, C. S. (2004), The impact of a-weighting sound pressure level measurements during the evaluation of noise exposure, *in* 'Conference NOISE-CON', pp. 12–14.

Polychronopoulos, S., Skarlatos, D. & Mourjopoulos, J. (2014), 'Efficient filter-based model for resonator panel absorbers', *Journal of the Audio Engineering Society* **62**(1/2), 14–24.

Rindel, J. H. (2011), Echo problems in ancient theatres and a comment to the 'sounding vessels'described by vitruvius, *in* 'Proc. The acoustics of ancient theatres Conference, Patras'.

Rindel, J. H. (2018), 'Open plan office acoustics–a multidimensional optimization problem', *Proceedings of DAGA2018, Munich, Deutsche Gesellschaft für Akustik* .

Romadhona, I. C., Yahya, I. et al. (2017), 'On the use of coupled cavity helmholtz resonator inclusion for improving absorption performance of wooden sound diffuser element', *Procedia engineering* **170**, 458–462.

Schlittmeier, S. J. & Liebl, A. (2015), 'The effects of intelligible irrelevant background speech in offices–cognitive disturbance, annoyance, and solutions', *Facilities* .

Selamet, A. & Lee, I. (2003), 'Helmholtz resonator with extended neck', *The Journal of the Acoustical Society of America* **113**(4), 1975–1985.

Selamet, A., Xu, M., Lee, I.-J. & Huff, N. (2005), 'Helmholtz resonator lined with absorbing material', *The Journal of the Acoustical Society of America* **117**(2), 725–733.

Shi, X. & Mak, C. M. (2015), 'Helmholtz resonator with a spiral neck', *Applied Acoustics* **99**, 68–71.

Storn, R. & Price, K. (1997), 'Differential evolution–a simple and efficient heuristic for global optimization over continuous spaces', *Journal of global optimization* **11**(4), 341–359.

Tang, S. (2005), 'On helmholtz resonators with tapered necks', *Journal of Sound and Vibration* **279**(3-5), 1085–1096.

Van der Aa, B. (2012), Ground buried resonators analytical and numerical modelling of their noise reducing effect for sound propagating outdoors from traffic noise sources.

Ver, I. L. & Beranek, L. L. (2006), *Noise and Vibration Control Engineering-Principles and Applications, Wiley, 2006: Noise and Vibration Control Engineering-Principles and Applications*, Vol. 1, Bukupedia.

Vigran, T. (2004), 'Conical apertures in panels; sound transmission and enhanced absorption in resonator systems', *Acta acustica united with Acustica* **90**(6), 1170–1177.

Vorländer, M. (2007), *Auralization: fundamentals of acoustics, modelling, simulation, algorithms and acoustic virtual reality*, Springer Science & Business Media.

Wang, C. & Bradley, J. (2002), 'A mathematical model for a single screen barrier in open-plan offices', *Applied Acoustics* **63**(8), 849–866.

Yuan, M., Yang, F. & Pang, Z. (2019), 'Deep subwavelength split ring neck acoustic resonator', *Results in Physics* **13**, 102322.